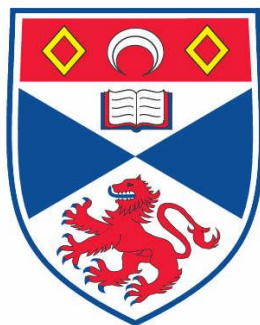


*Metal Organic Frameworks
as Lewis Acid Catalysts*

Laura Mitchell



This thesis is submitted in partial fulfilment for the degree of
PhD
at the
University of St Andrews

2014

Supervisors: Dr Matthew L. Clarke and Prof. Paul A. Wright

Declarations

1. I, Laura Mitchell, hereby certify that this thesis, which is approximately 57 000 words in length, has been written by me, that it is the record of work carried out by me and that it has not been submitted in any previous application for a higher degree.

I was admitted as a research student in September 2010 and as a candidate for the degree of PhD in September 2011; the higher study for which this is a record was carried out in the University of St Andrews between 2010 and 2014.

Date..... Signature of Candidate.....

2. I hereby certify that the candidate has fulfilled the conditions of the Resolution and Regulations appropriate for the degree of PhD in the University of St Andrews and that the candidate is qualified to submit this thesis in application for that degree.

Date..... Signature of Supervisor.....

3. In submitting this thesis to the University of St Andrews I understand that I am giving permission for it to be made available for use in accordance with the regulations of the University Library for the time being in force, subject to any copyright vested in the work not being affected thereby. I also understand that the title and the abstract will be published, and that a copy of the work may be made and supplied to any bona fide library or research worker, that my thesis will be electronically accessible for personal or research use unless exempt by award of an embargo as requested below, and that the library has the right to migrate my thesis into new electronic forms as required to ensure continued access to the thesis. I have requested the appropriate embargo below. The following is an agreed request by candidate and supervisor regarding the electronic publication of this thesis:

Embargo on all of printed copy and electronic copy for the same fixed period of two years on the following ground: publication would preclude future publication.

Date Signature of Candidate

Signature of Supervisor

Acknowledgements

I would like to thank a few people for all their help and support during this project. Firstly, I wish to thank Dr Matt Clarke and Prof. Paul Wright, for not only giving me the opportunity to take part in this research, but also for all their support and guidance. Their enthusiasm, dedication and wealth of knowledge have been invaluable, and the success of the project would not have been possible without them. I also express my gratitude to my industrial supervisor, Dr Nadia Acerbi, who has also been an integral source of knowledge and ideas.

I have had the opportunity to collaborate with other academics and researches and they have helped by providing their vital specialist knowledge. I thank Prof. Marco Daturi, Dr Alex Vimont and Ms. Maralene Renouf for hosting me at Laboratoire Spectrochimie Caen where I undertook in-situ IR experiments. I thank Prof Sharon Ashbrook and Dr Valerie Seymour for their collection and analysis of solid-state NMR data. I am grateful to Prof. Richard Walton and Mr Luke Daniels for their help with EXAFs and XANEs experimental techniques. I am appreciative to Mrs Sylvia Williamson for all her help and training in adsorption and thermal analysis.

I have had the opportunity not only to carry out my own research but also work with some exceptional people within both the Clarke and Wright groups past and present. I am especially grateful to Dr John Mowat who has been an exceptional help with experiments and scientific discussion. I would also like to thank Dr Jose Fuentes who has had provided much of his expertise in organic synthesis and has been much help and support in this last four years. My thanks also go to the project students that have contributed to the scientific research in this thesis; namely Patrick Williamson, Barbora Ehrlichová and Grace Turner.

I would like to thank the people most important in my life who have provided endless support when I needed it most, my family. I am forever grateful to my parents, Lesley and Paul Mitchell, who without their continued support and enthusiasm I would not be here. I would like to thank William, Edward, Paula, Jessica and Jacob Mitchell who have always been there for me and gave me something else to focus on when I needed it. To my grandparents and other members of my family I have not mentioned, who have always generously supported me throughout my education, I am grateful.

Finally, to my partner Lewis Downie I am eternally grateful, not only for your endless scientific advice and proof reading, but for always being there for me and even pushing me. I look forward to our future together.

*This thesis is dedicated to my grandfather,
John Carson*

Abstract

Lewis acids are widely used in the pharmaceutical industry, generally homogeneously, to perform reactions such as C-C or C=N bond formation and acetalisation. Typically, metal salts such as those of Ti, Fe and especially Sc are used, the last typically as the triflate. Metal organic frameworks (MOFs) containing such metals should act as heterogeneous, removable and reusable catalysts for similar reactions if they can be prepared in stable forms and with large, open pores and metal cation sites that can be rendered coordinatively unsaturated. Families of novel MOFs with different structure types and cations have therefore been prepared and their activity has been examined in carbonyl ene C-C bond forming reactions, Friedel-Crafts-Michael additions and imine formation reactions. Their activities have been compared with those of the well-known HKUST-1(Cu), MIL-100(Fe) and MIL-101(Cr) solids examined as catalysts previously. In particular, divalent transition metal bisphosphonates and dicarboxylates with pore sizes from 10 – 20 Å and scandium carboxylates (MIL-68(Sc), MIL-88D(Sc), MIL-100(Sc), MIL-101(Sc)) have been tested. Synthetic procedures were optimised according to commercial constraints for the known MOFs STA-12(Ni) and MIL-100(Sc).

While good activities are observed for Ni-based MOFs and in a number of the scandium-based solids, MIL-100(Sc) is by far the best Lewis acid catalyst for a range of reactions. In particular, MIL-100(Sc) is very active even when used without pre-dehydration, is readily recyclable with minor loss of activity and shows fully heterogeneous activity. It outperforms both MIL-100(Fe) and MIL-101(Cr), each commonly reported as versatile catalysts in the literature. Careful synthesis of bulky substrates shows that the activity is derived from reactions within the internal pore system. Furthermore, MIL-100(Sc) is able to perform tandem reactions - such as dehydration followed by carbonyl ene reaction - in which the Lewis acid sites catalyse two steps. The Lewis acidic sites of the excellent Lewis acid catalyst MIL-100(Sc) has been examined in detail by *in situ* IR using adsorption of CO and CD₃CN as probe molecules and compared with other MIL-100 materials.

The work has been extended to the examination of MOFs containing two different metals, by substitutional approaches within the metal nodes (e.g. Sc-Al, Sc-Fe, Sc-Cr, Sc-Ni, Sc-Co within the trimeric M₃O(O₂C-) ₆ nodes of MIL-100). In addition, series of

Sc-Fe MIL-100 materials have been prepared that contain α -Fe₂O₃ nanoparticles in the pores of the structure. These composites show higher specific catalytic activity for Lewis acid catalysis than MIL-100(Sc), even though some scandium has been replaced with iron: the origin of this behaviour is discussed. MIL-100(Sc/Fe) has also been explored as a bifunctional catalyst in tandem Friedel-Crafts-oxidation reactions. MIL-100(Sc₆₀/Fe₄₀) was found to give exceptionally high conversions in the Friedel-Crafts-oxidation tandem reaction of 2-methyl indole and ethyl trifluoropyruvate to form a ketone, outperforming the many other materials tested and giving the best balance of the two different types of catalytic sites required to catalyse the reaction.

MIL-100(Sc) has also been prepared containing 50% of mono-fluorinated trimesate ligands in the framework for the first time. This fluorinated MIL-100(Sc) has been post-synthetically modified by addition of a di-phenylphosphino group as confirmed by solid state NMR. This can act as a starting point for the future generation of MOF-supported metal phosphine catalysts.

Abbreviations

ABTC	3,3',5,5'-azobenzenetetracarboxylic acid
ap	as-prepared
aq	aqueous
a.u.	arbitrary units
BDC	1, 4-benzene-dicarboxylic acid
BET	Brunauer-Emmett-Teller
BPDC	4,4'- biphenyldicarboxylate
br	broad
BTAPA	1, 3, 5-benzene tricarboxylic acid tris [<i>N</i> -(4-pyridyl) amide]
BTC	1, 3, 5-benzene tricarboxylic acid
Cat	catalyst
CHDC	<i>trans</i> -1, 4-cyclohexanedicarboxylate
CHN	Elemental analysis
COD	1,5-cyclooctadiene
CPO	Coordination polymer of Oslo
°C	degrees Celsius
d	doublet
DCE	dichloroethane
DCM	dichloromethane
DFT	density functional theory
DHTP	2,5-dihydroxyterephthalic acid
DMF	dimethylformamide
DMSO	dimethyl sulfoxide
EDX	energy dispersive X-ray (spectroscopy)
ED	ethylenediamine
e.e.	enantiomeric excess
et	ethyl
eq.	equivalents
ESI	electron spray ionisation
ESR	electron spin resonance
EXAFS	extended X-ray absorption fine structure
FT	Fourier transform
g	grams
H ₃ PDC	3,5-pyrazoledicarboxylic acid
H ₄ L	<i>N,N'</i> -piperazinebis-(methylenephosphonic acid)
H ₄ LL	<i>N,N'</i> -bipiperidine(methylenephosphonic acid)
HKUST	Hong-Kong University of Science and Technology
h	hours
Hz	hertz
ICP	inductively coupled plasma
IGA	intelligent gravimetric analysis
IR	infra-red spectroscopy
IRMOF	isoreticular metal organic framework
K	Kelvin
L	ligand
M	metal

me	methyl
MIL	Materiaux de l'Institut Lavoisier
mins	minutes
ml	millilitres
MOF	metal organic framework
mol	mole(s)
mol%	percentage molar equivalent(s)
m.p.	melting point
MS	mass spectrometry
nm	nanometre
NMR	nuclear magnetic resonance
OAc	acetate
OMe	methoxy
OTf	triflate
Ph	phenyl
ppm	parts per million
PTFE	polytetrafluoroethylene
PXRD	powder X-ray diffraction
pymo	2-hydroxypyrimidinolate
q	quartet
RT	room temperature
s	singlet
SEM	scanning electron microscope
STA	St Andrews University
t	triplet
TGA	Thermogravimetric analysis
<i>t</i> -Bu	tertiary butyl group (-C(CH ₃) ₃)
<i>tert.</i>	tertiary
THF	tetrahydrofuran
TOF	turnover frequency
UiO	Universitetet i Oslo
UV	ultra-visible
wt%	weight percentage
XANES	X-ray absorption near edge structure
ZSM-5	Zeolite Socony Mobil

Contents

1.	Introduction	1
1.1.	Zeolites	1
1.2.	Metal organic frameworks	3
1.2.1.	Metal carboxylate metal organic frameworks	4
1.2.1.1.	MOF-5	5
1.2.1.2.	HKUST-1	5
1.2.1.3.	CPO-27	6
1.2.1.4.	MIL-100/101	7
1.2.1.5.	MIL-88	9
1.2.1.6.	soc-MOF	10
1.2.1.7.	MIL-68	10
1.2.2.	Metal phosphonate metal organic frameworks	11
1.2.2.1.	STA-12	11
1.2.2.2.	STA-16	13
1.3.	MOFs in catalysis	14
1.3.1.	Advantages of MOFs in catalysis	14
1.3.2.	Size selectivity of MOFs in catalysis	14
1.3.3.	Use of MOFs with coordinatively unsaturated metal sites in catalysis	15
1.3.3.1.	Exploiting coordinatively unsaturated metal sites	16
1.3.4.	Functionalisation of the organic ligand	17
1.3.5.	Post synthetic modification	19
1.4.	Mixed metal MOFs	21
1.4.1.	Direct synthesis of mixed metal MOFs from mixtures of metal salts	21
1.4.2.	Mixed metal MOFs from ligand that coordinates a second metal	23
1.4.3.	Post synthetic introduction of nanoparticles	26
1.4.4.	Post synthetic modification of MOFs containing auxiliary ligands	28
1.4.5.	Post synthetic modification of MOFs with ligands and metals	29
1.5.	References	32
2.	Characterisation	37
2.1.	Diffraction	37
2.2.	Powder X-ray diffraction	38
2.3.	Structural refinement: Rietveld and Le Bail	40
2.4.	Adsorption	42
2.4.1.	Physisorption: Measurement of porosity (N ₂ adsorption)	42
2.4.2.	Chemisorption: Measurement of chemisorption at Lewis acid sites via IR of absorbent probe molecules	44
2.5.	Ultra-Visible spectroscopy	47
2.6.	X-ray absorption (XAS)	48
2.7.	Scanning electron microscopy (SEM) and Energy dispersive X-ray spectroscopy (EDX)	50
2.8.	Thermogravimetric analysis	52
2.9.	Elemental analysis (CHN)	52
2.10.	References	53

3.	Synthesis, optimisation and characterisation of known MOF materials	54
3.1.	Introduction	54
PART A	MOF synthesis, characterisation and optimisation	
3.2.	Synthesis of known MOF materials	55
3.2.1.	CPO-27	55
3.2.2.	STA-12	56
3.2.2.1.	Synthesis of STA-12(M) (where M= Ni, Co, Mg)	56
3.2.2.2.	Optimisation of synthesis of STA-12(Ni)	58
3.2.3.	Optimisation of synthesis of MIL-100(Sc)	65
3.3.	Conclusion Part A	71
PART B	Characterisation of the Lewis acidic sites of MIL-100(Sc)	
3.3.	Probing of Lewis acidic sites of MIL-100(Sc) using in-situ IR	73
3.3.1.	Temperature effects on MIL-100(Sc)	74
3.3.1.1.	As-prepared MIL-100(Sc)	74
3.3.1.2.	Methanol-activated MIL-100(Sc)	75
3.3.2.	Deuterated acetonitrile dosing on as-prepared and methanol-activated MIL-100(Sc)	75
3.3.3.	CO adsorption of as-prepared and methanol-activated MIL-100(Sc) at 423 K and 523 K	77
3.3.3.1.	As-prepared MIL-100(Sc) heated at 423 K and CO dosed at 100 K	77
3.3.3.2.	As-prepared MIL-100(Sc) heated at 523 K and CO dosed at 100 K	79
3.3.3.3.	Methanol activated MIL-100(Sc) heated at 423 K and CO dosed at 100 K	79
3.3.3.4.	Methanol activated MIL-100(Sc) heated at 523 K and CO dosed at 100 K	80
3.4.	Conclusion	81
3.5.	References	81
4.	Lewis acidic MOFs as catalysts for C-C and C=N bond-forming reactions	83
4.1.	Intermolecular carbonyl ene reaction using Lewis acidic metal organic frameworks as catalysts	83
4.1.1.	Intermolecular carbonyl ene reactions catalysed by MOFs containing divalent metals	88
4.1.2.	Intermolecular carbonyl ene reactions catalysed by MOFs containing trivalent metals	89
4.1.3.	Effects of synthesis method on catalyst activity	94
4.1.4.	Recoverability and reusability of STA-12(Ni) and MIL-100(Sc)	96
4.1.5.	Intermolecular carbonyl ene reaction with less activated alkenes and enophiles	98
4.1.6.	Tandem deprotection carbonyl ene reactions	101
4.1.7.	The effect of raising the activation temperature of MIL-100(Sc)	103
4.2.	Conjugate addition of electron deficient olefins to indole	104
4.2.1.	Conjugate addition of 2-methylindole to methyl vinyl ketone catalysed by divalent and trivalent MOFs	104
4.2.2.	Conjugate addition of other indoles to vinyl ketones catalysed by divalent and trivalent MOFs	110

4.2.3.	Surface catalysis or catalysis inside the pore?	112
4.3.	Imine formation	116
4.3.1.	Imine formation reaction of benzyl amine and fluoroacetophenone with a range of MOF materials	116
4.3.2.	Imine formation using MIL-100(Sc) with varying amines and carbonyl compounds	119
4.4.	Conclusion	121
4.5.	References	123
5.	Synthesis characterisation and catalytic performance of mixed metal MOFs	126
5.1.	Introduction	126
5.2.	Synthesis of mixed metal MIL-100(Sc/M) M= Al, Cr, Fe	126
5.2.1.	MIL-100(Sc/Fe)	126
5.2.2.	MIL-100(Sc/Fe) with included α -Fe ₂ O ₃ nanoparticles	132
5.3.	Other mixed metal MIL-100	141
5.3.1.	MIL-100(Sc/Al)	142
5.3.2.	MIL-100(Sc/Cr)	147
5.3.2.	Introduction of divalent metals into MIL-100	149
5.4.	HKUST-1(Cu/Ru)	152
5.5.	Catalysis using mixed metal MIL-100 materials	155
5.5.1.	Carbonyl ene reaction	155
5.5.2.	Conjugate addition of electron deficient olefins to indole	156
5.6.	Use of mixed metal MIL-100 as bifunctional catalysts	159
5.6.1.	Deacetalisation/Friedel-Crafts reaction of indole and related substrates with trifluoroacetaldehyde ethyl hemiacetal	159
5.6.2.	Oxidation of alcohols catalysed by various MOF materials	162
5.6.3.	One-pot deacetalisation/Friedel-Crafts reaction and oxidation	164
5.7.	Conclusion	170
5.8.	References	171
6.	Post synthetic modification	173
6.1.	Introduction	173
6.2.	Synthesis of fluorinated MIL-100(Sc)	174
6.3.	Functionalisation of MIL-100(Sc) with diphenylphosphine	178
6.4.	Conclusion	183
6.5.	References	183
7.	Experimental	184
7.1.	General procedures	184
7.2.	Ligand synthesis	184
7.3.	MOF synthesis	186
7.4.	FTIR experimental	190
7.5.	MOF catalysis	191
7.5.1.	Carbonyl ene reaction	191
7.5.2.	Conjugate addition of indole to electron deficient olefin	194
7.5.3.	Synthesis of larger substrates for the indole reaction	196
7.5.4.	Conjugate addition of large substrate indole to electron deficient olefin	198
7.5.5.	Imine synthesis over MOFs	199
7.5.6.	Tandem C-C bond forming-oxidation catalysis	201

7.6.	References	207
8.	Conclusions and future work	208
8.1.	Conclusion	208
8.2.	Future work	212

1. Introduction

Minimising environmental impact in chemical industry has become a very important issue and the need to achieve a greener approach to synthetic chemistry has resulted in an increased demand for cleaner syntheses with less waste. There is a need for more useful heterogeneous catalysts in order to improve catalyst reusability and enable catalyst separation. Heterogeneous catalysts that display the same level of function and selectivity as homogeneous catalysts are therefore required. Another attractive proposition is to develop multifunctional catalysts that can catalyse sequential transformations and thereby reduce waste and simplify operation.

Lewis acid catalysis is widely used in the pharmaceutical industry for acylation, alkylation, cyanation and aldol type reactions, generally using homogeneous catalysts. By preparing these catalysts in a way that they may easily be recycled they could become more commercially and environmentally attractive. This was first achieved by immobilising Lewis acids on solid supports.¹ Kobayashi *et al.*¹ were able to demonstrate that encapsulating scandium trifluoro-methanesulfonate, Sc(OTf)₃, into a solid polymer support, gave a highly active Lewis acid catalyst for several carbon-carbon bond formation reactions. Once the reaction had reached completion, the catalyst could be removed by filtration and reused without any decrease in catalytic activity. High activity was not only seen for encapsulated scandium but also analogous osmium-, palladium- and ruthenium-containing compounds. However, the materials' performance was very solvent dependent and required a high mol% of catalyst compared to homogeneous catalysts.¹ Polymers also present issues with decomposition during reaction and difficulties in impregnation with and retention of the catalyst. Porous inorganic-organic hybrid materials containing active sites could be a further step forward as supported catalysts and single site heterogeneous catalysts.²

1.1. Zeolites

Microporous zeolites (with pores of up to 10 Å in free diameter) are crystalline inorganic materials that have proved successful in heterogeneous catalysis due to their high chemical and thermal stability, shape selectivity that derives from well-defined pore systems, recoverability and recyclability. They were first used as catalysts in the 1960s and have been widely exploited in industry ever since. The zeolite ZSM-5 is an

aluminosilicate with a crystalline framework structure that gives channels of diameter 5-5.5 Å. The structure is built from chains of five membered rings (rings made up of five tetrahedrally-coordinated cations and five oxygen atoms), with the rings themselves linked by bridging oxygen atoms (Figure 1.1).³

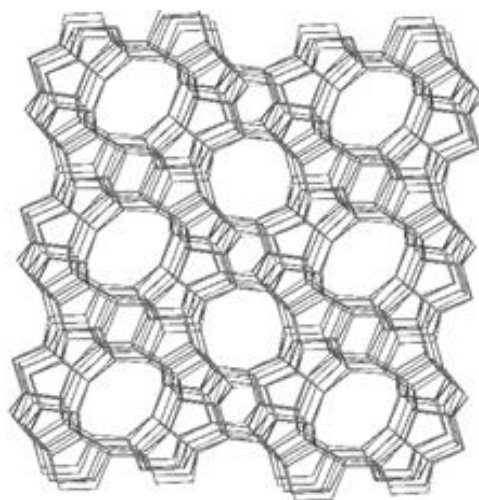
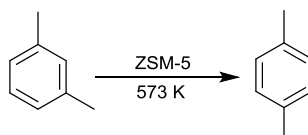


Figure 1.1: Zeolite structure ZSM-5. Representation gives only T-T connectivity showing five membered ring chains which connect to give sheets. Channel system limited by ten-membered rings (O atoms omitted for clarity)

ZSM-5 is widely used in the petrochemical industry because it becomes very acidic when aluminium (III) replaces silicon (IV) in tetrahedral cation sites and a proton is present for charge balance. The material is useful for acid-catalysed reactions, such as the isomerisation of *m*-xylene to *p*-xylene (Scheme 1.1). The catalyst is also shape selective due to its pore size which allows para-xylene product to diffuse out more quickly than the meta- (or ortho-) isomers.⁴



Scheme 1.1: Isomerisation of meta-xylene to para-xylene using ZSM-5

Zeolites have been very useful in industry for bulk chemical reactions: however they suffer from limitations in fine chemical production due to:

- (i) difficulties in introducing chemical variations to tune or strongly alter their properties,

- (ii) they do not promote a wide range of reactions when compared to homogeneous catalysts,
- (iii) it is very difficult to create zeolites that can deliver exclusive stereochemical control.
- (iv) Pore sizes and dimensions tend to be limited to 1 nm.

1.2. Metal organic frameworks

Metal organic frameworks (MOFs) (Figure 1.2) are structures that possess 3-dimensional frameworks made up of metal cations linked by organic ligands. They are commonly porous, crystalline structures with strong metal-to-ligand (or oxy-cluster of metal cations-to-ligand) interactions.⁵

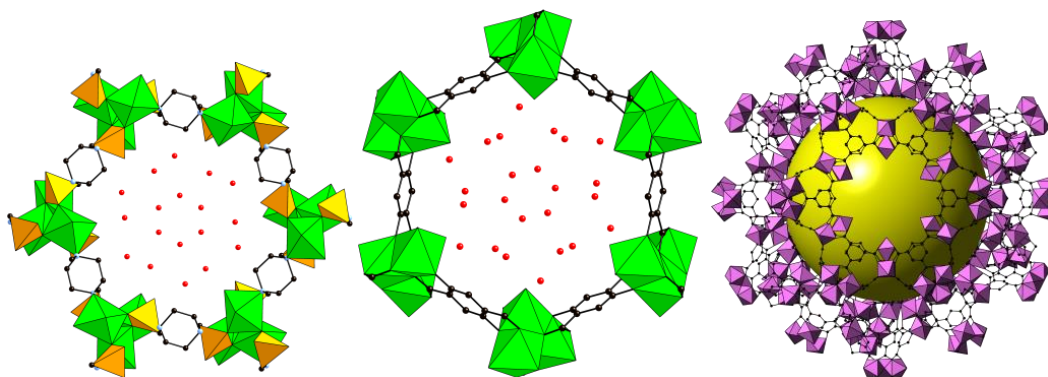


Figure 1.2: Three examples of different types of MOFs that have potential use in catalysis (From left STA-12 (metal bis(phosphonate))⁶, CPO-27 (divalent metal carboxylate)⁷, MIL-100 (trivalent metal carboxylate)⁸

The MOFs' pore size, shape and local internal environment can be varied and tuned depending on the metal cation and organic linker used. A large range of metals have been used in the synthesis of MOFs, however the organic linker used has been more limited, mainly to phosphonates, carboxylates, amine carboxylates (Figure 1.3) and imidazolates.

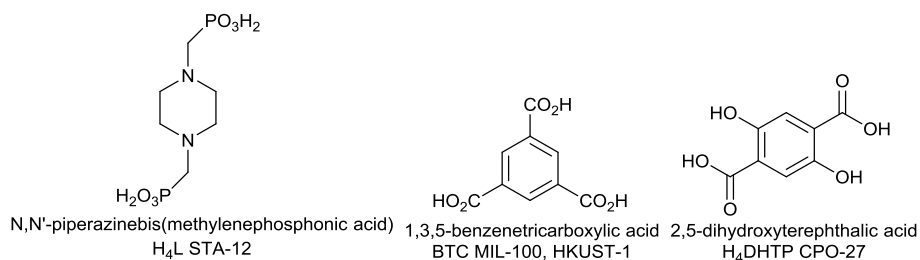


Figure 1.3: Examples of typical organic linkers used in the synthesis of MOFs

MOFs have many potential uses in gas storage and separation, drug delivery, biomedical imaging and catalysis.⁹ The frameworks can have surface areas of up to 4500 m²g⁻¹ or more and a pore size of up to 30 Å, explaining why gas storage has been an important aspect of MOF research.¹⁰ MOFs are readily synthesised, often from relatively inexpensive starting materials and so could be applicable on an industrial scale.

MOFs have the potential to escape some of the limitations of zeolites as catalysts; the mild conditions required for synthesis allow the MOFs to be tailored and modified by the addition of a wide chemical variety of moieties. For example, many transition metals and organic groups can be built into the structure. By incorporating such functionality it should be possible to optimise them for specific reactions and make them more useful for the fine chemical industry.¹¹

The presence of coordinatively unsaturated sites which can act as Lewis acid sites opens up the materials' potential use as recyclable Lewis acidic catalysts (Figure 1.4).

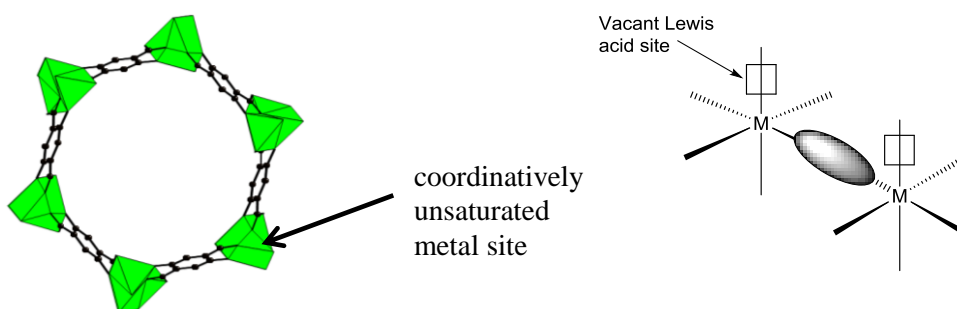


Figure 1.4: Coordinatively unsaturated site of dehydrated CPO-27 (Ni) MOF synthesised using 2-5,-dihydroxyterephthalic acid (DHTP) and divalent metal ion

MOFs also have limitations: they are less thermally stable and more moisture sensitive (due to hydrolysis of M-O-C bonds) than zeolites and removal of guest solvent can in some cases lead to structural collapse.¹² In most MOFs there is no accessible metal site, and where there are coordinatively unsaturated sites, there is usually only one type.

1.2.1. Metal carboxylate metal organic frameworks

Carboxylate-containing MOFs were studied in this project due to their range of pore sizes and their availability containing many of the metals that have previously been known in homogeneous catalysis as active Lewis acid catalysts, including Sc³⁺, Y³⁺,

Fe^{3+} and Cu^{2+} .¹³⁻¹⁷ This permitted the comparison of MOFs with different chemistry and structure and so indicated which properties are beneficial for catalysis.

1.2.1.1. MOF-5

MOF-5 was one of the early and prototypical examples of MOFs and there has been much research into its structure and properties. The discovery of MOF-5 by Eddaoudi *et al.*¹⁸ has led to many carboxylate-containing MOFs being synthesised over recent years, including frameworks with dinuclear, trinuclear and tetranuclear cationic building units and rigid carboxylate ligands such as 1,4-benzenedicarboxylate, 1,3,5-benzene tricarboxylate, etc. Importantly, many of the frameworks do not collapse after the removal of guest solvent and therefore exhibit permanent microporosity. The network of MOF-5 is made up of two components; the “ $\text{Zn}_4\text{O}(\text{O}_2\text{C})_6$ ” core which gives the structure rigidity and prevents collapse of the framework when dehydrated and the dicarboxylate ligand. The Zn^{2+} cations remain in 4-fold coordination upon solvent removal.¹⁹ The structure of MOF-5 inspired the targeted synthesis of many other MOFs, via isorecticular synthesis* which led to the IRMOF series of materials with the same topology but with dicarboxylate linkers of different lengths, and therefore with different pore sizes.²⁰ Although the development of MOF-5 is of intrinsic interest in MOF synthesis the material was not used in this project because it does not possess coordinatively unsaturated sites. MOF-5 has been used in catalysis by the introduction of a secondary metal into the structure as discussed in section 1.4.

Carboxylate MOFs have been widely researched in the last ten years by a combination of both experimental and theoretical methods, the latter to create virtual libraries of potentially viable MOF structures. This in turn has led to the development of many MOF structures with pore sizes that extend to the mesoporous range (greater than 20 Å).²¹

1.2.1.2. HKUST-1

HKUST-1 ($\text{Cu}_3(\text{BTC})_2(\text{H}_2\text{O})_3 \cdot x\text{H}_2\text{O}$, (BTC= 1,3,5-benzene tricarboxylic acid) (trimesic acid)) was one of the first MOF materials discovered that not only maintained structural

*Isorecticular synthesis- synthesis of MOFs that have the same framework topology, but may have linkers of different dimensions

integrity after solvent removal but from which coordinated solvent molecules could be removed to give Lewis acid sites.²² The material has been used as a ‘benchmark’ in catalysis, for example as a Lewis acid catalyst.²³ This structure contains copper cations linked by 1,3,5-benzene tricarboxylate (BTC) in paddle-wheel $\text{Cu}_2(\text{O}_2\text{C})_4$ sub-units to form $\text{Cu}_3(\text{BTC})_2$.²⁴ The rigid structure contains dimeric metal nodes and ‘octahedral’ units that contain two Cu^{2+} cations bound to four oxygen atoms from the BTC ligands and also to axial water molecules, the structure of which is shown in Figure 1.5. Water molecules can be removed by heating and can be replaced by coordinating adsorbates. HKUST-1 has three different window sizes, the largest of which is approximately circular (9 Å in diameter). The water coordinated to the metal cation can be removed by heating to leave a Lewis acid site on the copper. This does not change the oxidation state of the metal and only a slight reduction of cell volume (due to shrinkage of the $\text{Cu}_2\text{C}_4\text{O}_8$ unit) is observed.²⁵ HKUST-1 has been explored extensively as a Lewis acid catalyst (Section 1.3.3.1).

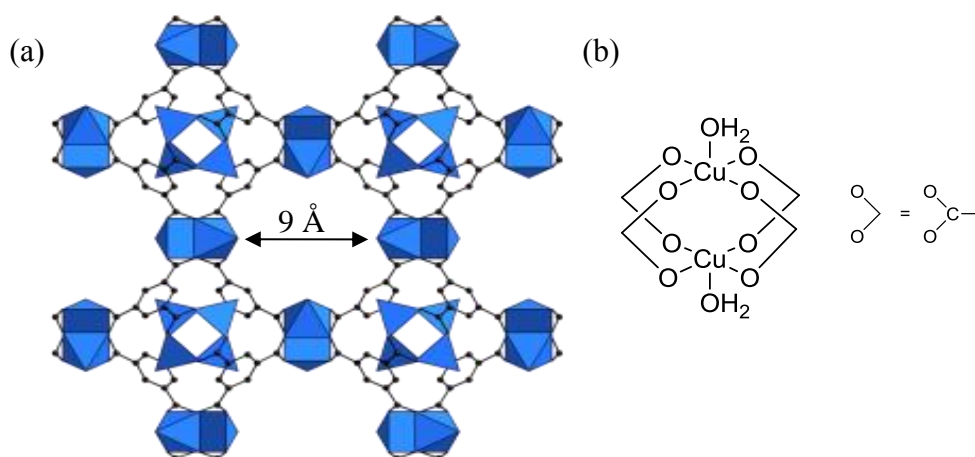


Figure 1.5: (a) HKUST-1, also known as $\text{Cu}_3(\text{BTC})_2$ where BTC = 1,3,5-benzene tricarboxylate. CuO_5 units shown as blue tetragonal pyramids, and 9 Å pore dimension indicated. H atoms omitted for clarity (b) Dimeric $\text{Cu}_2(\text{O}_2\text{C})_4(\text{OH}_2)_2$ unit of HKUST-1 structure

1.2.1.3. CPO-27

CPO-27 (M) (M=Co, Ni) was reported by Dietzel *et al.*,²⁶ and is isostructural with MOF-74(Mg, Zn) reported by Yaghi *et al.* It is a divalent metal carboxylate MOF, synthesised using 2,5-dihydroxyterephthalic acid (DHTP) (Figure 1.3), and forms a 3-dimensional framework with a honeycomb-like structure containing hexagonal channels

~11 Å in free diameter (Figure 1.6). The framework consists of helical chains of edge-sharing MO_6 octahedra. In the as-prepared material the metal cation is bound to five oxygens from the ligand (two from phenoxy group and three from the carboxylate groups of the ligand) and one from water.^{7, 27}

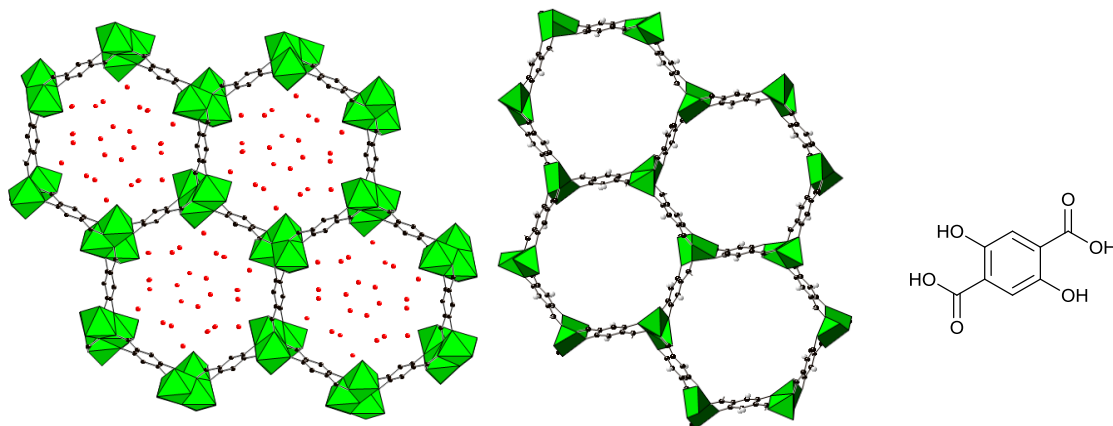


Figure 1.6: Channels of hydrated and dehydrated CPO-27(Ni) and structure of DHTP used in the solvothermal synthesis of the material

Physisorbed water can be removed from the structure which increases the pore volume in the channels to 60% of the total volume. Chemisorbed water bound to the metal cation can then also be removed from the metal site upon further heating. This leaves a stable structure with a coordinatively unsaturated metal cation. When the water is removed the geometry of the metal coordination changes from octahedral to square-pyramidal, however, due to the rigid nature of the ligand the unit cell volume of the material stays approximately the same. The activated metal site has a high enthalpy of adsorption, and so it readily adsorbs other molecules such as CO_2 , NO etc.²⁷

1.2.1.4. MIL-100/101

MIL-100 (M(III) trimesate(1,3,5-benzene tricarboxylic acid (BTC)) (where $\text{M}=\text{Cr}$, Al , Fe , V , Ga or Sc) and MIL-101 (M(III) terephthalate (1,4-benzene dicarboxylic acid (1,4-BDC))), are a series of trivalent metal carboxylates. First reported using Cr , and subsequently with other trivalent metals, these are among the largest pore carboxylate framework structures, with cage diameters varying from 25-34 Å.⁸ Their structures were determined by Férey *et al.*,²¹ by the use of computational methods, and confirmed by refinement against synchrotron X-ray powder diffraction. The structures of MIL-100 and MIL-101 are composed of supertetrahedral building blocks (Figure 1.7(b)). Trimers

of, for example, Cr octahedra (Figure 1.7(a)) linked by rigid carboxylate ligands occupy the four vertices of the supertetrahedra, linked either along the edge of the supertetrahedra (in the case of BDC for MIL-101) or over the face (using BTC to give MIL-100) by the carboxylate ligands. The supertetrahedra are linked by corner-sharing, to give a framework that contains two different types of supercages. The smaller of these types of cages are built from rings of five supertetrahedra only, whereas the larger cages are built from rings of five and of six supertetrahedra, and so there are larger windows into the larger supercages. After removal of guest solvent, the diameters of the smaller cage are ~ 25 Å (with a window size of 6 Å) for MIL-100 (Figure 1.7(c)). MIL-101 has cage diameter of ~ 30 Å diameter (window size 14 Å) for the smaller supercage. For the larger supercage the connection of pentagonododecahedra gives a cage diameter of ~ 29 Å (with window size 8.6 Å) for MIL-100 (Figure 1.7(c)) and ~ 34 Å (with window size 16 Å) for MIL-101.

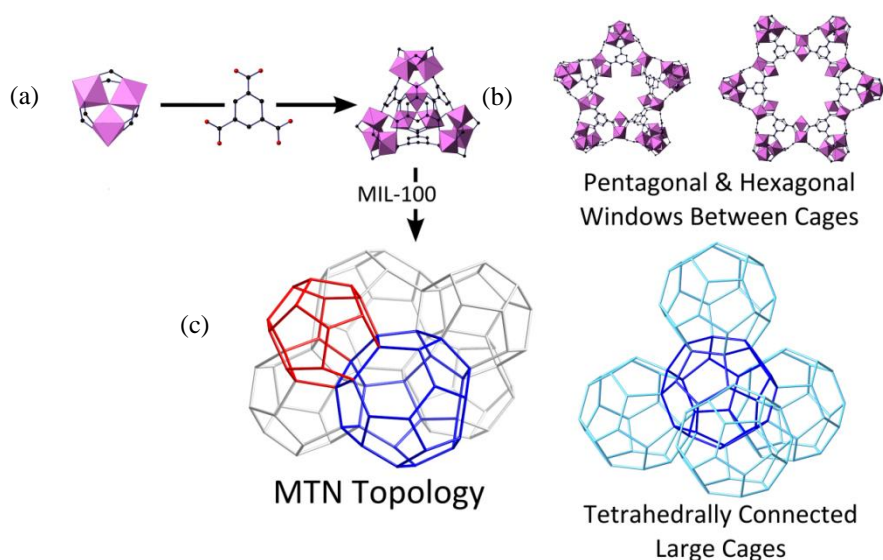


Figure 1.7: (a) Trimers of metal (III) O_6 octahedra. (b) Supertetrahedra (c) MIL-100 with two types of cages present²⁸

MIL-100 was one of the first structures to exhibit a framework with two different pore sizes: meso- (pore diameter of 20-500 Å) and microporous (pore diameter of 2-20 Å).²⁹ It was observed that the removal of chemisorbed water from chromium sites led to the formation of Lewis acid sites leading to potential use in Lewis acid catalysis.³⁰ In order to maintain charge balance in the material a hydroxide or fluoride ion is also part of the cluster, bound to one of the metal sites in the trimer. This cannot be removed by gentle heating, so this metal cation cannot be rendered coordinatively unsaturated.

1.2.1.5. MIL-88

There is also an isorecticular (for isorecticular, see MOF-5 section) set of MIL-88 metal (III) carboxylate MOFs, first reported by Serre *et al.*³¹ Like MIL-100 and MIL-101, the MIL-88 materials contain trivalent metal cations in trimers, linked by (in this case) linear dicarboxylate linkers of increasing length to give triangular bipyramidal cages opening out to one-dimensional channels. The MIL-88(Fe) materials are synthesised using a soluble iron source and fumarate acid ligand (MIL-88A), terephthalic acid (MIL-88B), naphthalene-2,6-dicarboxylic acid (MIL-88C), and 4,4'-biphenyldicarboxylic acid (MIL-88D) (structure of MIL-88B and MIL-88D shown in Figure 1.8. Each material consists of three metal cations in trimeric metal units bound to a μ_3 -oxygen atom. A further four oxygen atoms from carboxylate ligands are bound to the metal with a sixth site occupied by a solvent molecule; this can be removed to form a coordinatively unsaturated site.³² MIL-88 type solids have also been reported for Cr, Sc and In.³²⁻³⁴

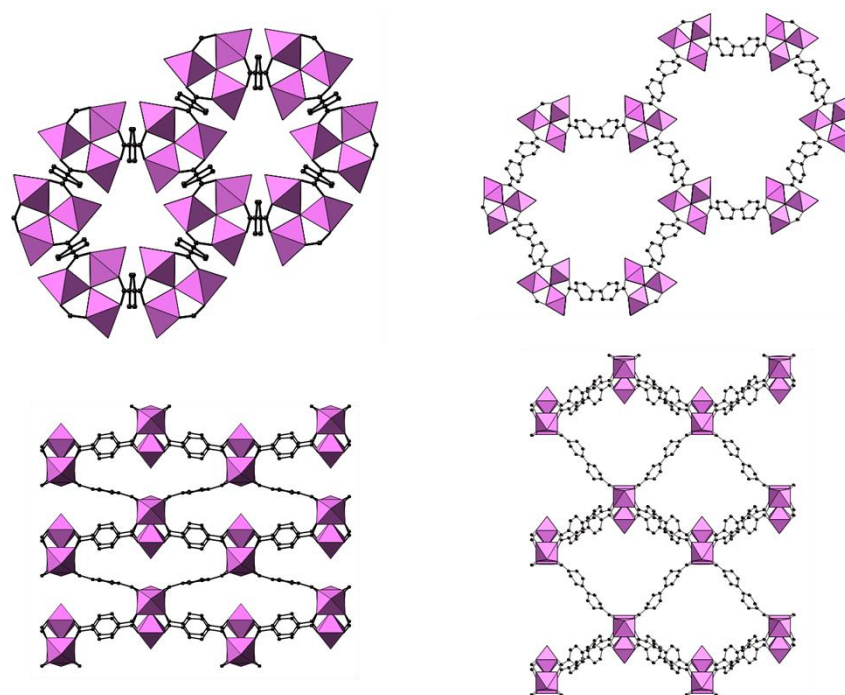


Figure 1.8:(a) MIL-88B (b) MIL-88D

The most remarkable feature of these solids is that they exhibit marked ‘breathing effects’ when the desolvated form is exposed to different polar solvents. Whereas MIL-88(B) adsorbs no N_2 when desolvated, when it is exposed to polar solvents (e.g.

methanol) the molecules are taken up and the unit cell ‘framework’ volume of MIL-88B(Cr) expands by up to 125%.³³ MIL-88D(Cr) and MIL-88D(Fe) display similar breathing behaviour, although certain synthetic routes to MIL-88D(Fe) can result in a non-breathing interpenetrated solid with two interwoven MIL-88D structures.³⁵

1.2.1.6. socMOF

This structure, which like MIL-88, MIL-100 and MIL-100 contains building units containing trimers of trivalent cations, was first reported by Liu *et al.* using In^{3+} cations as well as the 3,3',5,5'-azobenzenetetracarboxylate linker.³⁶ The name, socMOF, derives from the square-octahedral nature of trimer-ligand connectivity. Each trimer is bound to six organic linkers to form a 3-dimensional structure (Figure 1.9). The structure has a small pore diameter of 5 Å but is a highly porous material with a BET surface area of $1384 \text{ m}^2\text{g}^{-1}$.^{32, 37} Mowat *et al.* reported the Sc^{3+} analogue of this structure in 2011.³² This analogue was used in this project due to its small pore size (which would be too small to allow access of the substrates used into the pore) and so to determine whether catalytic conversion of large molecules reactions were occurring in the pores or at the surface.

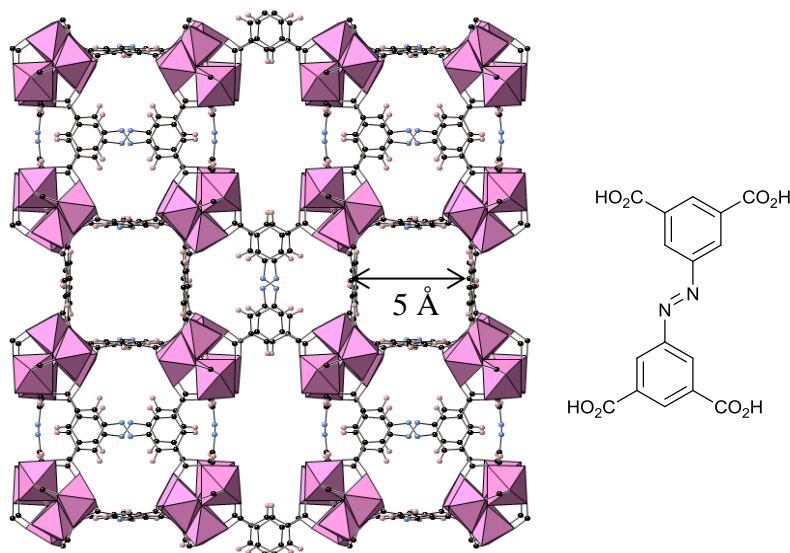


Figure 1.9: Structure of SocMOF(In) and ABTC ligand

1.2.1.7. MIL-68

MIL-68 is a further trivalent metal carboxylate MOF, with terephthalate groups as linkers. The material was initially reported using V^{3+} and since has been reported using

Al³⁺, Fe³⁺, In³⁺ Ga³⁺ and, during the period of this thesis, as the Sc³⁺ form.³⁸⁻⁴¹ MIL-68 consists of MO₄(OH)₂ chains of corner sharing octahedra. The metal hydroxide chains orientate to form two different pore channels creating a ‘kagome lattice’ structure. The smaller triangular pore has a free dimension of 6 Å and the larger hexagonal channels has a diameter of 17 Å (Figure 1.10). MIL-68(Ga) was found to have a BET surface area of 1117 m²g⁻¹, however this is reduced significantly in other MIL-68 materials with MIL-68(Fe) displaying a BET surface area of 665 m²g⁻¹. Due to the bonding of the metal in this material no unsaturated cation sites are present, even after heating, which allows catalytic comparison with other scandium-containing MOF materials.⁴⁰

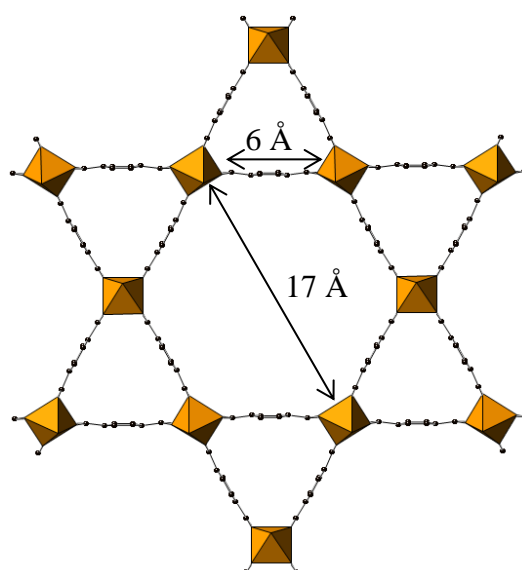


Figure 1.10: MIL-68(Fe) viewed from the c axis, showing both hexagonal and triangular pores

1.2.2. Metal phosphonate metal organic frameworks

1.2.2.1. STA-12

There are relatively few examples of porous phosphonate MOFs. Groves *et al.*⁴² synthesised the first large pore metal phosphonate MOF, STA-12 (Figure 1.11).^{6, 42} This was synthesised from a metal acetate (divalent metals; nickel, cobalt, iron and magnesium) and N, N'-piperazinebis(methylenephosphonic acid) (synthesised from a simple Mannich reaction) and exhibits a large surface area (626 m²g⁻¹) and pore size (10 Å). The flexibility of the organic ligand in STA-12 permits the porous structure to form. It is made up of helical chains of MO₅N (M = divalent metal) edge-sharing octahedral linked by the piperazine units. Each MO₅N coordination octahedron comprises of a

metal bound to four oxygen atoms from two different phosphonate groups, a fifth oxygen from chemisorbed water and a nitrogen atom from the piperazine ring. In fully hydrated STA-12 the uncoordinated P=O bonds (of which are one per phosphonate group) point towards the pore where the oxygen atom hydrogen bonds to the water present in the pore (Figure 1.11).⁶ Water in the pore can be removed by heating in two steps; first removal of physisorbed water from the pore and then chemisorbed (coordinated) water from the metal site. The removal of the chemisorbed water causes some structural rearrangement (but a pore size of about 10 Å is retained) and the formation of a MO₄N 5-fold metal coordination environment. One in three of the phosphonate P=O groups remains pointing into the channels upon dehydration.

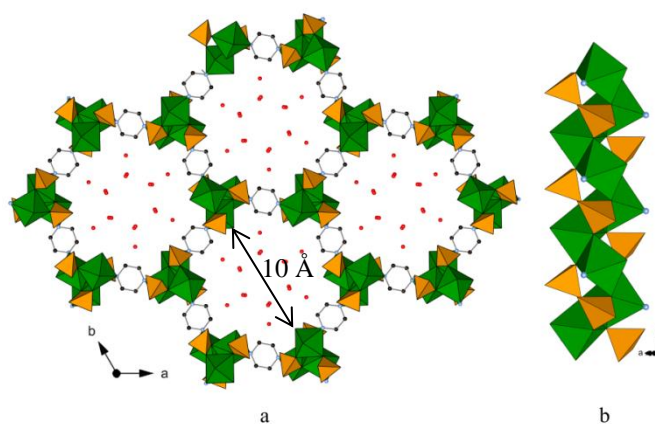


Figure 1.11: Fully hydrated STA-12 (in the yellow phosphonate tetrahedron one phosphonate P=O group oxygen atom points into the channel)

After water loss there is a slight structural distortion of the structure but crystallinity and porosity is retained leaving the vacant site on the metal accessible and with potential Lewis acidic properties (Figure 1.12).⁶

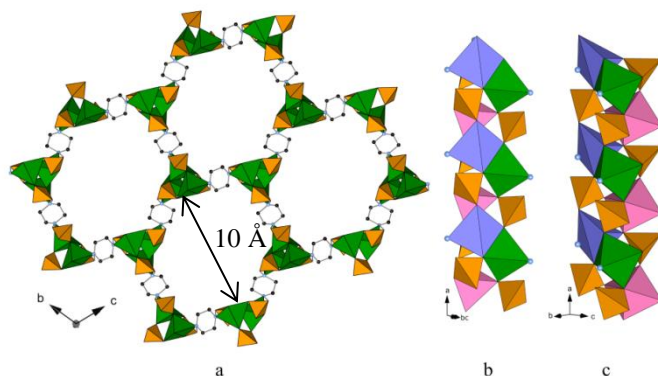


Figure 1.12: Dehydrated STA-12. Only one in three of the original $P=O$ oxygen atoms now project into the pore. Coordinatively unsaturated metal sites are potentially available for Lewis acid catalysis

1.2.2.2. STA-16

Recently, Wharmby *et al.*⁴³ have synthesised a phosphonate MOF structure isoreticular with STA-12 but with larger pore channels by changing the organic ligand from N,N' -piperazinebis(methylenephosphonic acid) (H_4L) (used in the synthesis of STA-12) (Figure 1.3) to N,N' -4,4'-bipiperidinebis(methylenephosphonic acid) (H_4LL). STA-16 was synthesised hydrothermally using cobalt acetate and N,N' -4,4'-bipiperidinebis(methylenephosphonic acid) in water (Figure 1.13).⁴³ The metal cation has the same octahedral coordination geometry (MO_5N) as in STA-12 with nitrogen from the piperazine ring, four oxygen atoms from two different phosphonate tetrahedra and the fifth oxygen from chemisorbed water.

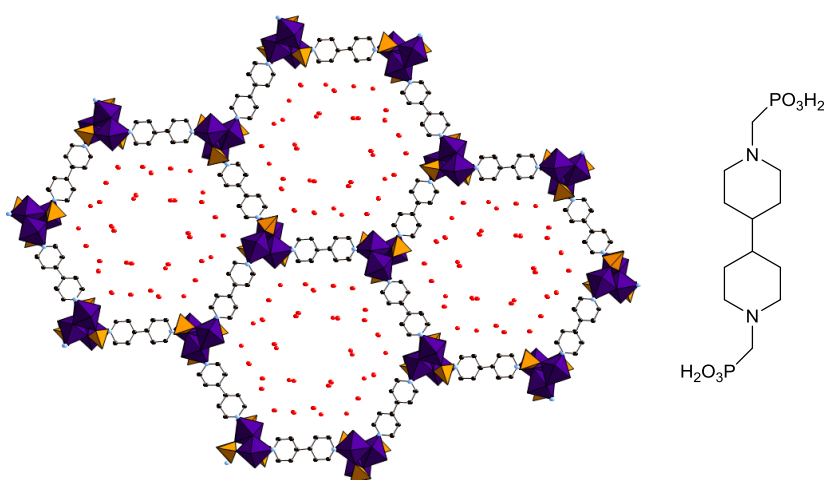


Figure 1.13: STA-16 structure with H_4LL ligand

When dehydrated no loss of crystallinity was observed. However as seen in STA-12 the formation of a five coordinate metal site results in distortion of the structure after the loss of chemisorbed water. The change in coordination of the Co^{2+} in STA-16(Co) is coincident with a colour change from purple to blue. The pore volume of STA-16 (Co) was determined using nitrogen adsorption data as $0.68 \text{ cm}^3 \text{ g}^{-1}$. The use of nonlocal density functional theory (DFT) calculations for N_2 gave a pore size of 18.5 \AA . This is the largest pore metal phosphonate MOF synthesised to date, and has potential Lewis acidic properties due to the formation of unsaturated metal sites when dehydrated.⁴³

1.3. MOFs in catalysis

1.3.1. Advantages of MOFs in catalysis

MOFs possess structural and chemical features that suggest they may have significant potential use as heterogeneous catalysts for the synthesis of fine chemicals. In terms of chemical variety the constituent framework metal cations can be almost any metal cation of interest, if the correct synthetic conditions and organic linkers are chosen. The very high surface areas, tuneable hydrophobicity and readily controlled pore sizes are all attractive features of MOF frameworks as designer catalysts, in contrast to the more restricted chemistry and pore geometry of silicate-based micro- and mesoporous materials. Many MOFs can be prepared with a high density of coordinatively unsaturated metal cation sites which may then act as Lewis acids (Figure 1.4).⁴⁴ Additionally the mild conditions of MOF synthesis enables the inclusion of organic functional groups within the framework linkers which can then be further modified to include catalytically-active metals. Finally, the use of chiral linkers offers a direct route to singly enantiomeric MOFs and so potentially chiral catalysts.

If MOFs can be prepared that are stable under reaction conditions of catalytic conversion, they can offer shape selective, recyclable, reusable, and even enantioselective catalysts for a wide range of fine chemicals syntheses where zeolites and related solids have limitations. Some of these features are discussed in greater detail below.

1.3.2. Size selectivity of MOFs in catalysis

Pore window diameter can make MOF catalysis size selective as the entry of molecules larger than the pore window will not occur. Size selectivity within a MOF has been

illustrated by Xamena *et al.*¹² when using a palladium-containing MOF, which had two different hexagonal pore windows of 4.8 Å and 8.8 Å, for alkene hydrogenation (Figure 1.14).¹² Hydrogenation was carried out on both 1-octene and cyclododecene using Pd-MOF as the hydrogenation catalyst; 1-octene was fully converted but cyclododecene did not react. Cyclododecene is a larger molecule than 1-octene and cannot diffuse into the pore where the catalytically active site is located, therefore no hydrogenation occurs.¹²

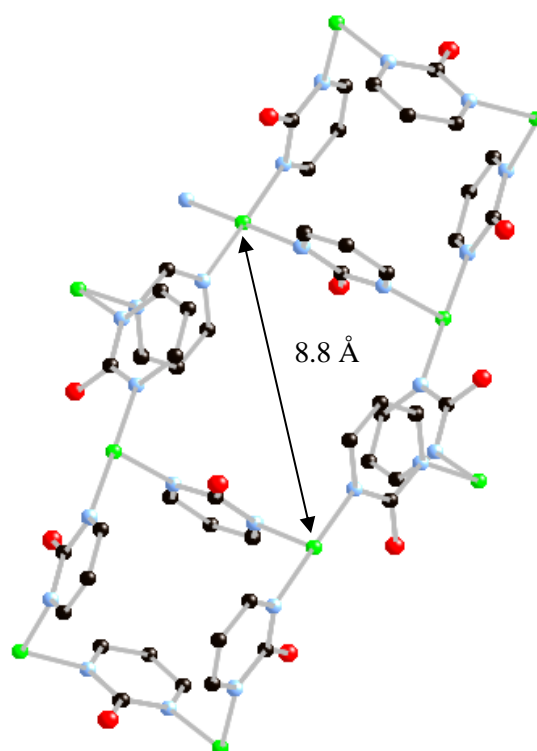


Figure 1.14: Pd-MOF illustrating two different pore size windows¹²

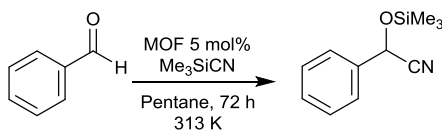
1.3.3. Use of MOFs with coordinatively unsaturated metal sites in catalysis

As already noted, for some MOFs the removal of chemisorbed solvent can form coordinatively unsaturated metal cation sites. The open metal site can then undergo solvent exchange, act as a Lewis acid or be used to graft other prospective catalysts onto the metal.²⁴ The high concentration of metal sites within a MOF and their potential accessibility due to the framework porosity make MOFs very interesting as potential catalysts. Initial research on MOFs concentrated more on adsorption than catalysis and many catalytic publications are fairly recent (i.e. during the duration of the research of this PhD thesis). They have been used as catalysts, for acetalisation of aldehydes with methanol,⁴⁵ cyanosilylation of carbonyl compounds,^{30, 44, 46, 47} Knoevenagel reactions,^{47-49,50} acetal formation,⁵¹ isomerisation of α -pinene oxide,^{23, 52} Diels-Alder reactions,^{53, 54}

Prins condensation of β -pinene and paraformaldehyde,⁵⁵ Beckmann rearrangement,⁵⁶ aza Michael reaction,⁵⁷ oxidative cross-dehydrogenative coupling of phenols and formamides,⁵⁸ Pechmann reaction,⁵⁹ aerobic epoxidation of olefins⁶⁰ and epoxide ring opening reactions.⁶¹

1.3.3.1. Exploiting coordinatively unsaturated metal sites

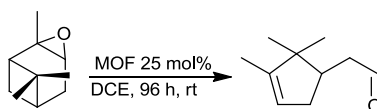
There is a significant number of literature examples in which the metal sites have been used for Lewis acid catalysis. Most MOFs reported with active metal sites contain a solvent molecule that can be easily removed by simply heating under vacuum. An early report by Schlichte *et al.*⁴⁴ described the use of $\text{Cu}_3(\text{BTC})_2(\text{H}_2\text{O})_3 \cdot x\text{H}_2\text{O}$, (BTC= 1,3,5-benzene tricarboxylic acid) HKUST-1, which could be dehydrated allowing the vacant site on Cu(II) to act in selective Lewis acid catalysis for the cyanosilylation of aldehydes and ketones. Dehydration to form $\text{Cu}_3(\text{BTC})_2$ enabled aldehydes to coordinate to the metal and cyanosilylation could occur with trimethylsilyl cyanide to form cyanohydrin derivatives (Scheme 1.2).



Scheme 1.2: Cyanosilylation of benzaldehyde

The cyanosilylation of benzaldehyde proceeded with moderate yield (57%) and high selectivity (88%). The heterogeneous nature of the catalyst was confirmed by filtration tests.⁴⁴ MIL-101 (Cr) (with window sizes of up to 16 Å) was also used in the cyanosilylation and was found to be superior to HKUST-1, with 98.5% conversion after 3 h at 313 K in heptane.³⁰ This is just one example of the many catalytic reactions carried out using HKUST-1.^{45, 62, 63}

Due to the presence of carboxylic acid groups in HKUST-1 which could be protonated to give additional Bronsted acidity (and contribute to the catalytic activity), the Lewis acidity of the metal sites were probed specifically. Alaerts *et al.*²³ were able to exploit the isomerisation of α -pinene oxide to campholenic aldehyde (Scheme 1.3) to determine whether catalytic activity could be accounted for by Lewis or Bronsted acid sites.



Scheme 1.3: Isomerisation of α -pinene epoxide to form campholenic aldehyde

It was previously found that in the isomerisation reaction Lewis acid catalysts were much more active, (conversion 85%) with greater selectivity (85% selective to campholenic aldehyde) than Bronsted acid catalysts which reacted to form many by-products (e.g. *p*-cymene and *trans*-sobrerol).⁶⁴ The reaction was carried out in different solvents with a 1:1 ratio of HKUST-1: α -pinene oxide. Selective conversions to campholenic aldehyde of up to 85% were observed when using solvent DCE (dichloroethane); however the reaction was very solvent dependent. Low conversions were seen for solvents such as THF (tetrahydrofuran) or acetonitrile that compete as ligands for Cu, or when pyridine was added. The high activity in the non-coordinating solvent DCE reflected the fact that the reaction was catalysed by the Lewis acid site.²³ Although most MOF materials tested show low conversions the selectivity to the desired product is high. MIL-100(Fe) was shown to have similar selectivity to HKUST-1 with an improvement in conversion from 8 % to 22% in 6 h.⁴³

Not only has MIL-100(Fe) been shown to be an active Lewis acid catalyst but it has also been used as an oxidation catalyst.⁵¹ It has been effectively used in the oxidation of diphenylmethane using tert-butylhydroperoxide to form benzophenone with high selectivity to product and conversions of up to 50%.⁵¹

1.3.4. Functionalization of the organic ligand

MOFs have also been used as catalysts by modifying the organic linker such that it contains other functionalities. It should be noted that the synthesis process in this case can result in existing metal sites being blocked by the extra functionality.⁴⁹

Hasegawa *et al.*⁴⁹ used this approach with organic ligands containing basic groups to create heterogeneous base catalysts. They made use of amide groups on the linker where the N-H group acts as an electron acceptor and C=O groups act as electron donors so providing two alternative hydrogen bonding sites. Employing the use of three amide groups as functional sites and three pyridyl functions as coordination groups (to stop amide-amide interaction) gives the bridging ligand, 1,3,5-benzene tricarboxylic acid

tris[*N*-(4-pyridyl)amide (4-btapa)], which was used to make a new class of base catalyst, $\{[\text{Cd}(4\text{-btapa})_2(\text{NO}_3)_2] \cdot 6\text{H}_2\text{O} \cdot 2\text{DMF}\}_n$ (Figure 1.15).⁴⁹

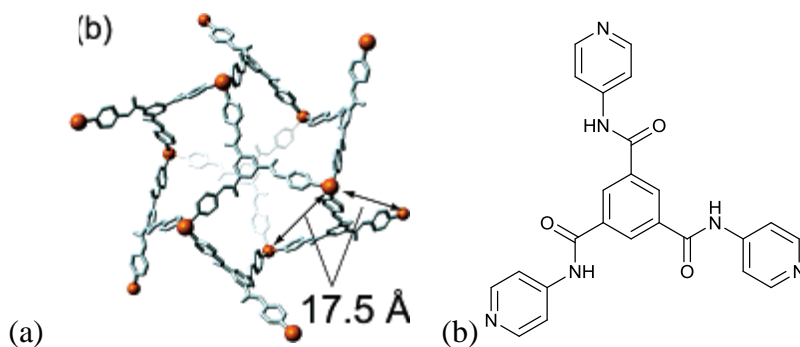


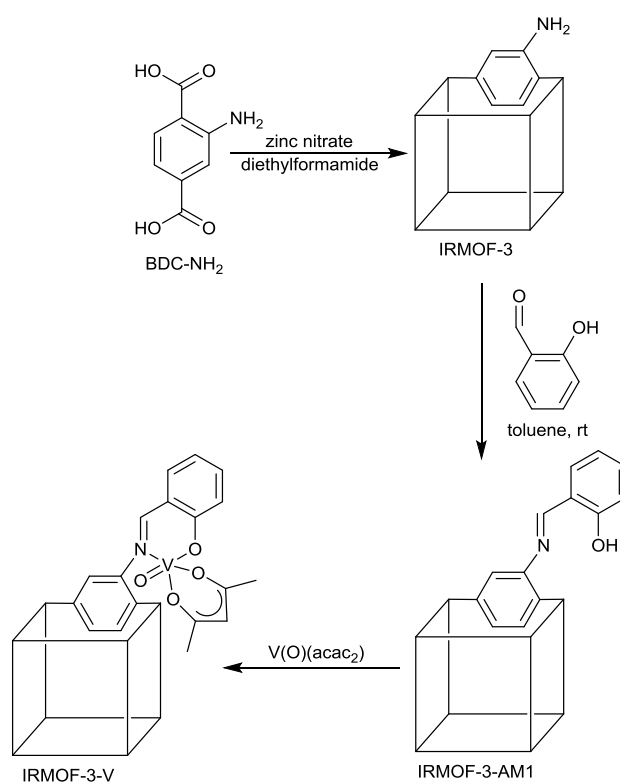
Figure 1.15: (a) $\{[\text{Cd}(4\text{-btapa})_2(\text{NO}_3)_2] \cdot 6\text{H}_2\text{O} \cdot 2\text{DMF}\}$ where brown spheres represent cadmium and grey bonds represent the ligand 4-btapa. Diagram taken from *The Journal of American Chemical Society* with permission⁴⁹ (b) 4-btapa ligand

The Knoevenagel condensation reaction was used to test the basic catalytic activity of the material in order to compare to the many possible homogeneously-catalysed routes. Benzaldehyde and active methylene compounds were used to carry out the test, with 98% conversion to malononitrile after 3 h, but there was no activity observed with larger substrates. From this it was proposed that the reaction occurred within the pores. It was also found that the catalyst could be recycled and reused without any loss of activity. Not only was this a breakthrough due to the synthesis of a new class of material but it was also an active heterogeneous catalyst for C-C bond formation, even if the Knoevenagel reaction is relatively easy to catalyse.

The introduction of different functional groups has been widely used in the synthesis of MIL-101 in order to increase the gas adsorption capabilities of the materials. However, the introduction of a sulphonic acid group on the ligand has been implemented in order to increase the catalytic activity of the material in esterification reactions. The introduction of the sulphonic acid group is carried out before MOF synthesis in order to increase stability of the S-MIL-101 material synthesised. The material can be used in the esterification reaction of acetic acid with n-hexanol. Conversion of product increases from 20% in MIL-101 to 60% by using MIL-101 with the sulphonic ligand. S-MIL-101 can be recycled up to 5 times without any loss in activity.⁶⁵

1.3.5. Post-synthetic modification

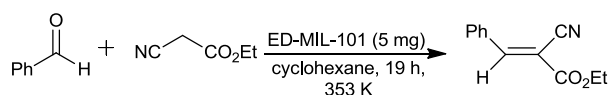
The introduction of functionality into a MOF after synthesis is another topic that has been extensively explored. This can be achieved by exploitation of functional groups present on the organic ligand which can undergo reactions to give the MOF new chemical and physical properties.⁶⁶ The use of this “post-synthetic” modification was reported with IRMOF-3, synthesised solvothermally with $\text{Zn}(\text{NO}_3)_2 \cdot 4\text{H}_2\text{O}$ and 2-amino-1,4-benzene dicarboxylic acid. The structure contains a 2-amino group that is not involved in coordination leaving it available for modification. After synthesis IRMOF-3 was dehydrated and reacted with acetic anhydride in dichloromethane to form the new IRMOF-3-AM1 (Scheme 1.4). Evidence of the reaction occurring was obtained using both NMR and ESI-MS (electron spray ionisation- mass spectroscopy). The acetylation reaction of IRMOF was also found to go to completion after 3 days (^1H NMR). The reaction was confirmed to be heterogeneous by checking that no metal, ligand and modified ligand were found in the solution. Crystallinity of the structure was retained after reaction.



Scheme 1.4: Acetylation of IRMOF-3-AM1 by reaction of IRMOF-3 with acetic anhydride

The amine group of IRMOF-3 not only undergoes acetylation reactions but also condensation reaction to produce a salicylidene moiety which can then be used to bind to other metal complexes (for example V(O)acac₂). This molecule was found to catalyse the oxidation of cyclohexane with 40% conversion; however, there was loss of structural integrity after the reaction limiting its usefulness as a catalyst for this reaction. However, the results did show that covalently modifying the organic ligand of a MOF post-synthesis can lead to active catalysts.⁶⁷

Post-synthetic modification of MIL-101(Cr) has led to promising results by taking advantage of the presence of unsaturated metal sites in the framework. It has previously been established that dehydration of MIL-101(Cr) causes loss of chemisorbed water thus leaving a Lewis acidic site on the chromium. This can then be exploited by introduction of ligands that can coordinate to this site. Hwang *et al.*⁵⁰ were able to functionalise MIL-101(Cr) using ethylenediamine as ligand; one amine group acts as a ligand for chromium and another amine is available to act as a base catalyst within the framework. The immobilisation of the ethylenediamine to form ED-MIL-101(Cr) caused no loss in crystallinity to the framework. The presence of ethylenediamine on the unsaturated chromium site in the MOF is confirmed using IR (the aliphatic C-H stretching frequency decreases when the ethylenediamine is coordinated) and also by N₂ adsorption which reveals a decrease in pore size.



Scheme 1.5: Knoevenagel condensation using ED-MIL-101 as Lewis acid

The catalytic activity of ED-MIL-101(Cr) was tested in a Knoevenagel condensation of benzaldehyde and ethyl cyanoacetate (Scheme 1.5). It was found to give high conversion to *trans*-ethyl cyanocinnamate (97.7%) with 99.1% selectivity and could be recycled and reused three times without any loss in activity. There is evidence that the reaction takes place in the pores as substrates that are too large to fit in the pores do not react.

It has been shown that MOFs are an exciting range of porous materials that are emerging for applications in many areas of chemistry. However, their use in catalysis is still in its infancy and much more work is needed.

1.4. Mixed metal MOFs

Mixed metal MOF materials can be of advantage as further catalytic properties can be introduced into the structures (as shown in chapter 5 and 6). These materials can be synthesised using several different approaches in order to introduce the metals:

- (i) direct MOF synthesis using more than one metal source;
- (ii) MOF synthesis from metal salts and bridging ligands that contain a secondary metal coordinated to them;
- (iii) post-synthetic metalation of a MOF that contains auxiliary ligands;
- (iv) post-synthetic introduction of metallic nanoparticles;
- (v) post-synthetic introduction of ligands and secondary metal.

1.4.1. Direct synthesis of mixed metal MOFs from mixtures of metal salts

Relatively few examples of mixed metal MOFs synthesised in a direct synthesis from a mixture of metal salts approach have been cited in the literature. Wang *et al.*⁶⁸ have synthesised MOFs containing both Mn^{3+} and Fe^{3+} that are connected via alternate carboxylic and azide bridges. The mono metallic MOFs were also synthesised for comparison. The manganese materials were found to exhibit antiferromagnetic behaviour and the iron counterpart demonstrated ferromagnetic behaviour. The mixed metal system was found to have no order and the positions of the metals were distributed randomly. The material exhibited both antiferromagnetic and ferromagnetic behaviour. The unit cell of the material decreases in size with introduction of more iron into the material.⁶⁸

There has been a recent interest in the synthesis of mixed metal MIL-53, in particular Cr/Fe and Fe/V. MIL-53(V) was found to form MIL-47 when heated to remove unreacted 1,4-benzenedicarboxylic acid. This is due to the irreversible oxidation of vanadium from V^{3+} to V^{4+} . It was later found that in the absence of air a fully open form of MIL-53(V) (after dehydration) could be formed that could be hydrated reversibly (Figure 1.16).⁶⁹

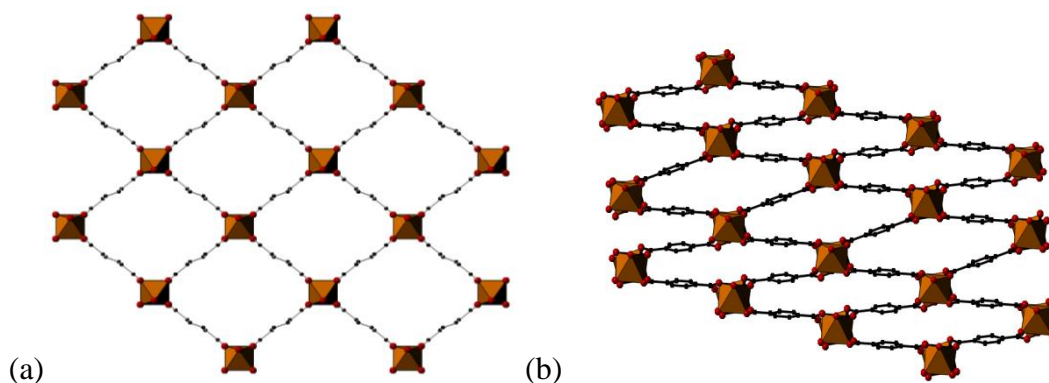


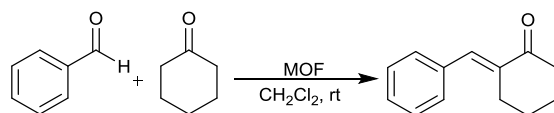
Figure 1.16: MIL-53 Fe (a) open pore form (b) closed pore form

MIL-53 and MIL-47 are both synthesised using 1,4-benzenedicarboxylic acid and differ only by the oxidation state of the metal and whether bridging M-O-M links have protons attached. MIL-53 possesses trivalent metals (e.g. Cr^{3+}) and forms a μ_2 -hydroxide bridge whereas MIL-47 has tetravalent metals (such as V^{4+}) with μ_2 -oxo bridges. Unlike MIL-53, MIL-47 remains in the open pore form and is not influenced by the introduction of guest molecules. The MIL-53 structure has been synthesised using different cations and the flexibility of the structure depends on the metal cation. MIL-53(V, Cr, Al) all form an open pore structure after heating but in MIL-53(Fe) and MIL-53(Sc) the samples only slightly expand after heating and stay in the closed pore form.⁷⁰ This led to the idea that by synthesising mixed metal MIL-53 it should be possible to modify the flexibility of MIL-53. Initially chromium was introduced into the MIL-53(Fe) structure; the synthesis was reported in two alternative ways. Nouar *et al.*⁷¹ synthesised MIL-53($\text{Cr}_{0.6}\text{Fe}_{0.4}$) using a direct synthesis, slowing down the reactivity of Fe^{3+} by using metallic iron to match the slower reactivity of the chromium nitrate.⁷¹ IR, Mossbauer and EXAFS confirmed the presence of both iron and chromium in the structure. When dehydrated the pores close and upon heating the structure opens to form a large pore material, similar to that observed in MIL-53(Ga) but different to that of both MIL-53(Cr) and MIL-53(Fe). The material had an uptake of $1200 \text{ m}^2\text{g}^{-1}$ and readily goes from closed pore material to open pore upon nitrogen uptake. This work demonstrates that mixed metal MOFs can have properties different from their end members.

Separately, MIL-53(Al/Cr) has been synthesised by introducing 1% chromium nitrate into the synthesis of MIL-53(Al), which allowed the material to be probed using ESR spectroscopy, and the transformation between low temperature closed pore and high

temperature open pore form could then be followed. Here the second metal acts as a spectroscopic probe.⁷²

Shi *et al.*⁷³ have reported the synthesis of a copper-bismuth MOF with a 3,5-pyrazoledicarboxylic acid (H₃PDC) ligand which has the potential to be used in the diastereoselective synthesis of (E)- α,β -unsaturated ketones. The material was synthesised hydrothermally using a mixture of CuCO₃.Cu(OH)₂, Bi(NO₃)₃.5H₂O and H₃PDC and the product has a 1:3 copper:bismuth ratio with all sites independent of one another in the asymmetric unit. The material synthesised was then tested in the cross condensation reaction of benzaldehyde and cyclohexanone. In dichloromethane, 90% conversion after 68 h with over 99% selectivity to (E)-2-benzylidenecyclohexanone was observed (Scheme 1.6).



Scheme 1.6: Reaction of benzaldehyde with cyclohexanone to give (E)-2-benzylidenecyclohexanone

Although the material did not outperform its homogeneous equivalent it did increase the rate of reaction and it could be recycled without loss of activity or structural integrity.⁷³ Previously the same group had reported bimetallic Zn/lanthanide MOFs and the same H₃PDC ligand; these materials consisted of an inorganic subunit within the MOF materials and the inclusion of the lanthanide metals made it highly efficient for photoluminescence.⁷⁴

1.4.2. Mixed metal MOFs from ligands that contain second metal

Catalytic sites can also be introduced by modification of the organic ligand prior to synthesis of the MOF. The preparation of MOFs containing (salen)Mn bridging ligands with Zn cations and biphenyldicarboxylate linker (Figure 1.17)⁷⁵ is an example of this procedure. The catalytically active metal site is part of the (salen)Mn bridging ligand. The Zn cations, are building units of the structure rather than active sites. The BPDC bridging ligand is a coordinative group binding to the zinc to facilitate the formation of a porous framework.

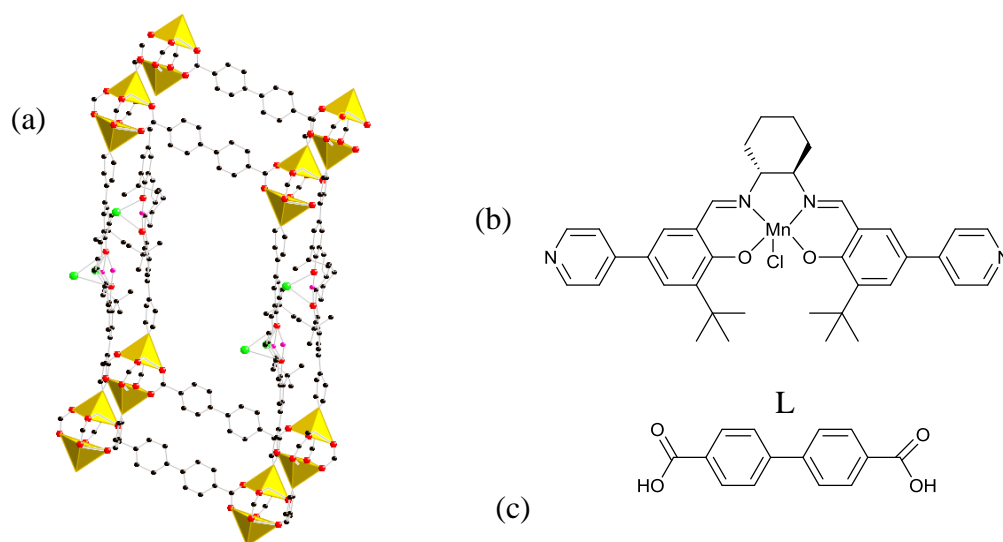
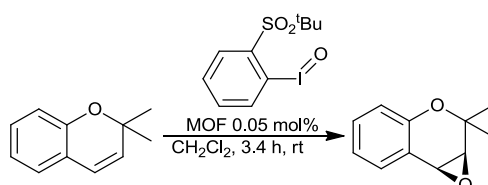


Figure 1.17: (a) MOF containing chiral Mn (salen) bridging ligand (b) (salen)Mn bridging ligand (c) biphenyldicarboxylate (BPDC) ligand

The combination of (salen)Mn ((R,R)-(2)-1,2-cyclohexanediamino-N,N'-bis(3-tert-butyl-5-(4-pyridyl)salicylidene)Mn^{III}Cl (Figure 1.17) as a catalytic bridging ligand along with zinc and the BPDC bridging ligand forms a robust pillared paddle wheel structure. The MOF was found to be an active and enantioselective catalyst for olefin epoxidation when using an oxidant, in this case 2-(tertbutylsulfonyl)iodosylbenzene (Scheme 1.7).



Scheme 1.7: 2,2-dimethyl-2H-chromene epoxidation

The reaction gave a 71% yield of the epoxide with 82% e.e. after 3.4 h using 0.05 mol% 2-(tertbutylsulfonyl)iodosylbenzene. The catalyst was recycled and reused without any loss of enantioselectivity. However there was a small loss of activity after the third cycle. Compared to the homogeneous (salen)Mn catalyst, the MOF showed promising results because the homogeneous catalyst loses activity after a few minutes due to oxidation of the salen ligand through reactive interaction with other catalysts; this oxidation is not observed in the MOF reaction as these interactions are prevented by site isolation.

The synthesis of a chiral MOF has been achieved using adapted salen as a bridging ligand with titanium or nickel as the complexed cations (Figure 1.18).^{76, 77}

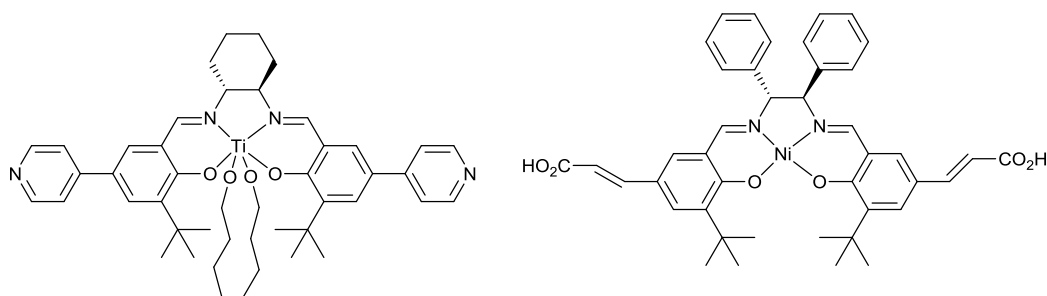
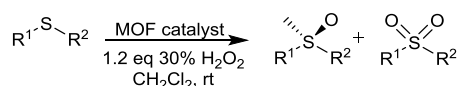


Figure 1.18: (a) titanium metallosalen bridging ligand (b) nickel metallosalen bridging ligand

The titanium metallosalen bridging ligand (Figure 1.18(a)) has been introduced into both cadmium- and zinc- containing MOFs which are then active and enantioselective catalysts for sulfoxidation reactions (Scheme 1.8).^{76, 78} The catalyst was found to give conversions of up to 77% after 72 h with enantioselectivity of up to 64% and high selectivities to the sulfoxide. Enantioselectivity was found to increase when bulkier R-groups were used i.e. when a methyl group was substituted with an isopropyl group the e.e. increased from 33% to 55%. However conversion decreased due to slower diffusion of larger substrates into the pore of the MOF. Although the reaction using a MOF was slower than if a homogeneous catalyst was used, an enhancement of enantioselectivity was observed at comparable selectivity and conversion.



Scheme 1.8: Enantioselective oxidation of sulfides catalysed by MOF

The use of nickel as the metal in the bridging ligand (Figure 1.18(b)) has been successfully implemented in the catalytic coupling reaction of CO₂ with epoxides to give cyclic carbonates with moderate yield and enantioselectivity.

It has also been reported that cobalt in the bridging ligand is an active catalyst for hydrolytic kinetic resolution of epoxides and epoxide ring opening reactions.^{79, 80} The hydrolytic kinetic resolution of epoxides was shown to give higher conversions and enantioselectivity using the MOF catalyst than over homogeneous catalyst. The catalyst could also be easily recycled without any loss in activity or enantioselectivity.

The use of salen bridging ligands has been adapted further to synthesise catalytically active MOFs that consists of a manganese-containing bridging ligand and a range of rare earth metals and these have been found to have catalytic activity in the epoxidation of olefins.⁸¹

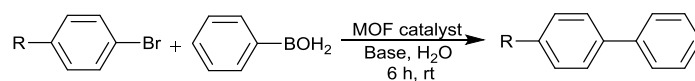
1.4.3. Post-synthetic introduction of nanoparticles

Introduction of nickel as metal nanoparticles into MIL-120 has made the material an active catalyst for hydrogenation; the material was compared to the supported nickel metal supported on alumina in the hydrogenation of benzene to cyclohexane. The catalyst was prepared by impregnation of the MIL-120(Al) by nickel nitrate solution. This allows the MOF material to act as a support for nickel (which sits in the pores of the MOF), although increasing the loading of nickel did cause nickel oxide to be formed. In the hydrogenation of benzene, the material was found to give full conversion with both 15 and 20 wt% nickel content at 463 K. At higher temperatures, the lower nickel loading of 15% outperforms that of the 20% loaded material and is significantly better than Ni/Al₂O₃ supported material. For MIL-120(Al/Ni), better performance was attributed to weaker interactions between the MOF material and the nickel, allowing more freedom for its interaction with the substrates. The material was also used in a continuous flow reactor and still maintained 95% conversion after 30 h. No degradation was found from the material after reaction, as determined by PXRD.⁸²

The use of nickel nanoparticles has also been attempted in conjunction with palladium nanoparticles in MIL-101. This is carried out using metal-organic vapour deposition (MOVCD) and nickel:palladium ratios were confirmed using EDX. The material was used as an effective catalyst for the reduction of 3-heptanone with conversion of 80% after 35 h using 20% loading of Pd₃Ni₂. In order for the reaction to proceed it was found that both metals were required and palladium and nickel catalysts could not separately achieve similar activity.⁸³

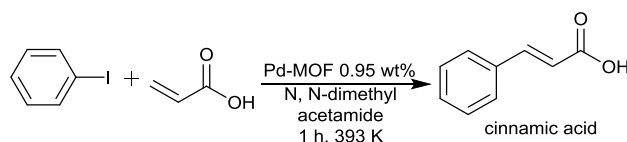
The use of palladium nanoparticles in MIL-101(Cr) has also been shown to be an active catalyst for the Suzuki–Miyaura Reactions in the presence of water. The reaction was found to give up to 99% conversion with varying substrates with low levels of palladium leaching observed. The catalyst could be recycled up to 10 cycles, although a

gradual transformation of the MOF to MIL-88B occurred.⁸⁴ The same catalyst was also found to be active in the Ullmann coupling reactions of aryl chlorides.⁸⁵



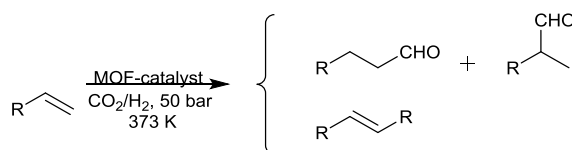
Scheme 1.9: Suzuki–Miyaura reaction in the presence of water catalysed by Pd/MIL-101(Cr)

ED-MIL-101 (discussed in section 1.3.5) can also be used to immobilise metal salts into the MOF structure by formation of ammonium groups which then react with the salt by PdCl_4^{2-} anionic exchange. When impregnated with Pd salt the framework can be used in a Heck reaction (Scheme 1.10) and gives 99% conversion of iodobenzene with acrylic acid to form cinnamic acid. The impregnation of other metals onto the framework opens up many potential uses of the frameworks and the development of their structures.



Scheme 1.10: Heck reaction of iodobenzene and acrylic acid with ED-MIL-101 (Cr) impregnated with Pd salts as catalyst

Rhodium nanoparticles have been used in MOF-5, MIL-101 and IRMOFs as active catalysts in hydroformylation (Scheme 1.11).⁸⁶⁻⁸⁸ The structure of the MOF was found to be important in controlling the activity and selectivity. MOF-5 was found to give conversion of 100% with smaller substrates e.g. n-hex-1-ene gave 100% conversion with 80% selectivity to the aldehyde and a n/l* ratio of aldehydes of 1.2 after 21 h. However the n/l ratio could be increased if the reaction was carried out over a shorter period of time to 3 although this was shown to have a decrease on the selectivity to aldehydes. MIL-101 gave high conversions with larger substrates such as n-dodec-1-ene which could not be obtained with MOF-5.



Scheme 1.11: Hydroformylation of alkene to formed linear and branched aldehydes

* n/l – branched to linear ratio

1.4.4. Post-synthetic modification of MOFs containing auxiliary ligands

Post-synthetic modification has been exploited to permit the addition of a secondary metal into the MOF structure. Three approaches have been taken. The first is by addition of metal to the organic ligand present in the MOF material. This has been reported by Bloch *et al.*⁸⁹ in which they used a 2,2'-bipyridine-5,5'-dicarboxylic acid ligand to synthesise MOF-253(Al) (Al in the framework). The bipyridyl unit can be used to complex a transition metal, in this case palladium (Figure 1.19). The aluminium gives no coordinatively unsaturated sites so only the palladium is active in catalysis. Further metals have been included within the material in this manner e.g. Cu, Pt, and Ru.⁸⁹⁻⁹²

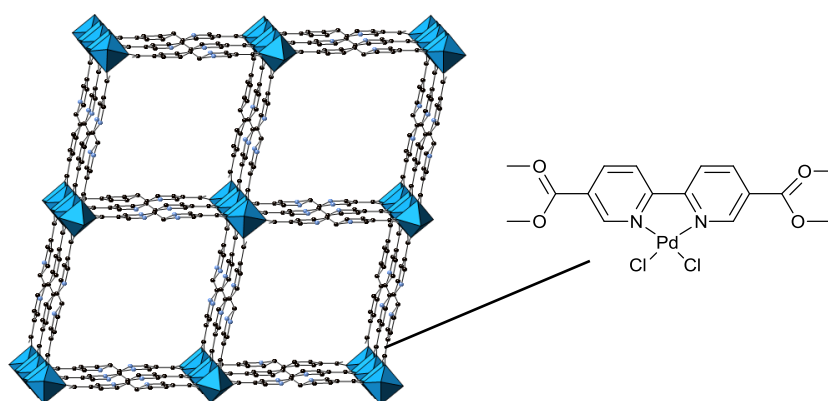


Figure 1.19: MOF-253 structure with 2,2'-bipyridine-5,5'-dicarboxylic acid ligand with Pd complexed to the ligand⁸⁹

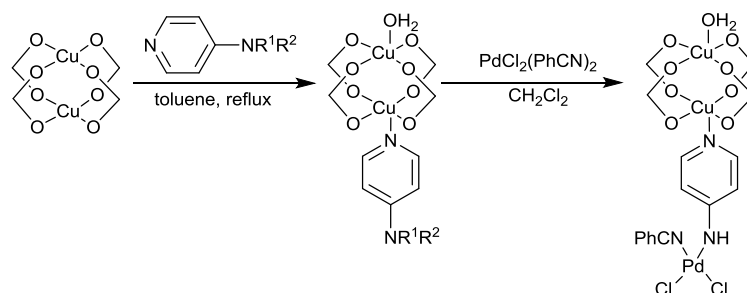
Both ruthenium- and copper- containing MOFs have been shown to be effective catalysts in oxidation reactions. Ruthenium-containing MOF-253 is synthesised by the post-synthetic addition of $[\text{RuCl}_4(\text{dms})]_2$ to MOF-253(Al) as described above for Pd. This has then been used for the oxidation of alcohols to form ketones (Scheme 1.12). The catalyst showed high selectivity to the desired product with conversions of up to 99%. No evidence of metal leaching was observed and the catalyst could be recycled up to 6 times without any loss in activity or crystallinity of the MOF.



Scheme 1.12: Oxidation of 1-phenylethanol to form acetophenone in dichloromethane catalysed by MOF-253-Ru

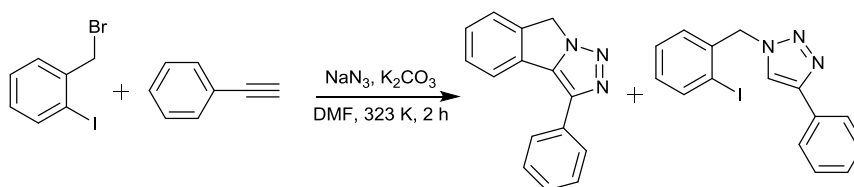
1.4.5. Post-synthetic modification of MOFs with ligands and metals

Another approach that can be used in order to introduce a secondary metal is by post-synthetic introduction of an organic ligand that binds to the structural metal. The organic ligand can then be used to bind a secondary metal in the structure. This has been demonstrated by Arnanz *et al.*⁹³ A dehydrated sample of HKUST-1 was reacted with aminopyridine. The pyridyl group bound to the coordinatively unsaturated Cu²⁺ sites. The MOF was then reacted with a palladium complex in order to form a bimetallic MOF in which the amino function coordinates to palladium (Scheme 1.13).⁹³



Scheme 1.13: Formation of palladium containing HKUST-1(Cu) MOF by addition of aminopyridine followed by palladium compound

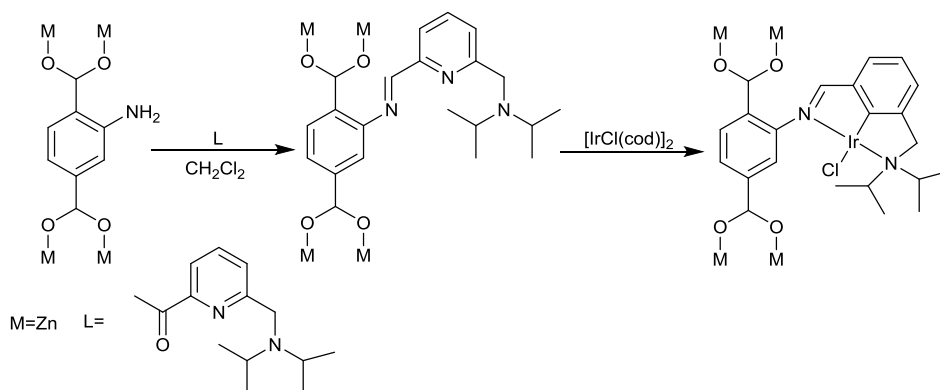
The addition of the palladium to the material opens up the prospect of a bimetallic MOF consisting of two different metals that can have different uses in catalysis. The material was tested in the one pot Sonogashira/click reactions of 2-iodobenzyl bromide, NaN₃, and alkynes (Scheme 1.14).



Scheme 1.14: One pot Sonogashira/click reactions of 2-iodobenzyl bromide and phenylacetylene to form 3-phenyl-8H-[1,2,3]triazolo[5,1-a]isoindole (Sonogashira coupling product) or 3-iodo-4-((4-phenyl-1H-1,2,3-triazol-1-yl)methyl)benzene-1-ylidium (intermolecular click reaction product)

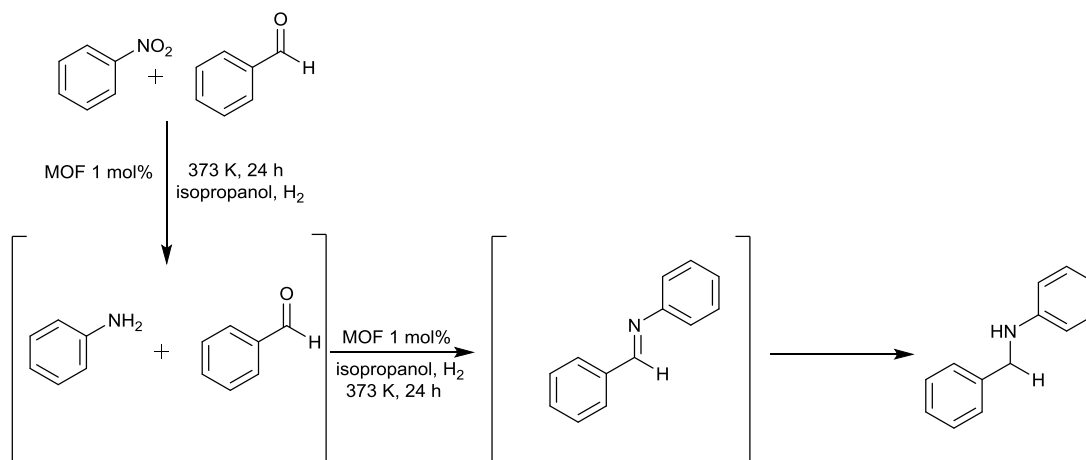
The catalyst proved successful for the formation of isoindoles with conversions of 100% in the reaction shown in Scheme 1.14. It was shown that selectivity is reversed towards an intermolecular click reaction product when the temperature of the reaction is increased over 323 K. Interestingly, it was found that the copper sites were of importance in the reaction as the reaction did not proceed at all when the palladium compound $\text{Pd}(\text{MeCN})_2\text{Cl}_2$ alone was used. The recyclability of the material depended on the substrate used, when using 2-iodobenzyl bromide the conversion decreases after each cycle and also the crystallinity of the material decreases. However, when using the substrate 1-(azidomethyl)-2-iodobenzene no loss in activity was observed.

One final approach in the introduction of a secondary metal into the structure is the post-synthetic covalent modification of the MOF with ligand and metal. In this case a functional group in the bridging ligand reacts with a ligand containing further functionality. This approach has been used to synthesise iridium-containing UiO-66 and IRMOF-3.⁹⁴ The addition of the chelating group 6-((diisopropylamino)methyl)picolinaldehyde that can react with an amino function on the benzene dicarboxylic acid (BDC) ring, which then allows for the addition of iridium precursor (Scheme 1.15).



Scheme 1.15: BDC-NH₂ ligand of IRMOF-3 which is reacted with chelating ligand 6-((diisopropylamino) methyl)picolinaldehyde and then further addition of iridium precursor

This catalyst has been used successfully to catalyse the formation of secondary amines. The reaction involves the initial reduction of nitrobenzene to aniline then the reaction of an aldehyde with aniline formed to give an aldimine which is then hydrogenated to form a secondary amine (Scheme 1.16). The reaction was shown to give conversions of over 99% with selectivity to the amine product of greater than 99%.



Scheme 1.16: Use of IRMOF-3 with iridium in the formation of amines from the reaction of aldehyde with nitrobenzene

Large pore Lewis acidic MOFs have been used in catalytic reactions such as cyanosilylation, isomerisation and oxidation. Conclusions regarding the effects of pore size, bridging ligand and metal centre on the activity or selectivity of these isolated examples are difficult to draw. Thus, a greater understanding of the molecular basis of the catalyst productivity is needed. Lewis acid catalysis is a huge field of organic chemistry, but thus far only a few examples of simple model reactions have been

investigated. There is therefore a need to examine the suitability of MOFs more widely in catalysis. The use of different MOFs in varying catalytic reactions has been explored in this project, in order to create a library of MOFs suitable for different reactions and explore factors important in determining the activity of the MOF.

There has been some interesting work where conventional MOF bridging ligands were combined with modified homogeneous catalysts to produce a MOF that contains inert structural metal sites along with catalytic metal sites. A more ambitious approach would be the design of multi metallic MOFs that are capable of catalysing consecutive reactions. This approach has been investigated in different ways with some interesting catalytic outcomes.

1.5. References

1. S. Kobayashi and R. Akiyama, *Chem. Commun.*, 2003, 449-460.
2. J. M. Thomas, *Design and Applications of Single-Site Heterogeneous Catalysts*, Imperial College Press, London, 2012.
3. G. T. Kokotailo, S. L. Lawton, D. H. Olson and W. M. Meier, *Nature*, 1978, **272**, 437-438.
4. O. Cappellazzo, G. Cao, G. Messina and M. Morbidelli, *Ind. Eng. Chem. Res.*, 1991, **30**, 2280-2287.
5. J. Lee, O. K. Farha, J. Roberts, K. A. Scheidt, S. T. Nguyen and J. T. Hupp, *Chem. Soc. Rev.*, 2009, **38**, 1450-1459.
6. S. R. Miller, G. M. Pearce, P. A. Wright, F. Bonino, S. Chavan, S. Bordiga, I. Margiolaki, N. Guillou, G. Férey, S. Bourrelly and P. L. Llewellyn, *J. Am. Chem. Soc.*, 2008, **130**, 15967-15981.
7. P. D. C. Dietzel, R. Blom and H. Fjellvag, *Eur J. Inorg. Chem.*, 2008, 3624-3632.
8. O. I. Lebedev, F. Millange, C. Serre, G. Van Tendeloo and G. Férey, *Chem. Mater.*, 2005, **17**, 6525-6527.
9. W. B. Lin, *Top. Catal.*, 2010, **53**, 869-875.
10. G. Férey, C. Mellot-Draznieks, C. Serre and F. Millange, *Acc. Chem. Res.*, 2005, **38**, 217-225.
11. D. Farrusseng, S. Aguado and C. Pinel, *Angew. Chem. Int. Ed.*, 2009, **48**, 7502-7513.
12. F. Xamena, A. Abad, A. Corma and H. Garcia, *J. Catal.*, 2007, **250**, 294-298.
13. S. Kobayashi, *Eur. J. Org. Chem.*, 1999, 15-27.
14. S. Kobayashi, *Synlett*, 1994, 689-701.
15. T. Kitanosono and S. Kobayashi, *Adv. Synth. Catal.*, 2013, **355**, 3095-3118.
16. D. A. Evans, S. W. Tregay, C. S. Burgey, N. A. Paras and T. Vojtkovsky, *J. Am. Chem. Soc.*, 2000, **122**, 7936-7943.
17. K. Wakita, G. B. Bajracharya, M. A. Arai, S. Takizawa, T. Suzuki and H. Sasai, *Tetrahedron-Asymmetry*, 2007, **18**, 372-376.
18. M. Eddaoudi, H. L. Li, T. Reineke, M. Fehr, D. Kelley, T. L. Groy and O. M. Yaghi, *Top. Catal.*, 1999, **9**, 105-111.

19. H. L. Li, C. E. Davis, T. L. Groy, D. G. Kelley and O. M. Yaghi, *J. Am. Chem. Soc.*, 1998, **120**, 2186-2187.
20. H. Li, M. Eddaoudi, M. O'Keeffe and O. M. Yaghi, *Nature*, 1999, **402**, 276-279.
21. G. Férey, C. Mellot-Draznieks, C. Serre, F. Millange, J. Dutour, S. Surble and I. Margiolaki, *Science*, 2005, **309**, 2040-2042.
22. A. Corma, H. Garcia and F. X. L. Xamena, *Chem. Rev.*, 2010, **110**, 4606-4655.
23. L. Alaerts, E. Seguin, H. Poelman, F. Thibault-Starzyk, P. A. Jacobs and D. E. De Vos, *Chem.-Eur. J.*, 2006, **12**, 7353-7363.
24. S. S. Y. Chui, S. M. F. Lo, J. P. H. Charmant, A. G. Orpen and I. D. Williams, *Science*, 1999, **283**, 1148-1150.
25. C. Prestipino, L. Regli, J. G. Vitillo, F. Bonino, A. Damin, C. Lamberti, A. Zecchina, P. L. Solari, K. O. Kongshaug and S. Bordiga, *Chem. Mater.*, 2006, **18**, 1337-1346.
26. P. D. C. Dietzel, Y. Morita, R. Blom and H. Fjellvag, *Angew. Chem. Int. Ed.*, 2005, **44**, 6354-6358.
27. P. D. C. Dietzel, B. Panella, M. Hirscher, R. Blom and H. Fjellvag, *Chem. Commun.*, 2006, 959-961.
28. A. Vimont, J. M. Goupil, J. C. Lavalley, M. Daturi, S. Surble, C. Serre, F. Millange, G. Férey and N. Audebrand, *J. Am. Chem. Soc.*, 2006, **128**, 3218-3227.
29. P. L. Llewellyn, S. Bourrelly, C. Serre, A. Vimont, M. Daturi, L. Hamon, G. De Weireld, J. S. Chang, D. Y. Hong, Y. K. Hwang, S. H. Jung and G. Férey, *Langmuir*, 2008, **24**, 7245-7250.
30. A. Henschel, K. Gedrich, R. Kraehnert and S. Kaskel, *Chem. Commun.*, 2008, 4192-4194.
31. C. Serre, F. Millange, S. Surble and G. Férey, *Angew. Chem. Int. Ed.*, 2004, **43**, 6285-6289.
32. J. P. S. Mowat, S. R. Miller, A. M. Z. Slawin, V. R. Seymour, S. E. Ashbrook and P. A. Wright, *Microporous Mesoporous Mater.*, 2011, **142**, 322-333.
33. S. Surble, C. Serre, C. Mellot-Draznieks, F. Millange and G. Férey, *Chem. Commun.*, 2006, 284-286.
34. H. Yang, F. Wang, Y. Kang, T.-H. Li and J. Zhang, *Dalton Trans.*, 2012, **41**, 2873-2876.
35. M. Dan-Hardi, H. Chevreau, T. Devic, P. Horcajada, G. Maurin, G. Férey, D. Popov, C. Riekkel, S. Wuttke, J.-C. Lavalley, A. Vimont, T. Boudewijns, D. de Vos and C. Serre, *Chem. Mater.*, 2012, **24**, 2486-2492.
36. Y. Liu, J. F. Eubank, A. J. Cairns, J. Eckert, V. C. Kravtsov, R. Luebke and M. Eddaoudi, *Angew. Chem. Int. Ed.*, 2007, **46**, 3278-3283.
37. J. Moellmer, E. B. Celer, R. Luebke, A. J. Cairns, R. Staudt, M. Eddaoudi and M. Thommes, *Microporous Mesoporous Mater.*, 2010, **129**, 345-353.
38. K. Barthelet, J. Marrot, G. Férey and D. Riou, *Chem. Commun.*, 2004, 520-521.
39. Q. Yang, S. Vaesen, M. Vishnuvarthan, F. Ragon, C. Serre, A. Vimont, M. Daturi, G. De Weireld and G. Maurin, *J. Mater. Chem.*, 2012, **22**, 10210-10220.
40. A. Fateeva, P. Horcajada, T. Devic, C. Serre, J. Marrot, J.-M. Greneche, M. Morcrette, J.-M. Tarascon, G. Maurin and G. Férey, *Eur. J. Inorg. Chem.*, 2010, 3789-3794.
41. C. Volkringer, M. Meddouri, T. Loiseau, N. Guillou, J. Marrot, G. Férey, M. Haouas, F. Taulelle, N. Audebrand and M. Latroche, *Inorg. Chem.*, 2008, **47**, 11892-11901.

42. J. A. Groves, S. R. Miller, S. J. Warrender, C. Mellot-Draznieks, P. Lightfoot and P. A. Wright, *Chem. Commun.*, 2006, 3305-3307.
43. M. T. Wharmby, J. P. S. Mowat, S. P. Thompson and P. A. Wright, *J. Am. Chem. Soc.*, 2011, **133**, 1266-1269.
44. K. Schlichte, T. Kratzke and S. Kaskel, *Microporous Mesoporous Mater.*, 2004, **73**, 81-88.
45. A. Dhakshinamoorthy, M. Alvaro and H. Garcia, *Adv. Synth. Catal.*, 2010, **352**, 3022-3030.
46. L. Maria Aguirre-Diaz, M. Iglesias, N. Snejko, E. Gutierrez-Puebla and M. Angeles Monge, *Crystengcomm*, 2013, **15**, 9562-9571.
47. S. Neogi, M. K. Sharma and P. K. Bharadwaj, *J. Mole. Catal. A: Chem.*, 2009, **299**, 1-4.
48. J. Gascon, U. Aktay, M. D. Hernandez-Alonso, G. P. M. van Klink and F. Kapteijn, *J. Catal.*, 2009, **261**, 75-87.
49. S. Hasegawa, S. Horike, R. Matsuda, S. Furukawa, K. Mochizuki, Y. Kinoshita and S. Kitagawa, *J. Am. Chem. Soc.*, 2007, **129**, 2607-2614.
50. Y. K. Hwang, D. Y. Hong, J. S. Chang, S. H. Jung, Y. K. Seo, J. Kim, A. Vimont, M. Daturi, C. Serre and G. Férey, *Angew. Chem. Int. Ed.*, 2008, **47**, 4144-4148.
51. A. Dhakshinamoorthy, M. Alvaro, P. Horcajada, E. Gibson, M. Vishnuvarthan, A. Vimont, J.-M. Greneche, C. Serre, M. Daturi and H. Garcia, *ACS Catal.*, 2012, **2**, 2060-2065.
52. A. Dhakshinamoorthy, M. Alvaro, H. Chevreau, P. Horcajada, T. Devic, C. Serre and H. Garcia, *Catal. Sci. Tech.*, 2012, **2**, 324-330.
53. B. Gole, A. K. Bar, A. Mallick, R. Banerjee and P. S. Mukherjee, *Chem. Commun.*, 2013, **49**, 7439-7441.
54. K. S. Jeong, Y. B. Go, S. M. Shin, S. J. Lee, J. Kim, O. M. Yaghi and N. Jeong, *Chem. Sci.*, 2011, **2**, 877-882.
55. M. Opanasenko, A. Dhakshinamoorthy, Y. K. Hwang, J.-S. Chang, H. Garcia and J. Cejka, *ChemSusChem*, 2013, **6**, 865-871.
56. M. Opanasenko, M. Shamzhy, M. Lamac and J. Cejka, *Catal. Today*, 2013, **204**, 94-100.
57. L. T. L. Nguyen, T. T. Nguyen, K. D. Nguyen and N. T. S. Phan, *Appl. Catal., A*, 2012, **425**, 44-52.
58. N. T. S. Phan, T. T. Nguyen and P. H. L. Vu, *ChemCatChem*, 2013, **5**, 3068-3077.
59. M. Opanasenko, M. Shamzhy and J. Cejka, *ChemCatChem*, 2013, **5**, 1024-1031.
60. M. J. Beier, W. Kleist, M. T. Wharmby, R. Kissner, B. Kimmerle, P. A. Wright, J.-D. Grunwaldt and A. Baiker, *Chem.-Eur. J.*, 2012, **18**, 887-898.
61. A. Dhakshinamoorthy, M. Alvaro and H. Garcia, *Chem.-Eur. J.*, 2010, **16**, 8530-8536.
62. A. Dhakshinamoorthy, M. Alvaro and H. Garcia, *ACS Catal.*, 2011, **1**, 48-53.
63. A. Corma, M. Iglesias, F. Xamena and F. Sanchez, *Chem.-Eur. J.*, 2010, **16**, 9789-9795.
64. K. Wilson, A. Renson and J. H. Clark, *Catal. Lett.*, 1999, **61**, 51-55.
65. Y. Zang, J. Shi, F. Zhang, Y. Zhong and W. Zhu, *Catal. Sci. Tech.*, 2013, **3**, 2044-2049.
66. Z. Q. Wang and S. M. Cohen, *J. Am. Chem. Soc.*, 2007, **129**, 12368.
67. M. J. Ingleson, J. P. Barrio, J. B. Guilbaud, Y. Z. Khimyak and M. J. Rosseinsky, *Chem. Commun.*, 2008, 2680-2682.

68. Y.-Q. Wang, Q. Yue, Y. Oi, K. Wang, Q. Sun and E.-Q. Gao, *Inorg. Chem.*, 2013, **52**, 4259-4268.
69. H. Leclerc, T. Devic, S. Devautour-Vinot, P. Bazin, N. Audebrand, G. Férey, M. Daturi, A. Vimont and G. Clet, *J. Phys. Chem. C*, 2011, **115**, 19828-19840.
70. F. Millange, N. Guillou, R. I. Walton, J.-M. Greneche, I. Margiolaki and G. Férey, *Chem. Commun.*, 2008, 4732-4734.
71. F. Nouar, T. Devic, H. Chevreau, N. Guillou, E. Gibson, G. Clet, M. Daturi, A. Vimont, J. M. Greneche, M. I. Breeze, R. I. Walton, P. L. Llewellyne and C. Serre, *Chem. Commun.*, 2012, **48**, 10237-10239.
72. M. Mendt, B. Jee, N. Stock, T. Ahnfeldt, M. Hartmann, D. Himsl and A. Poepl, *J. Phys. Chem. C*, 2010, **114**, 19443-19451.
73. F.-N. Shi, A. R. Silva, T.-H. Yang and J. Rocha, *Crystengcomm*, 2013, **15**, 3776-3779.
74. C. B. Liu, R. A. S. Ferreira, F. A. A. Paz, A. Cadiau, L. D. Carlos, L. S. Fu, J. Rocha and F. N. Shi, *Chem. Commun.*, 2012, **48**, 7964-7966.
75. S. H. Cho, B. Q. Ma, S. T. Nguyen, J. T. Hupp and T. E. Albrecht-Schmitt, *Chem. Commun.*, 2006, 2563-2565.
76. W. Xuan, C. Ye, M. Zhang, Z. Chen and Y. Cui, *Chem. Sci.*, 2013, **4**, 3154-3159.
77. Y. Ren, X. Cheng, S. Yang, C. Qi, H. Jiang and Q. Mao, *Dalton Trans.*, 2013, **42**, 9930-9937.
78. C. Zhu, X. Chen, Z. Yang, X. Du, Y. Liu and Y. Cui, *Chem. Commun.*, 2013, **49**, 7120-7122.
79. C. Zhu, G. Yuan, X. Chen, Z. Yang and Y. Cui, *J. Am. Chem. Soc.*, 2012, **134**, 8058-8061.
80. T. Zhang, F. Song and W. Lin, *Chem. Commun.*, 2012, **48**, 8766-8768.
81. A. Bhunia, M. A. Gotthardt, M. Yadav, M. T. Gamer, A. Eichhoefer, W. Kleist and P. W. Roesky, *Chem.-Eur. J.*, 2013, **19**, 1986-1995.
82. Y. Wan, C. Chen, W. Xiao, L. Jian and N. Zhang, *Microporous Mesoporous Mater.*, 2013, **171**, 9-13.
83. J. Hermannsdoerfer, M. Friedrich, N. Miyajima, R. Q. Albuquerque, S. Kuemmel and R. Kempe, *Angew. Chem. Int. Ed.*, 2012, **51**, 11473-11477.
84. V. Pascanu, Q. Yao, A. B. Gomez, M. Gustafsson, Y. Yun, W. Wan, L. Samain, X. Zou and B. Martin-Matute, *Chem.-Eur. J.*, 2013, **19**, 17483-17493.
85. B. Yuan, Y. Pan, Y. Li, B. Yin and H. Jiang, *Angew. Chem. Int. Ed.*, 2010, **49**, 4054-4058.
86. T. Van Vu, H. Kosslick, A. Schulz, J. Harloff, E. Paetzold, H. Lund, U. Kragl, M. Schneider and G. Fulda, *Microporous Mesoporous Mater.*, 2012, **154**, 100-106.
87. V. Toan Van, H. Kosslick, A. Schulz, J. Harloff, E. Paetzold, M. Schneider, J. Radnik, N. Steinfeldt, G. Fulda and U. Kragl, *Appl. Catal., A*, 2013, **468**, 410-417.
88. V. Toan Van, H. Kosslick, A. Schulz, J. Harloff, E. Paetzold, J. Radnik, U. Kragl, G. Fulda, C. Janiak and T. Nguyen Dinh, *Microporous Mesoporous Mater.*, 2013, **177**, 135-142.
89. E. D. Bloch, D. Britt, C. Lee, C. J. Doonan, F. J. Uribe-Romo, H. Furukawa, J. R. Long and O. M. Yaghi, *J. Am. Chem. Soc.*, 2010, **132**, 14382-14384.
90. K. C. Szeto, K. O. Kongshaug, S. Jakobsen, M. Tilset and K. P. Lillerud, *Dalton Trans.*, 2008, 2054-2060.

91. F. Carson, S. Agrawal, M. Gustafsson, A. Bartoszewicz, F. Moraga, X. Zou and B. Martin-Matute, *Chem.-Eur. J.*, 2012, **18**, 15337-15344.
92. Y.-Y. Liu, K. Leus, T. Bogaerts, K. Hemelsoet, E. Bruneel, V. Van Speybroeck and P. Van Der Voort, *ChemCatChem*, 2013, **5**, 3657-3664.
93. A. Arnanz, M. Pintado-Sierra, A. Corma, M. Iglesias and F. Sanchez, *Adv. Synth. Catal.*, 2012, **354**, 1347-1355.
94. M. Pintado-Sierra, A. M. Rasero-Almansa, A. Corma, M. Iglesias and F. Sanchez, *J. Catal.*, 2013, **299**, 137-145.

2. Characterisation

The structural characterisation of crystalline MOF materials is fundamental to the investigation of their behaviour as catalysts. Samples for this thesis were therefore investigated using a range of methods to determine details of physical properties relevant to catalysis: structure; porosity; presence of coordinatively unsaturated sites; morphology. The background to these techniques is discussed in this chapter.

2.1. Diffraction

X-ray diffraction (XRD) was the principal technique used for characterisation and analysis of the purity of MOF materials. This technique was used to identify phases and determine their unit cell parameters. Crystalline materials are periodically repeating structures made up of identical building blocks, or unit cells. A unit cell is described by ‘unit cell parameters’ defined by their vectors a , b and c and the angles between them, α , β and γ . There are 7 different symmetry groups that can be used to describe the geometric arrangement of lattice points and within these 7 different symmetry groups there are up to four types of lattice centring: primitive (P), lattice points at each of the corners of the unit cell; body-centred (I), lattice points at each of the corners and in the middle of the unit cell; face-centred (F), lattice point at each of the corners and also on the centre of all the faces of the unit cell; and base-centred (C), lattice points at each of the corners and in the middle of two opposite faces.^{1,2}

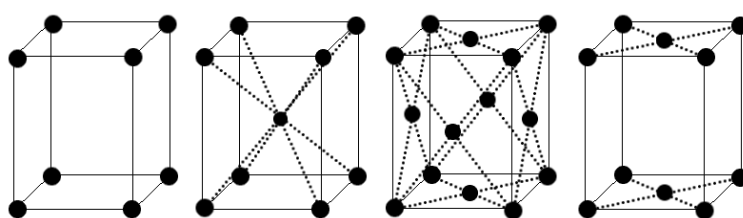


Figure 2.1: Lattice centring (a) primitive, (b) body-centred, (c) face-centred and (d) base centred

The combination of symmetry groups and lattice centres gives 14 different lattices referred to as the ‘Bravais lattices’ (Table 2.1). In the unit cell further symmetry can be defined due to the arrangement of the atoms. This symmetry is described in terms of point groups caused by centring, proper and improper rotation axes, screw axes (rotation and translation), mirror planes and glide planes (reflection and translation).

Combining the point groups and the Bravais lattices gives 230 different space group symmetries.²

Table 2.1 The seven crystal systems with lattice parameter conditions and Bravais lattice types

System	Unit cell dimension	Bravais lattice
Triclinic	$a \neq b \neq c / \alpha \neq \beta \neq \gamma$	<i>P</i>
Monoclinic	$a \neq b \neq c / \alpha = \beta = 90^\circ \neq \gamma$	<i>P, C</i>
Orthorhombic	$a \neq b \neq c / \alpha = \beta = \gamma = 90^\circ$	<i>P, C, I, F</i>
Tetragonal	$a = b \neq c / \alpha = \beta = \gamma = 90^\circ$	<i>P, I</i>
Hexagonal	$a = b \neq c / \alpha = \beta = 90^\circ \gamma = 120^\circ$	<i>P</i>
Rhombohedral	$a = b = c / \alpha = \beta = 120^\circ \gamma \neq 90^\circ$	<i>P</i>
Cubic	$a = b = c / \alpha = \beta = \gamma = 90^\circ$	<i>P, I, F</i>

Miller indices (of the form (hkl)) are used to define planes in lattices and crystals. These are used to describe the orientation and separation of lattice planes in a unit cell. For a given unit cell with unit cell parameters *a*, *b* and *c* the intercept of the first plane out from the origin with the *x*, *y*, and *z* axis is at *a/h*, *b/k* and *c/l*.²

2.2. Powder X-ray diffraction

Powder X-ray diffraction was used to establish phase purity and unit cell dimensions of the known materials that were studied. The small crystallite size of the materials, whilst advantageous for catalysis, precluded their study by single crystal X-ray diffraction.

X-ray diffraction was initially observed by Max von Laue in 1912 when he showed that white radiation incident onto a crystal gave rise to a ‘diffraction pattern’. These results were interpreted by Lawrence Bragg in terms of ‘reflections’ of monochromatic X-rays by crystal planes, which arose from the effects of constructive interference. The monochromatic X-rays must have a wavelength of the order of a typical crystal spacing to interact ($\sim 1 \text{ \AA}$). Bragg’s law is used to describe the ‘diffraction’ produced by the interaction of waves on planes of atoms.³

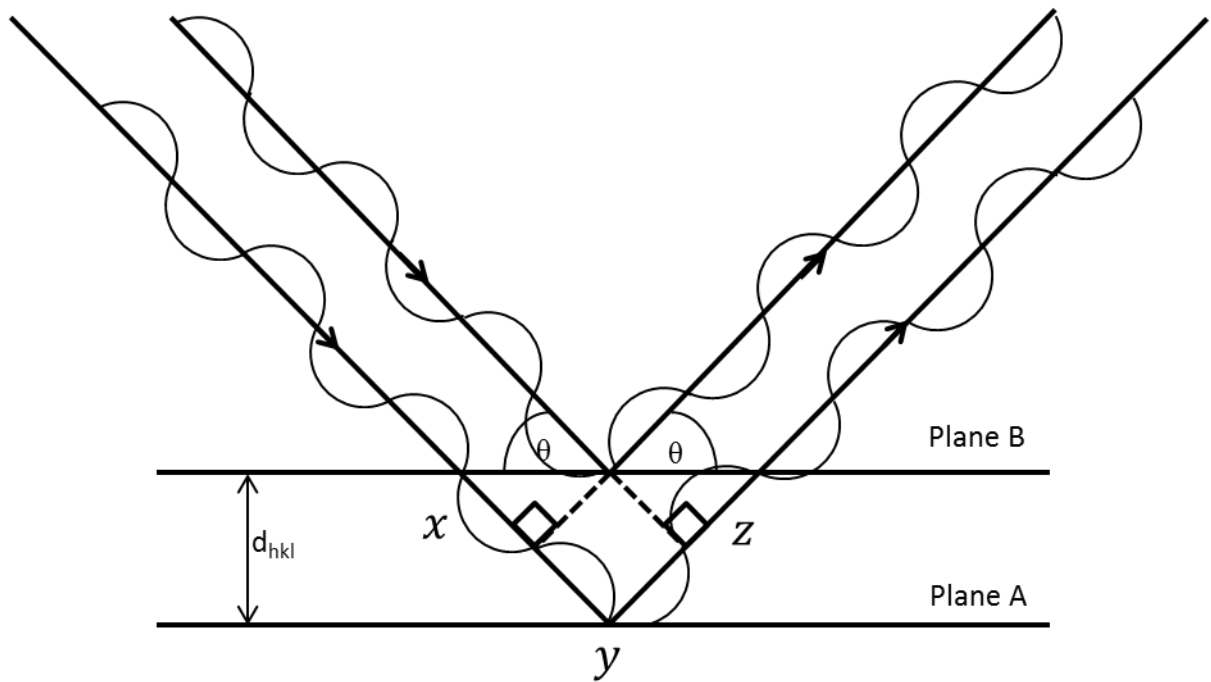


Figure 2.2: X-ray diffraction of two waves between two planes of lattice points in a crystal, showing example of constructive interference

Figure 2.2 schematically demonstrates the principle behind Bragg's law. In the planes of the material some of the waves are transmitted and some are 'reflected', with each plane of lattice points being an equal distance apart. Two waves are present in this diagram, with one wave being scattered from atoms in plane A and the second wave from atoms in plane B. From the diagram, the path difference must equal an integer number of wavelengths in order to preserve the constructive interference of the wave and hence cause diffraction. The path difference is defined in Bragg's equation in terms of d_{hkl} . By applying trigonometry, it can be said that xyz (and therefore yz) is equal to $d_{hkl} \sin \theta$ (equation 2.1 is obtained).⁴

where θ is the angle of incidence

$$xyz = 2d_{hkl} \sin \theta \quad 2.1$$

Where xyz is an integer number of wavelengths, this gives equation 2.2, Bragg's law, which needs to be satisfied for diffraction to occur.

$$n\lambda = 2d \sin \theta \quad 2.2$$

The scattering angle 2θ therefore depends on the interplanar spacing d_{hkl} . The positions of the peaks can be used to obtain the unit cell dimensions (and so the crystal system).

For powder diffraction, an X-ray source, monochromator and detector are required. X-rays are generated by accelerating electrons towards a metal target, causing some core shell electrons to be excited and ejected, and outer electrons to drop down to the new vacancy, emitting X-ray radiation as dissipated energy. PXRD was performed using Stoe STAD i/p diffractometers with either Cu $K_{\alpha 1}$ ($\lambda = 1.54060 \text{ \AA}$) or Fe $K_{\alpha 1}$ ($\lambda = 1.93604 \text{ \AA}$) X-radiation or a PANalytical Empyrean diffractometer with Cu $K_{\alpha 1}$ ($\lambda = 1.54060 \text{ \AA}$) radiation. Two different sources of radiation were required as strong fluorescence arises from cobalt-containing materials when using Cu K_{α} x-radiation. Fluorescence causes peaks to be obscured by producing a high background in the pattern (due to secondary emission of X-rays), so an iron source was required for some materials. Figure 2.3 shows schematically a powder X-ray diffractometer. Samples were measured using Debye-Scherrer (capillary mode), and transmission and flat plate (Bragg-Bentano) geometries. Debye-Scherrer geometry was used when samples were pre-dehydrated and sealed in a quartz capillary.

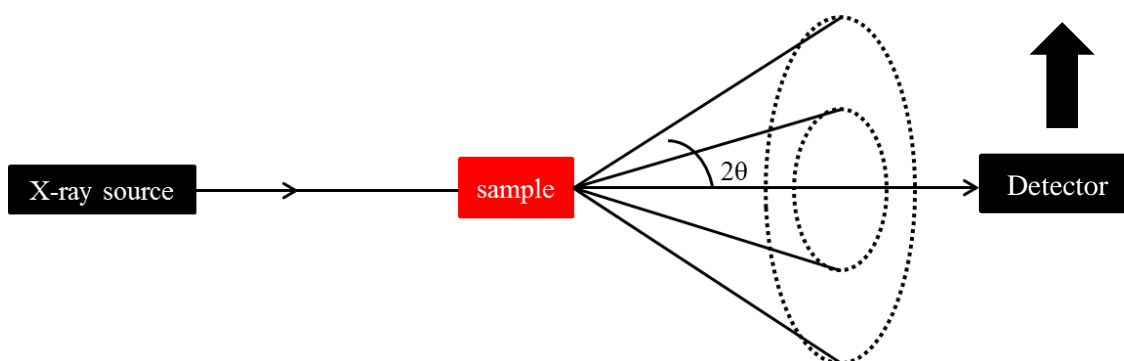


Figure 2.3: Schematic layout of a powder diffractometer

2.3. Structural refinement: Rietveld and Le Bail

In order to acquire structural data from PXRD, indexing for unit cell constants and space group assignment was performed, as well as model refinement (specifically Rietveld and Le Bail). Indexing the observed peaks in the diffraction pattern allowed for determination of the unit cell dimensions and potential space groups. In order to index unit cells, peak positions were located using the computer program Expo⁵ and supplied as input to the indexing programmes DICVOL⁶ or TREOR.⁷ Le Bail structureless

refinement could then be performed in order to confirm the space group choice and extract lattice parameters.

Rietveld refinement is used to extract structural information from powder diffraction patterns of crystalline structures. It compares the whole pattern simulated from a model to the observed diffraction data and then adjusts the model parameters accordingly to reduce the difference between the observed and calculated data according to the least squares method.

$$R = \sum w_i (y_i(\text{obs}) - y_i(\text{calc}))^2 \quad 2.6$$

Difference between observed and calculated pattern, where y_i is observed and calculated intensities and w_i is the weighting factor

Measures of how well the calculated data matches the observed data are reported as the fit parameters R_p and wR_p , which tend to zero with better fit.⁸

$$R_p = \frac{\sum |y_i(\text{obs}) - y_i(\text{calc})|}{\sum y_i(\text{obs})} \quad 2.7$$

$$wR_p = \left[\frac{\sum w_i (y_i(\text{obs}) - y_i(\text{calc}))^2}{\sum w_i (y_i(\text{obs}))^2} \right]^{1/2} \quad 2.8$$

Goodness of fit parameters in Rietveld refinement, where y_i is observed and calculated intensities and w_i is the weighting factor

Most of the materials examined in this thesis were compositional variants of known structures, so a model was available (unit cell, atomic positions). However, in the case of MIL-100 the structure is highly complex (independent atoms) and there is also significant disorder of residual solvent, so Rietveld refinement was not possible. Instead, the data was analysed by Le Bail refinement of the cubic unit cell parameter, a . Le Bail refinement is a structureless refinement in which instrumental and unit cell parameters are permitted to refine, and intensity can be attributed to allowed reflections. Refinements were carried out using the General Structure Analysis System (GSAS) software package⁹ and the EXPGUI interface.

2.4. Adsorption

2.4.1. Physisorption: Measurement of porosity (N₂ adsorption)

For the MOFs studied in this thesis, it was important to determine their porosity because this was a good guide to the accessibility of their pore space and therefore to their potential as high surface area catalysts. Determination of the permanent porosity of potential catalysts was measured using N₂ adsorption at 77 K. This was investigated either volumetrically using a Micrometrics Tristar II 3020 or gravimetrically using a Hiden-Isochem IGA.

Adsorption is when a molecule of either a liquid or gaseous adsorbate binds to a surface (adsorbent). This can be split into two sub-categories; physisorption and chemisorption. Physisorption is the long range interaction of adsorbate with the adsorbent forming weak bonds due to van der Waals forces. This interaction is weak. Chemisorption results from the exchange of charge between the adsorbate and the adsorbent for example an adsorbate on a Lewis acid site. The energy of this interaction is much higher and sometimes cannot be reversed. However it was important that chemisorbed species could be removed or exchanged in this project due to the need for catalytically active Lewis acid sites.¹⁰

Different models have been implemented in order to interpret the behaviour of adsorption on MOF materials. These include the Langmuir and Brunauer Emmett Teller (BET) models. The Langmuir model is not suitable for MOF materials due to its assumption that all adsorption sites are equivalent in energy with only monolayer coverage. MOF materials may be 1-, 2- or 3- dimensionally connected. They can consist of different organic ligands and metal cations, therefore have a range of different adsorption energies. Furthermore, the pores and cavities are large enough to permit more than monolayer adsorption. The BET model is a preferred alternative as it provides an extension to the Langmuir isotherm and considers multilayer adsorption. This allows adsorption to take place in the first layer on a range of sites with uniform energy and also on second and subsequent layers: it is a reliable approach to determine MOF surface areas.¹¹

Figure 2.4 shows a representation of the types of isotherms exhibited in materials classified by Brunauer, Denning, Denning and Teller (BDDT). Type I isotherms

represent Langmuir isotherms, typical of chemisorption and also of physisorption on microporous materials. The initial rise shows the filling of the micropores followed by a plateau when the pores are full. Type II and III isotherms are typical of multilayer adsorption on open surfaces. Type II arises when there is strong adsorbate-adsorbent interaction. Type III arises when there is weak adsorbate-adsorbent interactions and is rare. Type IV and V show characteristic ‘hysteresis loops’ which are indicative of both multilayer adsorption and condensation effects in mesopores (2-15nm).¹⁰

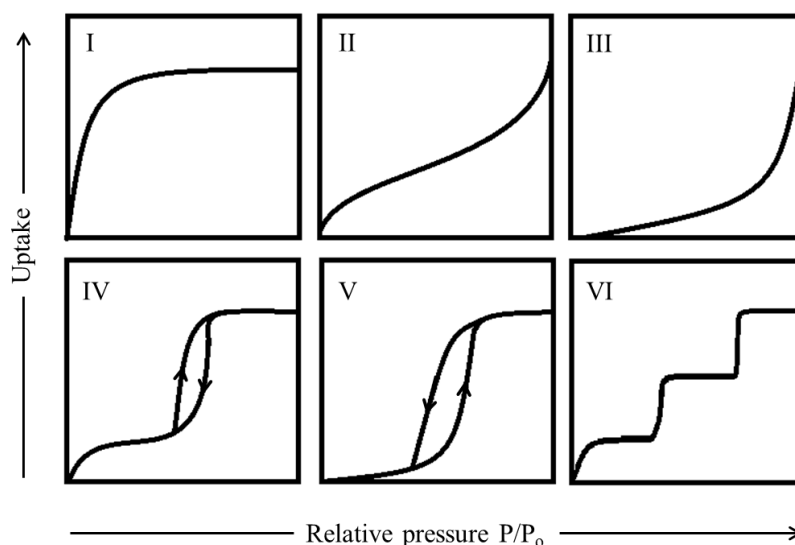


Figure 2.4: Brunauer, Denning, Denning and Teller (BDDT) classification of different isotherms

Type IV is commonly observed in mesoporous materials and can be observed (although without hysteresis) in MIL-100 materials (as discussed later, section 3.2.3). Two clear steps are observed due to the two different cage sizes in MIL-100 (Figure 2.5). From this isotherm different properties of the material can be determined including surface area ($1426 \text{ m}^2\text{g}^{-1}$) and pore volume ($0.59 \text{ cm}^3\text{g}^{-1}$). Type VI isotherms are obtained when adsorption is carried out with noble gases on well-defined solids.

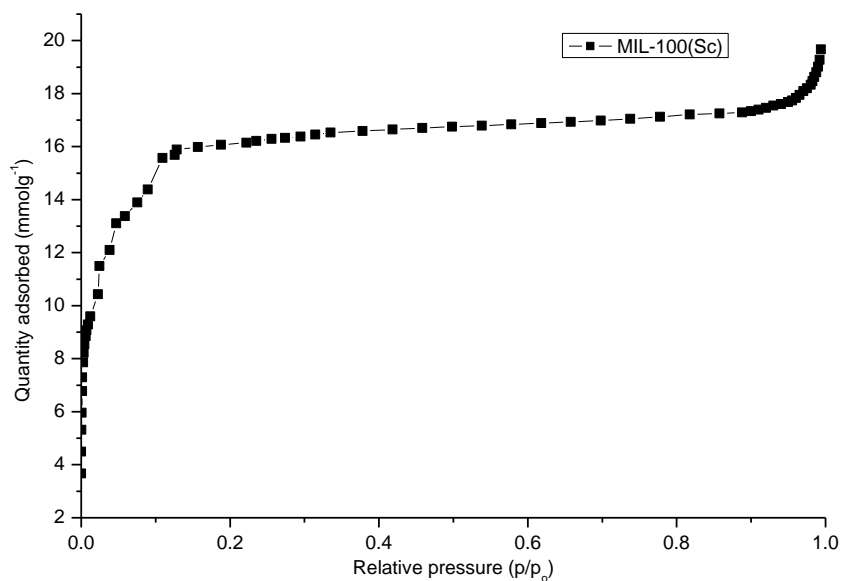


Figure 2.5: N_2 adsorption isotherm of MIL-100(Sc) at 77 K

2.4.2. Chemisorption: Measurement of chemisorption at Lewis acid sites via IR of absorbent probe molecules

FTIR spectroscopy is a common and widely used technique in both organic and inorganic chemistry. It is associated with the absorption of energy in the infra-red region by specific vibrational excitation between bonds and atoms that give rise to changes in dipole moments. It is used to identify functional groups and provide a fingerprint for molecules and also, in heterogeneous catalysis, to characterise active sites by the use of probe molecules that are IR-active.

The vibrational excitations can be split into two types; stretching and bending (Figure 2.6). These modes can be further subdivided into different categories.

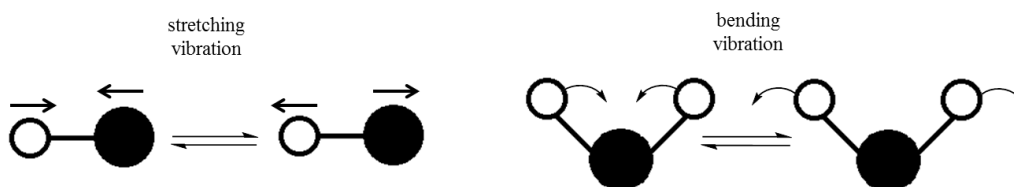


Figure 2.6: Stretching and bending vibration modes

Stretching modes may be either symmetric or asymmetric. Bending modes may be scissoring, rocking, twisting and wagging. Radiation is absorbed when the frequency of the radiation is the same as the vibrational frequency between atoms and bonds in the molecule. This causes a change in vibrational state of the molecule and heat is

subsequently released. The energy absorbed is related to increases in the rotational and vibrational energy of the molecules. This allows IR absorption due to changes in vibrational energy of a molecule to provide information required to identify the molecule.¹²

FTIR involves the absorbance of light at different frequencies at the same time and the amount of light absorbed is measured. A second pulse of light with different frequencies from those of the previous pulse is emitted and absorption measured. This process is repeated several times. In order to do this light is emitted from an IR source onto a beam splitter. This splits the light in which half of the light is directed onto a stationary mirror and the other onto a movable mirror (Figure 2.7). The light is then reflected back onto the beam splitter, recombined and directed at the sample.

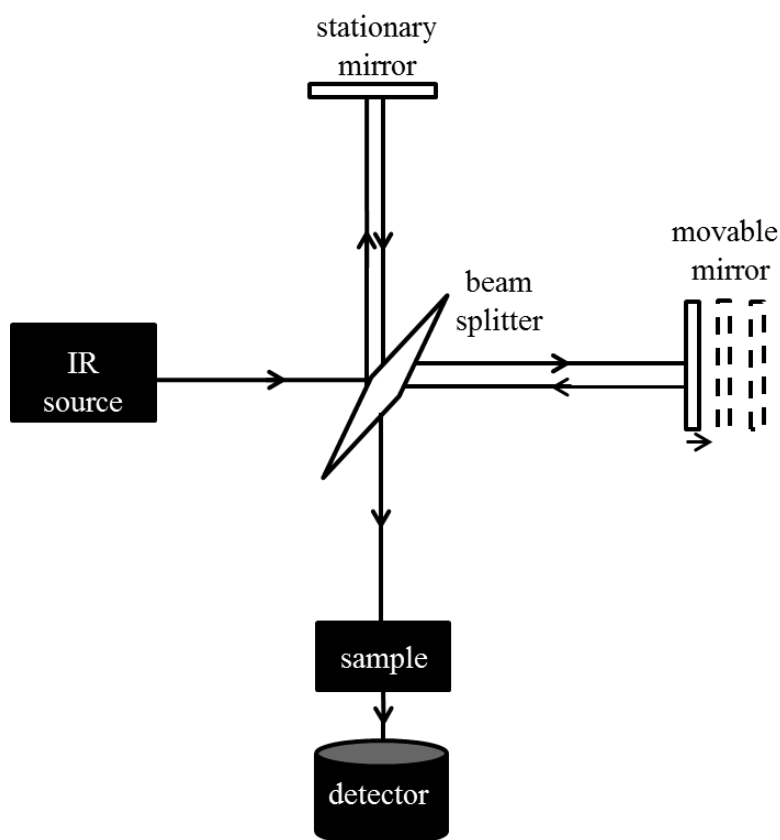


Figure 2.7: Diagram showing FTIR setup

Due to the movement of one of the mirrors the path length of one beam will be fixed and the other will differ. This causes interference in the beam and resultant signal known as the 'interferogram'. The interferogram provides information on every IR frequency from the source. When the light is absorbed into the sample, frequencies that

equal the vibrational frequency of the bonds (at specific wavelengths) are strongly attenuated but the light that passes through the sample is not. In order to interpret the information obtained in the interferogram Fourier transformation is required. Fourier transform is a mathematical technique used to decode the interferogram to give the spectrum (Figure 2.8).¹³

In this project IR spectroscopy was used to probe both the Lewis acid strength and the number of Lewis acid sites.¹ This was carried out using a Nicolet Nexus spectrometer equipped with an extended KBr beam splitting device and a mercury cadmium telluride (MCT) cryodetector (procedures used for these experiments are discussed in experimental section). Both CO and CD₃CN were used as probe molecules in this experiment. CO has been used previously in the study of HKUST-1.^{14, 15} The stretching frequency caused by the CO binding to a coordinatively unsaturated site can be recorded and the area of this frequency can then be used to determine the amount of Lewis acid sites present in the material. CD₃CN was also used as a probe molecule as the stretching frequency recorded from the metal binding to CD₃CN gave an indication of Lewis acid strength. The higher the stretching frequency the greater the Lewis acidic strength.

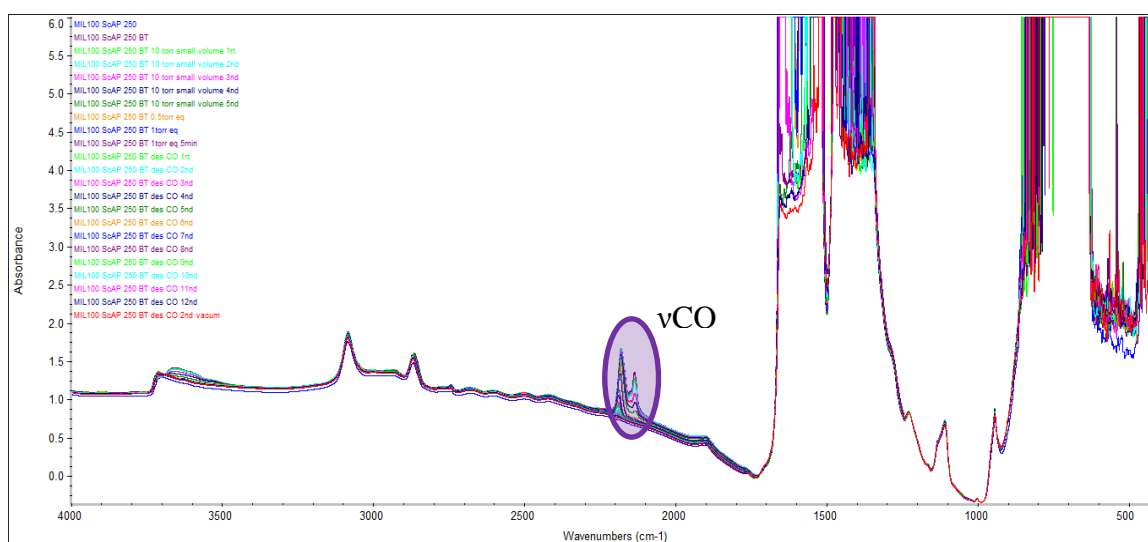


Figure 2.8: Infra-red spectra obtained for CO adsorption of MIL-100(Sc) with the ν CO stretch highlighted

¹ In Collaboration with Marlene Renouf, Alexander Vimont and Marco Daturi at the Laboratoire Catalyse et Spectrochimie, Université de Caen

2.5. UV-Visible spectroscopy

UV-spectroscopy has been used to observe changes in MOF composition and structure resulting from the introduction of transition metal cations into MOF materials. This will be discussed in Chapter 5. The technique is commonly used to probe transition metal ion incorporation and chemical state and sometimes to determine their concentrations (using the Beer-Lambert law; Equation 2.9).

$$\log\left(\frac{I}{I_0}\right) = \epsilon cl \text{ often stated as } \epsilon = A/cl \quad 2.9$$

Beer-Lambert law where I is the intensity of transmitted light, I_0 is the intensity of incident light, ϵ is the molar absorptivity, c is the concentration and l is the path length

Here we were interested in probing the influence of transition metal cations. A cation or ligand can absorb energy to excite the species to a higher electronic state (Figure 2.9). This can occur in a transition metal cation due to the transition of an electron into a higher energy orbital. The wavelength at which this absorption takes place is recorded using an optical spectrometer.¹³

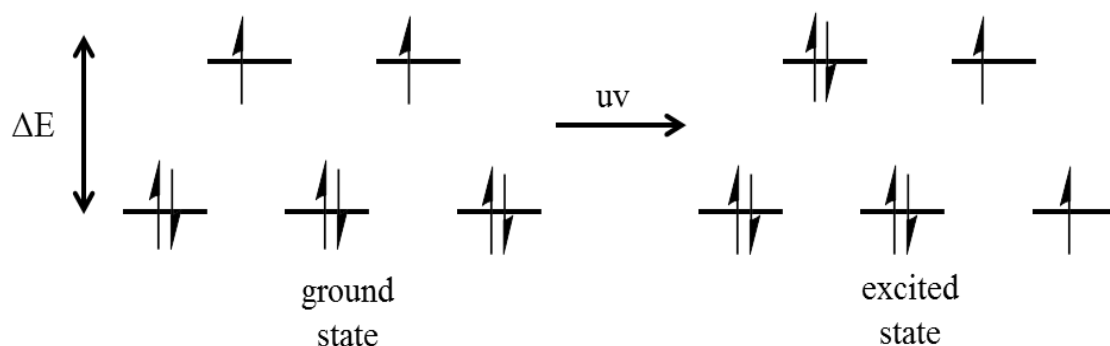


Figure 2.9: Absorption of a photon by a transition metal cation (d^8 , octahedral crystal field) in the ground state can lead to electronic excitation

In transition metal complexes several types of transitions can take place; most importantly the transition of electrons from lower to higher energy level orbitals e.g. $d-d$ transitions. These are typically spin disallowed and are associated with weak colours. A further transition is commonly caused by charge transfer. This is caused by the transition of an electron from a localised orbital on an atom to an adjacent atom. This transition is spin allowed and commonly associated with strong absorption bands and intense colours. A typical UV spectrum obtained for MIL-100 is shown in (Figure

2.10).¹² The spectra show the UV absorption of MIL-100(Sc) compared to MIL-100(Sc/Ni) in which a clear difference can be seen. Sc^{3+} contains no d electrons therefore no d-d transitions would be expected for energy level transitions in the transition metal cation, although UV bands do occur from the adsorption by the organic ligand (< 300 nm). When Ni^{2+} is introduced into the structure a clear change can be observed in the visible part of the spectrum due to the excitation of d-electrons (broad bands at 350-520 nm and 550-900 nm). This is discussed further in chapter 5.

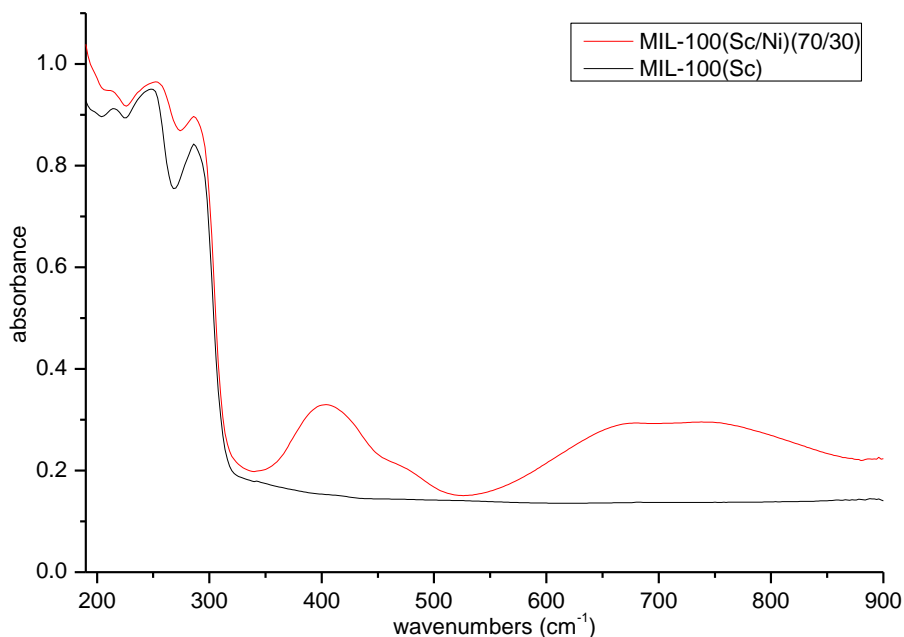


Figure 2.10: UV-visible spectrum of MIL-100(Sc) compared to MIL-100(Sc/Ni)

UV spectroscopy was carried out using a Jasco V-650 UV visible spectrometer with accompanying Jasco software over a range of 190-900 nm.

2.6. X-ray absorption spectroscopy

In this thesis the use of X-ray absorption spectroscopy was employed in order to determine oxidation states of metals and the type of nanoparticles present. Both X-ray Absorption Near Edge Structure (XANES) and Extended X-Ray Absorption Fine Structure (EXAFS) were used (Figure 2.11). These techniques use the absorption of photons in materials to determine different features of the material in question. The absorption of an X-ray photon causes electron(s) to be excited into unoccupied states or ejected. This creates a vacant core hole which is then filled by another electron in a different state causing X-ray fluorescence or filled by another electron and associated

emission of an Auger electron (Figure 2.12). When a core electron absorbs energy greater or equal to its binding energy an absorption ‘edge’ results. Metal K-edges energies are used to determine oxidation states of materials.^{16, 17}

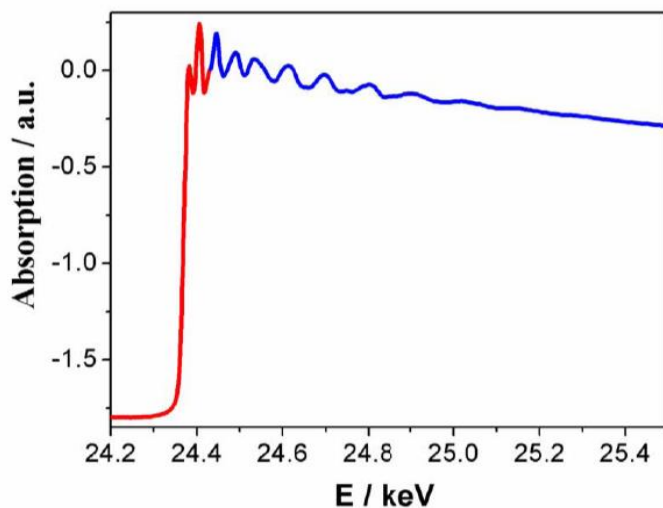


Figure 2.11: X-ray absorption spectra showing XANES region (red) and EXAFS region (blue)

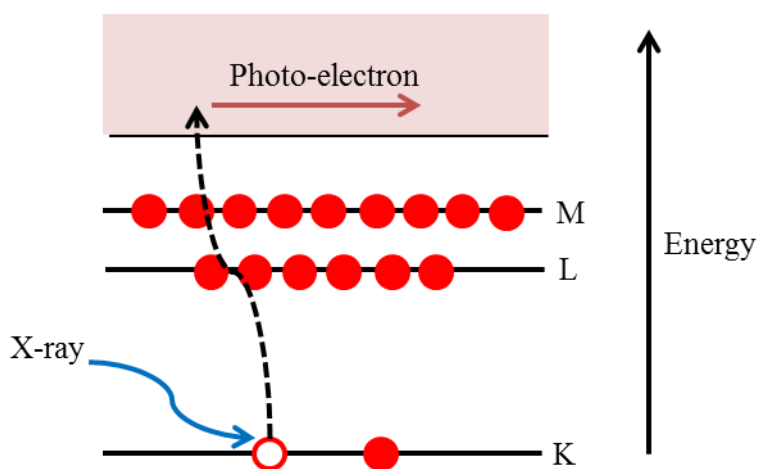


Figure 2.12: Schematic diagram of the photoelectric effect, X-ray being absorbed and core electron being ejected

XANES is the study of the features immediately at the absorption edge or 1% either side of it. The K-edge energy can be used to determine the oxidation state of a material. In this project the XANES was used to determine the oxidation state of materials by comparing their spectra to known compounds of a certain oxidation state (this is discussed in chapter 5).¹⁷

EXAFS allows for the determination of the chemical environment of selected atom type in terms of types and amount of nearest neighbouring atoms, distance between them and structural disorder which makes it a useful technique in determining local structure. It requires the modelling of known material and comparison of the known material with the new material.^{16, 18}

All the results obtained for both XANES and EXAFS were collected and analysed by Prof. Richard Walton and Luke Daniels at room temperature on beamline B18 of the Diamond Light Source in transmission mode from solid samples mixed with polyethylene powder to give suitable absorption at the K-edge. A Si (III) double-crystal monochromator was used to select the incident X-ray energy and scans performed in QUEXAFS mode. Data were normalised in the program *Athena*¹⁹ to yield XANES spectra and background subtracted EXAFS spectra. k^3 -weighted EXAFS spectra were analysed using *Artemis*,¹⁹ which implements the FEFF code, with coordination numbers of atomic shells fixed at expected values and shell distances, thermal parameters (σ^2) refined along with E_0 and S_0^2 (amplitude reduction factor).

2.7. Scanning electron microscopy (SEM) and Energy dispersive X-ray spectroscopy (EDX)

SEM and associated EDX were used in this study to obtain information on the morphology (size and shape) and the composition of materials (using energy dispersive X-ray spectroscopy, EDX). SEM is a microscopy that produces images of a material by focussing electron beams onto the material (Figure 2.13).

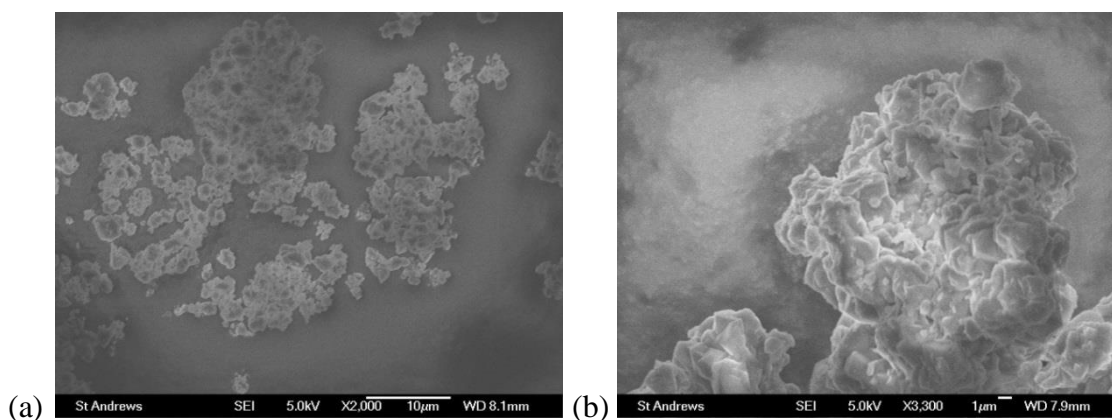
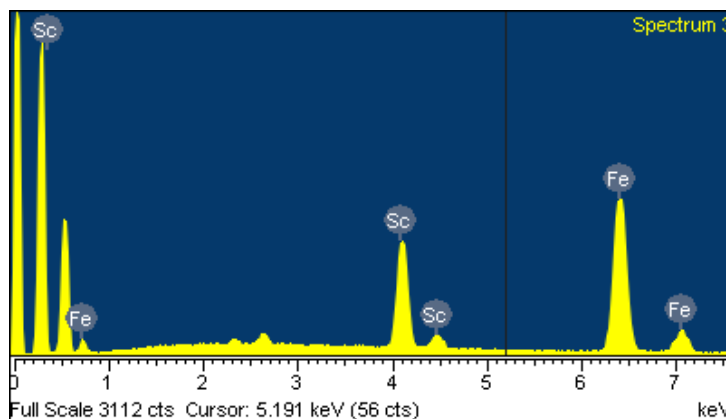


Figure 2.13: SEM images of MIL-100(Sc) at different magnifications using secondary electrons.

A beam of electrons is scanned across the surface of a sample creating an image by analysis of both secondary and backscattered electrons. SEM can be used for imaging at high resolution due to the very short wavelength of electrons at the energies that are typically used.^{20, 21}

EDX is a selected area chemical analysis probe, typically used to measure elements contained in a material. It is usually considered to be semi-quantitative. It is used in conjunction with SEM. It works by bombarding a sample with an electron beam, causing electrons to collide with the sample. Core electrons are then ejected from the surface (to a depth of around a few μm) of the material. Higher state electrons then drop down to fill the vacant core shells causing X-rays to be emitted as dissipated energy. The X-rays emitted have characteristic wavelengths related to the elements from which they are emitted, allowing elements present in the material to be determined. This is then plotted as a spectrum; instrument software converts these signals to relative elemental compositions. For major element the accuracy of the technique is usually $\pm 1\%$ however due to other uncertainties in composition of reference standards and correction errors of raw data the accuracy is said to be closer to $\pm 2\%$. Figure 2.14 shows a spectrum obtained from a mixed metal MIL-100 sample containing both scandium and iron. The peak position is characteristic of different elements and the intensity is used to determine the concentration of each of these elements. EDX measurements were obtained by a JEOL 5600 SEM with an Oxford INCA Energy 200 EDX system. This was carried out by selecting and specific area and mapping.



*Figure 2.14: EDX spectrum of a mixed scandium, iron form of MIL-100
(see chapter 5 for details)*

2.8. Thermogravimetric analysis (TGA)

TGA is used to measure the weight lost from a material as it is heated, usually with a constant heating rate.²² It is generally carried out in a flowing gas (typically N₂ or air). A known amount of sample is placed in a balance pan (generally platinum or alumina).

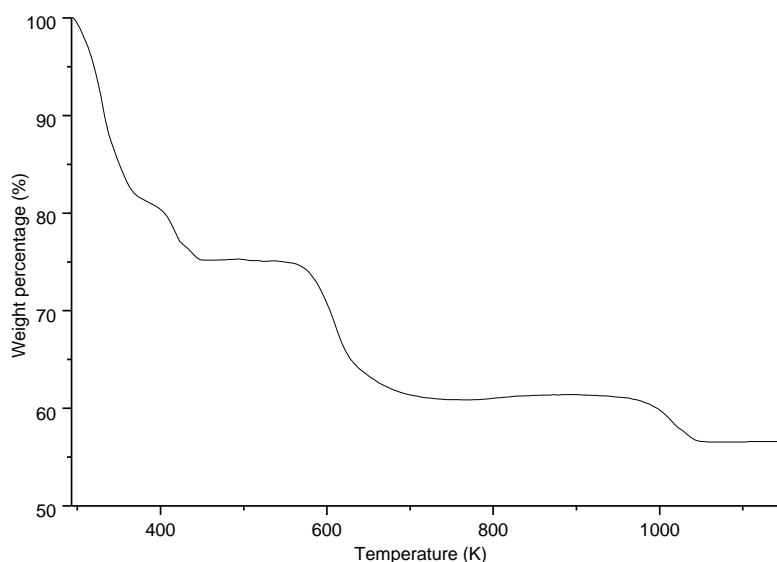


Figure 2.15: TGA of STA-12(Ni), percentage weight loss of the material from 293-1150 K. The weight loss of 15.5 % below 373 K is due to the loss of physisorbed water and of 5.1% below 523 K due to chemisorbed water. The weight loss after 523 K is caused by degradation of the structure and organic ligand

The material is then heated and weight measurements are taken. In the case of MOFs the weight losses are generally attributed to dehydration and degradation of the structure. A plot, as seen in Figure 2.15, of temperature vs. weight loss is made and weight losses can be assigned to different components of the material e.g. solvent, ligand, etc. TGA measurements were made using Netzsch TG209 and TGA 760 instruments.

2.9. Elemental analysis (CHN)

CHN is used to determine the organic content of a material. It is used to determine weight percentage of carbon, hydrogen, nitrogen and other heteroatoms (e.g. sulphur). It is commonly carried out by combustion, where a sample is burned at high temperatures in an excess of oxygen to form CO₂, H₂O, N₂ and NO_x, which can be separated and the weight percentage of each element determined.

2.10. References

1. A. R. West, *Basic Solid State Chemistry*, John Wiley & Sons, Ltd, UK, 1999.
2. C. Hammond, *The Basics of Crystallography and Diffraction*, Oxford University Press, USA, 2006.
3. W. Clegg, *Crystal Structure Determination*, Oxford University Press, USA, 1998.
4. U. C. London, Powder Diffraction on the Web, <http://pd.chem.ucl.ac.uk/pd/welcome.htm>.
5. A. Altomare, M. C. Burla, M. Camalli, B. Carrozzini, G. L. Cascarano, C. Giacovazzo, A. Guagliardi, A. G. G. Moliterni, G. Polidori and R. Rizzi, *J. Appl. Crystallogr.*, 1999, **32**, 339-340.
6. A. Boulfif and D. Louer, *J. Appl. Crystallogr.*, 1991, **24**, 987-993.
7. P. E. Werner, L. Eriksson and M. Westdahl, *J. Appl. Crystallogr.*, 1985, **18**, 367-370.
8. R. A. Young, *The Rietveld Method*, Oxford University Press, USA, 1996.
9. A. C. Larson and R. B. Von Dreele, *General Structure Analysis System (GSAS)*, Los Alamos National Laboratory, USA, 1994.
10. G. Attard and C. Barnes, *Surfaces*, Oxford University Press, USA, 1998.
11. T. Dueren, Y.-S. Bae and R. Q. Snurr, *Chem. Soc. Rev.*, 2009, **38**, 1237-1247.
12. S. Duckett and B. Gilbret, *Foundations of Spectroscopy*, Oxford University Press, USA, 2000.
13. L. M. Harwood and T. D. W. Claridge, *Introduction to Organic Spectroscopy*, Oxford University Press, USA, 1997.
14. S. Bordiga, L. Regli, F. Bonino, E. Groppo, C. Lamberti, B. Xiao, P. S. Wheatley, R. E. Morris and A. Zecchina, *Phys. Chem. Chem. Phys.*, 2007, **9**, 2676-2685.
15. C. Prestipino, L. Regli, J. G. Vitillo, F. Bonino, A. Damin, C. Lamberti, A. Zecchina, P. L. Solari, K. O. Kongshaug and S. Bordiga, *Chem. Mater.*, 2006, **18**, 1337-1346.
16. D. C. Koningsberger and R. Prins, *X-Ray Absorption – Principles, Applications, Techniques of EXAFS, SEXAFS and XANES*, John Wiley & Sons, 1988.
17. J. Als-Neilsen and D. McMorrow, *Elements of Modern X-ray Physics*, Wiley and Sons, 2001.
18. J. J. Boland, S. E. Crane and J. D. Baldeschwieler, *J. Chem. Phys.*, 1982, **77**, 142-153.
19. B. Ravel and M. Newville, *J. Synchrotron Rad.*, 2005, **12**, 537-541.
20. J. W. S. Hearle, *The use of the scanning electron microscope*, Pergamon Press, Oxford, 1972.
21. K. Jantscher, *Crystal structure determination in the scanning electron microscope: Fundamental and experimental problems*, AV Akademikerverlag, Saarbrücken, 2013.
22. P. J. Haines, *Principles of thermal analysis and calorimetry*, Royal Society of Chemistry, Cambridge, 2002.

3. Synthesis, optimisation and characterisation of known MOF materials

3.1. Introduction

This chapter addresses the synthesis of the previously-reported MOFs used as catalysts in the reactions described in later chapters: HKUST-1(Cu); MIL-100(Al, Cr, Fe, Sc); MIL-101(Cr); CPO-27(Co,Ni); STA-16(Co, Ni); MIL-100(Sc); STA-12(Co, Ni). For STA-12(Ni) and MIL-100(Sc), attempts to optimise their synthesis by reducing the use of undesirable solvents and by scaling up the preparations are described. Alternative methods of synthesis of STA-12 and MIL-100(Sc) were thought to be possible as well as desirable following the reported synthesis of Ag-organosulfonate MOFs¹ and some lanthanide containing MOFs² that made use of reflux and other ‘mild’ conditions of synthesis. Schlesinger *et al.*³ investigated the use of different synthesis methods for the production of HKUST-1(Cu). They compared the use of solvothermal, microwave assisted, mechanochemical, reflux and ultrasonic irradiation to determine the effects the synthesis method has on the material produced. It was found that solvothermal treatment, microwave irradiation and reflux all gave high yields of products with similar BET surface areas of ca. 1200 m² g⁻¹. They found that by changing the solvent to DMF the microwave-assisted synthesis could give materials with BET surface areas increased to 1499 m² g⁻¹. Lower increases in BET surface areas were observed in samples prepared solvothermally (up to 1323 m² g⁻¹). Changing the solvent in the reflux synthesis from a water/ethanol mixture to DMF gave strongly reduced surface areas. A high yield of high surface area material could be synthesised by microwave irradiation within 30 minutes compared to solvothermal treatments of 24 h. The use of these alternative synthesis techniques for MIL-100(Sc) and STA-12(Ni) are discussed in Part A.

The second Part B of this chapter addresses the characterisation of the Lewis acidic Sc³⁺ sites in MIL-100(Sc) used in this thesis. This was achieved by IR spectroscopy using CO and CD₃CN as probe molecules for the coordinatively unsaturated Sc³⁺ sites. This information is put into the context of previous IR studies of the same probe molecules on other MIL-100 materials and on CPO-27 and STA-12 (and -16) materials investigated as catalysts in chapters 4 and 5.

Part A: MOF synthesis, characterisation and optimisation

3.2. Synthesis of known MOF materials

Some of the materials for which the catalytic performance was assessed were synthesised solely according to the literature methods (STA-16,⁴ CPO-27,⁵ HKUST-1,⁶ MIL-88B(Sc),⁷ MIL-100(Cr,⁸ Fe⁹ and Al¹⁰) and MIL-101(Cr)¹¹). Each material was confirmed to be pure by PXRD (powder X-ray diffraction) and their porosity confirmed after activation. For STA-12(Ni) and MIL-100(Sc), which have been synthesised previously, efforts were made to investigate routes to their synthesis under milder conditions than reported, particularly with a view to making their synthesis acceptable in an industrial context.

3.2.1. CPO-27(Ni)

CPO-27(Ni) was synthesised using nickel acetate hexahydrate (1.48 mmol, 0.368 g), dihydroxyterephthalic acid (0.74 mmol, 0.147 g), water (10 ml) and tetrahydrofuran (10 ml) (2:1:750:166) in a Teflon-lined steel autoclave, mixed and heated at 383 K for 24 h. The material was analysed using PXRD and the observed pattern compared to a pattern simulated from a reported structure of the material. For CPO-27(Ni) the structure was from Dietzel (Figure 3.1).¹² Close agreement confirmed that phase had been synthesised pure.

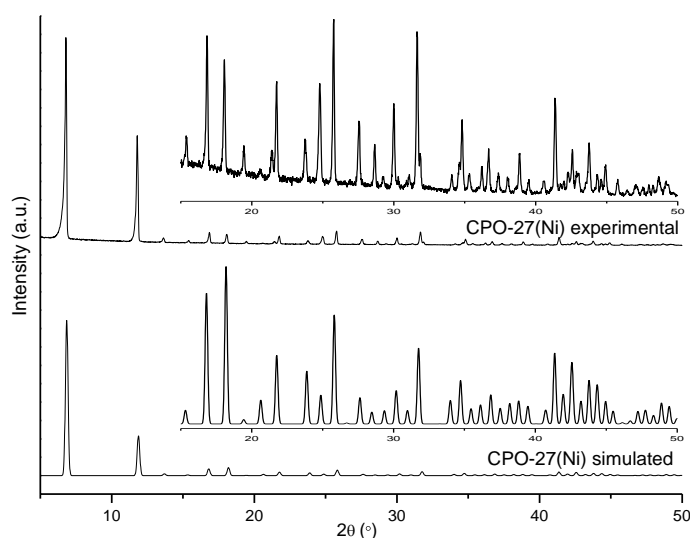


Figure 3.1: PXRD pattern of (above) CPO-27(Ni) synthesised solvothermally (72 h at 383 K) compared to that (below) simulated with expanded view for CPO-27(Ni) from the reported structure¹²

3.2.2. STA-12

The synthesis of STA-12(M) has been reported previously with various different divalent cations (cobalt, nickel, iron, manganese and magnesium) and the ligand N, N'-piperazinebis(methylenephosphonic acid) (synthesised from a simple Mannich reaction). In the Mg, Co, and Ni forms the material exhibits surface areas of ca. 600 m² g⁻¹ and a pore size diameter of ca. 9 Å.¹³ The first of these materials to be synthesised and studied was STA-12(Ni) reported by Groves *et al.*¹⁴ The material contains physisorbed water molecules in the hexagonal channels and chemisorbed water molecules bound to the nickel cations. The water is completely removed by heating at 523 K to form a solid with coordinatively unsaturated Ni²⁺ sites that are suitable for Lewis acid catalysis.

3.2.2.1. Synthesis of previously prepared STA-12(M) (where M= Ni, Co and Mg)

STA-12(Ni)¹⁴ and STA-12(Co, Mg)¹³ were first synthesised hydrothermally (see Table 3.1) using a 40 ml Teflon lined stainless steel autoclave placed in an oven at 493 K for 72 h. The relative molar amount of water used in the reactions is higher than that previously reported because it was found that at these higher values the crystallinity is improved. The resultant materials were analysed using PXRD, TGA and N₂ adsorption.

Table 3.1: Reaction conditions used to prepare different STA-12(M) samples

Metal source	Ligand	Ratio (M:L:H ₂ O:KOH)	Temperature (K)	Time (h)
Ni(OAc) ₂	H ₄ L	2:1:1500:0	493	72
Co(OAc) ₂	H ₄ L	2:1:1500:3	493	72
Mg(OAc) ₂	H ₄ L	2:1:1500:3	493	72

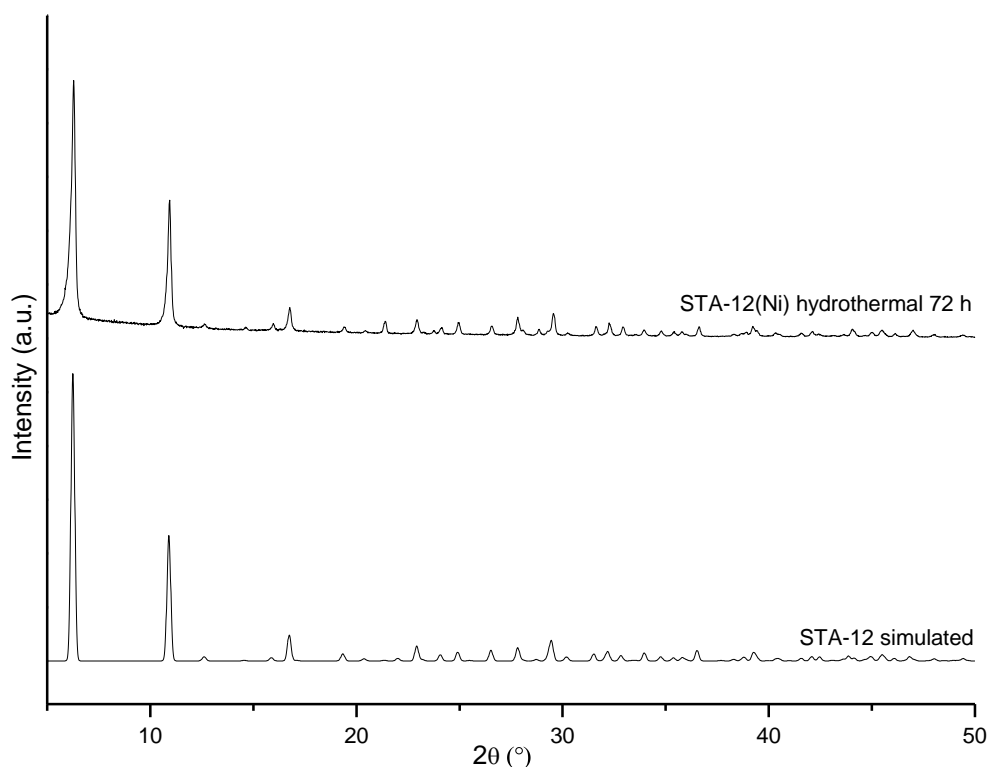


Figure 3.2: PXRD pattern of (a) simulated STA-12(Ni) compared to (b) STA-12(Ni) synthesised hydrothermally (72 h at 493 K)

The observed powder diffraction compares well with that predicted from the reported crystal structure (Figure 3.2). TGA analysis was carried out to compare with literature data and also so water loss could be quantified (chapter 4). The first decomposition step can be attributed to the loss of physisorbed water with a mass change of 18.5 % between 293 K and 383 K. The second mass change of 6.1% is caused by the loss of chemisorbed water which occurs between 383 K and 463 K (Figure 3.3 (a)). The other changes in mass are caused by the decomposition of the material at 573 K. N₂ adsorption of STA-12(Ni) at 77 K on a sample activated by heating at 523 K in vacuum indicated the structure was microporous and had a nitrogen uptake of 8.4 mmol g⁻¹ (at $p/p_0 = 0.4$) and a BET surface area of 626 m² g⁻¹ (Figure 3.3 (b)).

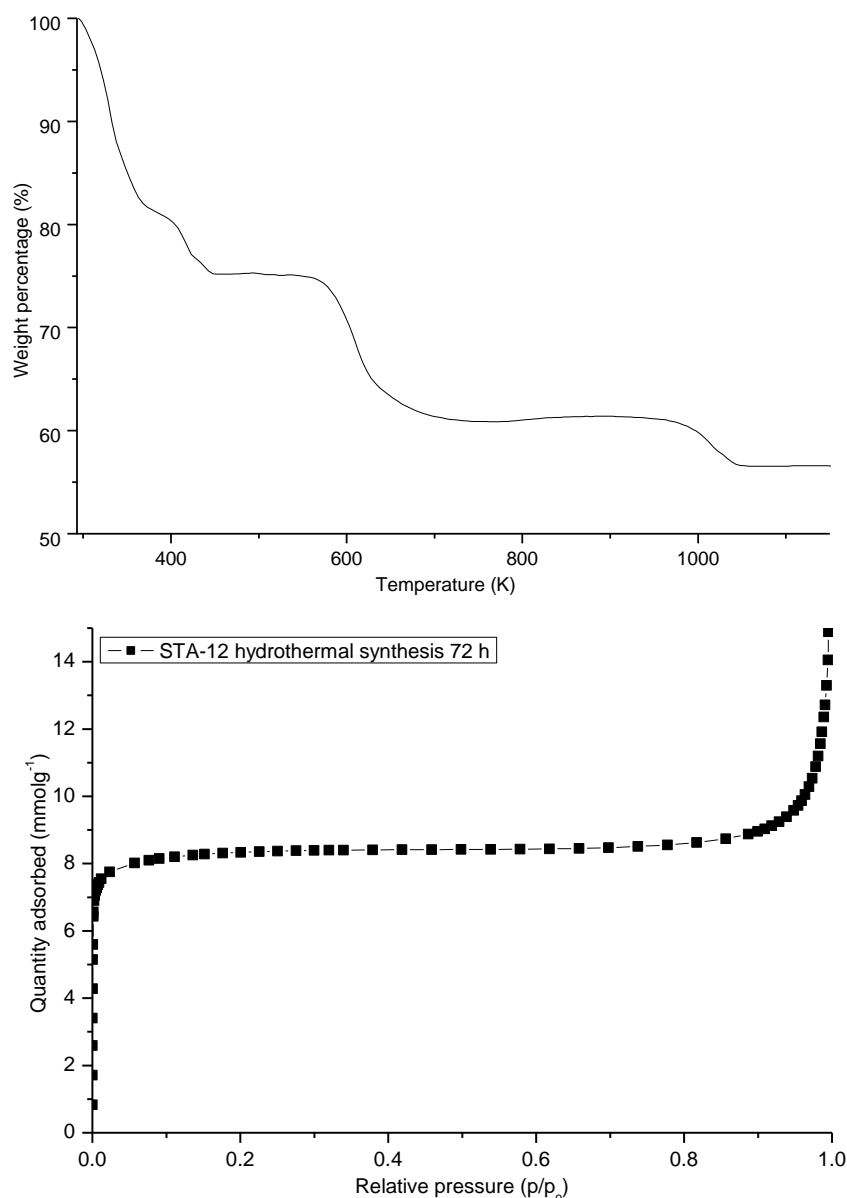


Figure 3.3: (above) TGA analysis, (below) N_2 adsorption of STA-12 (Ni) at reflux 77 K

3.2.2.2. Optimisation of the synthesis of STA-12(Ni)

The experimental method used to synthesis STA-12(Ni) was found to give a highly crystalline material with good N_2 uptake. However it was thought the long synthesis time of 72 h could be reduced by exploring alternative synthesis routes. Initially the original hydrothermal synthesis method was used and the reaction time reduced to 48 h, and then 24 h (PXRD Figure 3.4). The PXRD patterns show some minor broadening for the materials synthesised at lower synthesis times compared to that synthesised for 72 h (Table 3.2) which indicates that the crystallite size was slightly smaller in the shorter time synthesis.

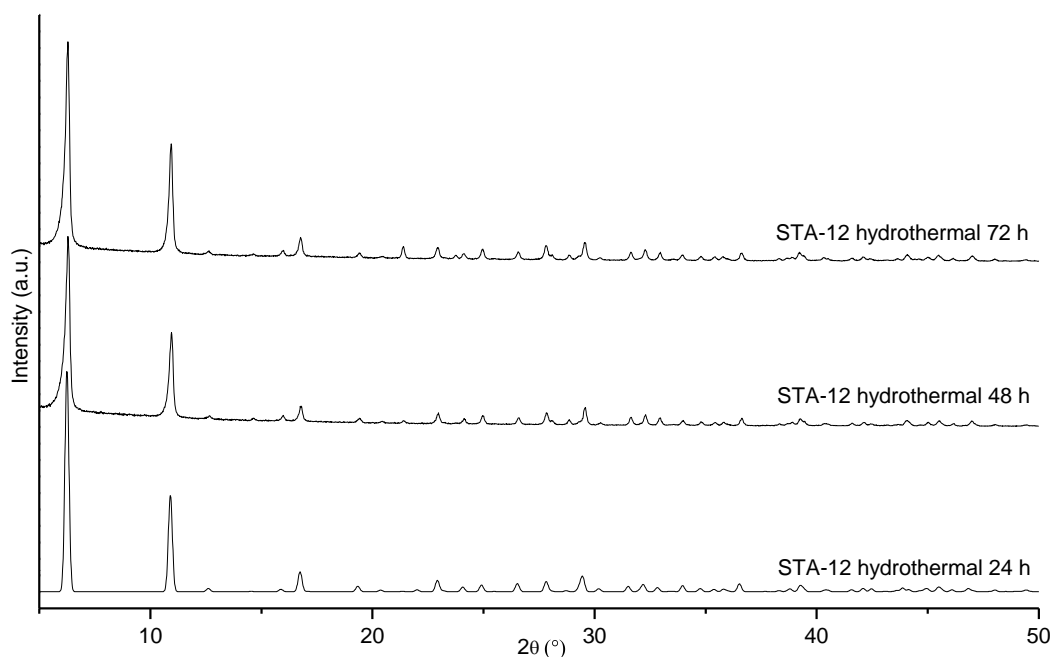


Figure 3.4: PXRD patterns of STA-12(Ni) synthesised hydrothermally for different times (a) 24 h (b) 48 h and (c) 72 h

Table 3.2: Comparison of crystallite size of STA-12 using different synthesis methods

Material	Observed broadening (FWMH) (°)	2θ (°)	crystallite size (nm)
microwave	0.276	23.77	52
24 h	0.179	23.76	75
48 h	0.174	23.77	78
72 h	0.171	23.76	81
Reflux	0.168	23.76	87

The synthesis time affected the N₂ uptake of the material more significantly (Figure 3.5). The N₂ uptake adsorption of the material dropped considerably if the material was only crystallised for 24 h (N₂ uptake of 2.77 mmol g⁻¹). The uptake almost doubles when the synthesis time is doubled to 48 h and increases further at 72 h accompanied by an increase in BET surface area (Table 3.3). Increasing the synthesis time beyond 72 h had no further increase of N₂ adsorption or crystallite size.

Table 3.3: BET surface area of STA-12(Ni) (at $p/p_0 = 0.4$) synthesised using different techniques

Synthesis time	BET surface area ($\text{m}^2 \text{g}^{-1}$)
24 h	246
48 h	412
72 h	626

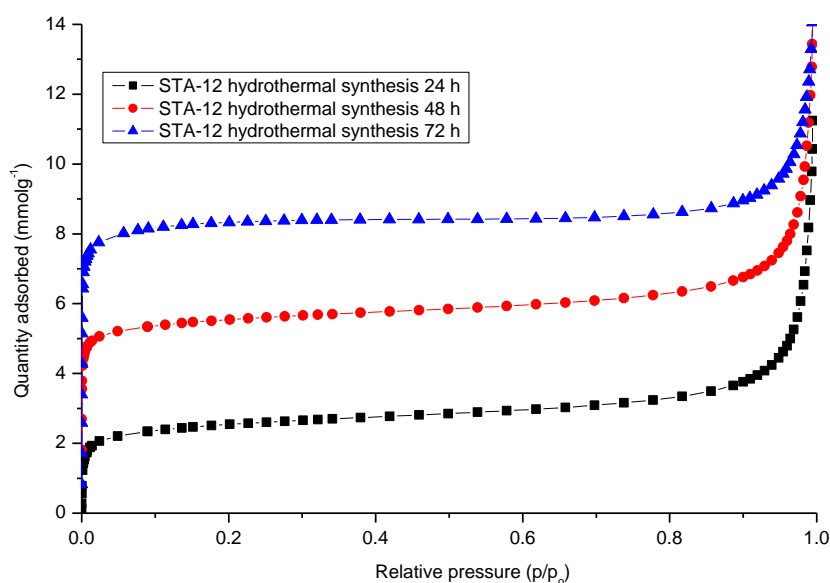
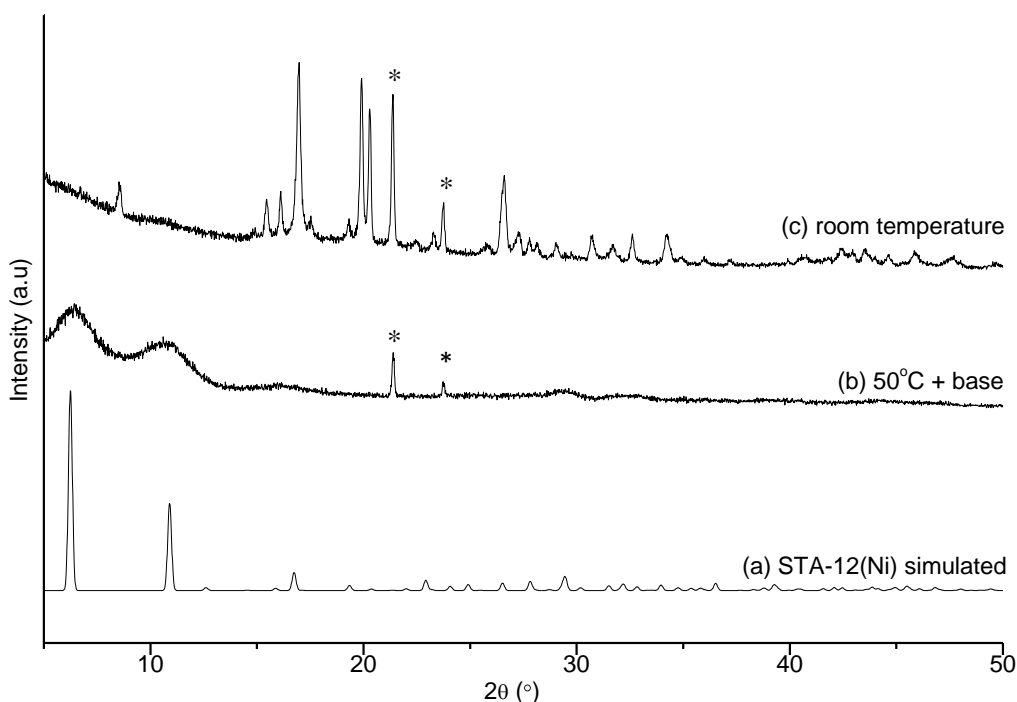


Figure 3.5: N_2 adsorption at 77 K of hydrothermally synthesised STA-12(Ni) for 24 h (black), 48 h (red) and 72 h (blue)

The temperature at which the hydrothermal reaction was carried out was varied in order to observe its effects on the resultant material. It was found that by lowering the temperature the crystallinity drops along with the nickel content in the final product. The colour of the materials is paler green than found for STA-12(Ni) synthesised at 493 K. The yield of the materials synthesised at lower temperatures also drops indicating 493 K is the optimum temperature for hydrothermal synthesis of STA-12(Ni).

Different methods were then investigated to determine if simpler methods of synthesis could be used; for example simply stirring the starting mixture at room temperature as previously shown to be possible for the synthesis of HKUST-1^{15, 16} and MOF-5.¹⁷ The synthesis of STA-12(Ni) at room temperature was attempted initially using the same

reactant ratio as used for the hydrothermal synthesis (Table 3.1) but this yielded disappointing results with only starting material recovered after 72 h. The H₄L ligand used for the reaction did not dissolve in water so alternative solvents in which the ligand would dissolve were tried on their own or mixed with water (ethanol, ethylene glycol and THF). However, again only starting material was recovered. The use of additional base in the reaction was also tried (base is required in the hydrothermal synthesis of STA-12(Co, Mg)). The H₄L ligand was dissolved in water and 2.5 M KOH. Ni(OAc)₂ was added and stirred for 24 h giving a very pale green solid at 323 K. PXRD (Figure 3.6) shows that the material formed was not STA-12(Ni) but the two broad reflections at 6 and 12° are where two very characteristic peaks of STA-12 appear. The material showed negligible BET surface area. The synthesis was tried for longer reaction times; however this showed no effect on the product.



*Figure 3.6: PXRD of attempted synthesis of STA-12(Ni) (a) simulated pattern of STA-12(Ni) (b) attempted synthesis of STA-12(Ni) at 323 K with added base and (c) attempted room temperature synthesis of STA-12(Ni) *denotes machine peaks*

Alternative methods of synthesis of STA-12 were sought. The use of reflux synthesis was attempted for STA-12(Ni) using the same reagents ratios as shown in Table 3.1 and refluxing for 8 h. The material was synthesised in high yield (92%), slightly increased from the hydrothermal technique (85%). The material was found to have BET surface

area of $652 \text{ m}^2 \text{ g}^{-1}$ comparable to the hydrothermally synthesised material (Figure 3.7 and Table 3.4).

Table 3.4: BET surface area of STA-12(Ni) synthesised using different techniques

Synthesis technique	BET surface area ($\text{m}^2 \text{ g}^{-1}$)
Solvothermal	626
Microwave	589
Reflux	652

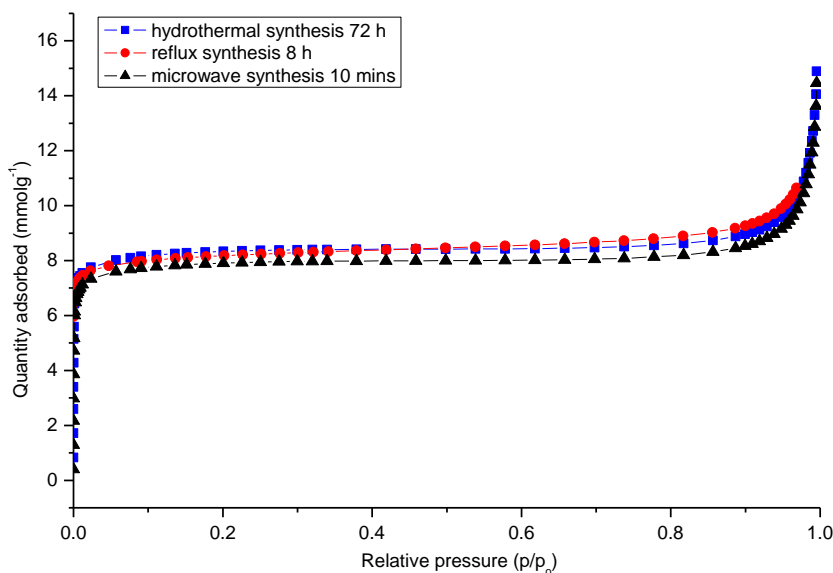


Figure 3.7: N_2 adsorption of STA-12(Ni) using different synthesis techniques; microwave synthesis (black), reflux synthesis (red) and hydrothermal synthesis (blue) (at 77 K)

Reflux synthesised STA-12(Ni) appeared to have good crystallinity observed from PXRD (Figure 3.8) and a larger crystallite size of around 100 nm compared to the 72 h hydrothermally-synthesised material which has a crystallite size of about 90 nm (Table 3.2).

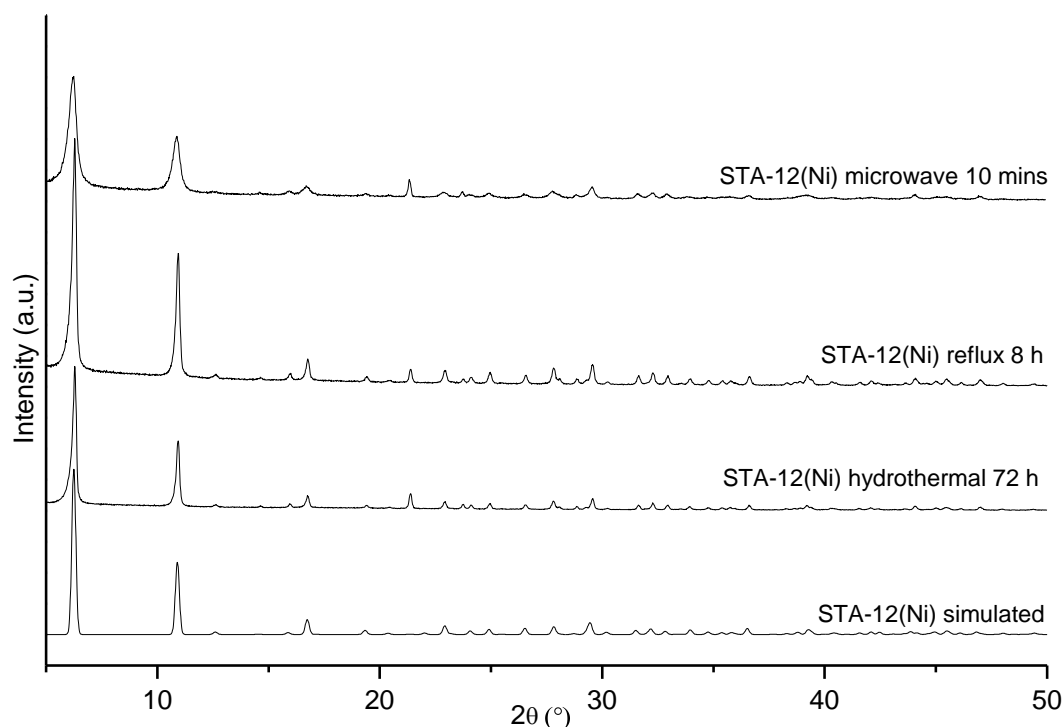


Figure 3.8: XRD of STA-12(Ni) synthesised using different techniques as labelled on spectra

After the success of the reaction using reflux conditions, the reaction temperature was decreased further to 363 K in order to determine if high temperatures were required. The desired material was no longer formed: the XRD pattern was a poor match and the BET surface area was reduced. The lowest temperature necessary for successful reaction was found to be 373 K.

One other synthesis technique that has also proved to be successful in MOF synthesis is the use of microwave irradiation. As mentioned previously this has previously been shown to give larger BET surface areas than other techniques and to achieve this in very short reaction times. The fast reaction heating allows for rapid kinetics of nucleation and crystal growth leading to the formation of small crystallites.¹⁸ The reaction was carried out using the same ratios as previously used (Table 3.1) but reaction time was reduced to 30 minutes and the reaction was carried out at various temperatures between 323 and 473 K. It was found that in order to synthesise STA-12 with good BET surface area a temperature of 373 K is required; this is similar to reflux conditions. The crystallite size of the material can then be calculated from the Scherrer equation (Figure 3.9 and Table 3.2) and is much smaller (52 nm) than that of the material synthesised by reflux. Although the crystallite size was reduced, the N₂ adsorption of the material remained

high and was similar to the value found for reflux-synthesised materials; the BET surface area is also similar (Figure 3.7 and Table 3.4).

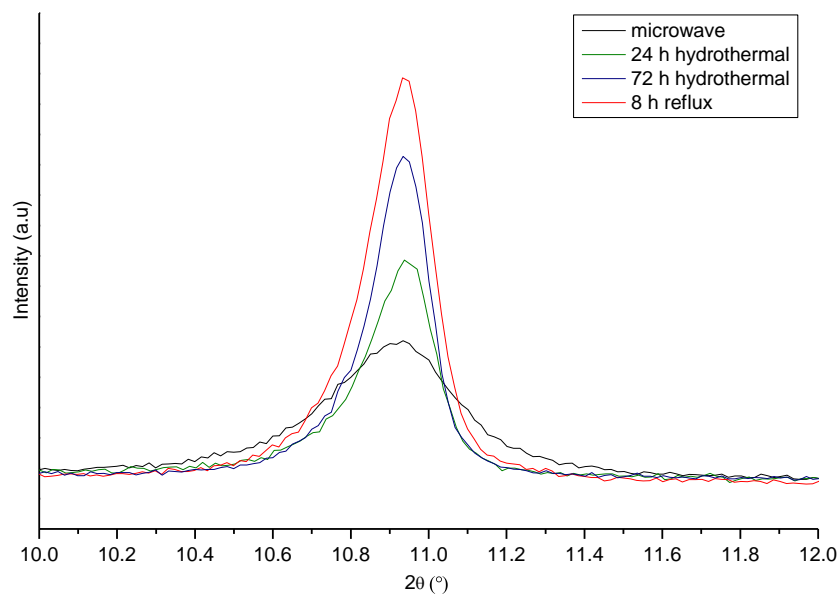


Figure 3.9: Expanded PXRD between 10° and 20° showing line broadening in STA-12(Ni): via microwave heating (black), hydrothermal synthesis (green), hydrothermal synthesis (blue) and reflux synthesis (red)

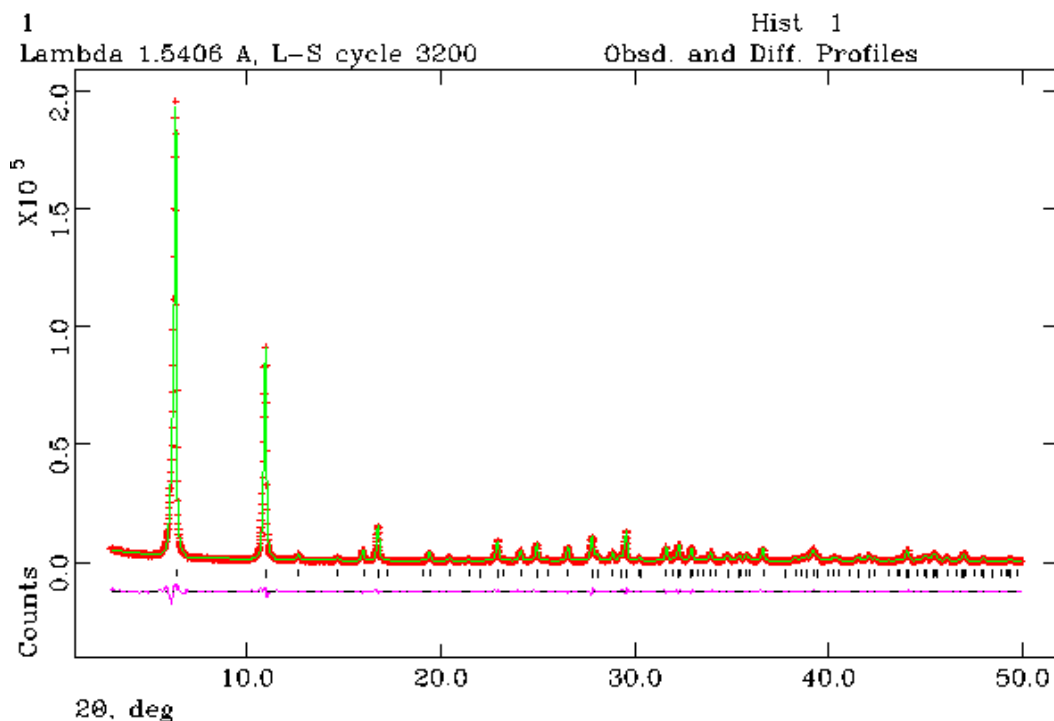


Figure 3.10: An example of a Rietveld refinement carried out on reflux-synthesised STA-12(Ni)

Using Rietveld refinement the unit cell of the materials were determined. Figure 3.10 is a Rietveld plot of the refinement carried out on reflux-synthesised STA-12. For these refinements the starting structure model was that obtained from the reported STA-12(Ni) structure.¹⁴

Rietveld refinement of the PXRD patterns in the $R\bar{3}$ space group for various synthesis methods suggests that the less crystalline materials have smaller a and c parameters.

Table 3.5: Unit cell parameters of STA-12(Ni) using different synthesis methods and their wRp

Synthesis method	a (Å)	b (Å)	c (Å)	wRp
24 h hydrothermal	27.9142(15)	27.9142(15)	6.23142(28)	0.0651
72 h hydrothermal	27.9368(3)	27.9368(3)	6.23212(9)	0.0499
microwave	27.904(7)	27.904(7)	6.2167(10)	0.0689
Reflux	27.9459(7)	27.9459(7)	6.23385(14)	0.0489

The results show that by changing the synthesis method from hydrothermal to reflux to microwave heating the reaction time required to produce materials with similar properties is subsequently reduced. The catalytic performance of these materials will be discussed in chapter 4.

3.2.3. Optimisation of the synthesis of MIL-100(Sc)

After the success of finding alternative ways to synthesise STA-12(Ni), a similar approach was taken for MIL-100(Sc). In this material there was interest in trying to find both a faster route and also an alternative solvent to that used in the solvothermal synthesis because DMF is a very undesirable solvent in industry due to its toxicity.

Marquez *et al.*¹⁹ successfully synthesised thin films of MIL-100 materials using microwave heating, therefore the use of microwave heating for MIL-100(Sc) was investigated. Starting mixtures were prepared using scandium nitrate hexahydrate, trimesic acid and DMF in a 3:2:600 ratio as previously described by Mowat *et al.*⁷ The microwave synthesis was carried out at 373 K for 30 minutes compared to the solvothermal approach which required 48 h at 423 K for crystallisation. PXRD patterns (Figure 3.11) show that the material has the MIL-100 structure. Unlike that observed in

the synthesis of STA-12(Ni), line broadening cannot be seen in the microwave-synthesised material and the crystallite sizes of the materials synthesised using different techniques is similar.

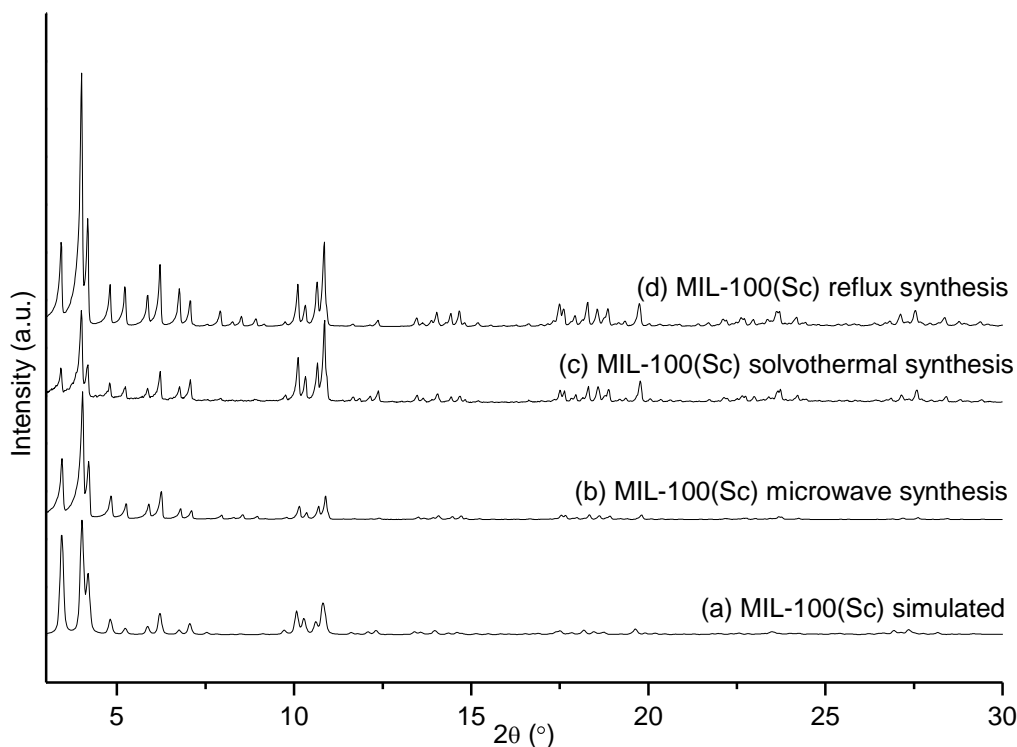


Figure 3.11: PXRD pattern of (a) simulated compared to (b) microwave synthesised (c) solvothermal synthesised and (d) reflux synthesised MIL-100(Sc)

N₂ adsorption of the microwave-prepared material is found to be very similar to that of the solvothermally-synthesised material with a BET surface area of 1414 m² g⁻¹ (Figure 3.12 and Table 3.6).

Table 3.6: BET surface area of MIL-100(Sc) synthesised using different techniques

Synthesis technique	BET surface area (m ² g ⁻¹)
Solvothermal	1426
Microwave	1414
Reflux	1556

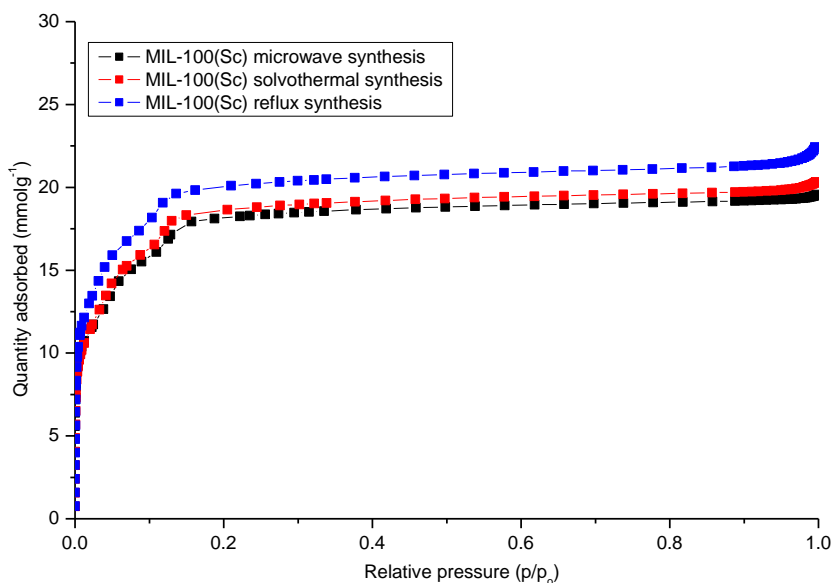


Figure 3.12: N_2 adsorption of MIL-100(Sc) using different synthesis techniques; microwave synthesis (black), reflux synthesis (red) and solvothermal synthesis (blue) (at 77 K)

When synthesising MIL-100(Sc) under reflux techniques, the material was shown to have improved crystallinity and also the BET surface area was increased (Table 3.6), above that found for materials prepared by either solvothermal or microwave-assisted synthesis. Therefore the reflux technique proved to be the best for this material, reducing reaction time to 8 h, increasing N_2 adsorption and maintaining high crystallinity.

The lowest temperature at which product was obtained was by heating at 353 K with stirring. However, in this case MIL-100(Sc) crystallinity decreases and the BET surface area was reduced to $958 \text{ m}^2 \text{ g}^{-1}$.

Another aim was to try and find an alternative solvent in which MIL-100(Sc) could be synthesised. Many different solvents and mixtures were attempted for the synthesis of this material but with little success. Water was used initially as it is the least toxic and the most abundant solvent however the reaction only returned starting materials. The temperature was varied from room temperature to 373 K to observe if an increase in temperature could help the MIL-100(Sc) synthesis. Similar reactions were carried out hydrothermally at higher temperatures (293 - 493 K). Microwave synthesis was also found not to produce the desired product over the same range of temperatures (293 - 493 K).

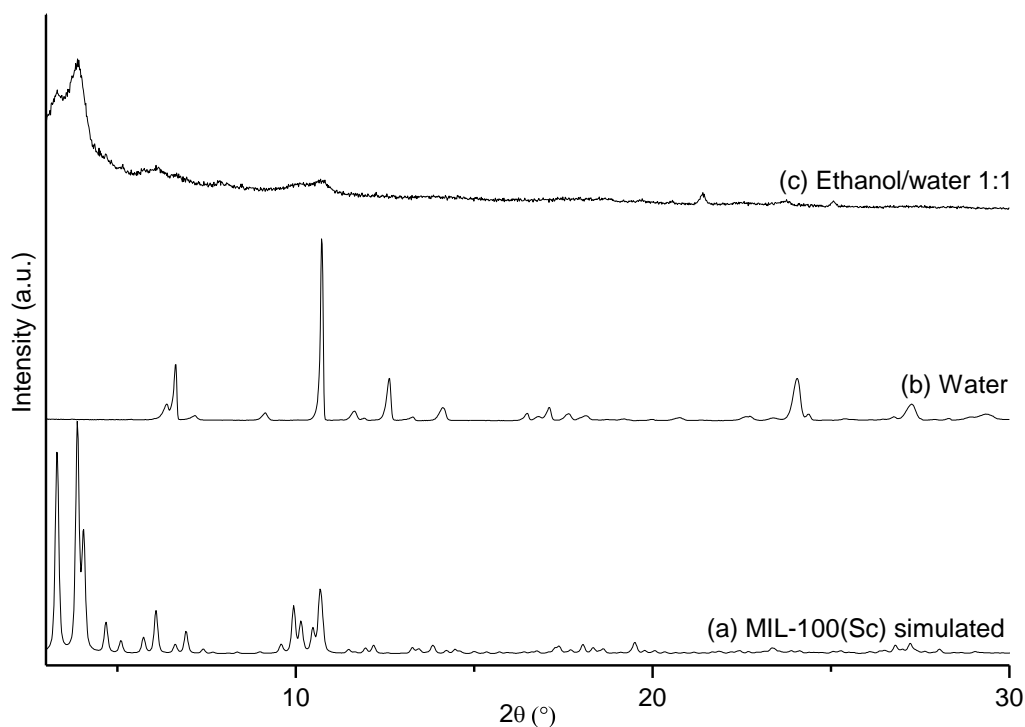


Figure 3.13: PXRD pattern of attempted synthesis of MIL-100(Sc) using different solvents under reflux (a) simulated compared to (b) water and (c) ethanol/water (1:1)

A mixture of ethanol and water under reflux gave a poorly crystalline material with a PXRD pattern that has broad peaks characteristic of MIL-100(Sc). A yield of only 22% was obtained as well as a very low BET surface area of $236 \text{ m}^2 \text{ g}^{-1}$. Many other solvents including pyridine, THF, dimethylacetamide, DMSO and acetonitrile were also tried with none yielding the desired product. Different sources of scandium and also alternative ester ligands of trimesic acid (which were successful in the synthesis of MIL-100(Fe) without HF)²⁰ were also tried, without success.

The use of propylene carbonate which is also a so called ‘green’ solvent yielded a different result from that obtained with DMF or any other solvent. The PXRD pattern (Figure 3.14) was indexed using the DICVOL method in the Fullprof suite of programs to give a unit cell of $a = 8.6573(2) \text{ \AA}$ $b = a$ and $c = 18.5234(8) \text{ \AA}$, space group $R\bar{3}$. The cell parameters matched that of $\text{Mn}_3(\text{BTC})_2$ ($R\bar{3}$, $a = b = 8.65(1) \text{ \AA}$ and $c = 18.491(4) \text{ \AA}$) a 3-dimensional coordination polymer (Figure 3.15) synthesised solvothermally using MnCl_2 , trimesic acid, and aqueous KOH in a ratio of 2:3:12 (3 days at 493 K).²¹

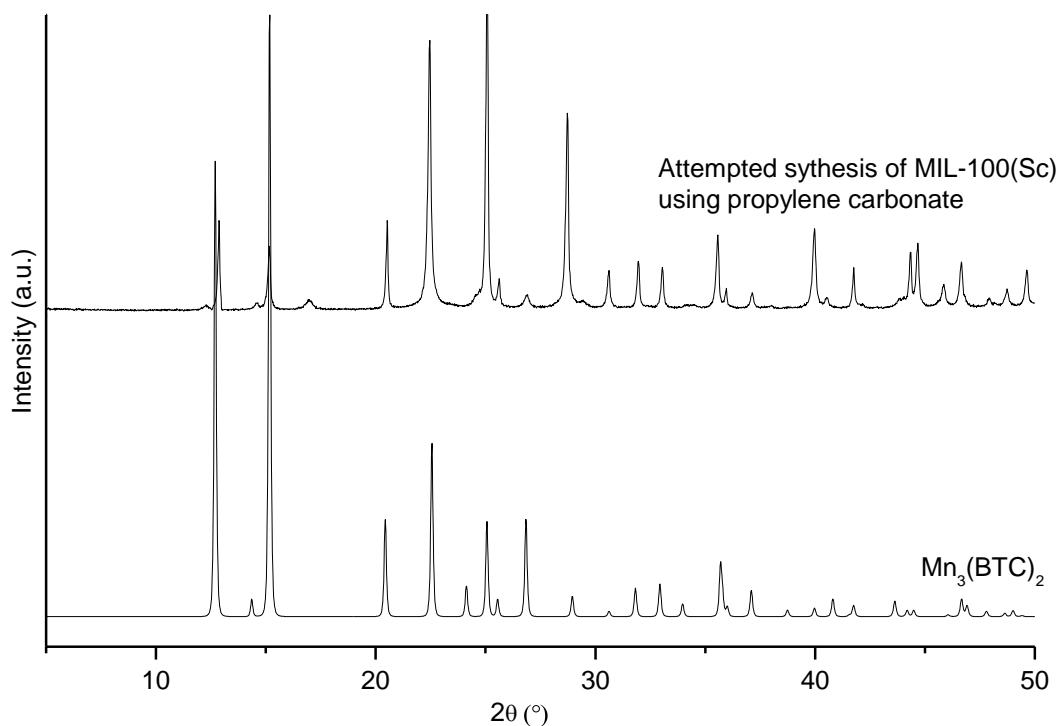


Figure 3.14: PXRD of attempted synthesis of MIL-100(Sc) using propylene carbonate compared to $Mn_3(BTC)_2$

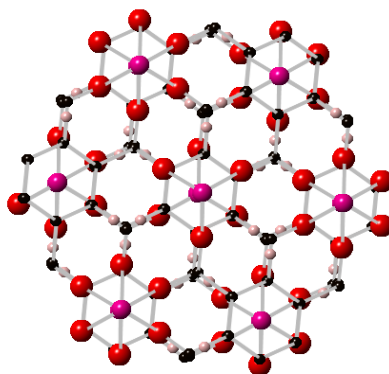


Figure 3.15: View down the c axis of $Mn_3(BTC)_2$. Scandium atoms are shown in pink spheres, red spheres represent oxygen atoms, black spheres are carbon atoms of the trimesic acid and white spheres hydrogen atoms

Figure 3.14 shows the PXRD pattern of the obtained material compared to a simulated pattern of $Mn_3(BTC)_2$. The peak positions of the materials are very similar but intensities differ strongly (Le Bail). Rietveld refinement was carried out in which modification of the initial $Mn_3(BTC)_2$ structure was explored, to determine if the Sc-

containing material was structurally related, but no success was achieved. The material is non-porous, with a very low BET surface area.

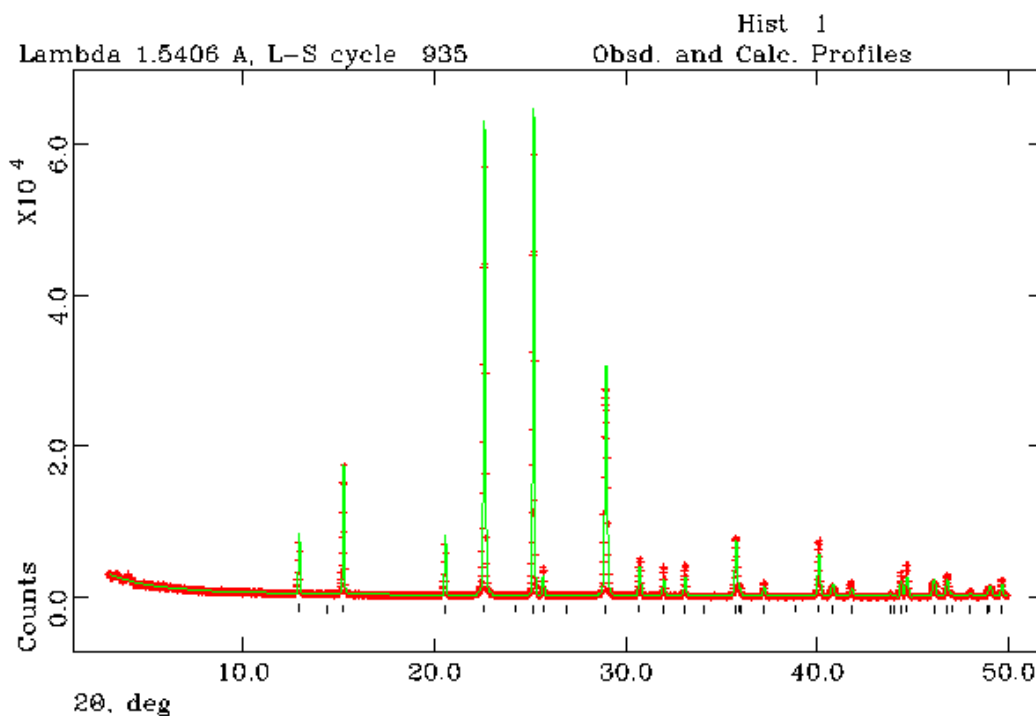


Figure 3.16: *Le Bail* fit of product obtained from synthesis of MIL-100(Sc) using propylene carbonate

The unsuccessful attempts of the synthesis of MIL-100(Sc) using alternative solvents suggest that DMF is required in the synthesis, possibly by directing the reaction towards the product. This led to the idea that, rather than completely eliminating DMF (which has proved to be unsuccessful) a mixture of other solvents with DMF could be used to reduce the overall DMF solvent usage. Synthesis using solvent mixtures of DMF/H₂O with H₂O contents >90% were successful, although the MIL-100(Sc) material synthesised displayed a slight decrease in crystallinity compared to the material synthesised in DMF alone. The yield of the product is reduced, to 54% compared to 89% obtained by reflux and the BET surface area was slightly reduced to 1089 m² g⁻¹ which in turn slightly affected catalytic activity (discussed in chapter 4). A relationship between the yield and BET surface area was observed with increasing DMF concentration. The same behaviour was also observed when using ethanol as the solvent combined with DMF but again the yield was reduced along with the surface area.

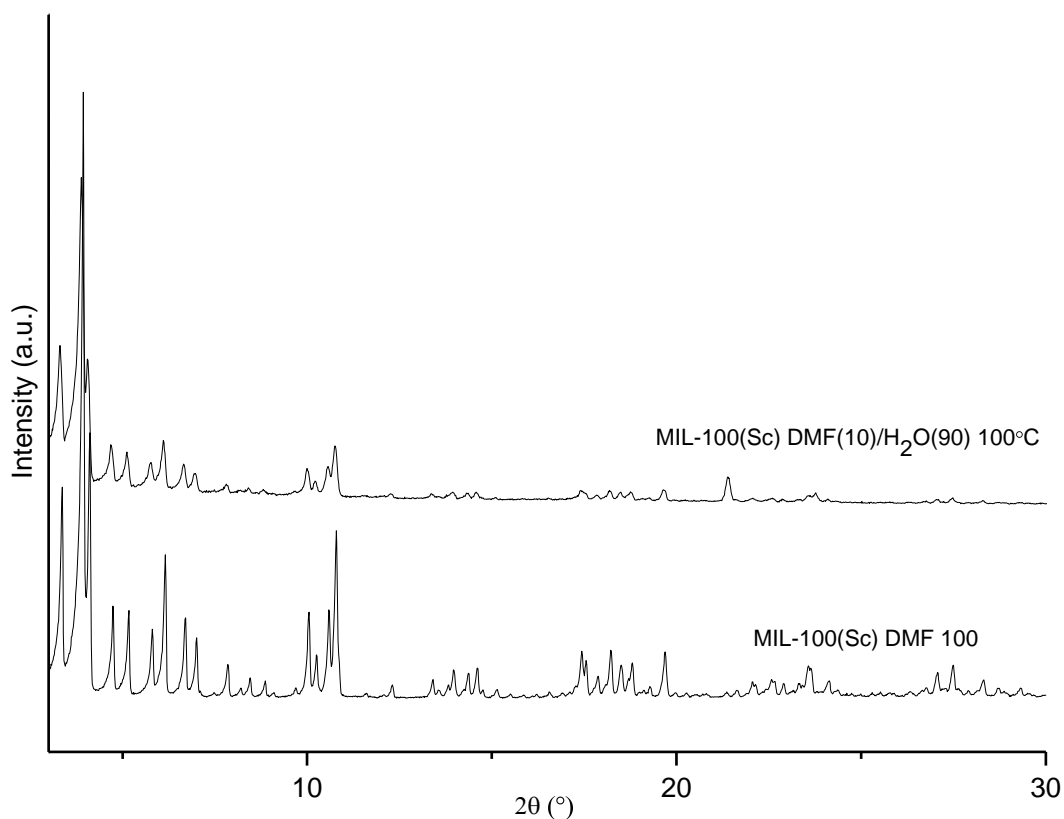


Figure 3.17: PXRD pattern of MIL-100(Sc) synthesised using a mixture of water (top) and DMF (bottom) compared to the material synthesised using 100% DMF

Faster more efficient routes to synthesising MIL-100(Sc) have been demonstrated with both microwave and reflux techniques greatly reducing the reaction time and maintaining high yields. Unfortunately, the use of alternative solvents for the synthesis of MIL-100(Sc) was not as successful, and the reaction appears to require DMF at least as a component of the reaction solvent. MIL-100(Sc) can be synthesised reducing the amount of DMF and introducing water or ethanol as a co-solvent.

3.3. Conclusion Part A

The synthesis of known MOF materials have been carried out and the successful modification of some of these syntheses has been achieved. It has been shown that hydrothermal synthesis of STA-12(Ni) requires 72 h for complete crystallisation, similar high surface areas can be obtained *via* syntheses of much shorter duration using alternative methods of synthesis. By simply changing the synthesis method to reflux, reaction time can be reduced from 72 to 8 h producing STA-12(Ni) with similar crystallite size, maintaining high crystallinity and high BET surface area. STA-12(Ni) can also be synthesised using microwave heating, reducing the synthesis time even

further and producing a material with much smaller crystallite size but comparable BET surface area. Unfortunately, after many attempts with different solvent combinations, room temperature synthesis was not achieved. The lowest temperature required for synthesis of STA-12(Ni) is 373 K.

Similar variations in synthesis methods were attempted for MIL-100(Sc). High yields, good crystallinity and high BET surfaces areas could be produced with shorter reaction times using microwave and reflux syntheses. Screening for an alternative solvent in the synthesis of MIL-100(Sc) proved very difficult and little advancement was made in this area as most other solvents simply returned starting material or non-crystalline material while reaction in propylene carbonate gave an alternative phase. Even though many different solvents, alternative ligands and other scandium sources were attempted, DMF appeared to be required for the synthesis of MIL-100(Sc) although it was possible to prepare MIL-100(Sc) with a 1:9 DMF:water mixture, albeit with a reduced yield and slightly decreased BET surface area.

Part B: Characterisation of the Lewis acidic sites of MIL-100(Sc)

3.4. Probing of Lewis acidic sites of MIL-100(Sc) using in-situ IR

In this section, the measurement of Lewis sites on MIL-100(Sc) activated in different ways is described. The method used to determine the number of accessible Lewis acid sites and their strength was the infra-red spectroscopy of the molecules CO and CD₃CN, which are effective probes for Lewis acidic, coordinatively unsaturated metal cation sites in MOFs, through interaction via their lone pairs.

Previously, such studies have been performed on MIL-100, CPO-27 and STA-12 solids that are tested as Lewis acid catalysts in this thesis. Table 3.7 and Table 3.8 gives the CO and C≡N (CD₃CN) vibration frequencies observed in a range of MOFs of these three structure types with different metal compositions. The free molecules show frequencies of 2143 (CO) and 2257 cm⁻¹ (CD₃CN) respectively. Previously, STA-12(Ni) and (Co) have been examined and CO frequencies of 2170 and 2140 cm⁻¹ have been measured for CO adsorbed on the coordinatively unsaturated Ni²⁺ and Co²⁺, respectively.²² Similarly CPO-27(Ni) has also been probed using CO. It was found that three separate bands are observed when the material is dosed with CO, at 2134 cm⁻¹ due to physisorbed CO, and at 2127 and 2110 cm⁻¹ due to CO bound to the Ni²⁺ site.²³

In this thesis, similar experiments were performed to follow the effects of different pre-treatments on the Sc³⁺ Lewis acidic sites in MIL-100(Sc). The synthesis of MIL-100(Sc) involves the use of DMF as a solvent, and this high boiling point solvent is not readily removed from the pores and the active sites. It has previously been shown that extraction of DMF by stirring in methanol for 24 h, followed by drying at 323 K, increases the surface area from 1242 cm⁻¹ to 1544 m² g⁻¹, corresponding to a significant increase in available porosity. In this thesis, the methanol activation was attempted at room temperature for 16 h and 5 days at 373 K (in an autoclave). No significant differences in the surface area were measured and the catalytic conversion in the Friedel-Crafts Michael addition reaction (see Chapter 4, Section 2) remained constant within experimental error.

The probing by IR of the Lewis acidity of the sample prepared with and without methanol washing and heated at different temperatures was therefore performed to establish the optimum activation conditions using this approach. The experimental IR

procedure used to probe MIL-100(Sc) is described in the Experimental Section 7.4 (P.188).

3.4.1. Temperature effects on MIL-100(Sc)

Using IR the Lewis acidic sites of both the as-prepared and methanol-activated MIL-100(Sc) materials after thermal activation were probed and compared to quantify the difference in their activities and compare them to previously-synthesised MIL-100 materials. Generally, dehydration at 423 K under vacuum is carried out before use in a reaction, and the materials are activated at 423 K and 523 K to investigate the effects of heating at a higher temperature. Deuterated acetonitrile (CD_3CN) and carbon monoxide (CO) were used as IR probes.

3.4.1.1. As-prepared MIL-100(Sc)

As-prepared MIL-100(Sc) was loaded into the IR spectrometer and heated to 523 K stepwise under vacuum with a heating dwell of 90 min at 423 K. An IR spectrum was collected every 25 K to follow solvent removal from the material.

Figure 3.18 shows the spectra in which the peaks at 2945 and 2873 cm^{-1} and are characteristic of DMF in the pores. These peaks decrease in intensity upon heating to 523 K, but are not completely removed. The peak at 3080 cm^{-1} remains unchanged, and is assigned to the C-H stretch of the trimesate linkers. In the lower region of the IR, peaks at 1111 and 892 cm^{-1} can also be attributed to DMF and are also observed to decrease in intensity.

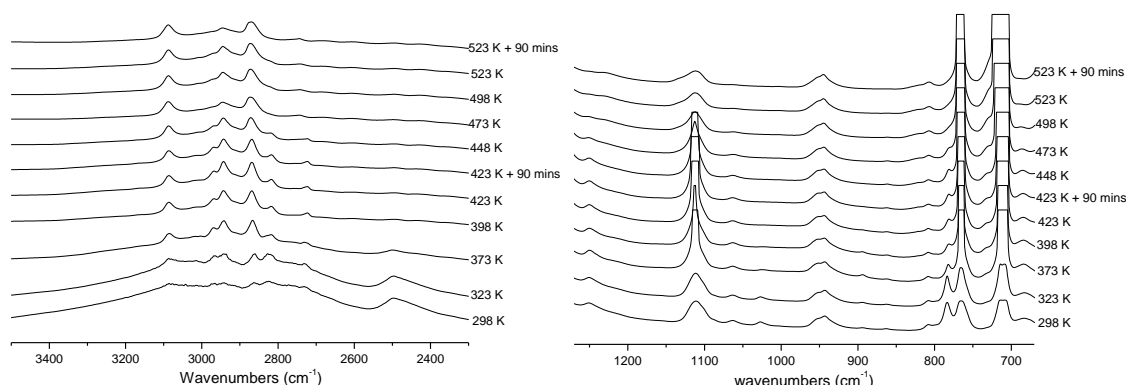


Figure 3.18: (a) IR spectra of as-prepared MIL-100(Sc) material from 2100 – 4000 cm^{-1} (b) IR spectra of as-prepared MIL-100(Sc) material from 670 – 1270 cm^{-1}

3.4.1.2. Methanol-activated MIL-100(Sc)

Methanol-activated MIL-100(Sc) was also investigated by FTIR and was heated from 298 K to 523 K. The most intense peak is observed at 3672 cm^{-1} , and this is attributed to the hydroxyl group of methanol, possibly bound to the Sc^{3+} sites Figure 3.19(a)). Methanol is removed completely upon heating to 448 K, as shown by the decrease in intensity of peaks at 3673 cm^{-1} , 3229 cm^{-1} , 3071 cm^{-1} , 3022 cm^{-1} , 2953 cm^{-1} , 2897 cm^{-1} and 2813 cm^{-1} , all corresponding to resonances of MeOH. The presence of residual DMF is also observed (2941 cm^{-1} , 2869 cm^{-1}). The presence of both DMF and methanol can also be observed in the mid IR (Figure 3.19(b)), where methanol removal is shown by decrease and removal in peaks at 1014 cm^{-1} and 754 cm^{-1} . The peak corresponding to that of DMF reduces as the temperature is increased.

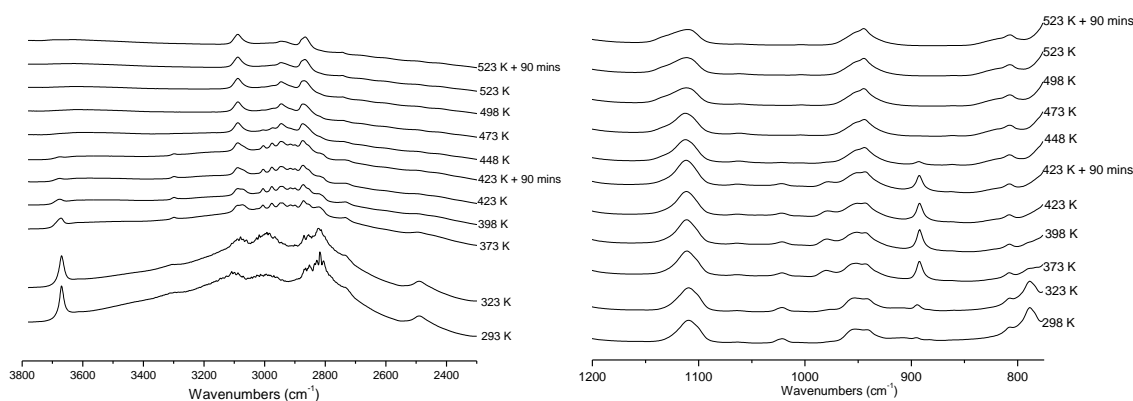


Figure 3.19: (a) IR spectra of methanol-activated MIL-100(Sc) material from $2250 - 3750\text{ cm}^{-1}$ (b) IR spectra of methanol-activated MIL-100(Sc) material from $770 - 1270\text{ cm}^{-1}$

3.4.2. Deuterated acetonitrile dosing of as-prepared and methanol-activated MIL-100(Sc)

As-prepared and methanol-activated materials were probed after thermal activation for the presence of Lewis acidic sites by CD_3CN . Acetonitrile was chosen as a probe molecule as it could help determine the strength of the Lewis acid sites. The nitrogen lone pair acts as an electron donor and binds to the vacant Lewis acid site. A higher shift in wavenumber is observed when electron donor-acceptor complexes form between the nitrogen and Lewis acid site. A higher wavenumber indicates a stronger interaction between the lone pair and vacant site therefore a stronger Lewis acid.^{6, 24, 25} Figure 3.20 shows before and after introduction of CD_3CN for both as-prepared MIL-100(Sc) and methanol-activated material.

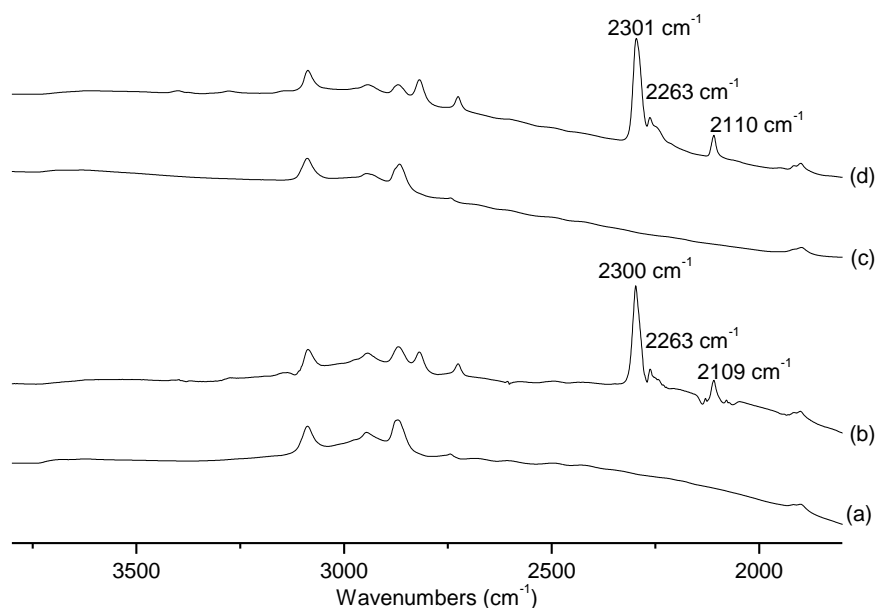


Figure 3.20: IR spectra of before and after CD_3CN dosing on as-prepared and methanol-activated MIL-100(Sc). (a) As-prepared MIL-100(Sc) heated to 523 K (b) After CD_3CN dosing (c) Methanol-activated MIL-100(Sc) heated to 523 K (d) After CD_3CN dosing

The peaks that are observed at $2300-2301\text{ cm}^{-1}$ and 2263 cm^{-1} can be attributed to the $C\equiv N$: group of CD_3CN adsorbed on the material, the former is due to the coordination to the unsaturated metal site Sc^{3+} and the latter due to physisorbed CD_3CN .

Table 3.7: CD_3CN Frequency shift of different coordinated MIL-100 as a probe of Lewis acidity

MOF	Chemisorbed CD_3CN frequency (cm^{-1})
APMIL-100(Sc)*	2300
MeOHMIL-100(Sc)**	2301
MIL-100(Fe) ²⁶	2304
MIL-100(Cr) ²⁷	2305
MIL-100(Al) ²⁸	2321

*As-prepared MIL-100(Sc). ** Methanol-activated MIL-100(Sc).

The results obtained for MIL-100(Sc) can be compared to those previously obtained in the literature for other MIL-100 materials. It should be noted that each one of these materials has been activated slightly differently to that of MIL-100(Sc). In the case of MIL-100(Al) the material was heated in DMF for 5 h at 423 K, filtered refluxed in

water at 373 K and finally heated under vacuum at 523 K for 5 h.²⁸ MIL-100(Cr) required washing with acetone and water and drying in air at room temperature.²⁷ MIL-100(Fe) was refluxed in water at 373 K for 3 h and dried at room temperature.⁹ Compared to previously probed MIL-100 materials including MIL-100(Al) (which has been found to give the highest apparent Lewis acidity when probed with CD₃CN) MIL-100(Sc) does not show as high strength Lewis acidity (Table 3.7). Volkringer *et al.* used CD₃CN to test the Lewis acidity of MIL-100(Al) which observed a shift of 2321 cm⁻¹ caused by the strong bonding of the CD₃CN species on the coordinatively unsaturated site of Al³⁺.²⁸ The higher shift of the coordinated material represents a higher Lewis acidity in the material. However the shift is similar to that of MIL-100(Cr)²⁷ and MIL-100(Fe)²⁶ (2305 cm⁻¹ and 2304 cm⁻¹) showing they have similar Lewis acidity to MIL-100(Sc) by this criterion.

3.4.3. CO adsorption of as-prepared and methanol-activated MIL-100(Sc) at 423 K and 523 K

To investigate further the Lewis acidity of MIL-100(Sc), CO adsorption was performed after activation at different temperatures to determine the concentration of coordinatively unsaturated sites. MIL-100 MOFs containing different metals have previously been probed by IR using CO so that the results can be compared.

3.4.3.1. As-prepared MIL-100(Sc) heated at 423 K and CO dosed at 100 K

As-prepared MIL-100(Sc) was initially heated to 423 K under vacuum for 4 h and then CO adsorption was carried out at 100 K. The material was dosed with CO from 1.04 μmol to 5.19 μmol and then at an ‘equilibrium’ pressure of 133 Pa, at which pressure all chemisorbing sites are expected to be occupied.

Small doses of CO are introduced into the sample to allow calibration of the $\nu(\text{CO})$ molar absorption coefficient because all admitted CO is expected to be taken up at these low pressures (see appendix). The band forming at 2182 cm⁻¹ can be attributed to chemisorption of CO on the sample, which increases due to the continuous increase in the concentration of CO molecules coordinated to the Sc³⁺ site Figure 3.22. Using the known concentration of CO, an accurate value was determined for the molar absorption coefficient.

Table 3.8: Frequency of coordinated CO bound to different metal forms of MIL-100 materials, and concentration of Lewis acid sites for each material

MOF	Activation temperature (K)	Chemisorbed CO frequency (cm ⁻¹)	No. of Lewis acid sites (mmol g ⁻¹)
APMIL-100(Sc)*	423	2180	0.59
MeOHMIL-100(Sc)**	423	2180	0.96
MIL-100(Fe) ²⁶	423	2192	1.94
MIL-100(Cr) ²⁷	423	2173	2.6
MIL-100(Al) ²⁸	423	2183	1.15
APMIL-100(Sc)*	523	2182	1.96
MeOHMIL-100(Sc)**	523	2180	1.96
MIL-100(Fe) ²⁶	523	2200, 2192, 2184	3.66
MIL-100(Cr) ²⁷	523	2170, 2166	3.5
MIL-100(Al) ²⁸	523	2183	1.8

*As-prepared MIL-100(Sc). **Methanol-activated MIL-100(Sc).

The total concentration/number of Lewis acid sites was then calculated from the absorbance measured at the higher pressure where all the sites are expected to be occupied. MIL-100(Sc) activated at 423 K was found in this way to have 0.59 mmol g⁻¹ sites. Compared to MIL-100(Fe) which has 1.94 mmol g⁻¹²⁶ and MIL-100(Cr) with 2.6 mmol g⁻¹²⁶ (activated at 423 K) (Table 3.8), MIL-100(Sc) has fewer sites, closer to MIL-100(Al) 1.15 mmol g⁻¹ at 423 K.²⁸ The strong band at 2137 cm⁻¹ at higher P_{co} results is from physisorbed CO, which has a C≡O vibration frequency similar to that observed for gas phase CO (2143 cm⁻¹). CO is observed in IR due to three types of interactions, the first of which is due to σ-bond interactions. This is the interaction between a lone pair on the carbon and an empty orbital which leads to a shift in electron density from CO to metal centre. The stronger the interaction the higher the wavenumber. The second interaction is due to π bonding caused by overlap of filled d orbitals in the metal and p orbitals in CO. Electrons are donating from the metal to empty π* antibonding orbital introducing more electron density into the CO molecule reducing the CO bond strength therefore reducing the wavenumber of the stretching frequency. The third interaction is very rare, it occurs when a pair of electrons from the carbon on the CO group π-bond to the metal. Like sigma bonding this also increases the metal carbon bond therefore increasing the wave number observed.^{24, 29, 30} In Lewis acid materials like the MIL-100 materials studied the π back donating interaction is much weaker than the σ bonding interaction therefore higher wavenumbers are observed.

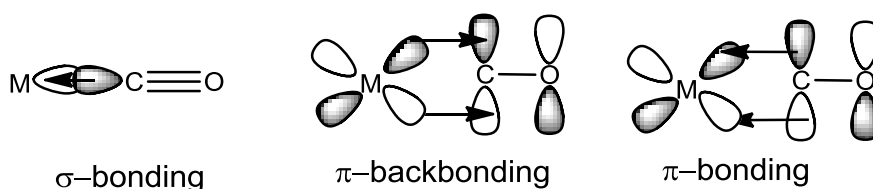


Figure 3.21: Interactions observed between metal and CO

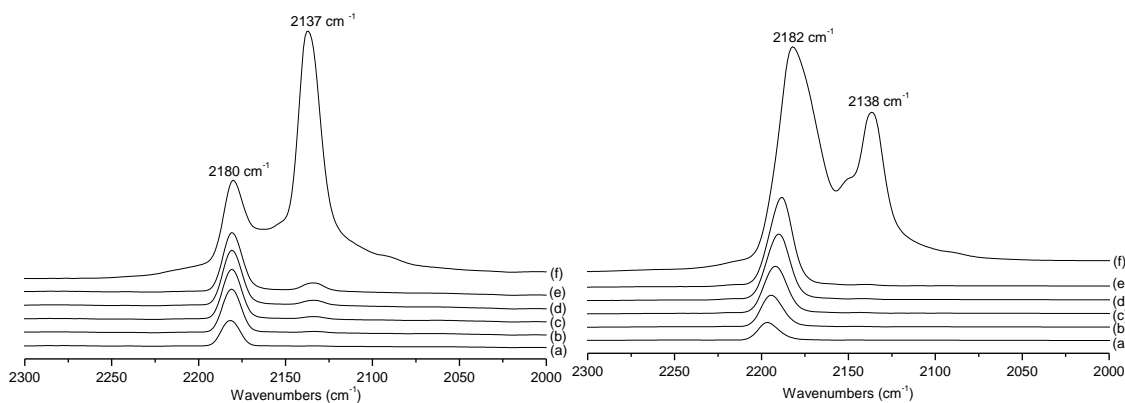


Figure 3.22: Infra-red spectra of MIL-100(Sc) as-prepared after activation at (i) 423 K (ii) 523 K and introduction of CO doses from 1.04 μmol (a) 2.08 μmol (b) 3.12 μmol (c) 4.16 μmol (d) 5.19 μmol (e) and the introduction of equilibrium pressure (f)

3.4.3.2. As-prepared MIL-100(Sc) heated at 523 K and CO dosed at 100 K

The experiment was also carried out on as-prepared MIL-100(Sc) activated at the higher temperature of 523 K. The molar adsorption coefficient of this material is 2.2 $\mu\text{mol}^{-1}\text{cm}$ (previous work from MIL-100(Cr) and MIL-100(Al) show they are both very similar at around 2.1 $\mu\text{mol}^{-1}\text{cm}$) and the amount of Lewis acidic sites is 1.96 mmol g^{-1} . This equates to ~ 1.5 active sites per trimer. Compared to MIL-100(Cr) and MIL-100(Fe) the amount of Lewis acidic sites is again much lower with 3.41 mmol g^{-1} sites in MIL-100(Cr) and MIL-100(Fe) 3.66 mmol g^{-1} (~ 2 active sites per trimer), but it is similar to that found in MIL-100(Al). These results show again DMF remain occluded and cannot all be easily removed by heating. Extraction *via* methanol was an alternative approach to DMF removal.

3.4.3.3. Methanol-activated MIL-100(Sc) heated at 423 K and CO dosed at 100 K

Methanol-activated MIL-100(Sc) treated by washing in methanol for 24 h was examined after thermal treatment at 423 K and then at 523 K to compare with as-prepared MIL-100(Sc) heated at these temperatures.

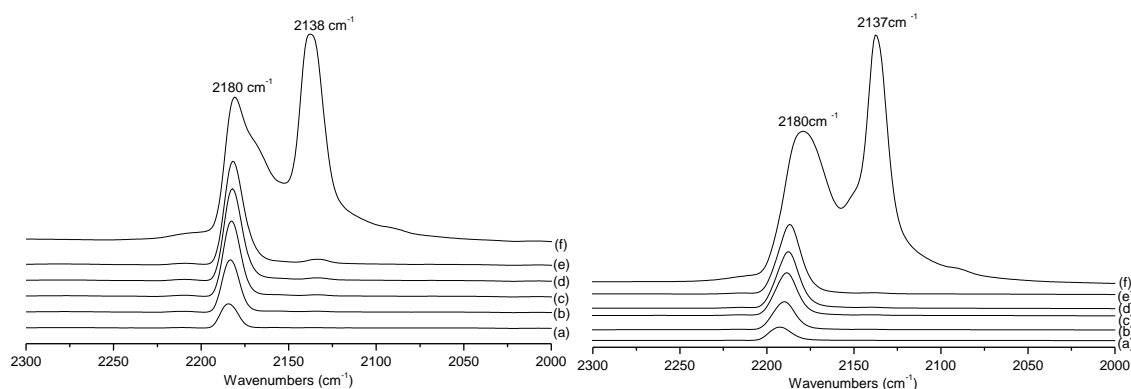


Figure 3.23: Infra-red spectra of methanol-activated MIL-100(Sc) after activation at (i) 423 K (ii) 523 K and introduction of CO doses from 1.04 μmol (a) 2.08 μmol (b) 3.12 μmol (c) 4.16 μmol (d) 5.19 μmol (e) and the introduction of equilibrium pressure (f)

After activation at 423 K the amount of Lewis acidic sites in the methanol-washed sample slightly increased to 0.8 mmol g⁻¹ compared to the untreated sample at the same temperature, but this remains lower than other materials in the MIL-100 series activated under similar conditions.

3.4.3.4. Methanol-activated MIL-100(Sc) heated at 523 K and CO dosed at 100 K

The same material was heated to 523 K and dosed with CO to determine the accessible Sc³⁺ sites. This gave a significant increased number of Lewis acid sites compared to the previous experiments, 1.96 mmol g⁻¹, this is a large increase from the material activated at 423 K but still lower than that of MIL-100(Cr) and (Fe).

This increase is caused by the removal of more DMF at this temperature. However, N₂ adsorption studies on MIL-100(Sc) heated at 523 K show an associated reduction in BET surface from 1544 m² g⁻¹ to 1256 m² g⁻¹ upon heating at 523 K. This may be caused by the formation of defects in the material due to the proximity of the heating temperature to the decomposition temperature. The same reduction in surface area was observed upon heating the as-prepared MIL-100(Sc) to 523 K. Furthermore, the material degassed at the higher temperature was less selective when used in the carbonyl ene reaction (see chapter 4) so that methanol washing followed by heating at 423 K was adopted as a standard activation.

3.5. Conclusion Part B

MIL-100(Sc) was probed using FTIR and probe molecules to determine the number and strength of Lewis acid sites present. Using CD₃CN as a probe molecule showed that the material had similar Lewis acidic strength to the previously synthesised materials MIL-100(Cr, Fe), but lower than that of MIL-100(Al). Both the as-prepared material and the methanol-washed material showed the DMF was retained in the structure even after heating to 523 K: methanol-washing removed some of this. The concentration of Lewis acid sites in the material was also measured, using CO as a probe molecule. The methanol-washed material had almost double the number of Lewis sites compared to the as-prepared material, but in each case this was lower than in MIL-100(Cr) or MIL-100(Fe). The amount of sites present at 523 K was similar for both materials which amounted to about 1.5 sites Lewis acid sites per trimer, again less than observed for MIL-100(Cr) or MIL-100(Fe). Although Lewis acidity of the materials is important it will be discussed in chapter 4 why the reduced strength of Sc³⁺ as a Lewis acid may actually be of benefit to MIL-100(Sc) in catalysis.

3.6. References

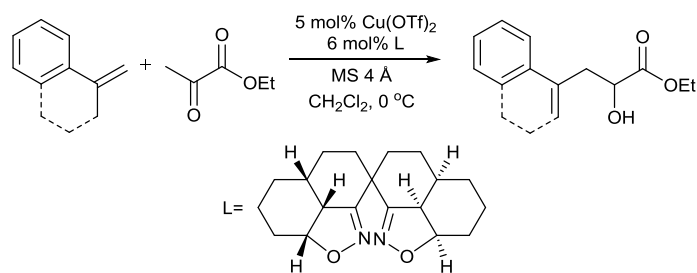
1. H. Fei, L. Paw U, D. L. Rogow, M. R. Bresler, Y. A. Abdollahian and S. R. J. Oliver, *Chem. Mater.*, 2010, **22**, 2027-2032.
2. C. M. MacNeill, C. S. Day, S. A. Gamboa, A. Lachgar and R. E. Noffle, *J. Chem. Crystallogr.*, 2010, **40**, 222-230.
3. M. Schlesinger, S. Schulze, M. Hietschold and M. Mehring, *Microporous Mesoporous Mater.*, 2010, **132**, 121-127.
4. M. T. Wharmby, J. P. S. Mowat, S. P. Thompson and P. A. Wright, *J. Am. Chem. Soc.*, 2011, **133**, 1266-1269.
5. P. D. C. Dietzel, Y. Morita, R. Blom and H. Fjellvag, *Angew. Chem. Int. Ed.*, 2005, **44**, 6354-6358.
6. L. Alaerts, E. Seguin, H. Poelman, F. Thibault-Starzyk, P. A. Jacobs and D. E. De Vos, *Chem.-Eur. J.*, 2006, **12**, 7353-7363.
7. J. P. S. Mowat, S. R. Miller, A. M. Z. Slawin, V. R. Seymour, S. E. Ashbrook and P. A. Wright, *Microporous Mesoporous Mater.*, 2011, **142**, 322-333.
8. P. Long, H. Wu, Q. Zhao, Y. Wang, J. Dong and J. Li, *Microporous Mesoporous Mater.*, 2011, **142**, 489-493.
9. P. Horcajada, S. Surblé, C. Serre, D.-Y. Hong, Y.-K. Seo, J.-S. Chang, J.-M. Greneche, I. Margiolaki and G. Férey, *Chem. Commun.*, 2007, 2820-2822.
10. C. Volkringer, D. Popov, T. Loiseau, G. Férey, M. Burghammer, C. Riekel, M. Haouas and F. Taulelle, *Chem. Mater.*, 2009, **21**, 5695-5697.
11. D.-Y. Hong, Y. K. Hwang, C. Serre, G. Férey and J.-S. Chang, *Adv. Funct. Mater.*, 2009, **19**, 1537-1552.
12. P. D. C. Dietzel, B. Panella, M. Hirscher, R. Blom and H. Fjellvag, *Chem. Commun.*, 2006, 959-961.

13. M. T. Wharmby, G. M. Pearce, J. P. S. Mowat, J. M. Griffin, S. E. Ashbrook, P. A. Wright, L.-H. Schilling, A. Lieb, N. Stock, S. Chavan, S. Bordiga, E. Garcia, G. D. Pirngruber, M. Vreeke and L. Gora, *Microporous Mesoporous Mater.*, 2012, **157**, 3-17.
14. J. A. Groves, S. R. Miller, S. J. Warrender, C. Mellot-Draznieks, P. Lightfoot and P. A. Wright, *Chem. Commun.*, 2006, 3305-3307.
15. J.-L. Zhuang, D. Ceglarek, S. Pethuraj and A. Terfort, *Adv. Funct. Mater.*, 2011, **21**, 1442-1447.
16. L. H. Wee, N. Janssens, S. R. Bajpe, C. E. A. Kirschhock and J. A. Martens, *Catal. Today*, 2011, **171**, 275-280.
17. D. J. Tranchemontagne, J. R. Hunt and O. M. Yaghi, *Tetrahedron*, 2008, **64**, 8553-8557.
18. J. Klinowski, F. A. Almeida Paz, P. Silva and J. Rocha, *Dalton Trans.*, 2011, **40**, 321-330.
19. A. G. Marquez, A. Demessence, A. E. Platero-Prats, D. Heurtaux, P. Horcajada, C. Serre, J.-S. Chang, G. Férey, V. Antonio de la Pena-O'Shea, C. Boissiere, D. Grosso and C. Sanchez, *Eur. J. Inorg. Chem.*, 2012, 5165-5174.
20. R. Canioni, C. Roch-Marchal, F. Secheresse, P. Horcajada, C. Serre, M. Hardidan, G. Férey, J.-M. Greneche, F. Lefebvre, J.-S. Chang, Y.-K. Hwang, O. Lebedev, S. Turner and G. Van Tendeloo, *J. Mater. Chem.*, 2011, **21**, 1226-1233.
21. S. O. H. Gutschke, M. Molinier, A. K. Powell, R. E. P. Winpenney and P. T. Wood, *Chem. Commun.*, 1996, 823-824.
22. S. R. Miller, G. M. Pearce, P. A. Wright, F. Bonino, S. Chavan, S. Bordiga, I. Margiolaki, N. Guillou, G. Feerey, S. Bourrelly and P. L. Llewellyn, *J. Am. Chem. Soc.*, 2008, **130**, 15967-15981.
23. S. Chavan, F. Bonino, J. G. Vitillo, E. Groppo, C. Lamberti, P. D. C. Dietzel, A. Zecchina and S. Bordiga, *Phys. Chem. Chem. Phys.*, 2009, **11**, 9811-9822.
24. J. S. Chen, J. M. Thomas and G. Sankar, *J. Chem. Soc., Faraday Trans.*, 1994, **90**, 3455-3459.
25. E. E. Platero, M. P. Mentrui and C. Morterra, *Langmuir*, 1999, **15**, 5079-5087.
26. H. Leclerc, A. Vimont, J.-C. Lavalley, M. Daturi, A. D. Wiersum, P. L. Llewellyn, P. Horcajada, G. Férey and C. Serre, *Phys. Chem. Chem. Phys.*, 2011, **13**, 11748-11756.
27. A. Vimont, J. M. Goupil, J. C. Lavalley, M. Daturi, S. Surblé, C. Serre, F. Millange, G. Férey and N. Audebrand, *J. Am. Chem. Soc.*, 2006, **128**, 3218-3227.
28. C. Volkringer, H. Leclerc, J.-C. Lavalley, T. Loiseau, G. Férey, M. Daturi and A. Vimont, *J. Phys. Chem. C*, 2012, **116**, 5710-5719.
29. A. Zecchina and C. O. Arean, *Chem. Soc. Rev.*, 1996, **25**, 187.
30. C. Morterra and G. Magnacca, *Catal. Today*, 1996, **27**, 497-532.

4. Lewis acidic MOFs as catalysts for C-C and C=N bond-forming reactions

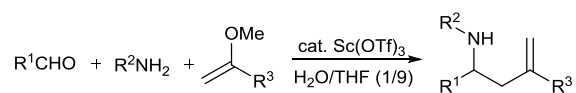
4.1. Intermolecular carbonyl ene reaction using Lewis acidic metal organic framework catalysts

Lewis acid catalysts are widely used within the pharmaceutical and fine chemical industries, mainly in homogeneous form and often for C-C bond formation reactions. Typically they include metals such as Ti^{4+} , Fe^{3+} , Cu^{3+} , Al^{3+} , Sn^{4+} , Zn^{2+} and Sc^{3+} .¹⁻⁴ The spiral bis(oxazolinyl) ('box') Cu(II) homogeneous catalyst has been shown to be an active catalyst in the carbonyl ene reaction of various olefins and ethyl glyoxalate (Scheme 4.1). This was originally reported by Evans *et al.*⁵ and later developed by Wakita *et al.*⁶ The reaction proceeded well with distilled ethyl glyoxalate to give high conversions and selectivity at low temperatures, and catalysis of this (and related reactions) using MOF catalysts is discussed in Section 4.1.1.



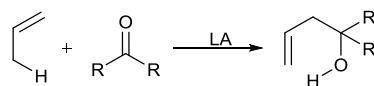
Scheme 4.1: Carbonyl ene reaction between an enophile and ethyl glyoxalate using a copper(II)-based homogeneous catalyst

Kobayashi reported the use of scandium triflate as a homogeneous catalyst in C-C bond formation reactions.^{1, 2, 7, 8} The same group has demonstrated the successful use of scandium triflate as a catalyst in aldol, Michael, Diels-Alder and Friedel-Crafts reactions. The catalyst has also been shown to be active in aqueous conditions, as seen in the Mannich-type reactions of an aldehyde, an amine, and a vinyl ether (Scheme 4.2). This reaction was shown to give high conversions (up to 93%) and the catalyst could be reused after the removal by column chromatography. The successful use of scandium in homogeneous catalysis led us to the investigation of its use in heterogeneous MOF form, as part of a metal organic framework.



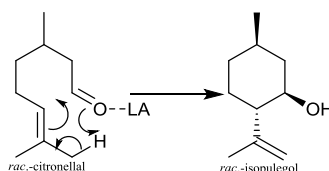
Scheme 4.2: Carbonyl ene reaction catalysed by scandium triflate in aqueous solution

There has been great interest in polymer-supported Lewis acid catalysts because these catalysts may be readily separated and recycled.⁷⁻⁹ However, they tend to be less active than homogeneous catalysts, have quite low loadings of active sites and are difficult to synthesise on a large scale. Zeolites impregnated with Lewis acidic metal cations have also attracted attention¹⁰⁻¹⁴ but low selectivity and relatively low porosity and pore size remains a problem. Metal organic frameworks (MOFs) containing the metals listed above should give heterogeneous catalysts for these types of reactions, introducing easy recovery and reusability of the catalyst especially if the cations can be prepared to be coordinatively unsaturated, or to allow ligand exchange at least one position. For this reason the MOFs HKUST-1(Cu), STA-12(Ni, Co), STA-16(Ni, Co), CPO-27(Ni,Co), MIL-100(Sc, Cr, Fe, Al), MIL-101(Cr), MIL-88(Sc) and socMOF(Sc) were investigated as Lewis acidic catalysts and the carbonyl ene reaction was chosen as a model reaction to test their Lewis acidity (Scheme 4.3).



Scheme 4.3: Lewis acid catalysed carbonyl ene reaction between an alkene with an allylic hydrogen and enophile

The reaction is potentially 100% atom efficient. Aside from the desirability of such reactions in a general sense, this means that at reaction completion, the heterogeneous catalyst can be filtered off and the solvent removed to leave the product.¹⁵



Scheme 4.4: Intramolecular carbonyl ene reaction of citronellal catalysed by a Lewis acid catalyst to form isopulegol

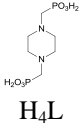
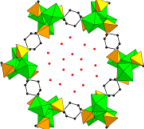
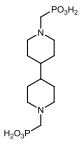
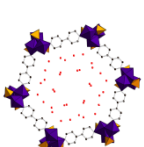
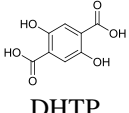
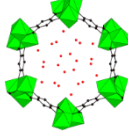
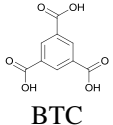
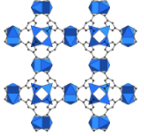
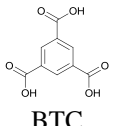
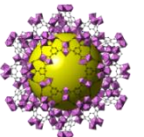
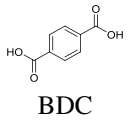
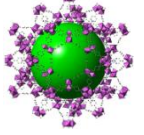
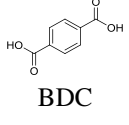
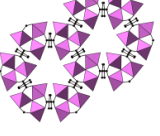

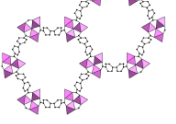
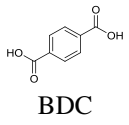
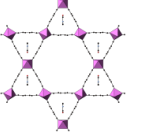
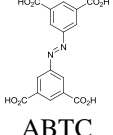
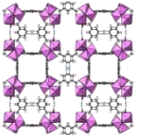
The zeolite Sn-Beta has been reported to be an active Lewis acid catalyst for the intramolecular carbonyl ene reaction of citronellal to form isopulegol, (Scheme 4.4)

with 98 % selectivity and 85% diastereoselectivity. Isopulegol can be catalytically hydrogenated to form menthol, which is widely used, especially in pharmaceuticals (for example in decongestants).¹⁶ The same reaction has been carried out to test the Lewis acidity of some MOFs including HKUST-1(Cu).¹⁷ It has been reported that HKUST-1(Cu) exhibits Lewis acidity upon removal of coordinated water to reveal coordinatively unsaturated metal sites.¹⁸ Alaerts *et al.* showed that HKUST-1 could be used as a selective catalyst for the formation of (-)-isopulegol. The reaction went to completion with 69% selectivity to the desired (-)-isopulegol, better than most other materials tested, with the exception of ZnBr₂. Lewis acid sites cause catalysts to be more selective for (-)-isopulegol so that it was suggested that Lewis acid sites are the active sites in the material, rather than Bronsted acid sites.¹⁷ HKUST-1(Cu) is a good benchmark material for comparison with other MOF catalysts because it has been studied in great detail.¹⁹⁻²⁶

Very recently, the complete process (intramolecular carbonyl ene and hydrogenation reactions) has been carried out using a palladium-doped-MIL-101(Cr) catalyst. This catalyses both reactions needed to form menthol in one reaction vessel without the need to isolate intermediates. The catalyst utilises the coordinatively unsaturated Cr³⁺ cations to carry out the Lewis acid catalysis and the palladium nanoparticles for the hydrogenation. The reaction achieved 70% conversion to the desired menthol product with 16% conversion to other menthol products.²⁷

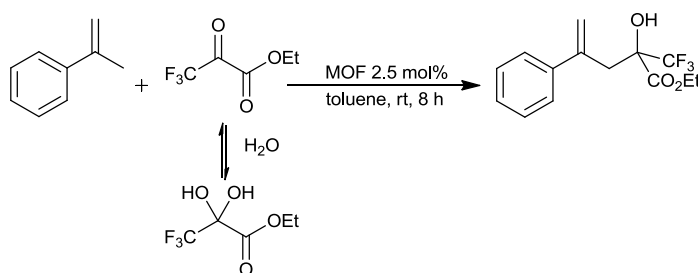
Otherwise, there remains relatively little research on the use of MOFs for catalysis of this attractive C-C bond-forming reaction, and indeed development of the scope and utility of the *intermolecular* carbonyl ene reaction is required irrespective of the benefits of catalyst recovery that can be expected using MOFs. The carbonyl ene reaction is a good method to form C-C bonds and can occur without any catalyst at elevated temperatures.²⁸ An intermolecular carbonyl ene reaction occurs between an alkene with an allylic hydrogen and an enophile. Lewis acid catalysts make the enophile more electrophilic, and therefore accelerate the reaction, enabling it to occur at much lower temperatures. To probe the activity of MOFs in the intermolecular carbonyl ene reaction many different materials with different metals and ligands (and consequently pore sizes) were tested. Each MOF used in catalysis was synthesised and characterised as described in chapter 3.

Table 4.1: Summary and some characteristics of MOF materials used in catalysis

MOF[Formula]	Ligand	Structure	BET surface area (m ² g ⁻¹)	Connectivity pore type and size /Å
STA-12(Ni/Co) ²⁹ [M ₂ L]	 H ₄ L		675(Ni) 506(Co)	1-D Channels 10
STA-16(Ni/Co) ³⁰ [M ₂ L]	 H ₄ L		1365(Co) 1247(Ni)	1-D Channels 16
CPO-27(Ni/Co) ³¹ [M ₂ (DHTP)]	 DHTP		1210(Ni) 1256(Co)	1-D Channels 11
HKUST-1(Cu) ¹⁷ [Cu ₃ (BTC) ₂]	 BTC		1273	3-D Cages 25 Windows 6
MIL-100 (Sc,Cr,Fe Al) ³²⁻³⁵ [M ₃ O(OH)(BTC) ₂]	 BTC		1526 (Sc) 1430 (Cr) 1363(Fe) 1255(Cr)	3-D Cages 25 & 30 Windows 5 & 9
MIL-101(Sc/Cr) ³⁶ [M ₃ O(OH)(BTC) ₂]	 BDC		640(Sc) 3250(Cr)	3-D Cages 29 & 34 Windows 12 & 16
MIL-88B(Sc) ³² [Sc ₃ O(OH)(BDC) ₃]	 BDC		<30	3-D Cage 7 Channel <2 (variable)
MIL-88D(Sc) ³⁷ [Sc ₃ O(OH)(BPDC) ₃]	 BPDC		886	3-D Cage 16 Channel 13 (interpenetrated)
MIL-68(Sc) ³⁷ [M ₃ (OH)(BDC)]	 BDC		202	1-D Channel 16
soeMOF(Sc) ³² [Sc ₃ O(ABTC) _{1.5} NO ₃ ⁻]	 ABTC		1384	3D network of 5Å channels

The first reactants tried were α -methylstyrene and ethyl trifluoropyruvate (Scheme 4.5).

A summary of the MOF materials used in catalysis is given in Table 4.1. The materials were chosen due to their differing properties of pore size, connectivity and cation type, to give a wide range. The flexible isoreticular phosphonate structures STA-12 and STA-16 gave the direct opportunity to compare the effect of pore size of the MOF. CPO-27 is a much more rigid structure than STA-12 which enabled the effect of flexibility to be measured. The comparison of trivalent and divalent metal containing MOFs could also be carried out over MIL-100, which can be made using different di- and trivalent metals. MIL-101 (which was available as the Cr- form) has a similar 3D structure to that of MIL-100, but with larger cage and window sizes. MIL-88B also has trimers of metal (III) cation, like MIL-100 and MIL-101 but shows interesting breathing effects depending on the solvent present and is related to MIL-88D but is likely to be an interpenetrated structure without breathing behaviour.



Scheme 4.5: Intermolecular carbonyl ene reaction of α -methylstyrene with ethyl trifluoropyruvate catalysed by various MOF materials

The intermolecular carbonyl ene reaction was expected to be relatively easy to catalyse and since both the reactants and products were less than 10 Å in dimension they would gain access to those MOFs with larger pores. The reaction typically requires an inert atmosphere to avoid the formation of a hydrate of ethyl trifluoropyruvate. All the MOF materials were tested in toluene as solvent to allow easy removal once the reaction had occurred, to prevent inhibition by solvent binding at the Lewis acid sites and to avoid possible issues of reproducibility that can arise when using protic solvents or those that can decompose to give reactive species (e.g. $\text{CH}_2\text{Cl}_2 \rightarrow \text{HCl} + \text{CCl}_4$). A loading of 2.5 mol% catalyst was used, based on mol% metal cation within the MOF (and so eliminating any differences due to the weight or stoichiometry of different ligands). The MOF materials were pre-activated under vacuum at elevated temperatures (STA-12,

523 K; STA-16, 423 K; CPO-27, 463 K; HKUST-1(Cu), 373 K; MIL materials, 423 K (consistent with TGA and IR data).

The conversion of the reaction can be monitored using $^{19}\text{F}\{^1\text{H}\}$ NMR in which three main signals could be seen; unreacted ethyl trifluoropyruvate ($\delta = -76.1$ ppm), hydrated ethyl trifluoropyruvate ($\delta = -82.7$ ppm) and the product ($\delta = -78.7$ ppm). In some cases an internal standard was used (1-fluoronaphthalene) and for some samples product conversions were checked by ^1H NMR. All analytical methods gave similar results, confirming the assay was quantitative.

4.1.1. Intermolecular carbonyl ene reactions catalysed by MOFs containing divalent metals

In our model reaction the benchmark MOF catalyst HKUST-1(Cu) gave a conversion of 31 % to product in 8 h and is only 2-3 times better than the uncatalysed reaction. Nickel-based MOFs were an improvement on HKUST-1(Cu). The comparison of MOF materials containing nickel and cobalt with different linkers (phosphonate and carboxylate) and pore sizes was probed. Water could be removed from each of these materials to form five-coordinate metal centres with a coordinatively unsaturated site.

Nickel-containing STA-12 gave a much higher conversion to product than its cobalt analogue (48 vs. 12%). The cobalt-containing MOF did not show increased conversion compared to the control (no catalyst) (Table 4.2). (Cobalt is better known for oxidation reactions and STA-12(Co) has been found to be a highly active oxidation catalyst by Beier *et al.*)³⁸

Surprisingly, increasing the pore size of the STA-12 material by the introduction of another 6-membered ring into the ligand as in STA-16 had no effect on the catalysis. It had been thought that by increasing the pore size the ease of access of the reactant to the coordinatively unsaturated site would be improved, in turn increasing the turnover rate. The results suggest that reaction, rather than diffusion, is rate-limiting.

Table 4.2: Carbonyl ene reactions of α -methylstyrene with ethyl trifluoropyruvate (Scheme 4.5) catalysed by divalent metal-containing MOFs

Entry	Catalyst	Reactant ^a (%)	Product ^a (%)	Hydrate ^a (%)	Other ^a (%)
1	no catalyst	85	12	2	1
2	HKUST-1(Cu)	54	31	9	6
3	STA-12(Ni)	44	48	7	1
4	STA-12(Co)	81	12	5	2
5	STA-16(Ni)	46	42	7	5
6	STA-16(Co)	80	6	13	1
7	CPO-27(Ni)	42	47	9	2
8	CPO-27(Co)	66	18	12	4

α -methylstyrene (2.7 mmol) and ethyl trifluoropyruvate (2.7 mmol) were added to a solution of activated MOF (2.5 mol%) in toluene (5 ml) and the solution was stirred at room temperature for 8 h. ^a Determined by $\{^1\text{H}\}^{19}\text{F}$ NMR.

Changing the ligand from a phosphonate to a 1,4-dioxido-2,5-benzenedicarboxylate in the form of CPO-27 (which distorts little upon dehydration when compared to STA-12) appeared to have no effect on the catalysis, as both STA-12(Ni) and CPO-27(Ni) show similar conversions. The decrease in activity when the metal is changed to cobalt is also observed in the CPO-27 series. In summary, it is clear that the divalent cation for the MOF-catalysed carbonyl ene reaction increases activity in the order $\text{Co}^{2+} < \text{Cu}^{2+} < \text{Ni}^{2+}$.

4.1.2. Intermolecular carbonyl ene reactions catalysed by MOFs containing trivalent metals

The previous results show divalent metal that some MOF materials are active in the carbonyl ene reaction but the conversion is modest, especially as the reaction works without the use of a catalyst. The STA-12(Ni) and CPO-27(Ni) catalysts are a modest improvement on this. Among homogeneous catalysts scandium(III) triflate is a well-known Lewis acid and has been widely used as a catalyst for C-C bond formation.^{1, 2} We therefore hypothesised that Sc(III) MOFs might be active Lewis acid catalysts so this prompted the investigation of Sc^{3+} and other trivalent metal-containing MOFs in the carbonyl ene reaction (Table 4.3).

MIL-100(Sc) is by far the most active and selective catalyst for this reaction, both compared with other scandium-containing MOFs, and also with other MIL-100 materials containing different trivalent cations. MIL-100(Sc) gave a high conversion of 99% with 99% selectivity for the product ethyl-2-hydroxy-4-phenyl-2-

(trifluoromethyl)pent-4-enoate. The MIL-100(Sc) could simply be filtered off from the reaction and the solvent removed under vacuum to give pure product (Figure 4.1). Notably, the solvent used for the reaction played a significant role in conversion. The conversion is strongly reduced if the reaction is conducted in polar solvents (methanol, conversion 31%; acetonitrile, 48%) which suggests inhibition by solvent binding at the active Lewis acidic Sc³⁺ site. MIL-100(Sc) can also attain 99% conversion without pre-activation at 423 K, suggesting that methanol (or water) molecules bound at the active sites can readily be displaced by reactant in the toluene reaction solvent

Table 4.3: Carbonyl ene reactions of α -methylstyrene with ethyl trifluoropyruvate (Scheme 4.5) catalysed by trivalent metal containing MOFs

Entry	Catalyst	Reactant ^a (%)	Product ^a (%)	Hydrate ^a (%)	Other ^a (%)
1	no catalyst	85	12	2	1
2	MIL-100(Sc)	0	99	0	1
3	MIL-100(Sc) ^b	0	99	0	1
4	MIL-100(Sc) ^c	69	24	5	2
5	MIL-100(Sc) ^d	52	39	6	3
6	MIL-100(Cr)	29	65	4	2
7	MIL-100(Fe)	42	46	8	4
8	MIL-100(Al)	56	29	5	3
9	MIL-101(Sc)	53	24	13	10
10	MIL-101(Sc) ^e	69	22	5	4
11	MIL-101(Cr)	36	58	5	1
12	MIL-88B(Sc)	55	26	17	2
13	MIL-88B(Sc) ^c	65	22	10	3
14	MIL-88D(Sc)	46	45	8	1
15	socMOF(Sc)	83	4	8	5

α -methylstyrene (2.7 mmol) and ethyl trifluoropyruvate (2.7 mmol) were added to a solution of activated MOF (2.5 mol%) in toluene (5 ml) and the solution was stirred at room temperature for 8 h. MOFs activated by stirring in methanol for 24 h, drying and heating at 423 K under vacuum for 5 h unless stated otherwise ^a Determined by ¹H/¹⁹F NMR. ^b Reaction carried out using as-prepared MIL-100(Sc) washed with methanol rather than activated by heating under vacuum. ^c Reaction solvent methanol. ^d Reaction solvent acetonitrile. ^e Did not pre-activate under vacuum at 423 K.

The lower activity of the other MIL-100 materials is observed for MIL-100(Cr), MIL-100(Fe) and MIL-100(Al), with conversions in the carbonyl ene reaction of only 65%, 48% and 29%, respectively and lower selectivity to desired product (Table 4.3). The Fe, Al, Cr materials would all be expected to be significantly Lewis acidic from IR measurements using probe molecules (discussed in chapter 3.3). MIL-100(Sc) therefore appears to have the balance of Lewis acidity needed in order to be an effective catalyst

in the reaction. The reactant is bound sufficiently strongly to be activated for reaction but the Lewis acidity is not so strong that it will inhibit desorption of initially bound solvent (methanol) or product. MIL-100(Sc) also showed superiority in its performance as it could achieve 99% conversion even without dehydration, something that is not observed for the other materials.

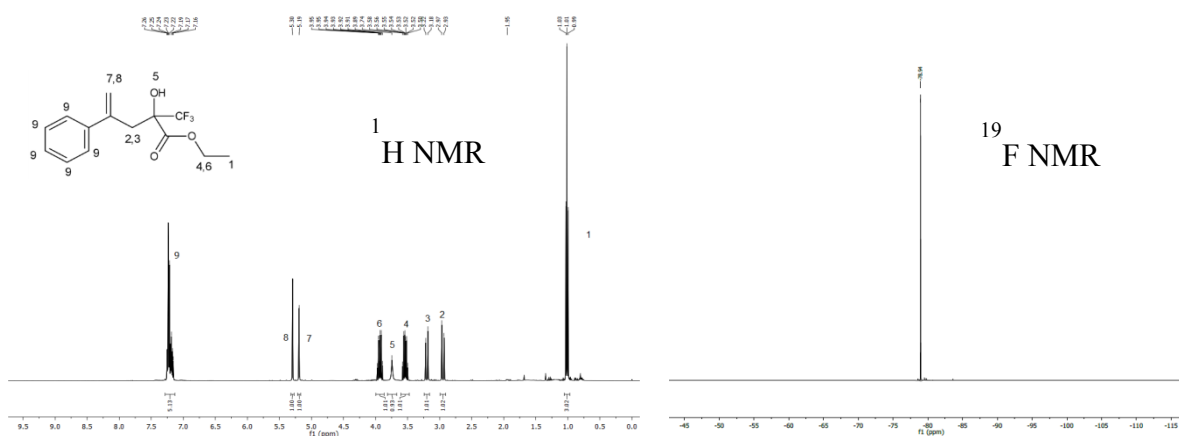


Figure 4.1: (left) ^1H and (right) ^{19}F NMR of reaction product from Scheme 4.5 after removal of catalyst by filtration and removal of solvent, without further purification

Due to the high activity of the scandium-containing MIL-100 a range of scandium-bearing MOF materials were tested, to determine whether the catalytic activity depended only on the presence of Sc^{3+} centres or whether the structure of the MOF was also important. MIL-101(Sc) was studied as it has similar cationic trimers and supercage structure to those of MIL-100(Sc). (It is built from benzene-1,4-dicarboxylic acid giving it a larger windows (12 and 16 Å) and cages (29 and 34 Å)). Because of these characteristics MIL-101(Sc) should have given as good if not better activity than MIL-100(Sc) due to its even larger window and pore size. However the material was found to be unstable upon heating (forming MIL-88B when heated under standard activation conditions) and did not have the same increase in surface area upon activation with methanol as MIL-100. MIL-101 has a similar structure to that of MIL-100 but contains larger windows and cages; this has been found by the increased BET surface area of MIL-101(Cr) ($2800 \text{ m}^2\text{g}^{-1}$) as compared to MIL-100(Cr) ($1500 \text{ m}^2\text{g}^{-1}$).^{39, 40} Synthesis of MIL-101(Sc) has been carried out by Yan-Tao *et al.*⁴¹ and further investigation at St. Andrews (B. Gonzalez Santiago) suggested a BET surface area comparable to MIL-101(Cr) at low activation temperature. However, when the

temperature of activation was increased, N₂ adsorption gave a lower value of 628 m²g⁻¹. This lowering of surface area could be caused by recrystallisation of the compound and therefore pore blocking of the material, hence the modest conversion of only 24%.³² The reaction was also tried with as-prepared MIL-101(Sc) which would not undergo the same recrystallisation observed at high temperatures, but this did not increase the performance of the catalyst.

Both MIL-88B and MIL-88D contain the same Sc₃O(O₂C-) ₆ trimer as MIL-100(Sc) so might be expected to have similar catalytic activity. MIL-88B is synthesised using the same ligand as MIL-101, benzene-1,4-dicarboxylic acid. However, it is formed at lower temperatures. ‘Breathing’ behaviour is exhibited in MIL-88B(Sc) which shows low adsorption of N₂ in the desolvated state.⁴² MIL-88B(Sc) porosity increases, expanding the overall cell volume by 60% when polar solvents (e.g. methanol) are absorbed.⁴³ From powder X-ray diffraction of MIL-88B immersed in toluene, it appears the material is in a closed pore state; this prohibits the reactants from entering the pores as the windows are not large enough for reactants to gain entry and allows only surface catalysis to occur, hence the lower conversion of 26%. The reaction solvent was changed to methanol to see if the reaction would proceed better if the MIL-88B material was in its ‘open pore’ form. However this was not the case and conversion to product decreased (Table 4.3. entry 13). Methanol and other polar solvents did appear to have a negative effect on the conversion (Table 4.3, entries 4 and 5) due to the Lewis acidic sites having a high affinity for methanol and therefore coordinating to scandium blocking the Lewis acid site.

The isorecticular larger pore structure MIL-88D was synthesised using biphenyl-4,4’-dicarboxylic acid. The analysis of MIL-88D(Sc) using powder X-ray diffraction found evidence of interpenetration (presence of a secondary structure within the structure) as previously seen with MIL-88D(Fe).⁴² This restricts access to the pore and could explain the modest conversion of 46%.

The modest conversion over socMOF can be rationalised by the small pore size (a 3-dimensional network of 5 Å channels); the substrates are too large to fit in, inhibiting access to the pore. This suggests, by comparison that the catalysis over MIL-100(Sc) occurs in the pores, and further evidence of this is presented in section 4.2.1.

Coordinatively unsaturated sites in the MIL-100(Sc) trimer therefore activate the carbonyl substrate to aid selective catalysis of the intermolecular carbonyl ene reaction with alkene substrate to form the product. MIL-100(Sc) is easily activated but also acts as a catalyst under the same conditions without activation, unlike the other MOF materials. The windows of 9 Å diameter allow substrates and reactant to flow in and out of the pore easily and the large cage size (30 Å) facilitates the ease of access to unsaturated coordinative Sc³⁺ sites (Figure 4.2).

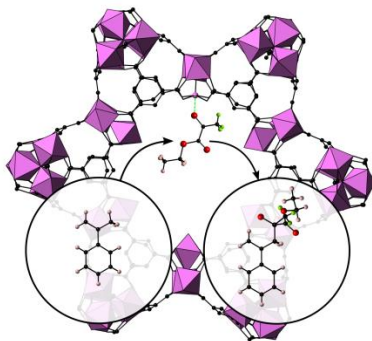


Figure 4.2: Schematic representation of the carbonyl ene reaction occurring in the pore of MIL-100(Sc)

To confirm that all of the catalytic activity was heterogeneous and that no leaching of Sc³⁺ cations had occurred, the catalyst was filtered off after 4 h and the reaction was allowed to continue without any catalyst present (Figure 4.3). Only a modest increase in conversion of 3% occurred after catalyst removal, consistent with the slow background reaction, and ICP-MS analysis on the reaction mixture found no evidence of scandium leaching from the MOF material.

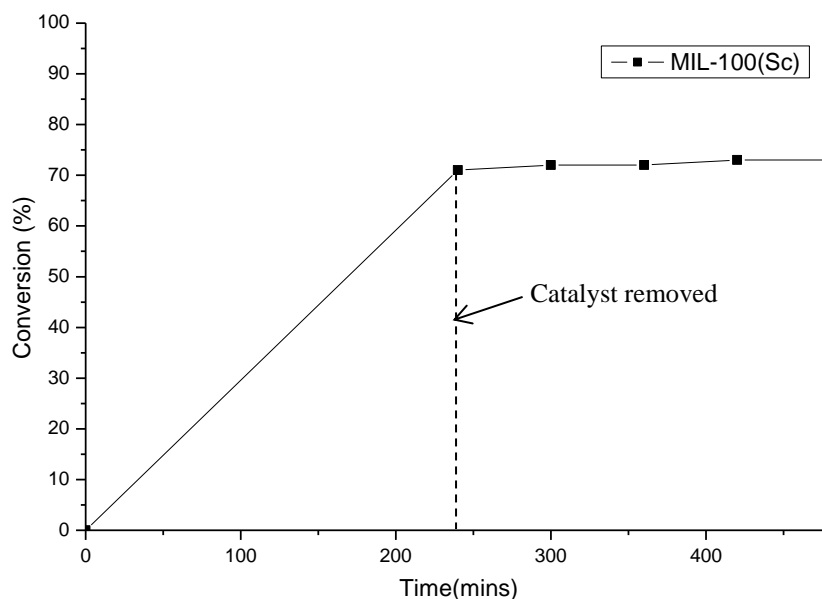


Figure 4.3: Graph showing conversion vs time for the carbonyl ene reaction in which MIL-100(Sc) catalyst is removed after 4 h and the reaction was continued with no catalyst present

4.1.3. Effects of synthesis method on catalyst activity

The STA-12(Ni) materials synthesised in chapter 3 using different synthesis methods were tested to determine if the method of synthesis had any effect on their overall catalytic activity. The carbonyl ene reaction was carried out for 8 h using each catalyst to quantify the activity of the materials. The hydrothermally-synthesised MOFs showed lower activity in catalysis (Table 4.4) as the reaction time for their synthesis was decreased. This may be due to the decrease in BET surface area observed previously, possibly caused by unreacted ligand blocking the pore of the structure reducing the access to Lewis acid.

No significant difference in the catalytic behaviour was observed between the materials synthesised at reflux (for 8 h) and those synthesised hydrothermally (72 h); both are found give similar conversions. These materials exhibited similar properties with regards to crystallite size, BET surface area and crystallinity. The use of microwave-synthesised STA-12(Ni) gave slightly increased conversion in this reaction. These results show that the catalytic performance of STA-12 slightly influenced properties that depend on its synthesis method and crystallisation time.

Table 4.4: Carbonyl ene reactions catalysed by STA-12(Ni): Effects of different synthesis methods on catalyst activity

Entry	Catalyst	Reactant ^a (%)	Product ^a (%)	Hydrate ^a (%)	Other ^a (%)
1	no catalyst	85	12	2	1
2	STA-12(Ni) 72 h ^b	44	48	7	1
3	STA-12(Ni) 48 h ^b	59	36	4	1
4	STA-12(Ni) 24 h ^b	69	25	5	1
5	STA-12(Ni) 8 h ^c	43	49	7	1
6	STA-12(Ni) 0.5h ^d	40	55	5	2

α -methylstyrene (2.7 mmol) and ethyl trifluoropyruvate (2.7 mmol) were added to a solution of activated MOF (2.5 mol%) in toluene (5 ml) and the solution was stirred at room temperature for 8 h.^a Determined by $\{^1\text{H}\}^{19}\text{F}$ NMR. ^b Synthesised hydrothermally at 493 K. ^c Synthesised under refluxing water at 373 K. ^d Synthesised using microwave heating in water at 373 K.

The same catalytic test was carried out using MIL-100(Sc) made using alternative synthesis methods and solvents (Table 4.5). Shorter reaction times (4 h) were used to stop the reaction going to completion and allow for a clearer comparison.

Table 4.5: Carbonyl ene reactions catalysed by MIL-100(Sc): effect of different synthesis methods on catalyst activity

Entry	Catalyst	Reactant ^a (%)	Product ^a (%)	Hydrate ^a (%)	Other ^a (%)
1	no catalyst	91	7	1	1
2	MIL-100(Sc) 48h ^b	27	71	2	1
3	MIL-100(Sc) 8h ^c	26	73	1	1
4	MIL-100(Sc) 0.5h ^d	27	70	2	1
5	MIL-100(Sc) ^e	30	62	7	1
6	Sc ₃ (BTC) ₂ (non-porous)	84	6	8	2

α -methylstyrene (2.7 mmol) and ethyl trifluoropyruvate (2.7 mmol) were added to a solution of activated MOF (2.5 mol%) in toluene (5 ml) and the solution was stirred at room temperature for 4 h. ^a Determined by $\{^1\text{H}\}^{19}\text{F}$ NMR. ^b Synthesised solvothermally in DMF at 423 K. ^c Synthesised under reflux in DMF at 413 K. ^d Synthesised using microwave irradiation in DMF at 413 K. ^e Synthesised under reflux using 9:1 water to DMF mixture at 373 K.

The synthesis method for MIL-100(Sc) did not have a strong effect on the catalytic activity of the material, with samples prepared via solvothermal, microwave and refluxing routes all giving materials yielding similar conversions, although MIL-100(Sc) synthesised using a 9:1 mixture of water and DMF appeared to give a slightly

lower conversion than when synthesised in DMF alone as a solvent. The slightly lower BET surface area ($1089 \text{ m}^2\text{g}^{-1}$) of the material may influence the activity of the material. The non-porous $\text{Sc}_3(\text{BTC})_2$ material synthesised using propylene carbonate showed no catalytic activity.

4.1.4. Recovery and reusability of STA-12(Ni) and MIL-100(Sc)

One of the potential advantages in using MOF materials as heterogeneous catalysts is their recyclability. Once each catalyst was filtered from the reaction, washed with solvent and dried, PXRD was used to investigate any structural changes. The reaction with α -methylstyrene and ethyl trifluoropyruvate was then repeated with recovered MOF material to see if any loss in activity could be observed (Table 4.6). The reusability of the active catalysts STA-12(Ni) and MIL-100(Sc) was determined.

The reaction was carried out, material recovered, dehydrated again and reused in the reaction. Some loss of material did occur when filtering after the initial reaction, so this was taken into consideration when the reaction was repeated and the amounts of reactants were adjusted accordingly. This experiment therefore measured the performance of the recycled catalysts and not the unoptimized technique for recovering the material, which could be optimised separately.

Table 4.6: Recycling of STA-12(Ni) and MIL-100(Sc) in the intermolecular carbonyl ene of α -methylstyrene with ethyl trifluoropyruvate

Entry	Catalyst	Cycle	Product ^a (%)
1	STA-12(Ni) ^b	1	64
2	STA-12(Ni) ^b	2	63
3	STA-12(Ni) ^b	3	63
4	MIL-100(Sc)	1	99
5	MIL-100(Sc)	2	96
6	MIL-100(Sc)	3	95
7	MIL-100(Sc)	4	95
8	MIL-100(Sc)	5	96

α -methylstyrene (2.7 mmol) and ethyl trifluoropyruvate (2.7 mmol) were added to a solution of activated MOF (2.5 mol%) in toluene (5 ml) and the solution was stirred at room temperature for 8 h (for MIL-100(Sc) or 16 h (for STA-12(Ni)). After each cycle the amount of reactant was adjusted to accommodate any loss when recovering material between cycles.

^a Determined by $\{^1\text{H}\}^{19}\text{F}$ NMR. ^b Reaction carried out for 16 h.

Table 4.6 shows that STA-12 (Ni) can be reused 3 times without any substantial loss of activity. PXRD patterns were taken on the material recovered in order to detect any changes in the structure. All patterns contained the same peaks with no major changes (Figure 4.4). A similar very minor drop in conversion and retention of structure as observed *via* XRD patterns was observed for MIL-100(Sc) (Table 4.6 and Figure 4.5).

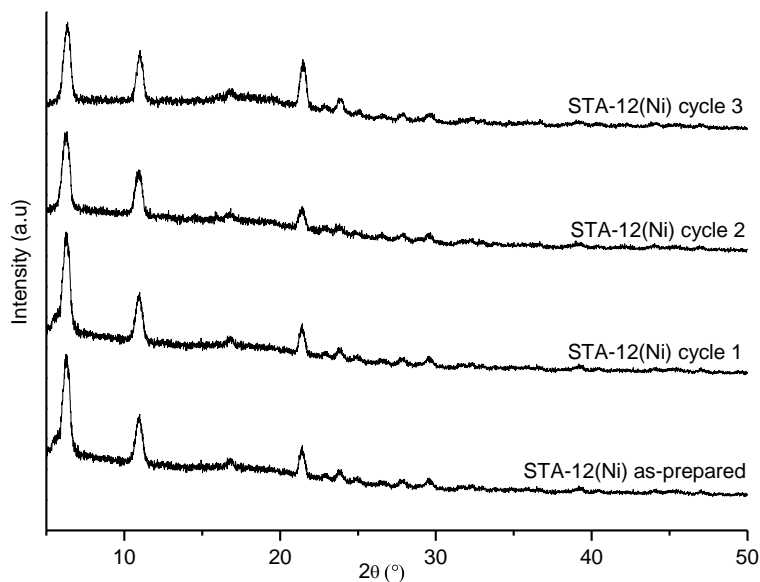


Figure 4.4: PXRD pattern of recovered STA-12(Ni) material after each cycle of reaction of α -methylstyrene with ethyl trifluoropyruvate in toluene stirred at room temperature for 8 h

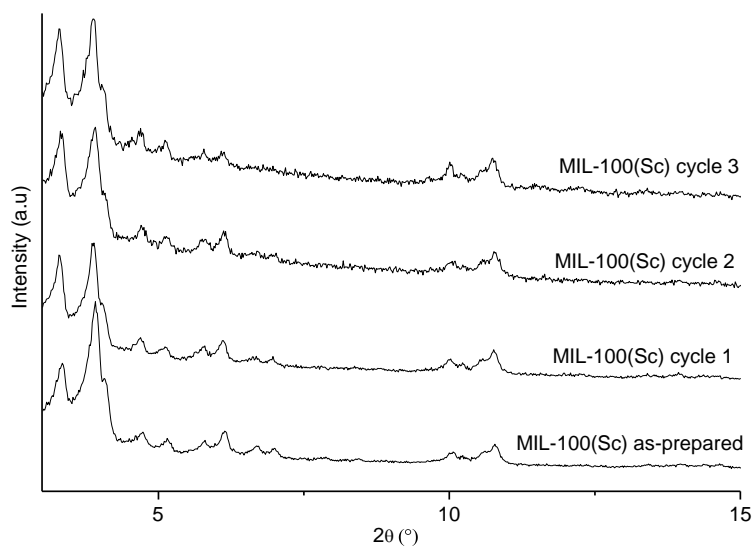


Figure 4.5: PXRD pattern of recovered MIL-100(Sc) material after each cycle of reaction of α -methylstyrene with ethyl trifluoropyruvate in toluene stirred at room temperature for 8 h

Furthermore, the conversion of reactants over MIL-100(Sc) (fresh and recycled) was followed using a reduced catalyst loading of 1.5 mol%, so the reaction could be easily followed. No deactivation was observed - the catalytic performance of the materials did not show significant differences (Figure 4.6). In each case the sigmoidal shape of the curve suggested an initial induction period, possibly as reactants diffuse to and products from the active site.

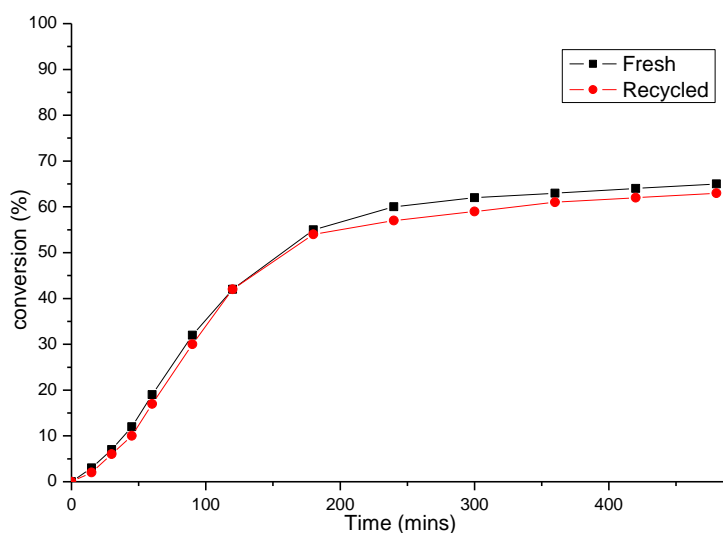
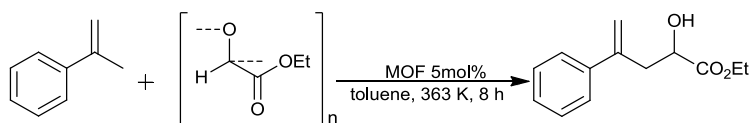


Figure 4.6: Graph showing conversion vs time for carbonyl ene reaction of α -methylstyrene (2.7 mmol) with ethyl trifluoropyruvate (2.7 mmol) using fresh and recycled MIL-100(Sc) (1.5 mol%) stirred in toluene (5 ml) at room temperature for 8 h

4.1.5. The intermolecular carbonyl ene reaction with less activated alkenes and enophiles



Scheme 4.6: Intermolecular carbonyl ene reaction of ethyl glyoxalate with α -methylstyrene catalysed by various MOF materials

Further investigation into the catalyst performance of MIL-100(Sc) was carried out by additional carbonyl ene reactions using a less activated enophile (ethyl glyoxalate) with α -methylstyrene (Scheme 4.6). Alternative alkenes - methylene cyclohexane and methylene cyclopentane - were also examined. Depolymerisation of ethyl glyoxalate polymer via distillation (at 423 K) before use is normally required for these reactions, so this protocol was initially adopted.⁴⁴ No reaction occurred when no catalyst was present

when α -methylstyrene is reacted with ethyl glyoxalate. However, MIL-100(Sc) catalyses this reaction and gave 84% conversion to product after 8 h at 363 K. This high activity was not observed with any other MOF materials tested (Table 4.7, entries 3-5) and is especially high compared to HKUST-1(Cu), which only achieves 6% conversion under the same conditions. By using the more activated alkenes, methylene cyclopentane and methylene cyclohexane, the product could be attained in even higher yields, reaching conversions of 99% in both cases. These reactions show these are more activated alkenes and the background reaction occurs at a significant rate without the presence of catalyst, but the introduction of 2.5 mol% catalyst more than doubles the conversion to product. This high level of performance could not be obtained by the chromium-containing MIL-100 (Table 4.7, entries 9 and 13) although it is still more active than the divalent MOFs tried in the reaction (such as HKUST-1(Cu)) (Table 4.7).

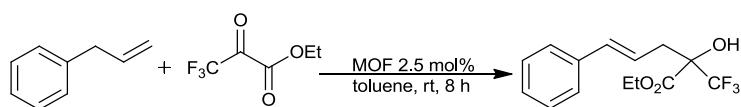
Table 4.7: Carbonyl ene reaction of ethyl glyoxalate with various alkenes catalysed by different MOF catalysts

Entry	Catalyst	Alkene	Product	Product (%)
1	no catalyst			0
2	MIL-100(Sc)	"	"	84
3	MIL-100(Cr)	"	"	55
4	STA-12 (Ni)	"	"	11
5	HKUST-1(Cu)	"	"	6
6	No catalyst			48
7	MIL-100(Sc)	"	"	99
8	MIL-100(Sc) ^a	"	"	97
9	MIL-100(Cr)	"	"	79
10	HKUST-1(Cu)	"	"	57
11	No catalyst			55
12	MIL-100(Sc)	"	"	99
13	MIL-100(Cr)	"	"	88
14	HKUST-1(Cu)	"	"	75

Alkene (2.7 mmol) and enophile (2.7 mmol) added to a suspension of activated MOF (5 mol%) in toluene (5 ml) and stirred at 363 K for 8 h. Conversion determined by ¹H NMR. ^a 2.5 mol% of catalyst/substrate.

The MOF materials promoted the carbonyl ene reaction of the less activated enophile, ethyl glyoxalate but, disappointingly, the same could not be said for the less activated alkenes. Both allyl benzene and 1-hexene were reacted in the presence of MIL-100(Sc). The reaction of allyl benzene and ethyl trifluoropyruvate was initially carried out at room temperature for 16 h in toluene (Table 4.8). The reaction was carried out without a catalyst present and after 16 h no conversion was observed.

Table 4.8: Reaction between allyl benzene and ethyl trifluoropyruvate catalysed by STA-12(Ni) and MIL-100(Sc)

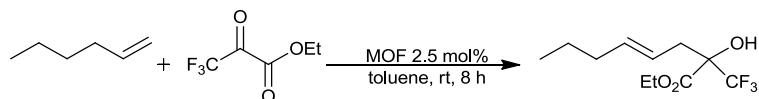


Entry	Catalyst	Reactant (%)	Product (%)	Hydrate (%)	Other (%)
1	STA-12(Ni)	81	6	11	2
2	STA-12(Ni) ^a	63	18	16	3
3	MIL-100(Sc)	70	7	18	5
4	MIL-100(Sc) ^a	43	34	20	3
5	MIL-100(Sc) ^b	29	54	15	2

Allyl benzene (2.7 mmol) and ethyl trifluoropyruvate (2.7 mmol) added to a suspension of activated MOF (2.5 mol%) in toluene (5 ml) and stirred at room temperature for 16 h. Conversion determined by ¹H/¹⁹F NMR. ^a Reaction carried out at 323 K. ^b Reaction carried out at reflux (383 K).

MIL-100(Sc) gave the highest conversion of allyl benzene, which was only slightly improved when the reaction was carried out at 323 K. When the reaction was carried out at reflux an increase in conversion was observed to 54% product (Table 4.8 entry 5). MIL-100(Sc) was also used with 1-hexene, however this also showed low conversion compared to the reactivity it had exhibited previously (Table 4.9). These results were disappointing: MIL-100(Sc) is not capable of catalysing the carbonyl ene reaction of these deactivated, terminal alkenes effectively.

Table 4.9: Reaction between 1-hexene and ethyl trifluoropyruvate catalysed by MIL-100(Sc) at varying temperature



Entry	Catalyst	Reactant (%)	Product (%)	Hydrate (%)	Other (%)
1	MIL-100(Sc)	67	12	18	3
2	MIL-100(Sc) ^a	59	16	21	4
3	MIL-100(Sc) ^b	53	30	15	2

1-hexene (2.7 mmol) and ethyl trifluoropyruvate (2.7 mmol) added to a suspension of activated MOF (2.5 mol%) in toluene (5 ml) and stirred at room temperature for 16 h. Conversion determined by $\{^1\text{H}\} \text{ } ^{19}\text{F}$ NMR.^a Reaction carried out at 323 K. ^b Reaction carried out at reflux.

4.1.6. Tandem deprotection carbonyl ene reactions

During investigation of the MOF-catalysed carbonyl ene reaction between ethyl trifluoropyruvate and α -methylstyrene, it was discovered that there was no need to carry out the reaction under strictly anhydrous conditions with MIL-100(Sc) - it was observed that any hydrate formed or present in the ethyl trifluoropyruvate would later be converted into product. With this in mind the reaction was carried out on the hydrated form of ethyl trifluoropyruvate. MIL-100(Sc) gave 99% conversion to the product (Table 4.10, entry 2). Although MIL-100(Cr) is also able to dehydrate the diol it gives much lower conversion than MIL-100(Sc) (Table 4.10, entry 3). No conversion occurred with STA-12(Ni) - the elimination of water from the hydrate may result in coordination to the uncoordinated Lewis acidic sites, rendering them catalytically inactive. Indeed, STA-12(Ni) can be seen slowly changing from its dehydrated form (orange) to its hydrated form (green) as this reaction progresses.

The ability of the MIL materials to act not only as a Lewis acid but also a deprotecting agent is advantageous. The hydrated form of ethyl trifluoropyruvate is likely to be a more shelf-stable reagent and furthermore is a common impurity in the commercial material.

Table 4.10: Tandem dehydration followed by carbonyl ene reaction catalysed by various MOF catalysts

Entry	Catalyst	Reactant	Product	Product (%)
1	No catalyst			0
2	MIL-100(Sc)	"	"	99
3	MIL-100(Cr)	"	"	55
4	STA-12(Ni)	"	"	0
5	HKUST-1(Cu)	"	"	12

α -methylstyrene (2.7 mmol) and enophile (2.7 mmol) were added to a solution of activated MOF (5 mol%) in toluene (5 ml) and the solution was stirred at 293 K for 16 h. Conversion determined by $\{^1\text{H}\}^{19}\text{F}$ NMR. ^a Recycled MIL-100(Sc)

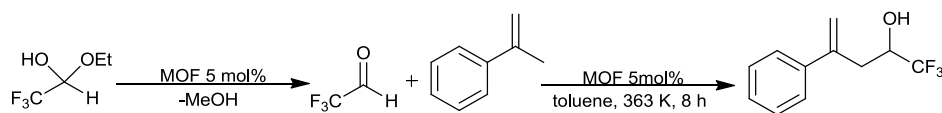
The depolymerisation of ethyl glyoxalate to form the monomer required for reaction was also investigated using MOF catalysts. In the case of ethyl glyoxalate, MIL-100(Sc) was tested using the polymeric form without cracking and distillation. The material gave full conversion and by simple removal of the catalyst and solvent, pure product was obtained. Eliminating the need for another step in the reaction, this type of reactivity has only been reported twice previously using homogeneous catalysts.^{5, 45} MIL-100(Sc) has the advantage that it can be recycled and still maintain a high conversion of 97% (Table 4.11).

Table 4.11: Tandem depolymerisation followed by carbonyl ene reaction catalysed by various MOF catalysts

Entry	Catalyst	Reactant	Product	Product (%)
1	No catalyst			0
2	MIL-100(Sc)	"	"	99
3	MIL-100(Sc) ^a	"	"	97
4	MIL-100(Cr)	"	"	52
5	HKUST-1(Cu)	"	"	0

α -methylstyrene (2.7 mmol) and ethyl glyoxalate (2.7 mmol) were added to a solution of activated MOF (5 mol%) in toluene (5 ml) and the solution was stirred at 363 K for 8 h. Conversion determined by ^1H NMR. ^a Recycled MIL-100(Sc)

The behaviour of MIL-100(Sc) as a deprotection agent in addition to being a Lewis acid catalyst was further replicated in the reaction of trifluoroacetaldehyde ethyl hemiacetal with α -methylstyrene (Scheme 4.7, Table 4.12).



Scheme 4.7: Deprotection of trifluoroacetaldehyde ethyl hemiacetal to form aldehyde and then reacting with α -methylstyrene catalysed by various MOF catalysts

The MOF materials facilitated the removal of ethanol (or methanol) from the trifluoroacetaldehyde ethyl hemiacetal to form the aldehyde required for the reaction to occur. The normal procedure is to generate trifluoroacetaldehyde gas from a solution of the hemiacetal in phosphoric acid, so that using a MOF catalyst eliminates the need for additional steps in the reaction. MIL-100(Sc) and MIL-100(Cr) were both active in this reaction. MIL-100(Sc) is simply removed from the reaction by filtration to give pure product in 99% yield (Table 4.12, entry 2). NMR spectra of these products can be found in the experimental section.

Table 4.12: Tandem deacetylation followed by carbonyl ene reaction catalysed by various MOF catalysts

Entry	Catalyst	Reactant	Product	Product (%)
1	No catalyst			0
2	MIL-100(Sc)	"	"	99
3	MIL-100(Cr)	"	"	59
4	HKUST-1(Cu)	"	"	30

α -methylstyrene (2.7 mmol) and trifluoroacetaldehyde ethyl hemiacetal (2.7 mmol) were added to a solution of activated MOF (5 mol%) in toluene (5 ml) and the solution was stirred at 363 K for 8 h. Conversion determined by ^{19}F NMR.

4.1.7. The effect of raising the activation temperature of MIL-100(Sc)

After probing MIL-100(Sc) using IR it was observed that the material exhibited stronger Lewis acidity and more Lewis acid sites by pre-activation at 523 K rather than 423 K. Catalytic tests were carried out on the materials activated at both temperatures. Two reactions were evaluated; a simple C-C bond formation reaction with activated substrate and a more demanding reaction with less activated substrates (Scheme 4.2 and Scheme in Table 4.8). It was thought that by heating to 523 K (hence creating more Lewis acidic sites) that catalytic activity could be increased. The reaction between allyl benzene and ethyl trifluoropyruvate (scheme in table 4.8) was attempted using 5 mol%

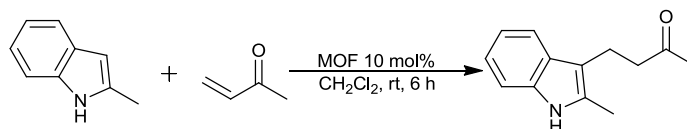
MIL-100(Sc). Pre-activation of MIL-100(Sc) carried out at 423 K gives a catalyst that gave 23% conversion to product in 8 h and 323 K. Pre-activation at 523 K caused conversion to product to decrease to 19% while other by-products were apparent in the NMR spectra. This could be due to the creation of defects in the MOF causing other catalytic sites to be produced and reducing the catalytic selectivity. The materials were also tested in a less demanding reaction, of α -methylstyrene with ethyl trifluoropyruvate, to form ethyl-2-hydroxy-4-phenyl-2-(trifluoromethyl)pent-4-enoate. Previous experiments using MIL-100(Sc) gave 99% conversion to product after 8 h when activated at 423 K. It was observed that when the material was activated at 523 K other by-products formed in the reaction causing the overall conversion to product to decrease to 85 % after 8 h. Therefore activating MIL-100(Sc) at 523 K or above appears to lead to the formation of defects which lead to the production of unwanted by-products at the expense of the desired product.

4.2. Conjugate addition of electron deficient olefins to indole

In order to explore the scope of reactions that MOF materials can be used to catalyse, the conjugate addition of indoles was investigated. This reaction is another example of a Lewis acid catalysed C-C bond formation that has 100% atom efficiency. The reaction is typically carried out in the presence of an aprotic solvent or a Lewis acid catalyst and requires careful monitoring to prevent polymerisation of the indole, which readily occurs under acidic conditions.⁴⁶ The MOF materials were thought to be potential catalysts for this reaction as most indole reactants are small enough to fit in the pores and so to access the Lewis acid sites.

4.2.1. Conjugate addition of 2-methylindole to methyl vinyl ketone catalysed by divalent and trivalent MOFs

Previous research performed by Yadav *et al.* used indium (III) chloride in the conjugate addition of electron deficient olefins to indole and reported a conversion of 92 % using 10 mol% catalyst after 2.5 h.⁴⁶ Initially 2-methylindole was reacted with methyl vinyl ketone in dichloromethane using 10 mol% MOF material which could easily be removed upon completion of the reaction (Scheme 4.8). The reaction was followed using ¹H NMR in which two triplets at ca. $\delta = 2.7$ ppm and $\delta = 2.9$ ppm could be observed from the product (4-(2-methyl-3-indolyl)butan-2-one). Using 10 mol% of MIL-100(Sc), a similar level of conversion (91%) was observed after just 1 h.



Scheme 4.8: Friedel-Crafts conjugate addition of 2-methylindole with methyl vinyl ketone catalysed by various MOF materials to produce 4-(2-methyl-3-indolyl)butan-2-one

The reaction does not proceed at all without the presence of a catalyst so that it is a good test reaction to determine the catalytic performance of the MOFs, and so a range of MOF catalysts was examined (Table 4.13).

STA-12(Ni) was a poor catalyst for this reaction, giving only 10% conversion to product. The larger substrates used in this reaction may find it harder to access the Lewis acidic site in the flexible pore of the material. CPO-27(Ni), which has similar pore size to STA-12(Ni) but is a much more rigid structure (where Ni²⁺ is more accessible in the dehydrated sample), gives a much higher conversion, highest amongst the materials examined except for the MIL-100 series.

MIL-100 materials outperformed the other materials tested, and among these MIL-100(Sc) is clearly the best catalyst, as previously observed in the carbonyl ene reaction. The conversion in dichloromethane as a solvent was 99%, in toluene 93%. Notably the conversion was much lower in the coordinating solvents acetonitrile (39%) and methanol (15%). This reduction of conversion in polar solvents was much greater than for the homogeneous scandium triflate, which gave 89-99% conversion in the same solvents. The inhibition effect due to binding of the polar solvent methanol at the Sc³⁺ site of MIL-100 is therefore much larger than for the ScOTf₃ site in the solution. For the other MIL-100 materials, MIL-100(Cr) exhibited good activity with a conversion of 79%, while MIL-100(Fe) and MIL-100(Al) showed quite poor activity in comparison, achieving only 40% and 48% conversion to product (Table 4.13, entry 10 and 11). The lower activity of MIL-100(Fe, Al, Cr) could possibly be caused by the blocking of Lewis acid sites by the indole material. Evidence supporting this has been carried out by Van de Voorde *et al.*⁴⁷ who reported the use of MIL-100(Cr, Fe and Al) as efficient indole contaminant removers. It was found that over 100% of the coordinatively unsaturated sites could be occupied after introduction of indole. The nitrogen of the indole substrate can bind to the Lewis acid site and the oxygen in the trimer may

hydrogen bond to the NH hydrogen of the indole. This could overall lead to a reduction in activity due to the strong bonding between the Lewis acid site and the substrate preventing catalysis from occurring.⁴⁷

Table 4.13: Conjugate addition of indole to 2-methylvinyl ketone catalysed by various MOFs

Entry	Catalyst	Solvent	Product ^a (%)
1	no catalyst	CH ₂ Cl ₂	0
2	Sc(OTf) ₃	CH ₂ Cl ₂	99
3	Sc(OTf) ₃	CH ₃ CN	89
4	Sc(OTf) ₃	Methanol	90
5	MIL-100(Sc)	CH ₂ Cl ₂	99
6	MIL-100(Sc)	Toluene	93
7	MIL-100(Sc)	Methanol	15
8	MIL-100(Sc)	CH ₃ CN	39
9	MIL-100(Cr)	CH ₂ Cl ₂	65
10	MIL-100(Fe)	CH ₂ Cl ₂	40
11	MIL-100(Al)	CH ₂ Cl ₂	48
12	MIL-101(Sc)	CH ₂ Cl ₂	51
13	MIL-101 (Cr)	CH ₂ Cl ₂	56
14	STA-12(Ni)	CH ₂ Cl ₂	10
15	STA-12(Co)	CH ₂ Cl ₂	7
16	CPO-27(Ni)	CH ₂ Cl ₂	68
17	CPO-27(Co)	CH ₂ Cl ₂	3
18	HKUST-1(Cu)	CH ₂ Cl ₂	11
19	MIL-88B(Sc)	CH ₂ Cl ₂	12
20	MIL-88D(Sc)	CH ₂ Cl ₂	66
21	MIL-68(Sc)	CH ₂ Cl ₂	7
22	SocMOF(Sc)	CH ₂ Cl ₂	0

2-methylindole (0.1312 g, 1 mmol) and methyl vinyl ketone (0.083 ml, 1 mmol) were added to a solution of CH₂Cl₂ (5 ml) with pre-activated MOF (10 mol%) and stirred for 6 h at RT. ^a Determined by ¹H NMR. Remaining mass balance was starting material.

Other scandium-containing materials were tested, but none could emulate the high activity of MIL-100(Sc). As expected, MIL-68 and socMOF have low activity. There are no coordinatively unsaturated Sc³⁺ sites in MIL-68 and socMOF has very small

pores that would not allow access of substrates to sites. This is shown by less than 10 % product being produced.

When the reaction was carried out using MIL-100(Sc) it was found that the material appeared brown in colour after reaction (originally it had been white) (Figure 4.7) and the N_2 adsorption at 77 K dropped from 25 mmol g^{-1} to 20 mmol g^{-1} (Figure 4.8). By simply washing with methanol under vacuum the material returned to its original white colour and the original porosity, as measured by N_2 uptake at 77 K, was restored (Figure 4.8). NMR analysis confirmed the wash was 8% final product which had been retained in the MOF. It seems likely that product retention is a potential issue for all these catalysts, but perhaps less severe for scandium than iron or chromium, as scandium is known to undergo ligand exchange reactions very rapidly.

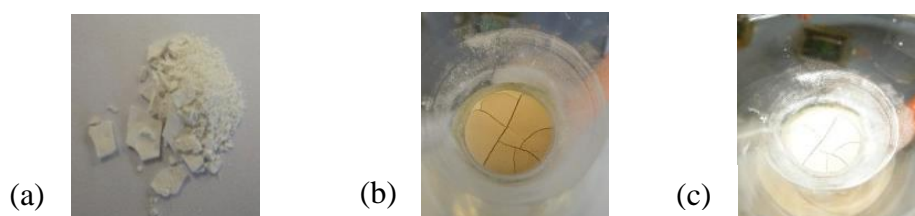


Figure 4.7: (a) MIL-100(Sc) (b) after reaction with 2-methylindole and methyl vinyl ketone (c) after methanol washing of material

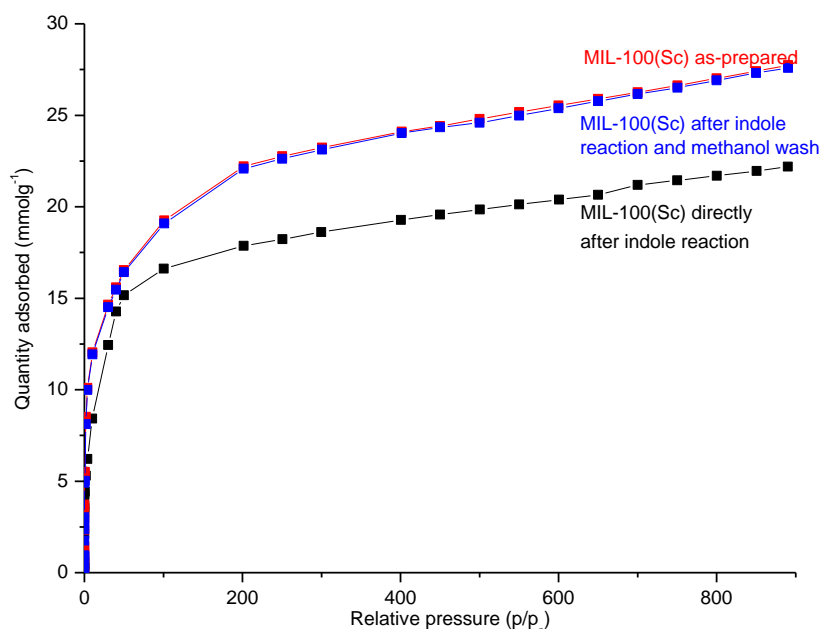


Figure 4.8: N_2 adsorption isotherms of MIL-100(Sc) before reaction of 2-methylindole with methyl vinyl ketone (red), after reaction (black) and after methanol washing (blue)

In order to determine the reusability of MIL-100(Sc) the material was recycled and conversion followed by NMR. The reaction was carried out using a reduced catalyst loading of 5 mol%. After each cycle MIL-100(Sc) was washed with methanol to remove products left in the pores. Using as-prepared MIL-100(Sc) 82% conversion to product was obtained with a conversion of 80% in each subsequent cycle. Each cycle gave similar reaction profiles over 360 minutes (Figure 4.9). The initial rate of reaction is rapid, attaining 70% conversion in the first 90 minutes and over 50% in the first 15 minutes. The reaction conversion significantly slows down after 90 minutes and up to 360 minutes only gains another 10%. This is consistent with product inhibition.

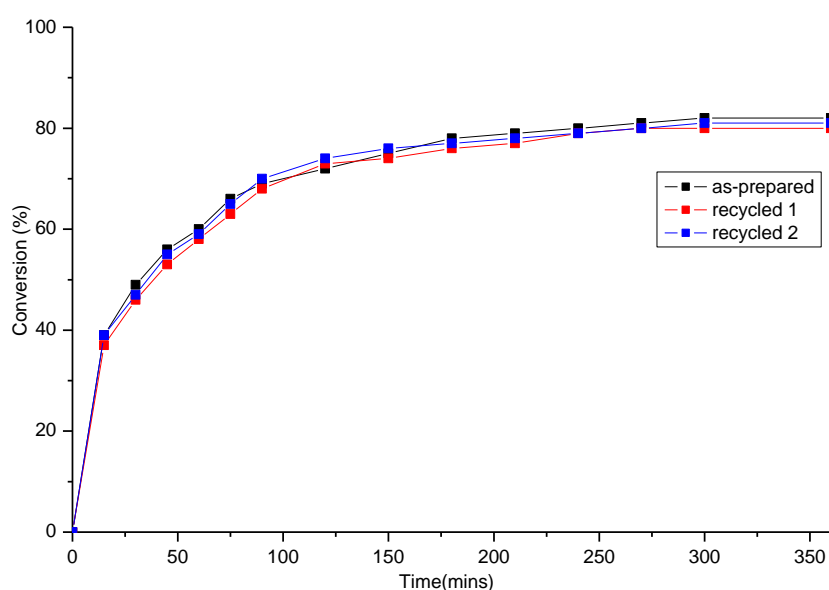


Figure 4.9: Formation of 4-(2-methyl-3-indolyl)butan-2-one catalysed by 5 mol% as-prepared and recycled MIL-100(Sc) over 6 h cycle stirred at room temperature in dichloromethane

PXRD patterns of MIL-100(Sc) after reaction and re-use show that there is no structural change after each cycle (Figure 4.10). The recycling of the MOF material was also carried out using 10 mol% to check for any drop in activity after reuse. No significant drops in conversion were observed. The material maintained high activity of 96% even after 5 cycles. To test the heterogeneity of the material the catalyst was removed from the reaction mixture after 30 minutes but the reaction was allowed to continue and followed by NMR. The reaction was found not to continue after catalyst removal (Table 4.14).

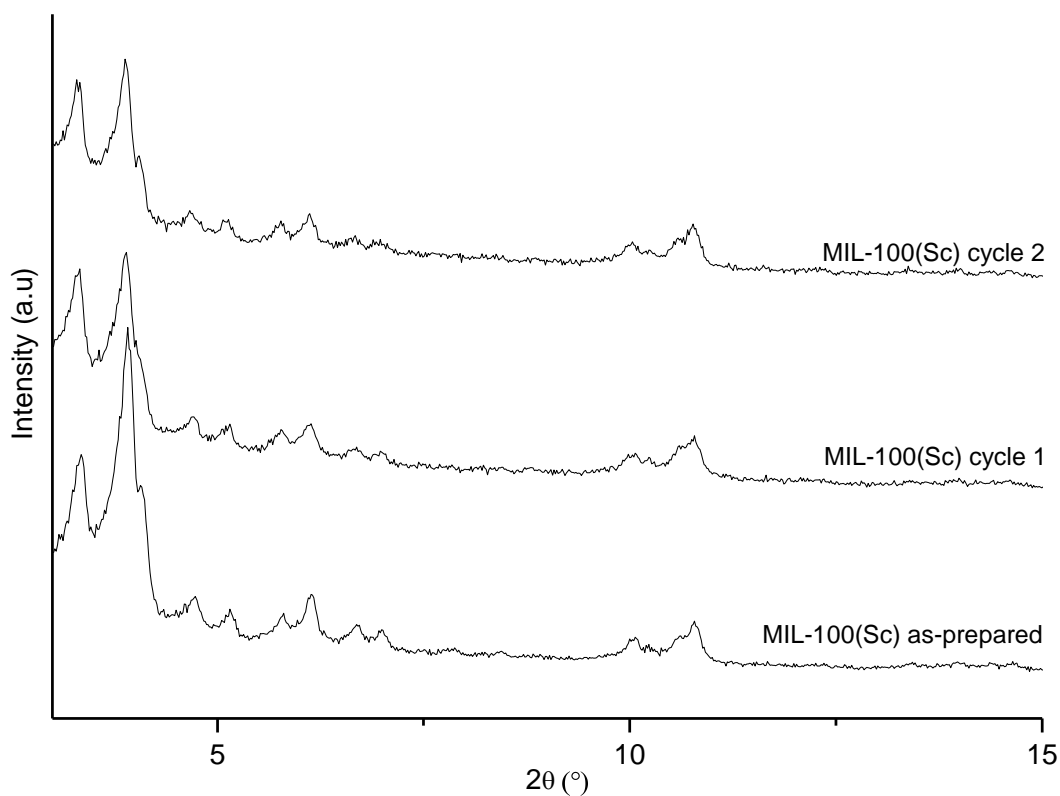


Figure 4.10: PXRD pattern of as-prepared material (MIL-100(Sc)) compared to material recovered after each reaction cycle

Table 4.14: Recycling of MIL-100(Sc) in the conjugate addition of indole to electron-deficient olefins

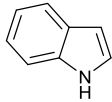
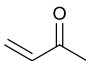
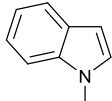
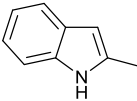
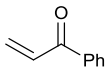
Entry	Cycle	Product(%) ^a
1	1	99
2	2	96
3	3	96
4	4	95
5	5	96
6 ^b	-	79
7 ^c	-	79

2-methylindole (0.1312 g, 1 mmol) and methyl vinyl ketone (0.083 ml, 1 mmol) were added to a solution of CH₂Cl₂ (5 ml) with pre-activated MOF (10 mol%) and stirred for 6 h at room temperature. ^a Determined by ¹H NMR. After each cycle the amount of reactant was adjusted to accommodate any loss when recovering material between cycles. ^b Reaction time 30 min. ^c Catalyst from entry 6 filtered off.

4.2.2. Conjugate addition of other indoles to vinyl ketones catalysed by divalent and trivalent MOF materials

The conjugate addition of indole to vinyl ketone was varied slightly using different indole and vinyl ketone substrates to investigate substrate scope (Table 4.15). The reactions with 1-methylindole and indole over MIL-100(Sc) show slightly lower conversions compared to that of 2-methylindole with vinyl ketone (88% and 89%). MIL-100(Cr) shows a significantly lower conversion when the substrate is changed to 1-methylindole, with a conversion of only 36%. A similar decrease in activity over MIL-100(Cr) is observed for the reaction of indole compared to 2-methylindole, but otherwise similar conversions are observed over the various MOFs investigated.

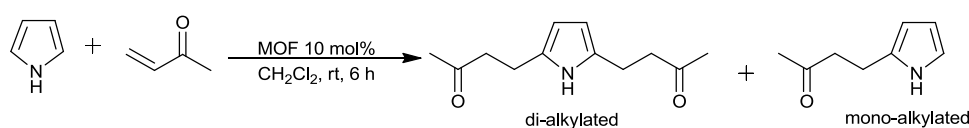
Table 4.15: Friedel-Crafts conjugate addition of varying indoles to different vinyl ketones catalysed by various MOF materials

Entry	Catalyst	Indole	Ketone	Product ^a (%)
1	Sc(OTf) ₃			90(90)
2	MIL-100(Sc)	"	"	89(87)
3	MIL-100(Cr)	"	"	40
4	MIL-88B(Sc)	"	"	15
5	CPO-27(Ni)	"	"	60
6	HKUST-1(Cu)	"	"	11
7	MIL-88D(Sc)	"	"	63
8	no catalyst		"	0
9	Sc(OTf) ₃	"	"	89(87)
10	MIL-100(Sc) ^b	"	"	88(88)
11	MIL-100(Cr)	"	"	36(35)
12	MIL-100(Fe)	"	"	25
13	MIL-100(Sc)			91(90)

Indole (1 mmol) and vinyl ketone (1 mmol) were added to a solution of CH₂Cl₂ (5 ml) with pre-activated MOF (10 mol%) and stirred for 6 h at room temperature. ^a Determined by ¹H NMR. ^b Reaction repeated using 1-methylnaphthalene as internal standard, giving same result.

Finally, the activity of MIL-100(Sc) for the conjugate addition of 2-methylindole with phenyl vinyl ketone was investigated. Even for the larger substrate high activity was maintained, resulting in 91% conversion.

The conjugate addition of electron deficient olefins to pyrrole was also carried out. This reaction has previously been observed to form both mono- and di-alkylated products (Scheme 4.9).⁴⁸ Our premise was that the shape and size constraints of the MOF pores will disfavour the formation of di-alkylated materials and could influence selectivity towards the formation of mono-alkylated pyrroles. Results of this reaction over three MOFs with different pore geometries are given in Table 4.16).



Scheme 4.9: Conjugate addition of pyrrole with methyl vinyl ketone

Table 4.16: Conjugate addition of pyrrole with methyl vinyl ketone catalysed by various MOF materials

Entry	Catalyst	Product ^a (%)	Ratio of di to mono product
1	No catalyst	35	1:3
2	MIL-100(Sc)	89	1:6
3	HKUST-1(Cu)	39	1:3
4	CPO-27(Ni)	41	1:6

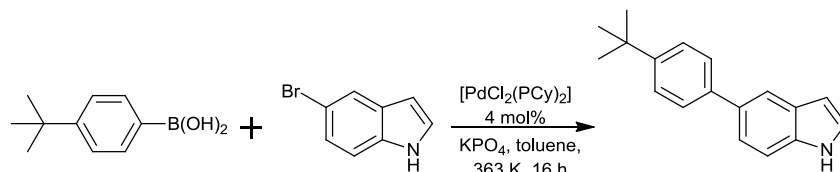
Pyrrole (1 mmol) and methyl vinyl ketone (1 mmol) were added to a solution of CH₂Cl₂ (5 ml) with pre-activated MOF (10 mol%) and stirred for 6 h at room temperature.

^aDetermined by ¹H NMR.

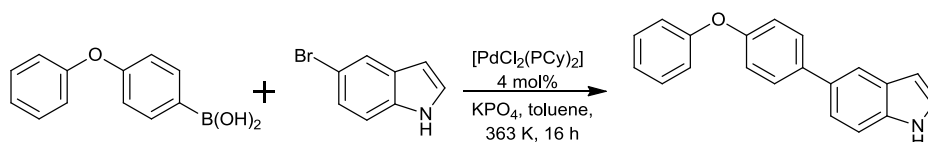
When MIL-100(Sc) was used to catalyse the reaction an overall conversion to product of 89% was achieved, with a selectivity of mono:di-alkylated material of 6:1. The material gave a much higher conversion than if no catalyst was present (35%) and also gives an increase in selectivity. HKUST-1(Cu) did not appear to have any effect on the reaction with a conversion (39%) not much higher than the control and no change in selectivity. CPO-27(Ni) did not show a large increase in activity (41%), however, it did prove to be more selective to the mono-alkylated product than HKUST-1 and the control.

4.2.3. Surface catalysis or catalysis inside the pore?

Previous evidence indicates that the reaction occurs in the pore by the change in colour and reduction in porosity after the reaction, as discussed in 4.2.1. In order to further probe whether the reaction occurred in the pore or on the surface of the catalyst, some of the MOF materials synthesised were reacted with indole substrates that would be too large to fit inside the pore of the materials. They were synthesised as shown in Scheme 4.10 and Scheme 4.11.

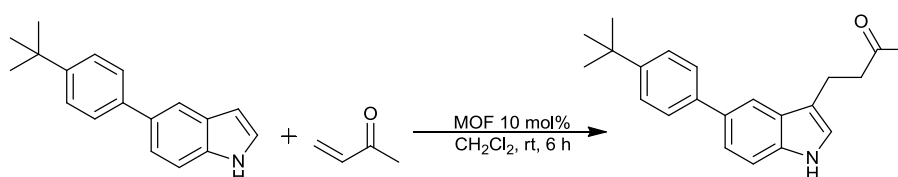


Scheme 4.10: Suzuki coupling reaction of 4-tert-butylphenylboronic acid with 5-bromoindole to form 5-(4-(tert-butyl)phenyl)-1H-indole



Scheme 4.11: Suzuki coupling reaction of 4-phenoxyphenylboronic acid with 5-bromoindole to form 5-(4-phenoxyphenyl)-1H-indole

These two bulky indoles were taken as substrates for the conjugate addition to methyl vinyl ketone.



Scheme 4.12: Friedel-Crafts conjugate addition of 5-(4-(tert-butyl)phenyl)-1H-indole with methyl vinyl ketone catalysed by various MOFs

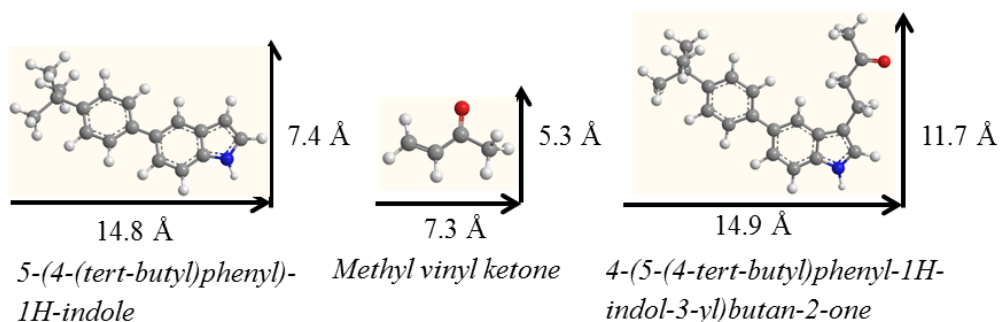
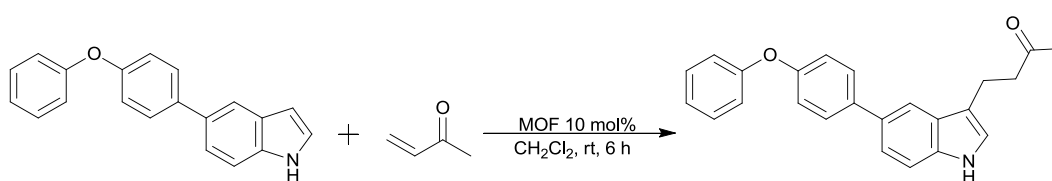


Figure 4.11: Scheme of reactants and product for larger substrate reactions and their dimensions



Scheme 4.13: Conjugate addition of 5-(4-phenoxyphenyl)-1H-indole to methyl vinyl ketone

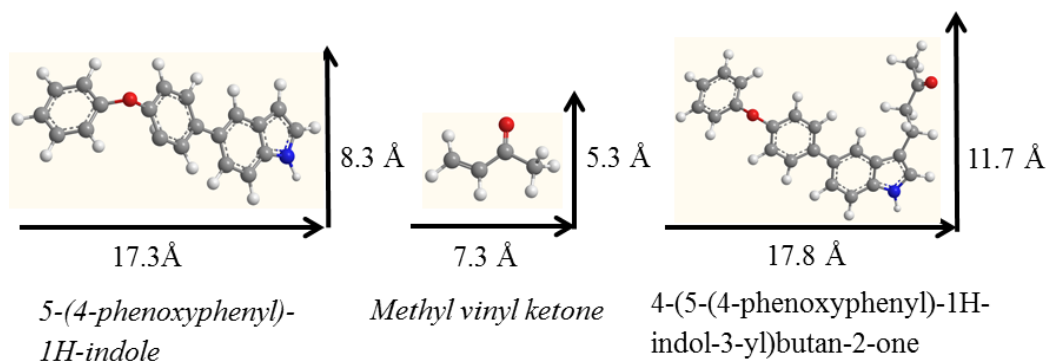


Figure 4.12: Scheme of reactants and product for larger substrate reactions and their dimensions

The product of Scheme 4.12, 5-(4-(*tert*-butyl)phenyl)-1H-indole, was synthesised. This has dimensions too large to fit through the windows/pores of most MOF materials (Scheme 4.12 and Figure 4.11). Sc(OTf)₃ was used as a control to gauge whether the reaction gave good conversion with a homogeneous catalyst which would not be hindered by size constraints. Sc(OTf)₃ gave a high conversion of 99% in the reaction (Table 4.17, entry 1). Normally MIL-100(Sc) had given similar overall conversions to those of the homogeneous catalyst but in this case the conversion was reduced significantly, with MIL-100(Sc) giving only 33% conversion (compared to the 90%

previously obtained with the smaller indole substrate). The window size of the MIL-100 structure is smaller than the reactant with dimensions of 5 and 9 Å. The small difference between window size and reactant size might allow the reactant to diffuse into the pore. However, evidence from N₂ adsorption and comparisons with previous reactions with this material suggest that no reactant gets into the pore. N₂ adsorption isotherms on the MIL-100(Sc) catalyst before and after the reaction observed no change in the N₂ uptake (Figure 4.13). Conversely, when a similar reaction with smaller substrates was carried out, N₂ adsorption decreases for MIL-100(Sc) recovered from the reaction mixture by simple filtration, in addition to a large colour change (section 4.2.1). This, combined with lack of colour change for the reaction using large substrates, suggests that the conversion observed for the material is caused by surface catalysis and does not occur in the pores.

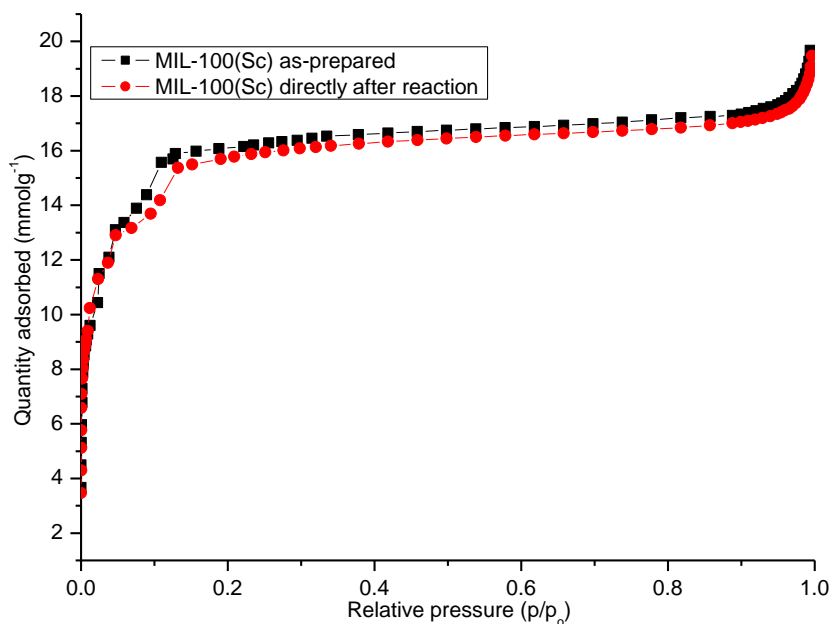


Figure 4.13: N₂ adsorption isotherms of MIL-100(Sc) before reaction of with 5-(4-(*tert*-butyl)phenyl)-1*H*-indole and methyl vinyl ketone (black), after reaction (red)

A similar reduction in activity was observed with other MOF materials (Table 4.17) which previously gave reasonable activities. CPO-27(Ni), which attained a conversion of 60 % with indole, had no activity with the larger substrate. CPO-27(Ni) has a channel of 11 Å which was thought would possibly be large enough for the substrate to access however this is found not to be the case. The rigid structure of the CPO-27(Ni) may prevent the access to any Lewis acid sites, thus inhibiting conversion.

Table 4.17: Conversion of reaction of 5-(4-(tert-butyl)phenyl)-1H-indole with methyl vinyl ketone (Scheme 4.12) catalysed by various MOFs

Entry	Catalyst	Conversion (%) ^a
1	no catalyst	0
2	Sc(OTf) ₃	99
3	HKUST-1(Cu)	10
4	CPO-27(Ni)	0
5	MIL-100(Sc)	33
6	MIL-88B(Sc)	15
7	MIL-88D(Sc)	9

5-(4-(tert-butyl)phenyl)-1H-indole (1 mmol) and methyl vinyl ketone (1 mmol) was added to a solution of CH₂Cl₂ (5 ml) with pre-activated MOF material and stirred for 6 h at room temperature. ^a Determined by ¹H NMR.

The second, even larger substrate, 5-(4-phenoxyphenyl)-1H-indol was also tested in order to confirm the low activity.

Reaction with 5-(4-phenoxyphenyl)-1H-indol gives similarly low conversion to that observed with 5-(4-(tert-butyl)phenyl)-1H-indole. Reactivity is not completely suppressed, which suggests some surface or near surface catalysis is still occurring.

Table 4.18: Conversion of reaction of 5-(4-phenoxyphenyl)-1H-indol with methyl vinyl ketone (Scheme 4.13) catalysed by MOF materials

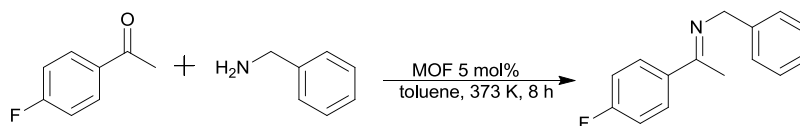
Entry	Catalyst	Conversion (%) ^a
1	Sc(OTf) ₃	84
2	MIL-100(Sc)	24
3	MIL-88B(Sc)	8
4	MIL-88D(Sc)	6

5-(4-phenoxyphenyl)-1H-indol (1 mmol) and methyl vinyl ketone (1 mmol) was added to a solution of CH₂Cl₂ (5 ml) with pre-activated MOF material and stirred for 6 h at room temperature. ^a Determined by ¹H NMR.

4.3. Imine Formation

4.3.1. Imine formation reaction of benzyl amine and fluoroacetophenone with a range of MOF materials

A further Lewis acid-catalysed reaction that could greatly benefit from a heterogeneous catalyst, eliminating the need for difficult purification procedures, is the formation of imines. This is of importance for the production of ketimines which is a greater challenge than the formation of aldimines, which can occur without a catalyst.



Scheme 4.14: Imine formation reaction of fluoroacetophenone and benzyl amine catalysed by MOF materials

Ketimines are typically synthesised using stoichiometric homogeneous ZnCl_2 and requiring a vacuum distillation step that is not suitable for every product. Unfortunately, ketimines are difficult to purify using column chromatography, since they hydrolyse easily, so that a heterogeneous catalyst that can obtain high conversions and that could simply be filtered off could be very useful for this reaction.⁴⁹

Initially the reaction of benzyl amine and 4-fluoroacetophenone was carried out at room temperature using MIL-100(Sc) because previous reactions had shown this material to outperform other MOF materials (Scheme 4.14 and Table 4.19). The reaction was found to give a modest conversion of 49% at room temperature. This is significantly higher than if no catalyst were present, where there is only 3% conversion. The temperature at which the reaction was carried out was increased, increasing the conversion to product to 60% at 333 K and 85% at 373 K. The reaction did not proceed past 85% conversion when the temperature was increased further.

One aim of this reaction was to try and get a catalyst that could give full conversion, and so reaction conditions were varied to achieve this. The equivalent of benzylamine used in the reaction was increased to attain a higher conversion; by increasing the equivalent of benzyl amine to 1.2 equivalents the reaction conversion was increased to 92% and then eventually >99% when using 2 equivalents. This allowed the MOF to be

simply filtered off and the excess benzyl amine could then be removed by a 0.1 M HCl acid wash. This eliminated the need for column chromatography or challenging purification steps to obtain the pure product. The activity of the other MIL-100 materials increased slightly with the increase of equivalents of benzyl amine however it is still low when compared to that of MIL-100(Sc) (Table 4.19, entries 10-14).

Other MOF materials were tested in the reaction and, as observed previously, MIL-100(Sc) outperformed the other materials. MIL-100(Cr) gave a disappointing conversion of 20%. The scandium-containing MOF MIL-88D(Sc) was also tried however it could not match the performance of MIL-100(Sc) (Table 4.19, entries 19 versus 21). This shows although the metal is important (as scandium containing MOFs gave higher conversion) the overall structure and ease of accessibility to the metal site is also important. The production of water in the reaction could attribute to the low activity of STA-12(Ni) as the water could be attracted to the metal site blocking reaction from occurring. It can be seen that the dehydrated STA-12(Ni) which is orange in colour after 10 minutes changes to the hydrated form, which is green in colour. This mirrors what was observed using hydrated ketone in the carbonyl ene reaction. Clearly MIL-100(Sc) is able to act as a Lewis acid and dehydrating agent, and presumably the fast ligand exchange with scandium prevents it from being inhibited by water. We also note that Sc(OTf₃) is water tolerant.¹

Table 4.19: Imine formation reaction of fluoroacetophenone and benzyl amine catalysed using various MOF materials and under different reaction conditions

Entry	Catalyst	Temperature (K)	Benzyl amine (equivalents)	Conversion(%) ^a
1	no catalyst	293	1	3
2	MIL-100 (Sc)	"	"	49
3	HKUST-1(Cu)	"	"	11
4	MIL-100 (Sc)	333	"	60
5	MIL-100(Cr)	"	"	20
6	MIL-100(Fe)	"	"	15
7	MIL-100(Al)	"	"	19
8	no catalyst	373	"	8
9	HKUST-1 (Cu)	"	"	20
10	MIL-100 (Sc)	"	"	85
11	MIL-100(Sc) ^b	"	"	85
12	MIL-100(Cr)	"	"	49
13	MIL-100(Fe)	"	"	27
14	MIL-100(Al)	"	"	31
15	MIL-88D(Sc)	"	"	35
16	STA-12(Ni)	"	"	5
17	MIL-100(Sc)	"	1.2	92
18	MIL-100(Sc)	"	1.5	95
19	MIL-100 (Sc)	"	2	>99
20	MIL-100(Cr)	"	2	55
21	MIL-88D(Sc)	"	2	40
22	HKUST-1(Cu)	"	2	23

^a 4' – Fluoroacetophenone (0.13 mmol) and benzylamine (0.13 mmol), 1-methylnapthalene (0.4mmol) were added to a solution of toluene (5ml) and pre-activated MOF (2.5 mol%) and stirred at 373 K for 8 h.
^b Recycled MIL-100(Sc) at 373 K.

The high activity of MIL-100(Sc) was retained after recovery and methanol washing of the material (Table 4.19, entry 11). PXRD showed no change in the structure after further cycles (Figure 4.14).

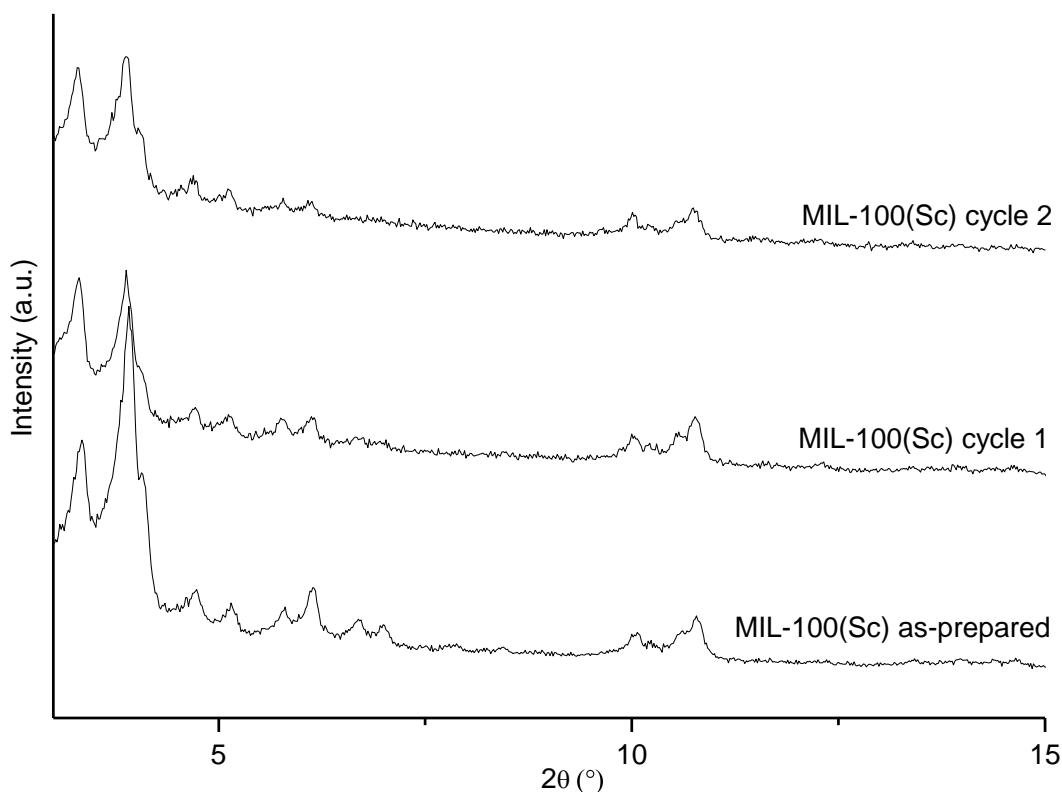
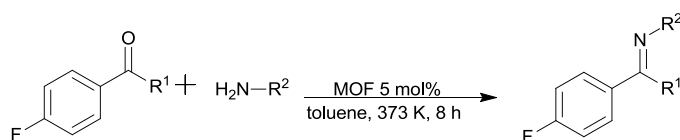


Figure 4.14: PXRD patterns of material recovered after each reaction cycle compared to as-prepared material

4.3.2. Imine formation using MIL-100(Sc) with varying amines and carbonyl compounds

The scope of the reaction MIL-100(Sc) was determined by using different amines and carbonyl compounds (Table 4.20, Scheme 4.15). The reaction of 4-fluorobenzaldehyde with benzyl amine was carried out. After 1 h the reaction had a conversion of 93% and eventually went to completion after 3 h (Table 4.20, entry 2). The control without catalyst already gave a conversion of 63 % however. Thus, while MIL-100(Sc) does catalyse this reaction it is not important from a practical perspective.



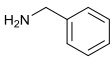
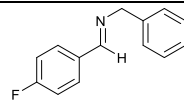
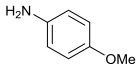
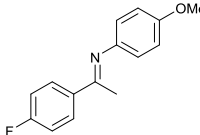
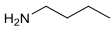
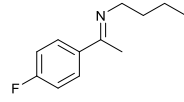
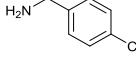
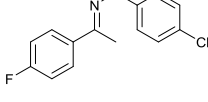
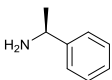
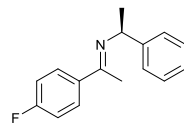
Scheme 4.15: Imine formation using varying amines

More challenging amine substrates were investigated using fluoroacetophenone rather than 4-fluorobenzaldehyde (making the reaction more difficult to catalyse). The reaction

between *p*-anisidine and fluoroacetophenone was found to give high conversions when the reaction was carried out at 373 K (Table 4.20, entry 3). Conversion of 92% to product was obtained which was then increased to full conversion by simply increasing the equivalents of benzyl amine to 2 and removing the excess benzyl amine by a weak acid wash after completion.

When using an aliphatic amine (butylamine) the conversion dropped to 70%. This could be attributed to the lower temperature of the reaction (343 K) with butyl amine due to its lower boiling point. Changing the substrate to chlorobenzyl amine found the reaction proceeded better when using the solvent hexane, even at lower temperatures (Table 4.20, entries 6 and 7).

Table 4.20: Imine formation reaction of fluoroacetophenone with a range of amines

Entry	R ¹	Temp (K)	Amine equivalents	R-NH ₂	Product	Product (%) ^a
1 ^b	H	293	1			63
2	H	"	"	"	"	93
3	CH ₃	373	"			82
4	CH ₃	"	2	"	"	>99
5 ^c	CH ₃	343	"			70
6	CH ₃	373	1			85
7	CH ₃	"	2	"	"	91
8 ^d	CH ₃	383	"			96
9	CH ₃	373	"	"	"	72

4' – Fluoroacetophenone (0.65 mmol) and 4-methoxyaniline (0.65 mmol), 1-methylnaphthalene (0.4 mmol) were added to a solution of toluene (5 ml) with pre-activated MOF (5 mol%) and stirred at 373 K for 8 h.^a Determined by ¹H NMR using 1-methylnaphthalene as internal standard. ^b no catalyst. ^c Solvent hexane. ^d Dean Stark apparatus used.

The final substrate investigated was (*S*)-1-phenylethylamine. In order to achieve high conversion in this reaction the temperature had to be increased and also the use of Dean

Stark apparatus was required to remove water formed in the reaction, which increased the conversion from 72% to 96%.

The imine formation reaction proved to be a successful reaction for MIL-100(Sc) and by simply optimising the reaction conditions for different substrates high and even full conversion to the required imine product was obtained.

4.4. Conclusion

These investigations demonstrate the ability of different MOF materials to act as heterogeneous and recyclable Lewis acid catalysts for a range of C-C and C=N bond formation reactions. MIL-100(Sc) proved to be the most successful of the MOF materials used in all the reactions attempted by a considerable margin. Not only could MIL-100(Sc) give a high catalytic activity, but it could also be easily recovered, and maintained its high activity even after 5 cycles. PXRD indicated that its structural integrity was maintained after each cycle. MIL-100(Sc) has many advantages over the other scandium materials used: it is easily synthesised, easily activated (sometimes not even requiring pre-activation before reaction), stable in air and can still be used after contact with moisture. Its large surface area and mesoporous cages enable the active sites in the material to be readily accessed (unlike socMOF, which has a window size too small to allow access to its active sites). The comparison of different MOFs has underlined that not only is the Lewis acidic metal cation used in the material important, but the environment of the active site is also critical.

It was initially thought that as MIL-100(Sc) gave high activity, other scandium containing MOFs would behave similarly. However, this has not been the case. Although it would be expected that MIL-101(Sc) would give similar if not higher activities than MIL-100(Sc) (due to its larger pore and window size) the instability of the material reduces its activity as it readily recrystallises to MIL-88B. The larger pore MIL-88D(Sc) was also expected to show high activity however studies (B. Gonzales) have shown there is a high chance that the structure is an interpenetrated one which reduces the window size and hinders access to the active sites. MIL-88B(Sc) remains in a 'closed pore' form when reactions are carried out in toluene, therefore, has no accessible Lewis acid sites. In a polar solvent that allows the material to be in its 'open pore' form but the catalytic activity still remains low because of strong solvent binding to scandium.

The synthesis of larger substrates has enabled investigation of whether the indole reaction occurs on the surface or in the pore of the structure. The results indicate that most of the reaction occurs within the pore of the material, although some sites must be accessible from the surface as some conversion of larger substrates still occurs.

MIL-100(Sc) was also compared to other trivalent metal containing MIL-100 materials in catalysis. This allowed for comparison of activities of different metals which could then be compared to results obtained in IR spectroscopy (discussed in section 3.3). Probing of Lewis acid acidity using CD₃CN indicated that MIL-100(Sc) has slightly lower Lewis acid strength compared to MIL-100(Fe, Cr) and was a weaker Lewis acid than MIL-100(Al). It was also found that MIL-100(Sc) contained fewer Lewis acid sites than MIL-100(Fe, Cr) with ~ 1.5 active sites per trimer, compared to 2 in MIL-100(Fe, Cr) after activation at similar conditions. More Lewis acid sites appeared to be present after activation at 523 K however when pre-activated at this temperature for catalysis more by-products were formed therefore pre-activation for each reaction was carried out at 423 K. MIL-100(Sc) easily outperformed each of these materials in various C-C bond forming reactions. It appears that MIL-100(Sc) obtains the optimum acid strength to allow substrates to be activated for catalysis and products to be released to give high yields. The higher Lewis acid strength of other materials in the series may be too strong to allow release of substrate from the Lewis acid site, preventing catalytic turnover from occurring. Figure 4.15 shows the larger of the windows in MIL-100(Sc) and the 5-fold coordinated Lewis acid site is also shown and provides an excellent example of a single site in a heterogeneous catalyst, as defined by Thomas.⁵⁰ This site possesses a good Lewis acidity for the reactions attempted compared to the other MOF materials tested. The 9 Å pore size allows for substrates of a specific size to access the site and reactants to leave the pore. Coordinating solvent and substrate can be exchanged when less polar solvents are used in the reaction. When polar solvents are used in the reaction, the performance of the material decreases, probably because the solvent binds to the Lewis acidic site and prevents further reaction from occurring.

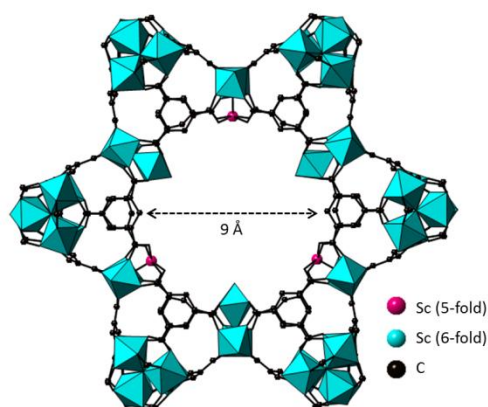


Figure 4.15: MIL-100(Sc) structure showing vacant Lewis acidic sites

This has shown that MIL-100(Sc) is one of the most useful MOF materials tested for Lewis acid catalysed reactions and could be a very useful catalyst for use in batch or flow reactors.

4.5. References

1. S. Kobayashi, *Synlett*, 1994, 689-701.
2. S. Kobayashi, *Eur. J. Org. Chem.*, 1999, 15-27.
3. A. G. M. Barrett and D. C. Braddock, *Chem. Commun.*, 1997, 351-352.
4. C. McDonagh and P. O'Leary, *Tetrahedron Lett.*, 2009, **50**, 979-982.
5. D. A. Evans, S. W. Tregay, C. S. Burgey, N. A. Paras and T. Vojkovsky, *J. Am. Chem. Soc.*, 2000, **122**, 7936-7943.
6. K. Wakita, G. B. Bajracharya, M. A. Arai, S. Takizawa, T. Suzuki and H. Sasai, *Tetrahedron: Asymmetry*, 2007, **18**, 372-376.
7. S. Kobayashi and S. Nagayama, *J. Am. Chem. Soc.*, 1996, **118**, 8977-8978.
8. S. Kobayashi and R. Akiyama, *Chem. Commun.*, 2003, 449-460.
9. H. Sellner, C. Faber, P. B. Rheiner and D. Seebach, *Chem.-Eur. J.*, 2000, **6**, 3692-3705.
10. A. Corma, M. T. Navarro and M. Renz, *J. Catal.*, 2003, **219**, 242-246.
11. A. Corma, M. E. Domine and S. Valencia, *J. Catal.*, 2003, **215**, 294-304.
12. K. P. Boroujeni, A. Zhianinasab and M. Jafarinasab, *J. Serb. Chem. Soc.*, 2013, **78**, 155-164.
13. J. C. Jansen, E. J. Creighton, S. L. Njo, H. vanKoningsveld and H. vanBekum, *Catal. Today*, 1997, **38**, 205-212.
14. E. M. El-Malki, R. A. van Santen and W. M. H. Sachtler, *J. Phys. Chem. B*, 1999, **103**, 4611-4622.
15. M. L. Clarke and M. B. France, *Tetrahedron*, 2008, **64**, 9003-9031.
16. A. Corma and M. Renz, *Chem. Commun.*, 2004, 550-551.
17. L. Alaerts, E. Seguin, H. Poelman, F. Thibault-Starzyk, P. A. Jacobs and D. E. De Vos, *Chem.-Eur. J.*, 2006, **12**, 7353-7363.
18. K. Schlichte, T. Kratzke and S. Kaskel, *Microporous Mesoporous Mater.*, 2004, **73**, 81-88.
19. F. Xamena, O. Casanova, R. G. Tailleux, H. Garcia and A. Corma, *J. Catal.*, 2008, **255**, 220-227.
20. A. Corma, H. Garcia and F. X. L. Xamena, *Chem. Rev.*, 2010, **110**, 4606-4655.

21. A. Corma, M. Iglesias, F. Xamena and F. Sanchez, *Chem.-Eur. J.*, 2010, **16**, 9789-9795.
22. A. Dhakshinamoorthy, M. Alvaro and H. Garcia, *Appl. Catal. A*, 2010, **378**, 19-25.
23. A. Dhakshinamoorthy, M. Alvaro and H. Garcia, *Chem.-Eur. J.*, 2010, **16**, 8530-8536.
24. A. Dhakshinamoorthy, M. Alvaro and H. Garcia, *Acs Catalysis*, 2011, **1**, 48-53.
25. I. Luz, F. X. Llabres i Xamena and A. Corma, *J. Catal.*, 2010, **276**, 134-140.
26. Y. Wu, L.-G. Qiu, W. Wang, Z.-Q. Li, T. Xu, Z.-Y. Wu and X. Jiang, *Transition Met. Chem.*, 2009, **34**, 263-268.
27. F. G. Cirujano, F. X. Llabres i Xamena and A. Corma, *Dalton Trans.*, 2012, **41**, 4249-4254.
28. M. L. Clarke, C. E. S. Jones and M. B. France, *Beilstein J. Org. Chem.*, 2007, **3**.
29. J. A. Groves, S. R. Miller, S. J. Warrender, C. Mellot-Draznieks, P. Lightfoot and P. A. Wright, *Chem. Commun.*, 2006, 3305-3307.
30. M. T. Wharmby, J. P. S. Mowat, S. P. Thompson and P. A. Wright, *J. Am. Chem. Soc.*, 2011, **133**, 1266-1269.
31. P. D. C. Dietzel, R. Blom and H. Fjellvag, *Eur. J. Inorg. Chem.*, 2008, 3624-3632.
32. J. P. S. Mowat, S. R. Miller, A. M. Z. Slawin, V. R. Seymour, S. E. Ashbrook and P. A. Wright, *Microporous Mesoporous Mater.*, 2011, **142**, 322-333.
33. A. Vimont, J. M. Goupil, J. C. Lavalley, M. Daturi, S. Surblé, C. Serre, F. Millange, G. Férey and N. Audebrand, *J. Am. Chem. Soc.*, 2006, **128**, 3218-3227.
34. P. Horcajada, S. Surblé, C. Serre, D.-Y. Hong, Y.-K. Seo, J.-S. Chang, J.-M. Grenèche, I. Margiolaki and G. Férey, *Chem. Commun.*, 2007, 2820-2822.
35. C. Volkringer, H. Leclerc, J.-C. Lavalley, T. Loiseau, G. Férey, M. Daturi and A. Vimont, *J. Phys. Chem. C*, 2012, **116**, 5710-5719.
36. O. I. Lebedev, F. Millange, C. Serre, G. Van Tendeloo and G. Férey, *Chem. Mater.*, 2005, **17**, 6525-6527.
37. L. Mitchell, B. Gonzalez-Santiago, J. P. S. Mowat, M. E. Gunn, P. Williamson, N. Acerbi, M. L. Clarke and P. A. Wright, *Catal. Sci. Tech.*, 2013, **3**, 606-617.
38. M. J. Beier, W. Kleist, M. T. Wharmby, R. Kissner, B. Kimmerle, P. A. Wright, J.-D. Grunwaldt and A. Baiker, *Chem.-Eur. J.*, 2012, **18**, 887-898.
39. P. L. Llewellyn, S. Bourrelly, C. Serre, A. Vimont, M. Daturi, L. Hamon, G. De Weireld, J. S. Chang, D. Y. Hong, Y. K. Hwang, S. H. Jung and G. Férey, *Langmuir*, 2008, **24**, 7245-7250.
40. G. Férey, C. Mellot-Draznieks, C. Serre, F. Millange, J. Dutour, S. Surblé and I. Margiolaki, *Science*, 2005, **309**, 2040-2042.
41. Y.-T. Li, K.-H. Cui, J. Li, J.-Q. Zhu, X. Wang and Y.-Q. Tian, *Chin. J. Inorg. Chem.*, 2011, **27**, 951-956.
42. S. Surblé, C. Serre, C. Mellot-Draznieks, F. Millange and G. Férey, *Chem. Commun.*, 2006, 284-286.
43. J. Mowat, Ph.D. Thesis, University of St. Andrews, 2012.
44. X. S. Wang, X. W. Wang, H. C. Guo, Z. Wang and K. L. Ding, *Chem.-Eur. J.*, 2005, **11**, 4078-4088.
45. T. Urushima, Y. Yasui, H. Ishikawa and Y. Hayashi, *Org. Lett.*, 2010, **12**, 2966-2969.
46. J. S. Yadav, S. Abraham, B. V. S. Reddy and G. Sabitha, *Synthesis-Stuttgart*, 2001, 2165-2169.

47. B. Van de Voorde, M. Boulhout, F. Vermoortele, P. Horcajada, D. Cunha, J. S. Lee, J.-S. Chang, E. Gibson, M. Daturi, J.-C. Lavalley, A. Vimont, I. Beurroies and D. E. De Vos, *J. Am. Chem. Soc.*, 2013, **135**, 9849-9856.
48. J. S. Yadav, S. Abraham, B. V. S. Reddy and G. Sabitha, *Tetrahedron Lett.*, 2001, **42**, 8063-8065.
49. J. Moskal and P. Milart, *Synthesis-Stuttgart*, 1984, 128-132.
50. J. M. Thomas, *Design and Applications of Single-Site Heterogeneous Catalysts, Clean Technology and Sustainability*, Imperial College Press, London, 2012.

5. Synthesis, characterisation and catalytic performance of mixed metal MOFs

5.1. Introduction

The synthesis of mixed metal MOFs, their characterisation and catalytic activity are discussed in this chapter. The introduction of different metals into the structure has previously been mentioned in chapter 1 as well as the different synthetic routes to the synthesis of mixed metal MOFs. The introduction of a secondary metal by immobilisation of a catalyst into the structure,¹⁻³ post-synthetic modification,⁴⁻⁶ introduction of nanoparticles⁷⁻⁹ and introduction of two or more metals in the original synthesis have all been used to form mixed metal materials.¹⁰⁻¹³ This chapter describes the use of a mixture of metals for direct mixed metal MOF synthesis. In particular, this technique will be used in the synthesis of mixed metal forms of MIL-100. The effects on structure that are caused by the additional metals and the properties of the materials as catalysts are described below.

5.2. Synthesis of mixed metal MIL-100(Sc)

MIL-100(Sc) exhibits high catalytic activity for C-C and C=N bond-forming reactions (chapter 4). However, the cost of scandium could make this catalyst relatively expensive. By replacing some of the scandium in the material with a cheaper more abundant metal the cost can be greatly reduced, hopefully with retention of catalytic activity. Both the introduction of divalent and trivalent metals was therefore carried out and the effects of this substitution on the catalytic activity has been studied.

5.2.1. MIL-100(Sc/Fe)

The introduction of iron into MIL-100(Sc) was initially tried as both metals can be used for the synthesis of MIL-100 materials. The two metal sources used were added in various ratios to synthesise final products with different metal ratios (Table 5.1). $\text{ScCl}_3(\text{aq})$ (prepared by dissolving Sc_2O_3 in a stoichiometric amount of HCl to produce $\text{ScCl}_3(\text{aq})$) and $\text{FeCl}_3 \cdot 6\text{H}_2\text{O}$ were found to give good control with regard to the final metal ratio in the MIL-100 and were the reagents of choice. Other metal sources (including scandium nitrate hydrate and iron nitrate nonahydrate) also gave materials of desired metal cation ratios. $\text{ScCl}_3(\text{aq})$ and $\text{FeCl}_3 \cdot 6\text{H}_2\text{O}$ were placed in a Teflon-lined steel autoclave with the appropriate ligand and solvent; in this case BTC and DMF.

They were then heated at 383 K for 24 h (Figure 5.1). MIL-100(Fe) was synthesised using the method previously published by Canioni *et al.*¹⁴

Table 5.1: Ratios of metals used in the synthesis of MIL-100(Sc/Fe)

Entry	Ratio (M ₁ :M ₂ :L:DMF)	MOF	Ratio by EDX
1	2.4:0.6:2:600	MIL-100(Sc ₈₀ /Fe ₂₀)	80/20
2	1.8:1.2:2:600	MIL-100(Sc ₆₀ /Fe ₄₀)	58/42
3	1.2:1.8:2:600	MIL-100(Sc ₄₀ /Fe ₆₀)	36/64
4	0.6:2.4:2:600	MIL-100(Sc ₂₀ /Fe ₈₀)	21/79

M₁ = Scandium source, M₂= Iron source, L=Ligand



Figure 5.1: Synthesised MIL-100(Sc/Fe) series

After removal from the oven and cooling, the products were filtered and the solids dried. In order to prepare the MOFs for catalysis they were washed, stirred in methanol for 24 h then filtered and dried. These materials were analysed using different characterisation techniques (PXRD, EDX, N₂ adsorption, TGA, UV-Visible and X-ray absorption spectroscopy (EXAFS/XANES)) to determine the structure, porosity and the metal content in the MOF.

The PXRD patterns of the materials show that the material are all pure MIL-100, although a slight reduction in crystallinity is observed as the iron content is increased (Figure 5.2).

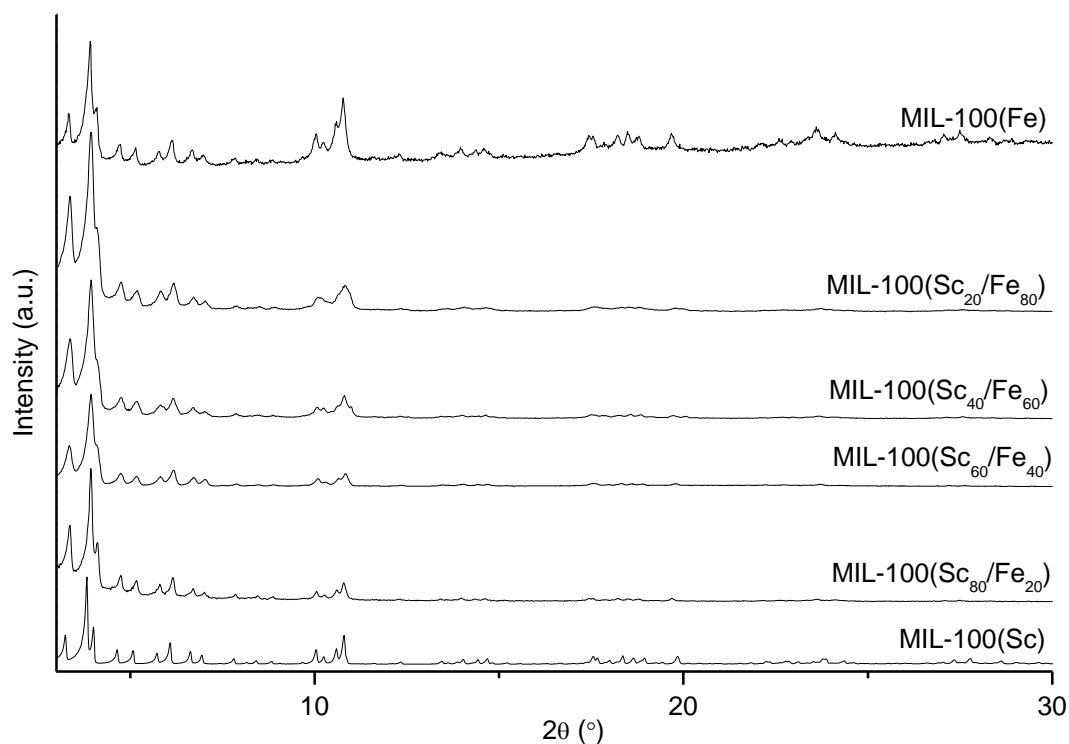


Figure 5.2: PXRD patterns of MIL-100(Sc/Fe) materials

EDX analysis of the materials confirms the ratio of scandium to iron contained in the material matches the amount of scandium and iron used in the initial synthesis within experimental error (Table 5.1). N₂ adsorption was used to quantify the surface areas of each material which are similar throughout with a BET surface area with a range of 1320-1350 m²g⁻¹ (Figure 5.3, Table 5.2). The adsorption shows that each material is mesoporous with each material having a similar 2-step adsorption, as discussed in the techniques chapter.

Table 5.2: BET surface area of MIL-100(Sc/Fe) materials (at $p/p_0 = 0.4$)

MOF	BET surface area (m ² g ⁻¹)
MIL-100(Sc)	1346
MIL-100(Sc ₈₀ /Fe ₂₀)	1322
MIL-100(Sc ₆₀ /Fe ₄₀)	1335
MIL-100(Sc ₄₀ /Fe ₆₀)	1345
MIL-100(Sc ₂₀ /Fe ₈₀)	1352
MIL-100(Fe)	1329

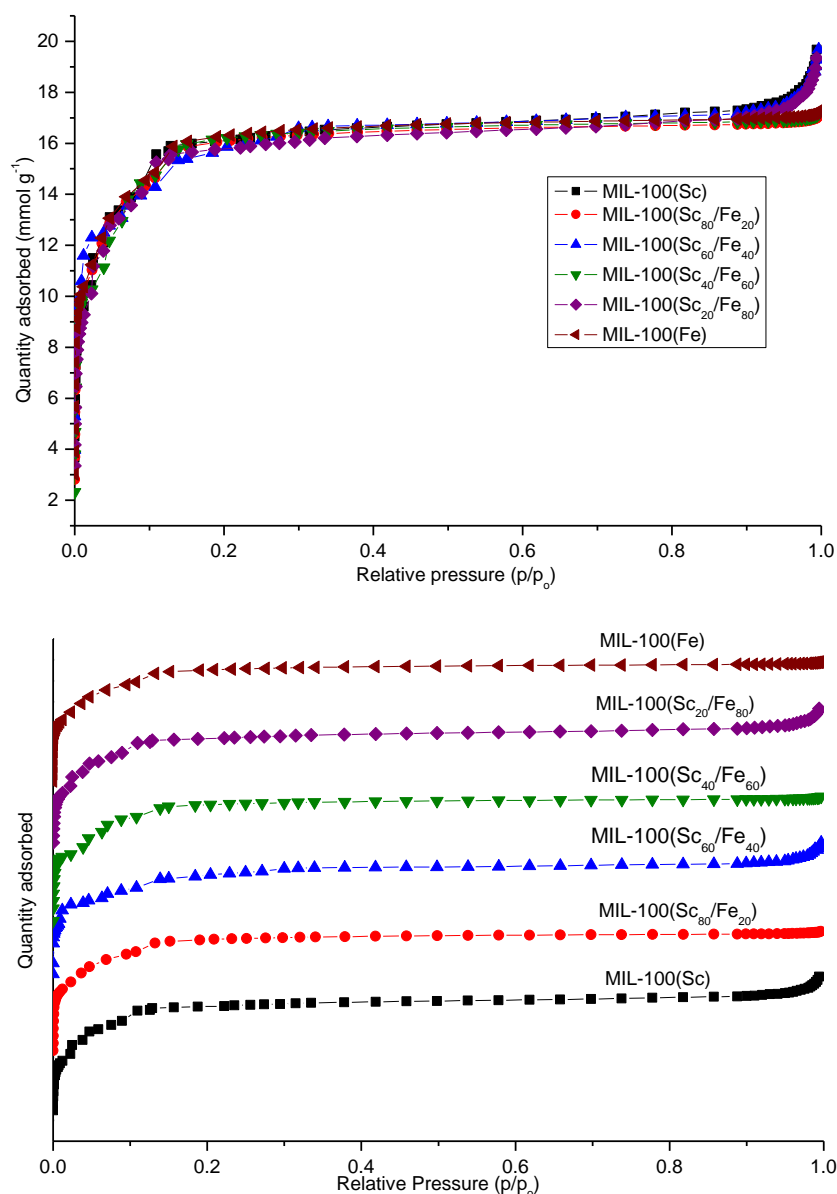


Figure 5.3: N₂ adsorption at 77 K (a) Comparison of mmol g⁻¹ uptake of mixed metal MIL-100 materials (b) Stacked view of N₂ isotherms (offset by 7 mmol g⁻¹)

Thermogravimetric analysis of the materials indicates that there is a decrease in the thermal stability of the materials as Fe is included: MIL-100(Sc₈₀/Fe₂₀) decomposes at a lower temperature than MIL-100(Sc) for example. A gradual decrease in the mass between 323 K and 600 K is caused by the loss of DMF. Finally, weight loss above 600 K is caused by the decomposition of the structure, leaving metal oxides (Figure 5.4). The overall weight percentage after calcination is higher for the iron-containing materials which is expected due to the higher mass of iron (Fe, 55.845 amu; Sc, 45.54 amu).

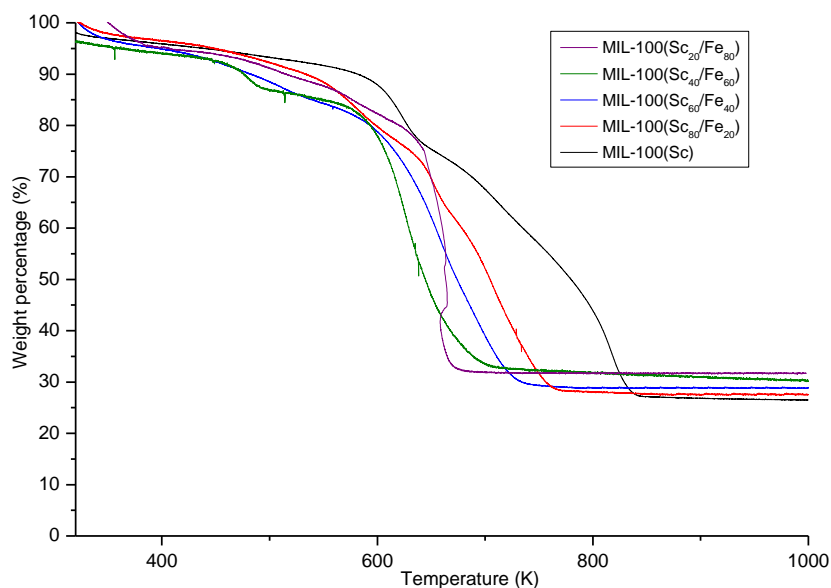


Figure 5.4: TGA carried out in air of (a) MIL-100(Sc) (black) (b) MIL-100(Sc₈₀/Fe₂₀) (red) (c) MIL-100(Sc₆₀/Fe₄₀) (blue) (d) MIL-100(Sc₄₀/Fe₆₀) (green) (e) MIL-100(Sc₂₀/Fe₈₀) (purple)

UV-visible spectroscopy was also used to follow the increase in the iron concentration in the materials. Scandium in the materials contains no d -electrons therefore does not absorb in the visible region. However, Fe^{3+} in the high spin state possesses d -electrons and absorption is detected from $d-d$ transitions. Absorption between 250 nm and 450 nm is likely to be caused by charge transfer between metal and ligand and $d-d$ transitions ${}^6\text{A}_{1g} \rightarrow {}^4\text{T}_{1g}$ and ${}^6\text{A}_{1g} \rightarrow {}^4\text{E}_g$. An increase in iron content can be observed by the increase in absorbance between 450-600 nm due to the ${}^6\text{A}_{1g} \rightarrow {}^4\text{T}_{2g}$ transition (Figure 5.5).^{15, 16} The absorptions observed are from $d-d$ transitions characteristic of octahedral Fe^{3+} , supporting a model where iron replaces scandium in the trimer.¹⁷

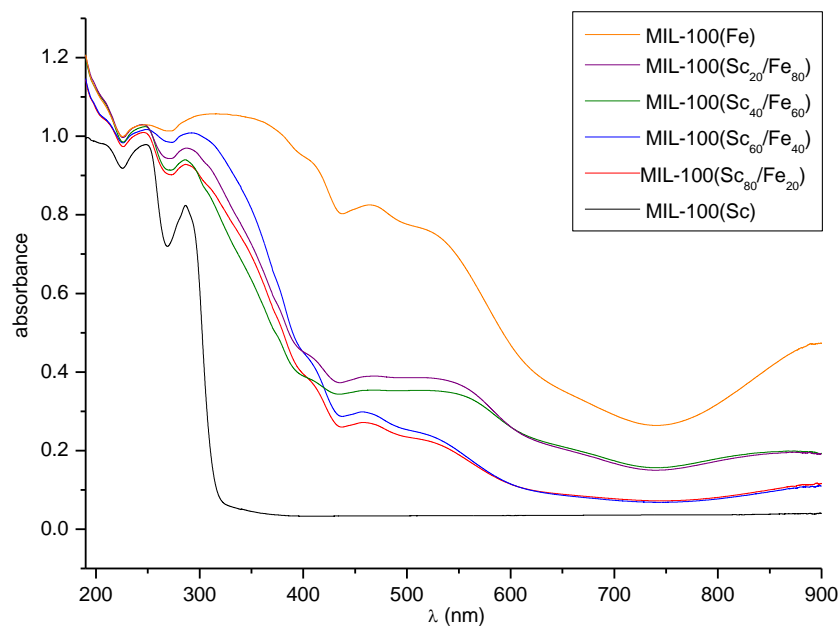


Figure 5.5: Comparison of UV-visible spectra of samples in the MIL-100(Sc/Fe) series

In order to detect any changes in the unit cell of the materials caused by the introduction of the smaller iron cation (ionic radii of iron (III) 78.5 pm; of scandium (III) 88.5 pm)¹⁸ analysis of the PXRD pattern was carried out. Rietveld refinement could not be carried out on the material due to the large unit cell and presence of disordered solvent in the materials. Instead, the Le Bail structureless refinement method was used in order to determine the unit cell.

MIL-100(Fe) was taken as having the same symmetry and unit cell as the mixed metal MIL-100 series so its symmetry ($Fd\bar{3}m$) and unit cell parameters ($a = 73.3402 \text{ \AA}$) were used as a starting point in the refinements.¹⁹ The $Fd\bar{3}m$ unit cell was found to fit well for all members of the series. A decrease in a parameter was observed with increasing amount of iron shown in Figure 5.6 as expected from Vegard's Law for solid solutions. The catalytic activity of members of the MIL-100(Sc/Fe) series was then measured as discussed further in Section 5.5.

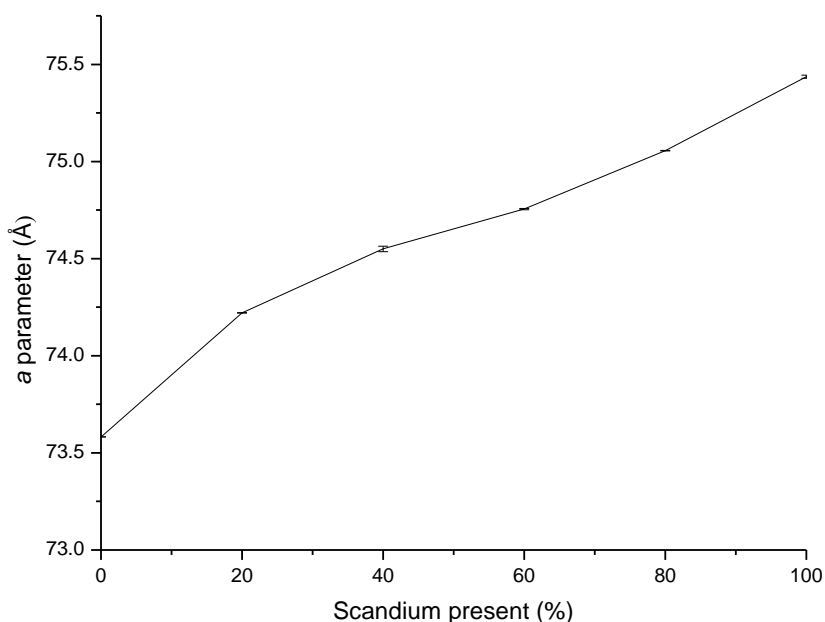
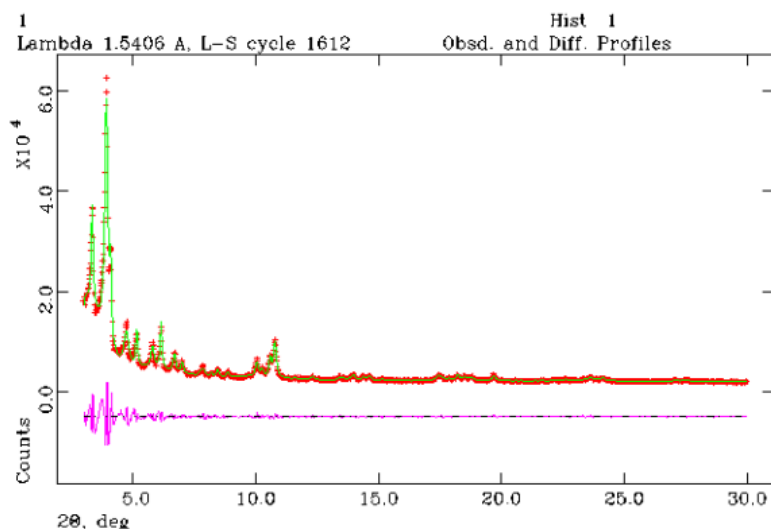


Figure 5.6: (a) *Le Bail* refinement of $Fd\bar{3}m$ structure less model against MIL-100(Sc_{60}/Fe_{40}) pattern giving $a \approx 74.755(3) \text{ \AA}$ (b) The cubic a parameter of each mixed metal material in the MIL-100(Sc/Fe) series as a function of Sc^{3+} content in the trimers ($Sc^{3+}/Sc^{3+} + Fe^{3+}$)

5.2.2. MIL-100(Sc/Fe) with included α - Fe_2O_3 nanoparticles

A second series of mixed metal materials was synthesised using an excess of iron salt ($FeCl_3 \cdot 6H_2O$). In the previous syntheses of MIL-100(Sc/Fe) materials the synthesis was carried out using a 3:2 ratio of metal:ligand: in these experiments the ratio of trivalent metal to ligand was varied for 4:2 to 7:2 (Table 5.3). These materials prepared with excess of Fe are described as MIL-100(Sc/Fe)Xs MOFs in the following discussion.

It was found that when using three equivalents of scandium and one of iron the MIL-100 material showed preference for scandium. No iron was incorporated into the material (Table 5.3, entry 1). Using two equivalents of scandium and 2.5 to 5 equivalents of iron MIL-100 materials with different properties were synthesised. The first significant difference observed in the materials was the colour – in this series the materials appeared pink, clearly different from the MIL-100(Sc/Fe) series, which solids were orange of different intensities.

Table 5.3: Molar ratios of metal sources used in the synthesis of mixed metal MIL-100(Sc/Fe)Xs

Entry	Ratio (Sc:Fe:L:DMF)	MOF	Ratio by EDX
1	3:1:2:600	MIL-100(Sc)	100
2	2:2.5:2:600	MIL-100(Sc ₉₀ /Fe ₁₀)Xs	89/11
3	2:3:2:600	MIL-100(Sc ₈₀ /Fe ₂₀)Xs	78/22
4	2:4:2:600	MIL-100(Sc ₆₀ /Fe ₄₀)Xs	64/36
5	2:5:2:600	MIL-100(Sc ₅₀ /Fe ₅₀)Xs	49/51

Xs = excess iron present, above that required to fill trimers L=BTC



Figure 5.7: Synthesised MIL-100(Sc/Fe)Xs series compared to MIL-100(Sc/Fe) series materials

Further analysis was carried out on this series of pink materials (MIL-100(Sc/Fe)Xs) (Figure 5.7). Initially PXRD analysis was used to determine if any structural changes were apparent. The pattern showed no other phases present apart from MIL-100(Sc). However a change in intensities of the peaks is observed. This is most marked between

$2\theta = 3$ and 4° where the first peak is of larger intensity than the second peak which was the opposite of what is observed in the MIL-100(Sc/Fe) series. A change is also noticeable between $2\theta = 6$ and 7° as the two peaks in this region are now of similar intensity (Figure 5.8).

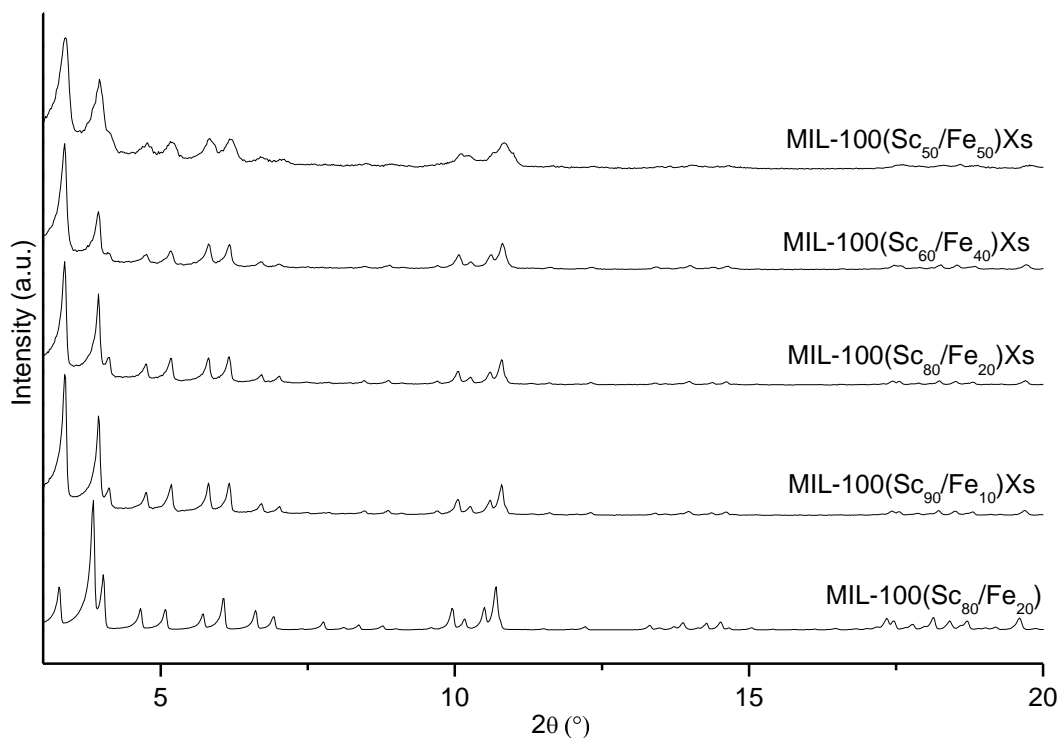


Figure 5.8: PXRD patterns of MIL-100(Sc/Fe)Xs materials

UV-visible spectroscopy shows significant differences between the spectra of the MIL-100(Sc/Fe) series and the MIL-100(Sc/Fe)Xs series. Weak absorptions from 450-550 nm are observed (Figure 5.5) caused by spin forbidden $d-d$ transitions in the MIL-100(Sc/Fe) series described in section 5.2.1. In Figure 5.9 the materials of same scandium/iron concentration have much stronger absorbance between 300 and 600 nm. This is likely to be caused by the presence of small iron oxide particles in the material.

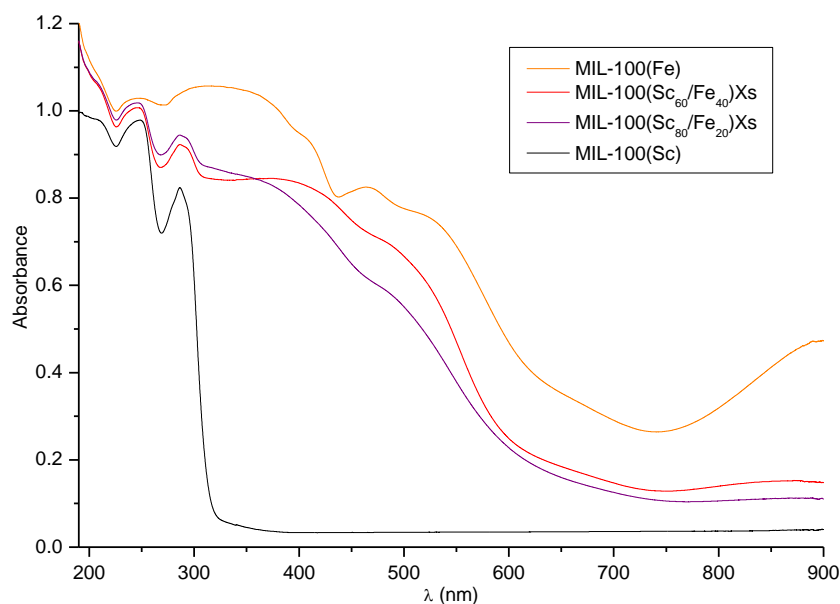


Figure 5.9: UV-visible spectroscopy of (a) MIL-100(Sc/Fe)Xs series compared to MIL-100(Sc) and MIL-100(Fe)

One explanation for the UV-visible spectroscopy and PXRD data is that Fe^{3+} oxide nanoparticles are present in the pores of the MOF materials. This was investigated further by X-ray absorption spectroscopy (XANES and EXAFS).^{*} MIL-100(Sc/Fe) and MIL-100(Sc/Fe)Xs materials were compared to the reference samples $\alpha\text{-Fe}_2\text{O}_3$ (hematite), $\gamma\text{-Fe}_2\text{O}_3$ (maghemite) and Fe_3O_4 (magnetite). The X-ray XANES showed the MIL-100(Sc/Fe) materials had K-edge energies to materials that contain iron in a 3+ state (Figure 5.10). All the materials in the MIL-100(Sc/Fe) series had similar spectra and also compare to previously published spectra of MIL-100(Fe), providing further evidence that iron is Fe^{3+} in the trimer of the materials.²⁰

Interestingly, the XANES spectra of the MIL-100(Sc/Fe)Xs materials show similarities to absorbance edge of hematite, $\alpha\text{-Fe}_2\text{O}_3$ suggesting at least part of the iron in this series of materials is caused by nanoparticles of $\alpha\text{-Fe}_2\text{O}_3$. This evidence shows that although some the iron is substituting in the iron trimers the remainder is due to $\alpha\text{-Fe}_2\text{O}_3$. An increase in the amount of $\alpha\text{-Fe}_2\text{O}_3$ -like signal is observed in the XANES spectra as the Fe/Sc molar ratio of increases (Figure 5.10). This was further probed by EXAFS analysis. This also showed the MIL-100(Sc/Fe)Xs materials had similar EXAFS spectra to $\alpha\text{-Fe}_2\text{O}_3$.

^{*} carried out by Prof. Richard Walton and Luke Daniels at Diamond Light Source

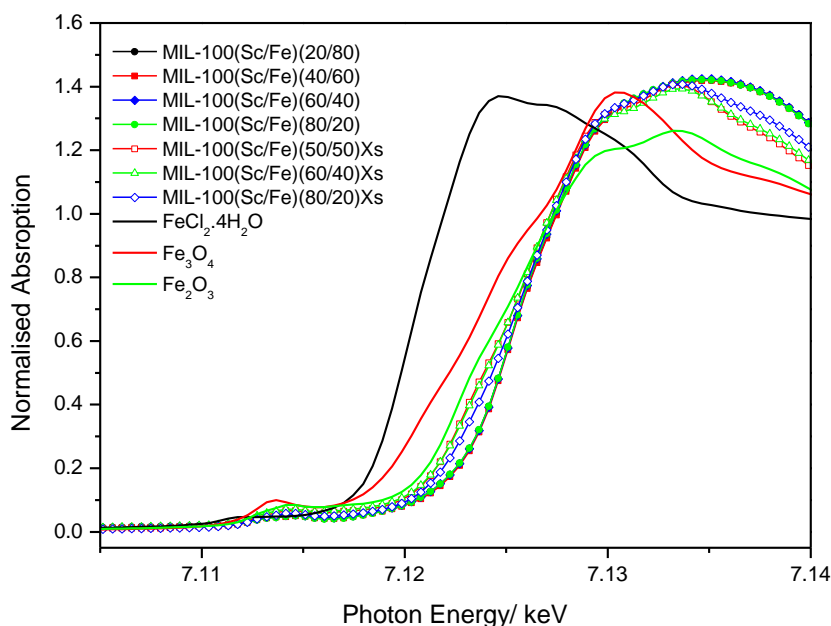


Figure 5.10: XANES spectra of MIL-100(ScFe) series and MIL-100(Sc/Fe)Xs series compared to reference samples α -Fe₂O₃, (hematite), γ -Fe₂O₃ (maghemite) and Fe₃O₄ (magnetite)

The Fourier-transformed EXAFs signals comparing α -Fe₂O₃, MIL-100(Sc₈₀/Fe₂₀)Xs and MIL-100(Sc₈₀/Fe₂₀) are shown in Figure 5.11. The Fourier-transforms represent the radial distribution of back scattering atoms around the central absorbing atom (Fe in this case). There is a phase shift in the EXAFs process so that the R values are all shifted compared to their real values. In each case EXAFs were modelled based on published MIL-100(Cr) data and each sample was tested against two different models. The first model contained Fe³⁺ with two Fe³⁺ nearest neighbours and the second in with Fe³⁺ which contained two Sc³⁺ nearest neighbours. Both models gave reasonable fits however the model which had Fe³⁺ with two Fe³⁺ nearest neighbours did provide better results than the Sc³⁺ model for the MIL-100(Sc/Fe) series. However this was not the case for the MIL-100(Sc/Fe)Xs series.

A peak in the FT signal at 2.5 Å is observed in MIL-100(Sc/Fe)Xs similar to that observed for α -Fe₂O₃ which is shown to increase as the amount of ‘Xs’ material is increased. It was also seen that the EXAFs data could not be satisfactorily fitted with MIL-100 data but in fact could be fitted using coordination numbers and distances of α -Fe₂O₃. The peak observed at 1-2 Å observed due to back scattering from the first shell of O atoms (Fe-O). This is strongest in MIL-100(Sc₈₀/Fe₂₀) however it is still present in

the ‘Xs’ material showing that although some of the iron is in nanoparticulate form some is also present in the trimers of the MOF.

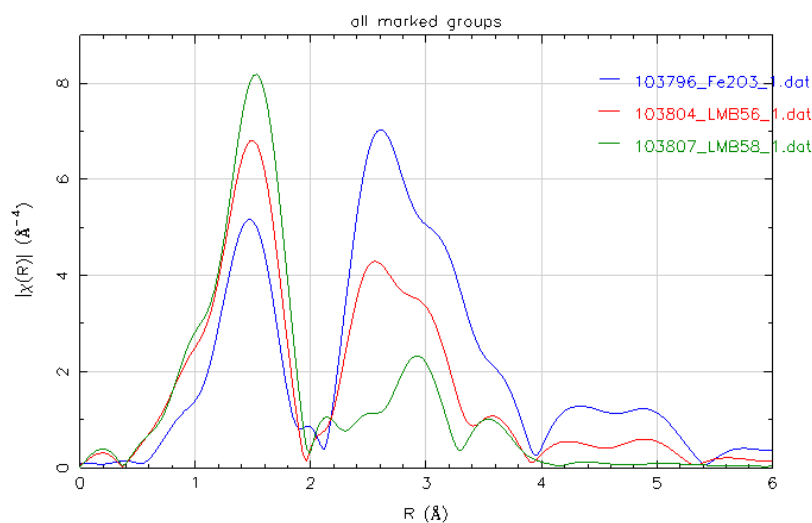


Figure 5.11: Fourier transform comparing $\alpha\text{-Fe}_2\text{O}_3$ (blue), MIL-100(Sc₈₀/Fe₂₀)Xs (red) and MIL-100(Sc₈₀/Fe₂₀) (green)

N₂ adsorption isotherms were obtained at 77 K for MIL-100(Sc/Fe)Xs materials. It was found that an increase of iron content (and $\alpha\text{-Fe}_2\text{O}_3$ signal measured by EXAFS) caused a reduction in the porosity. The BET surface area of the materials drops from 1325 m²g⁻¹ (MIL-100(Sc)) to 823 m²g⁻¹ for MIL-100(Sc₅₀/Fe₅₀)Xs which is a 37% reduction (Figure 5.12, Table 5.4). The reduction of N₂ capacity results partly from the additional mass of non-porous $\alpha\text{-Fe}_2\text{O}_3$ nanoparticles and also from the location of $\alpha\text{-Fe}_2\text{O}_3$ within the pores.

Table 5.4: BET surface area of MIL-100(Sc/Fe)Xs materials

MOF	BET surface area (m ² g ⁻¹)
MIL-100(Sc)	1346
MIL-100(Sc ₉₀ /Fe ₁₀)Xs	1325
MIL-100(Sc ₈₀ /Fe ₂₀)Xs	1172
MIL-100(Sc ₆₀ /Fe ₄₀)Xs	996
MIL-100(Sc ₅₀ /Fe ₅₀)Xs	823

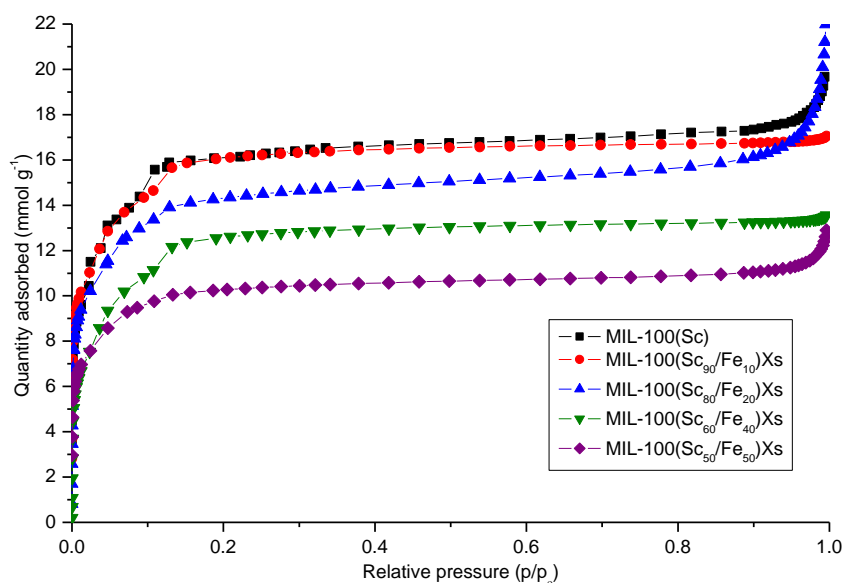
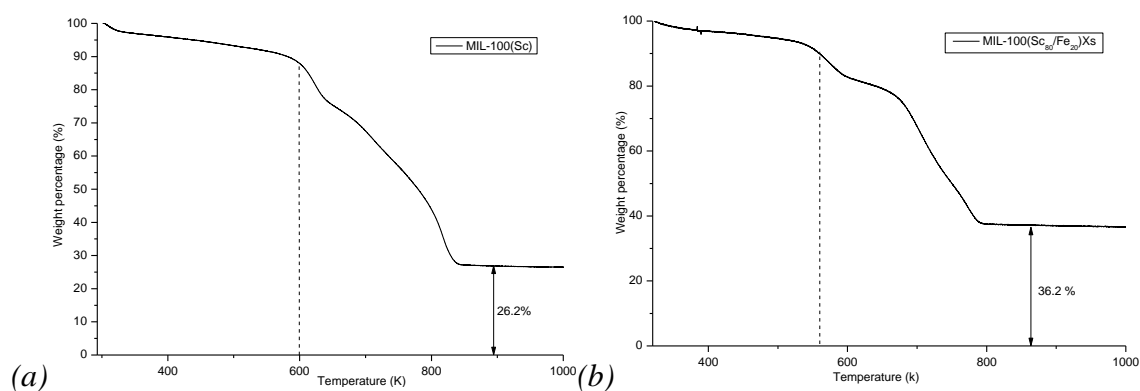


Figure 5.12: Comparison of N_2 adsorption isotherm at 77 K of mixed metal MIL-100Xs materials: MIL-100(Sc) (black), MIL-100(Sc_{90}/Fe_{10})Xs (red), MIL-100(Sc_{80}/Fe_{20})Xs (blue), MIL-100(Sc_{60}/Fe_{40})Xs (green), MIL-100(Sc_{50}/Fe_{50})Xs (purple)

TGA analysis of the materials shows that the materials are less thermally stable than MIL-100(Sc). Decomposition occurs at ca. 550 K rather than 600 K if iron is present (Figure 5.13). The residue after TGA of MIL-100(Sc) is around 26 wt % (Sc_2O_3) after thermal decomposition and between is 28-32% in MIL-100(Sc/Fe) series increasing with a higher ratio of iron. By contrast in the MIL-100(Sc/Fe)Xs materials a larger increase in the remainder of metal oxide left after calcination is observed. When TGA analysis was carried out on MIL-100(Sc_{80}/Fe_{20})Xs, 36.2% of remaining mass was observed from the metal oxides. This was 8% higher than what was observed in the equivalent MIL-100(Sc_{80}/Fe_{20}). This extra mass can be attributed to the α - Fe_2O_3 .



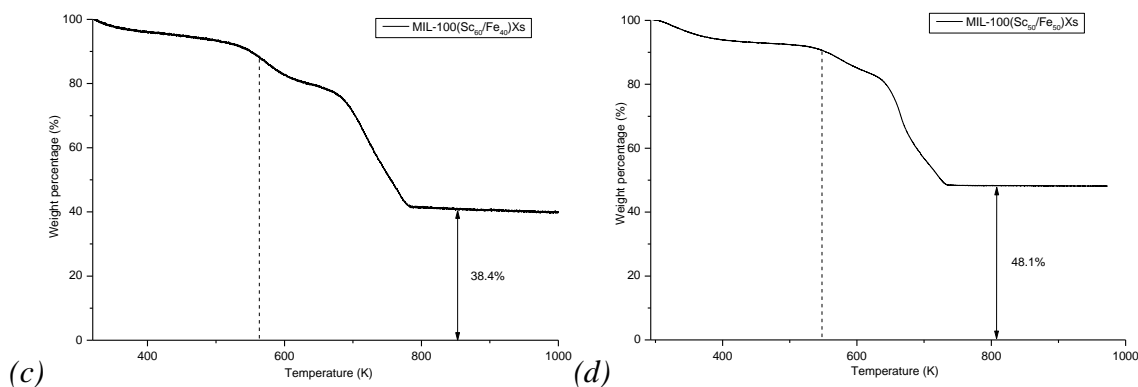


Figure 5.13: TGA under air showing oxide weight percentage remaining of (a) MIL-100(Sc), (b) MIL-100(Sc₈₀/Fe₂₀)Xs, (c) MIL-100(Sc₆₀/Fe₄₀)Xs, (d) MIL-100(Sc₅₀/Fe₅₀)Xs

The remaining mass left after calcination allowed for calculation of the amount of nanoparticles in the material. Using the TGA obtained for MIL-100(Sc) the molecular formula of the material was estimated as Sc₃O(OMe)₃(DMF)_{1.68}(BTC)₂. This allowed for scandium and iron to be substituted into the formula in order to calculate the amount of Fe₂O₃ using the molecular formula Sc_{1.8}Fe_{1.2}O(OMe)₃(DMF)_{1.68}(BTC)₂.zFe₂O₃. Taking this into consideration for MIL-100(Sc₈₀/Fe₂₀)Xs it is calculated that z will equal 0.65, MIL-100(Sc₆₀/Fe₄₀)Xs z will equal 1 and MIL-100(Sc₅₀/Fe₅₀)Xs it is calculated that z will equal 1.95. The presence of the Fe₂O₃ nanoparticulate in the pore should cause a reduction in porosity of 18% in MIL-100(Sc₆₀/Fe₄₀)Xs. The reduction in porosity of MIL-100(Sc₆₀/Fe₄₀)Xs was slightly larger than predicted which was found to be 25% (Figure 5.12). However, this evidence does point towards the nanoparticles being in the pores and not on the surface of the material.

The unit cell of the material was refined using the Le Bail method. There is an increase in the *a* parameter of the materials. Presumably this is caused by the materials having more scandium in the structure even though the overall ratio is 60/40 (Figure 5.14). This causes the unit cell of the excess materials to be larger due to the larger atomic radii of scandium. This then allows for the prediction of the amount of iron that is in the structure by comparing the *a* parameter of the MIL-100(Sc/Fe) series to the MIL-100(Sc/Fe)Xs series (Table 5.5).

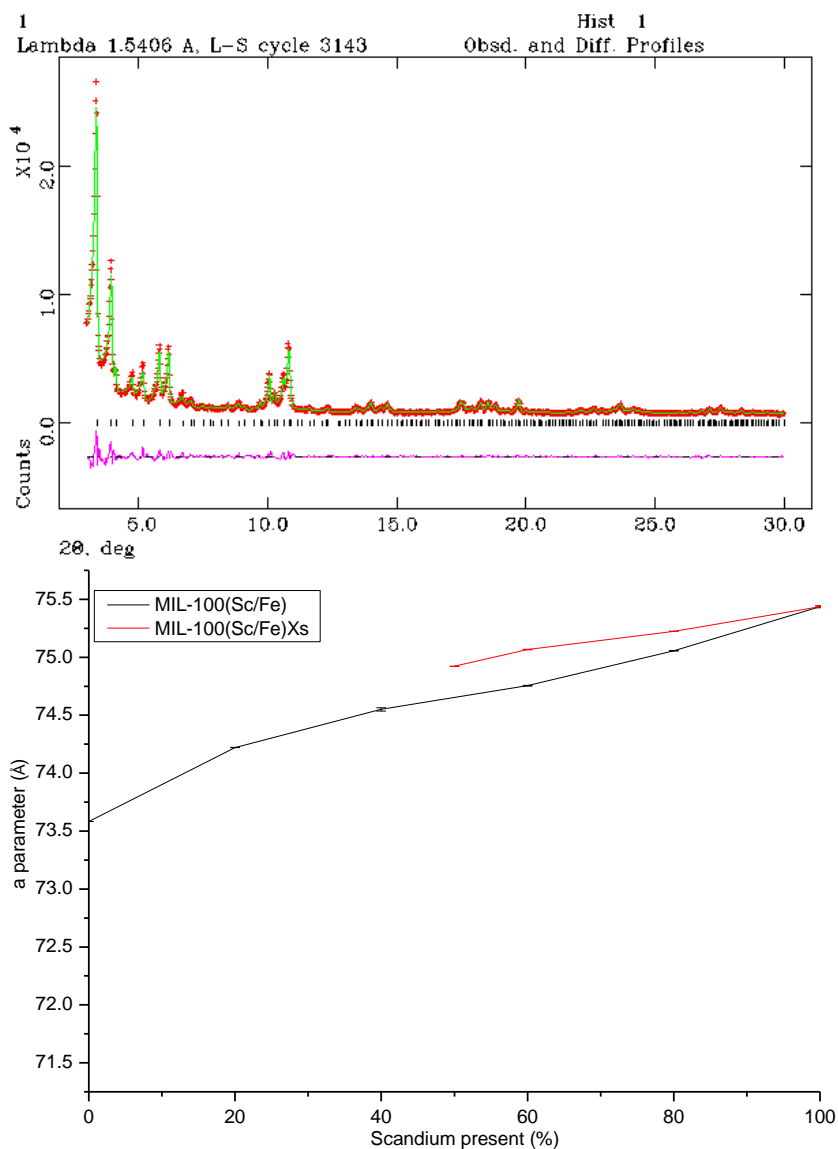


Figure 5.14: Le Bail refinement of MIL-100(Sc₆₀/Fe₄₀)Xs (b) cubic unit cell parameter of each mixed metal material in MIL-100(Sc/Fe) series with increasing amount of scandium compared to MIL-100(Sc/Fe)Xs series

Table 5.5: Properties of MIL-100(Sc/Fe)Xs series

MOF	Predicted Sc/Fe ratio in the framework ^b
MIL-100(Sc ₈₀ /Fe ₂₀)Xs	89/11
MIL-100(Sc ₆₀ /Fe ₄₀)Xs	81/19
MIL-100(Sc ₅₀ /Fe ₅₀)Xs	72/28

Further evidence to show that nanoparticles of Fe₂O₃ were contained in the pores of the MOF was obtained by TEM carried out by Amanda Anderson. This showed particles of 5-10 nm in the pore of the MOF (Figure 5.15).

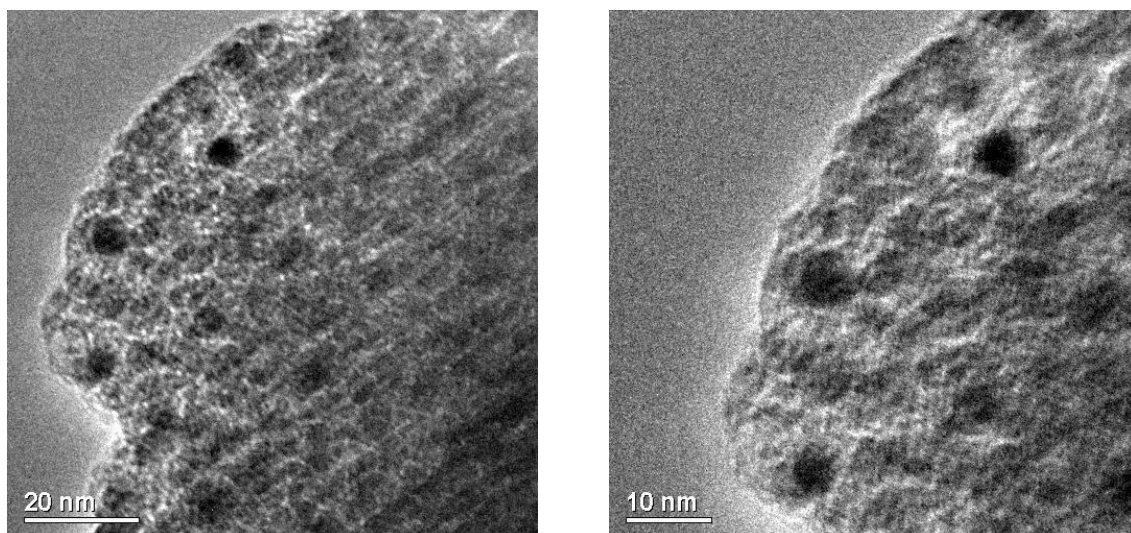


Figure 5.15: Transmission electron micrographs of MIL-100(Sc₆₀/Fe₄₀)XS, showing some particles without α -Fe₂O₃ nanoparticles (as determined by EXAFS) and others with nanoparticles of α -Fe₂O₃ from 5 – 10 nm in size.

The characterisation techniques used allowed for the identification of the extra framework α -Fe₂O₃ and allows a semi quantitative estimate of the amount of α -Fe₂O₃ in the MIL-100. TGA analysis helped quantify the amount of Fe₂O₃ in the structure by calculating the residual mass. Indicating that the nanoparticles are in the pore and not purely on the surface are obtained by PXRD and N₂ adsorption.

5.3. Other mixed metal MIL-100

Two other series of MIL-100(Sc, M), M= Al³⁺ and Cr³⁺, were prepared to compare with that of MIL-100(Sc,Fe). The pure phase MIL-100(Cr) and MIL-100(Al) have been reported previously.^{21, 22} In each case the solids were prepared as for MIL-100(Sc/Fe), with the Cr³⁺ and Al³⁺ metal cation sources being chromium chloride hexahydrate and aluminium nitrate hexahydrate. The experimental ratios of materials used to synthesise these materials are detailed in Table 5.6, along with *a* parameter, BET surface area and TGA residues.

Table 5.6: Experimental and characterisation details of mixed metal MIL-100

Sample Name	Molar ratio in Synthesis M ₁ :M ₂ :BTC:DMF	EDX Sc:M molar ratio	<i>a</i> / Å	TGA residue wt%	BET surface area (m ² g ⁻¹) ^a
MIL-100(Sc)	3:0:2:600		75.436(8)	26.2	1346
MIL-100(Sc ₈₀ Al ₂₀)	2.4:0.6:2:600	79:21	74.9231(21)	26.4	1312
MIL-100(Sc ₆₀ Al ₄₀)	1.8:1.2:2:600	63:37	74.6841(12)	25.2	1329
MIL-100(Sc ₄₀ Al ₂₀)	1.2:1.8:2:600	42:58	74.3204(7)	24.5	1309
MIL-100(Sc ₂₀ Al ₈₀)	0.6:2.4:2:600	19:81	73.9127(16)	22.9	1302
MIL-100(Al)	3:0:2:600		73.2356(2)	22.2	1295
MIL-100(Sc ₈₀ Cr ₂₀)	2.4:0.6:2:600	80:20	75.1452(2)	27.1	1335
MIL-100(Sc ₆₀ Cr ₄₀)	1.8:1.2:2:600	63:37	74.8045(12)	28.5	1328
MIL-100(Sc ₄₀ Cr ₆₀)	1.2:1.8:2:600	35:65	74.6121(15)	28.9	1330
MIL-100(Sc ₂₀ Cr ₈₀)	0.6:2.4:2:600	13:87	74.3145(5)	30.2	1301
MIL-100(Cr)	literature synthesis ¹⁴		73.6525(19)	30.5	1338

^a Measured by N₂ adsorption at 77 K

5.3.1. MIL-100(Sc/Al)

PXRD analyses show that a series of MIL-100(Sc/Al) materials have been prepared phase pure (Figure 5.17). Le Bail refinement against the PXRD of as-prepared materials shows a decrease in the unit cell as the concentration of Al (as determined by EDX) increases (Figure 5.16). This is expected due to the smaller ionic radius of Al³⁺ (67.5 nm) compared to that of Sc³⁺ (88.5nm)

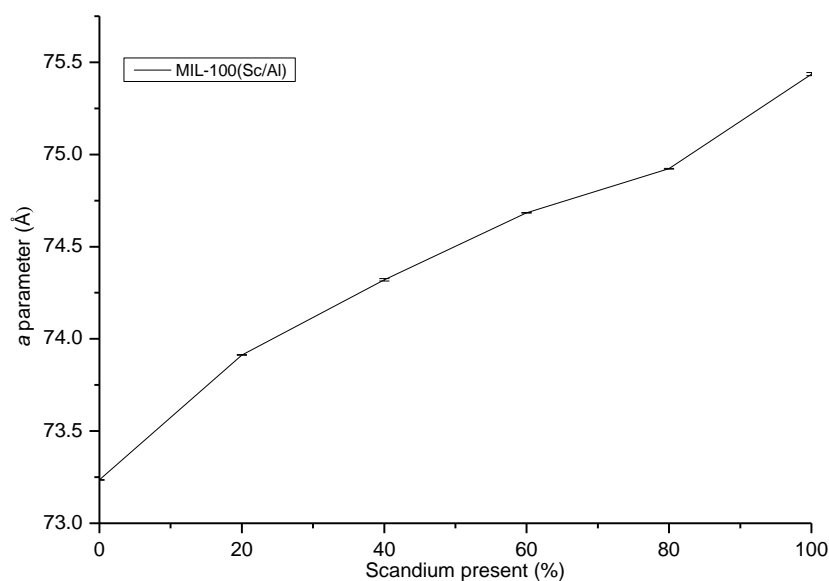


Figure 5.16: Unit cell a parameter of MIL-100(Sc/Al)

PXRD patterns obtained for the MIL-100(Sc/Al) series show that materials are structurally similar to MIL-100(Sc), although a slight decrease in crystallinity is observed with increased fraction of aluminium (Figure 5.17).

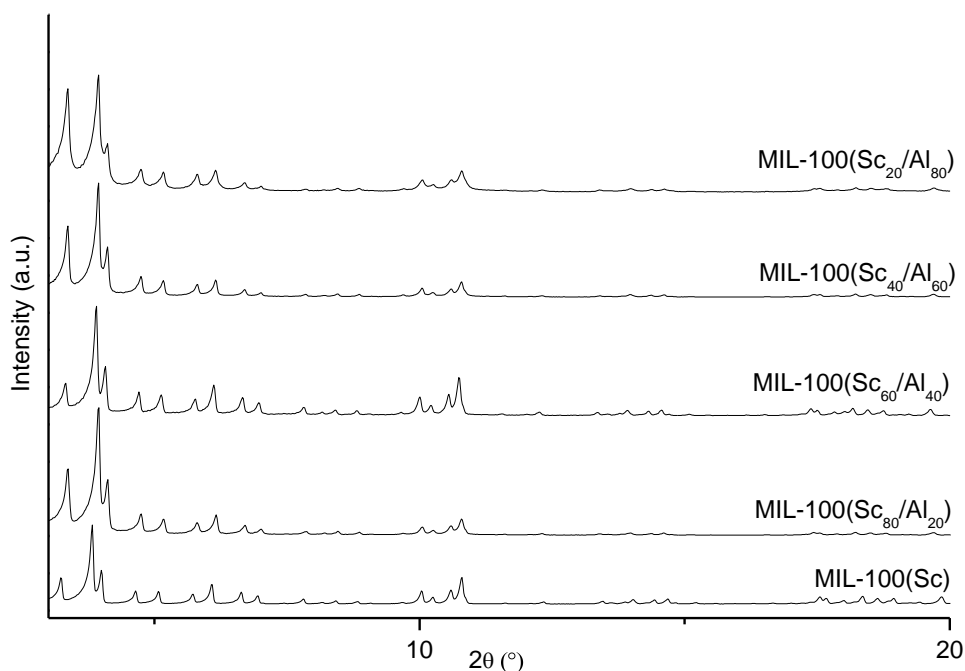


Figure 5.17: Comparison of PXRD of MIL-100(Sc), as-prepared MIL-100(Sc) with mixed metal MIL-100(Sc/Al)

TGA analysis shown in Table 5.6 indicates a reduction in the final residue as the amount of aluminium in the MIL-100 material is increased. This is to be expected due

to the smaller mass of aluminium. N₂ adsorption of the MIL-100(Sc/Al) shows similar uptake to that of MIL-100(Sc).

This series also gave the opportunity to try to determine by SS MASNMR whether the mixed Sc/Al materials contained a mixture of metals in the trimer or consisted of trimers occupied by either 3 Sc atoms or 3 Al atoms.

⁴⁵Sc and ²⁷Al MASNMR was carried out on the materials (Figure 5.18). The ²⁷Al spectra show a peak at -2.5 ppm typical of octahedral AlO₆, as measured previously for MIL-100(Al).²² This shows that the aluminium is present in the MIL-100 mixed metal structure. The ⁴⁵Sc MASNMR spectra displays a single broad resonance with an asymmetric line shape. There is a clear change in peak shape as the amount of scandium changes, with a broadened line shape at low Sc content. Two different environments are expected to be observed in the spectra due to one scandium being bound to a hydroxide ion (observed at 31 ppm)[†] and the other water (observed at 61 ppm)[†]. The spectra suggest that a higher proportion of Sc³⁺ cations are bound to hydroxide at lower scandium concentrations.

¹³C MASNMR was also carried out (Figure 5.19). Peaks at ca 173 ppm are assigned as carboxylate ¹³C. Each carboxylate ¹³C is linked (*via* O) to two different metal cations in a trimer. This could result in three different carboxylate ¹³C environments; 2Sc, Sc/Al or 2Al, depending on the metal composition of the trimer. A clear difference can be observed in the carbon peaks as the composition changes. The peak at 173 ppm in the carbon spectra is thought, on the basis of DFT calculations[†] to be due to carboxylate groups bound to two Sc³⁺ cations. The peak at 171 ppm is attributed to Sc/Al and 2Al environments and can clearly be seen to increase as the aluminium content increases. Although it cannot be determined whether the material contains mixed trimers of metal or full trimers of scandium and full trimers of aluminium it can be said that the metals are both successfully incorporated into the MIL-100 structure.

[†] From CASTEP simulation performed by Professor Sharon Ashbrook and Dr Valerie Seymour

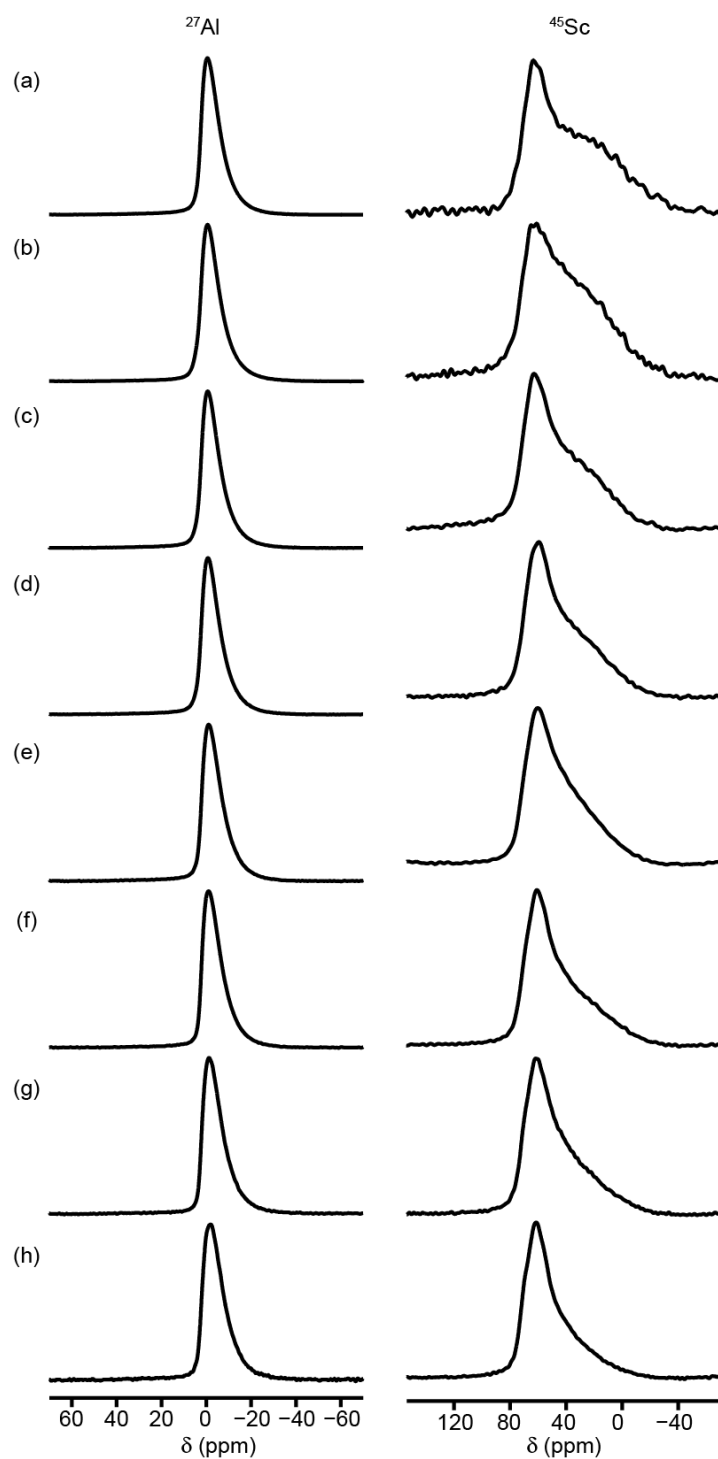


Figure 5.18: ^{27}Al and ^{45}Sc MASNMR spectra of (a) MIL-100($\text{Sc}_{10}/\text{Al}_{90}$) (b) MIL-100($\text{Sc}_{20}/\text{Al}_{80}$) (c) MIL-100($\text{Sc}_{30}/\text{Al}_{70}$) (d) MIL-100($\text{Sc}_{40}/\text{Al}_{60}$) (e) MIL-100($\text{Sc}_{50}/\text{Al}_{50}$) (f) MIL-100($\text{Sc}_{60}/\text{Al}_{40}$) (g) MIL-100($\text{Sc}_{70}/\text{Al}_{30}$) (h) MIL-100($\text{Sc}_{80}/\text{Al}_{20}$)

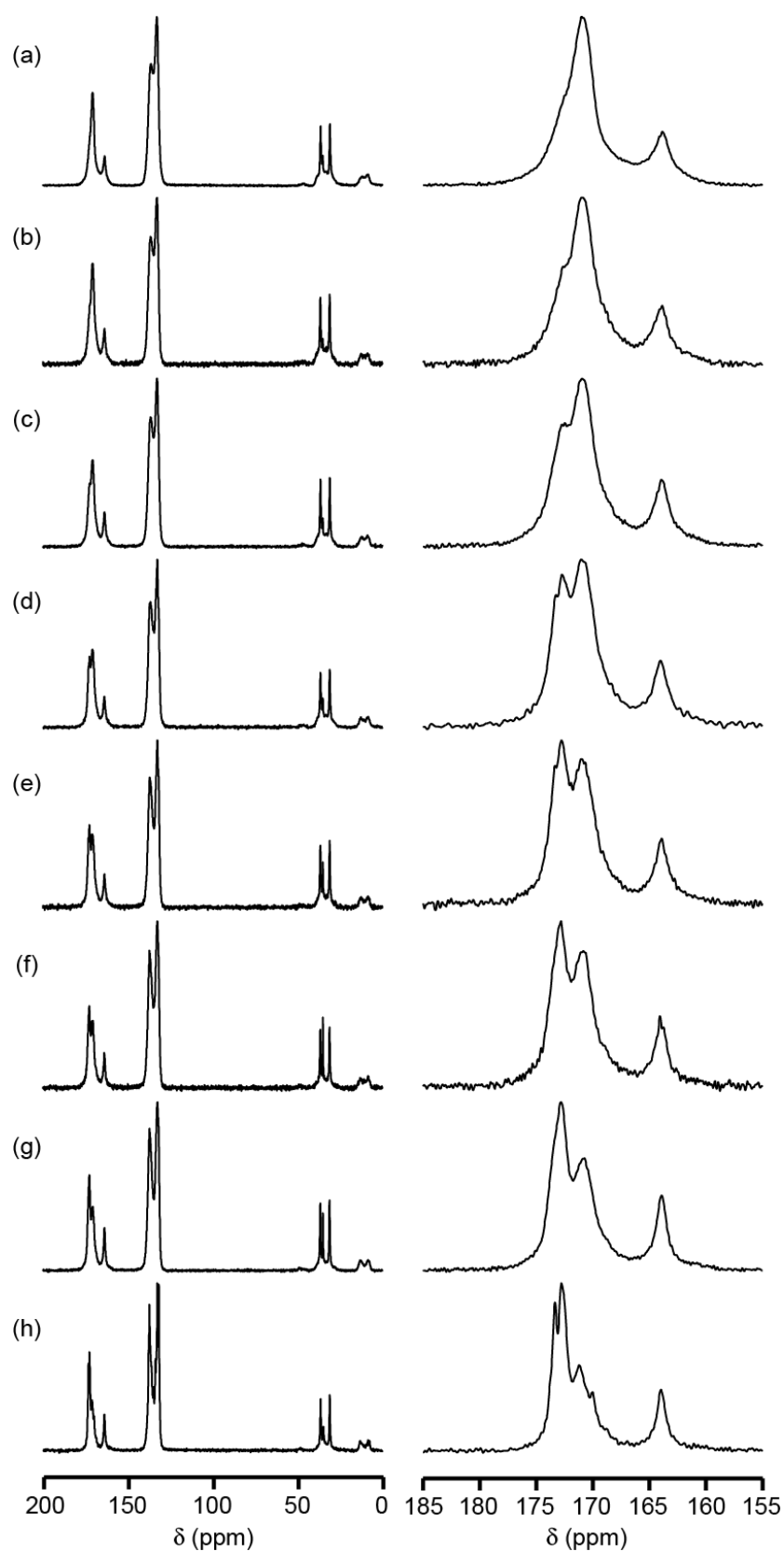


Figure 5.19: ^{13}C MASNMR of (a) MIL-100($\text{Sc}_{10}/\text{Al}_{90}$) (b) MIL-100($\text{Sc}_{20}/\text{Al}_{80}$) (c) MIL-100($\text{Sc}_{30}/\text{Al}_{70}$) (d) MIL-100($\text{Sc}_{40}/\text{Al}_{60}$) (e) MIL-100($\text{Sc}_{50}/\text{Al}_{50}$) (f) MIL-100($\text{Sc}_{60}/\text{Al}_{40}$) (g) MIL-100($\text{Sc}_{70}/\text{Al}_{30}$) (h) MIL-100($\text{Sc}_{80}/\text{Al}_{20}$)

5.3.2. MIL-100(Sc/Cr)

Similarly a MIL-100(Sc/Cr) series was synthesised to allow for catalytic comparison of the different materials. The details are given in Table 5.6. This series was initially characterised using PXRD which showed the materials were again structurally similar to MIL-100(Sc). A slight decrease in crystallinity as observed with increasing amounts of chromium which had been observed in previous mixed metal series.

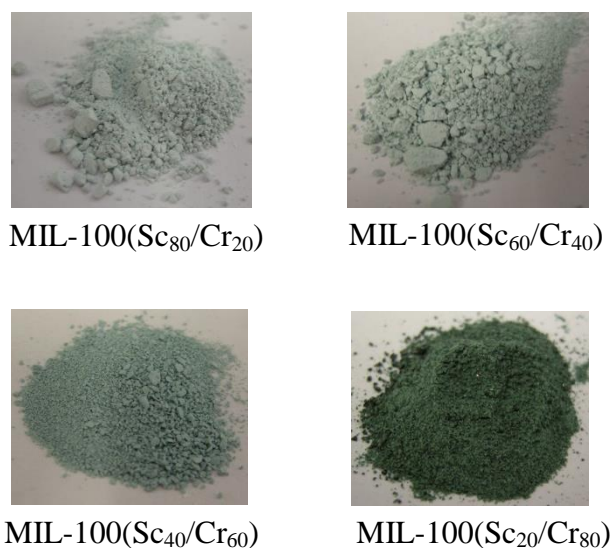


Figure 5.20: Synthesised MIL-100(Sc/Cr) series

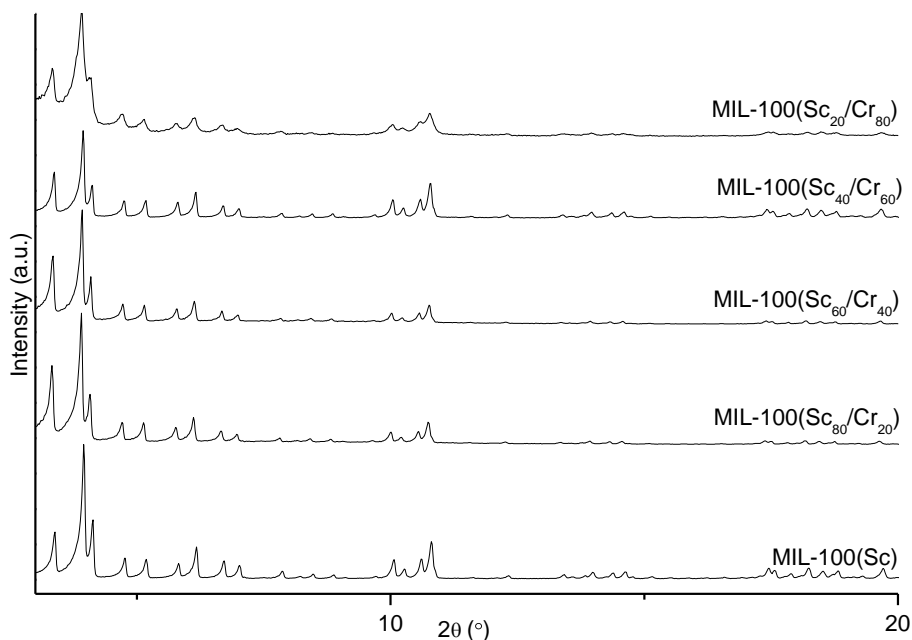


Figure 5.21: Comparison of PXRD of MIL-100(Sc), as-prepared MIL-100(Sc) with mixed metal MIL-100(Sc/Cr)

The PXRD patterns allow for the a parameter of the MIL-100(Sc/Cr) to be determined using structure less Le Bail refinement. This shows that the a parameter decreases as the amount of chromium is increased (Figure 5.22). This is due to the smaller ionic radii of chromium (75.5 pm).

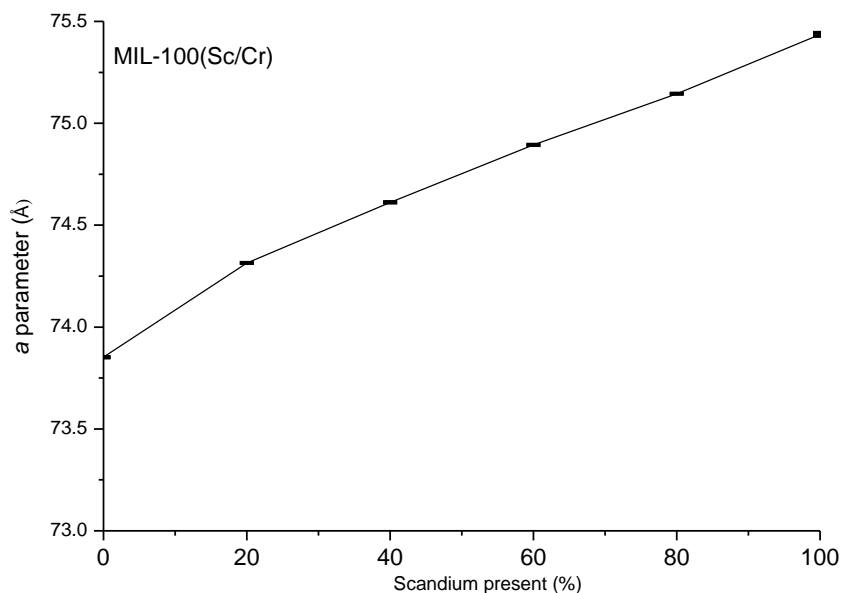


Figure 5.22: Unit cell a parameter of MIL-100(Sc/Cr)

TGA analysis of the material showed an increase in final residue after calcination as the amount of chromium was increased due to the greater weight of Cr_2O_3 than Sc_2O_3 and N_2 adsorption at 77 K of each material in the series indicates similar uptakes and surface areas (Table 5.6).

The UV spectrum shows the clear introduction of chromium into the MIL-100 structure. An increase of band strength at 400-500 nm and 520-800 nm is observed as the amount of chromium in the series is increased (Figure 5.23).

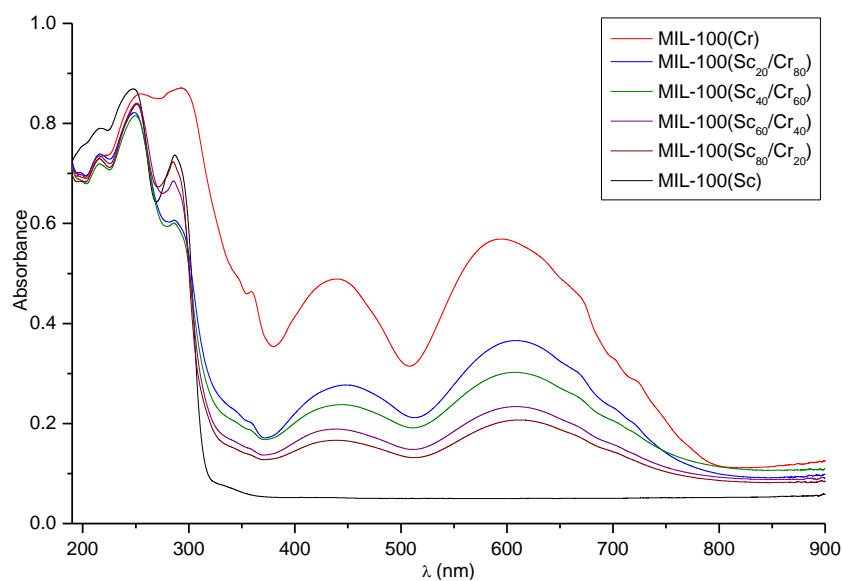


Figure 5.23: Comparison of UV-visible spectra of samples in the MIL-100(Sc/Cr) series

5.3.3. Introduction of divalent metals into MIL-100

The introduction of divalent metals into the MIL-100(Sc) material was also investigated. The synthesis of these materials was carried out as described in Table 5.7 using cobalt (II) chloride hexahydrate, nickel (II) acetate tetrahydrate and magnesium (II) chloride hexahydrate as sources for the divalent metal cations.

Table 5.7: Experimental and characterisation details of mixed metal MIL-100

Sample Name	Molar ratio in Synthesis $M_1:M_2:BTC:DMF$	EDX Sc:M molar ratio	TGA residue wt%	BET surface area (m^2g^{-1}) ^a
MIL-100(Sc)	3:0:2:600		26.2	1349
MIL-100(Sc ₉₀ Co ₁₀)	2.7:0.3:2:600	91:9	27.0	1355
MIL-100(Sc ₈₅ Co ₁₅)	2.55:0.45:2:600	84:16	27.5	1340
MIL-100(Sc ₈₀ Co ₂₀)	2.4:0.6:2:600	80:20	28.1	1333
MIL-100(Sc ₇₀ Co ₃₀)	2.1:0.9:2:600	69:31	29.1	1335
MIL-100(Sc ₉₀ Ni ₁₀)	2.7:0.3:2:600	89:11	26.9	1308
MIL-100(Sc ₈₀ Ni ₂₀)	2.4:0.6:2:600	81:18	28.0	1322
MIL-100(Sc ₇₀ Ni ₃₀)	2.1:0.9:2:600	70:30	28.9	1317
MIL-100(Sc ₇₀ Mg ₃₀)	2.1:0.9:2:600	71:39	25.4	1312

^a Measured by N₂ adsorption at 77 K

It was found that the maximum amount of divalent metal incorporated was 33%. When excess metal was added in the synthesis it remained in solution. This can be attributed to the need for the three metals in the trimer to have combined charge of at least 8+, to balance six carboxylate (-1) and one $\mu_3\text{O}$ (-2) charges). Whereas a charge greater than 8+ is possible for the 3 cations, since it can be balanced by the coordination of negatively charged hydroxyl groups (or halide anions) on the metal cations in place of water, there is no obvious mechanism to balance a combined charge on the metal cations of less than 8+.

Each material was characterised by PXRD, UV visible spectroscopy and N_2 adsorption analysis (Table 5.7). These analyses showed the series to be crystalline MIL-100 (Figure 5.24) materials with similar BET surface area to pure MIL-100(Sc) (Table 5.7).

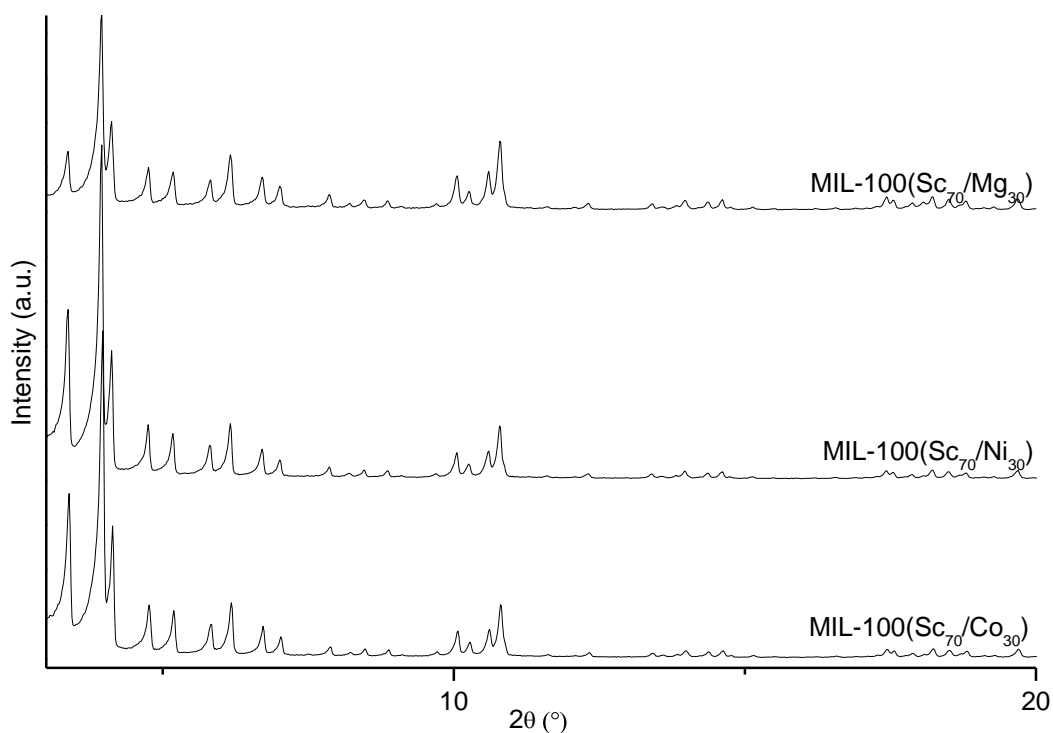


Figure 5.24: PXRD patterns of divalent mixed metal MIL-100(Sc)

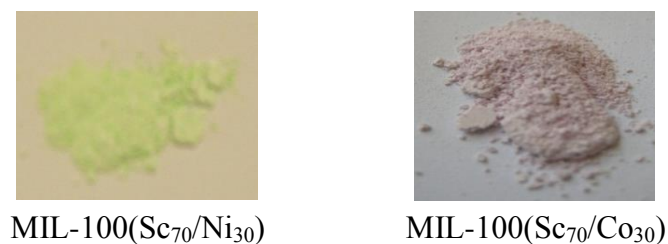
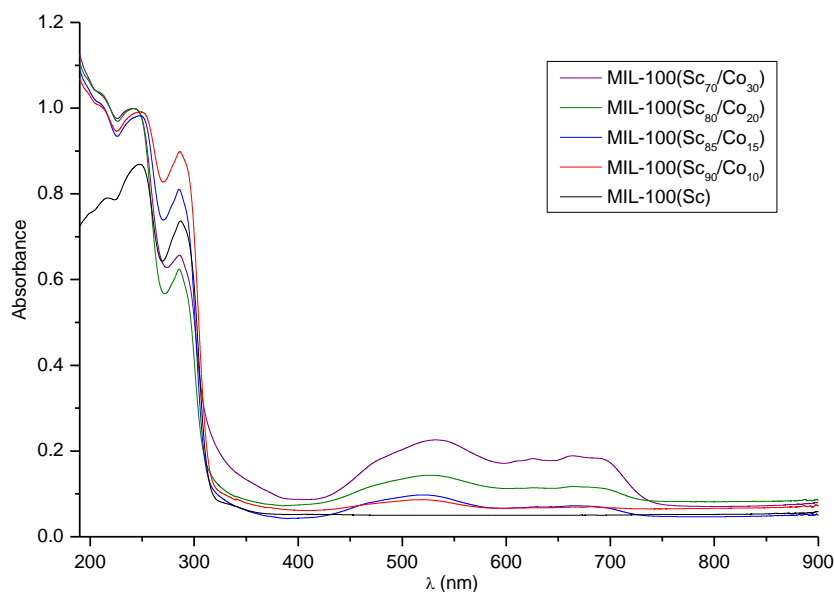


Figure 5.25: Divalent mixed metal materials synthesised (a) MIL-100(Sc₇₀/Ni₃₀) and (b) MIL-100(Sc₇₀/Co₃₀)

The metal ratios of the mixed metal materials were quantified by EDX analysis. The introduction of nickel and cobalt was accompanied by a distinct change in colour (Figure 5.25) which was then further analysed by solid state UV-visible spectroscopy (Figure 5.26).

The UV-absorption can be seen to increase as the amount of nickel or cobalt introduced into the material is increased. In MIL-100(Sc/Co) series two clear bands can be observed between 450-700 nm. This is typical of cobalt(II) in octahedral geometry. The bands are caused by the spin allowed transitions ${}^4T_{1g}(F) \rightarrow {}^4A_{2g}(F)$ and ${}^4T_{1g}(F) \rightarrow {}^4T_{2g}(F)$.^{23, 24} The band between 250 and 300 nm is likely to be caused by charge transfer from the ligand to the metal.



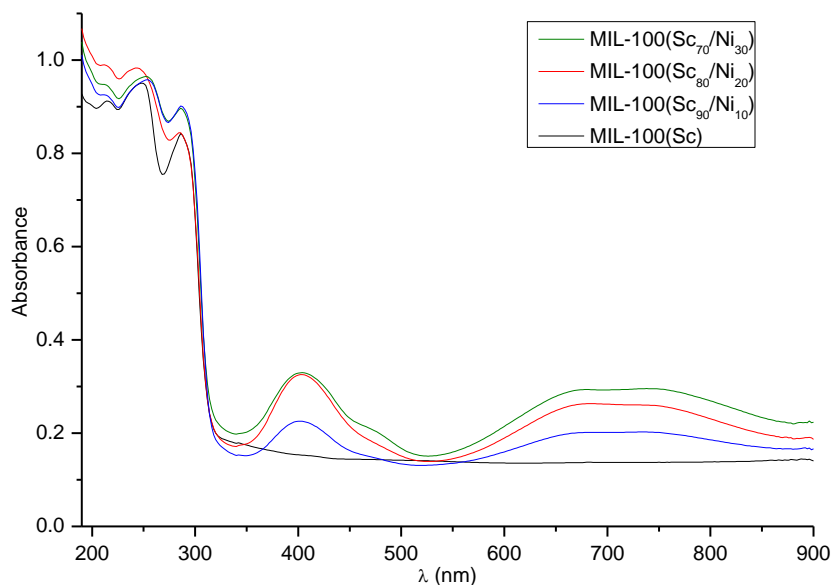


Figure 5.26: UV-visible spectroscopy of (a) MIL-100(Sc/Co) series compared to MIL-100(Sc) (b) MIL-100(Sc/Ni) series compared to MIL-100(Sc)

In the nickel containing series, two clear bands can also be observed, at 375-450 nm and 600-800 nm. These transitions are due to the spin allowed transitions of ${}^3A_{2g} \rightarrow {}^3T_{2g}$ and ${}^3A_{2g} \rightarrow {}^3T_{1g}$.²⁵ MIL-100(Sc/Mg) showed no change in absorption under using UV-absorption this is due to no *d* electrons being present in either scandium or magnesium.

5.4. HKUST-1 (Cu/Ru)

In chapter 4 the catalytic activity for HKUST-1(Cu) was measured for the carbonyl ene and related Lewis acid catalysed reactions. This was chosen as it is frequently discussed as a catalyst in the literature and so acts as a suitable comparison for the scandium MOFs. HKUST-1 is also of interest within the context of mixed metal MOF catalysts. Literature reports indicate that other metal forms of HKUST-1 can be prepared,^{26, 27} so a mixed (Cu/Ru) HKUST-1 is of interest as a mixed metal catalyst particularly as ruthenium is known to have properties for hydrogenation.²⁸⁻³¹ It was found that up to 10% of the Cu^{2+} could readily be substituted by Ru^{2+} , resulting in a colour change from blue to green (Figure 5.27). At higher concentrations of Ru a second crystalline phase appeared.

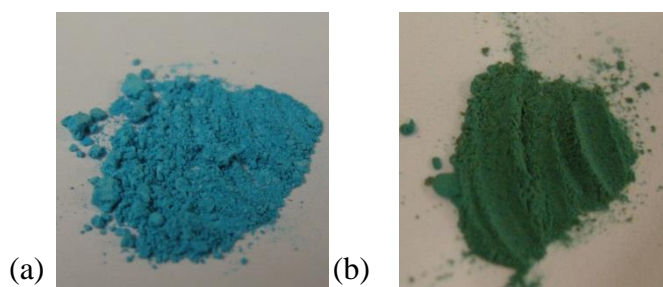


Figure 5.27: HKUST-1 materials (a) HKUST-1(Cu) (b) HKUST-1(Cu₉₀/Ru₁₀)

The material was characterised by PXRD and compared with HKUST-1(Cu) (Figure 5.28). The amount of ruthenium present in the material was determined by EDX analysis.

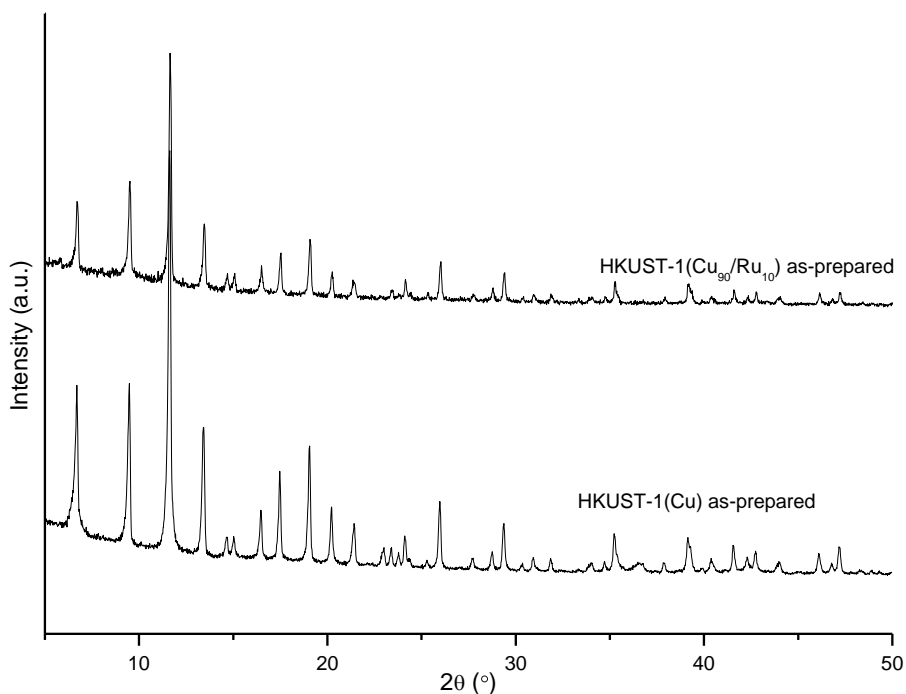


Figure 5.28: PXRD spectra of as-prepared HKUST-1(Cu) compared with HKUST-1(Cu₉₀/Ru₁₀)

The material was further characterised using N₂ adsorption. It was found that the N₂ adsorption was lower than that found for HKUST-1(Cu) with a surface area of 820 m²g⁻¹ compared to 965 m²g⁻¹ obtained for HKUST-1 (Figure 5.29).

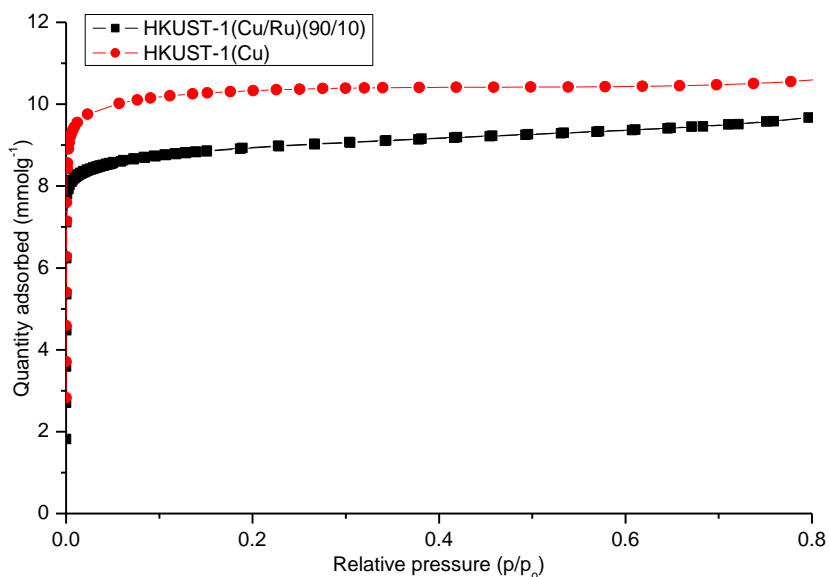


Figure 5.29: N_2 adsorption at 77 K of HKUST-1(Cu) compared to HKUST-1(Cu₉₀/Ru₁₀)

Further to this, XANES was carried out on the sample by Professor Richard Walton to determine the oxidation state of the material (Figure 5.30). This showed that the ruthenium was in fact in Ru^{3+} form—when compared to other octahedral Ru^{3+} containing materials it showed a similar XANES spectrum. Previously synthesised thin film MOF HKUST-(Ru) also showed the ruthenium was Ru^{3+} (with the ruthenium being counterbalanced by Cl^- or OH^-).^{26, 27}

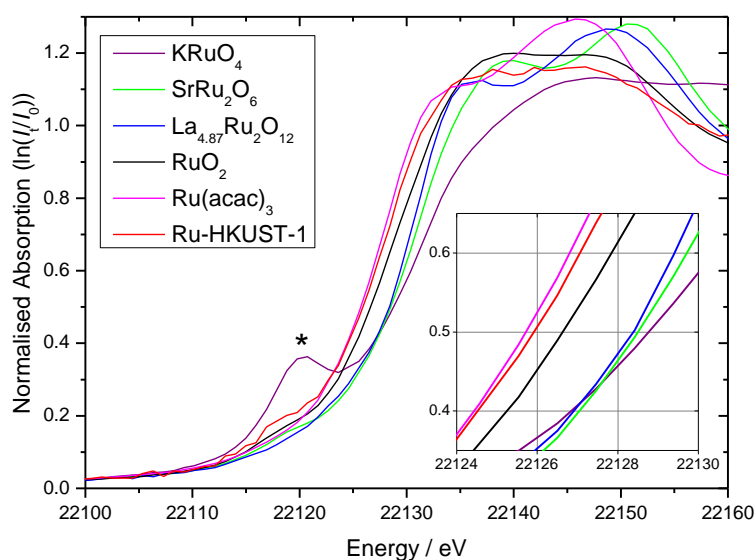


Figure 5.30: XANES spectrum for HKUST-1(Cu/Ru) compared to other ruthenium containing complexes

5.5. Catalysis using mixed metal MOF materials

The first catalytic aim was to measure the activity of all mixed metal MOFs as Lewis acid catalysts, to determine their effectiveness. More importantly, the synthesis of the mixed metal MOF materials introduced new and potentially active catalytic properties into the MIL-100(Sc) structure. The use of mixed metal MOFs in catalysis has been carried out previously^{6, 32} but, the use of different metal sites in the framework for different catalytic functions has not. Our main aim was to make use of active sites in close proximity in a MOF framework to carry out sequential reactions efficiently. As an example, C-C bond forming reactions and oxidation of alcohols were catalysed both separately and in tandem using a range of mixed metal MOFs.

5.5.1. Carbonyl ene reaction

MIL-100(Sc) was shown in chapter 4 to be an active catalyst for Lewis acid catalysed reactions such as the carbonyl ene reaction, more active than its Cr, Fe or Al counterparts. To monitor the effect of the isomorphous replacement of Sc by these metals, the activity was measured as a function of composition, using 5 mol% of metal centres (Sc, Cr, Fe, Al) compared to substrate. The amount of M sites was calculated according to the formula $M_3O(BTC)_2X_n$ (X_n refers to occluded solvent, the amount of which was determined by TGA). In addition the activity was measured for the MIL-100(Sc/Fe)Xs series of MOFs, keeping either the mass or the amount of trivalent metal constant for comparison. Initially the carbonyl ene reaction of α -methylstyrene with ethyl trifluoropyruvate was investigated (Figure 5.31). In each series where the scandium metal was replaced by another metal the catalytic activity can be observed to decrease as the amount of scandium decreases. The decrease in activity depended on which other metal was contained in the mixed metal MIL-100. The introduction of chromium into the series caused less reduction in overall activity and introduction of Fe had the biggest effect in overall activity reduction so that the activity for the reaction decreased in the order Sc>Cr>Fe>Al. Interestingly, in the material that contained α -Fe₂O₃ nanoparticles a high activity was maintained throughout the series indicating that α -Fe₂O₃ nanoparticles are active in this conversion (more active than Fe in the trimers).

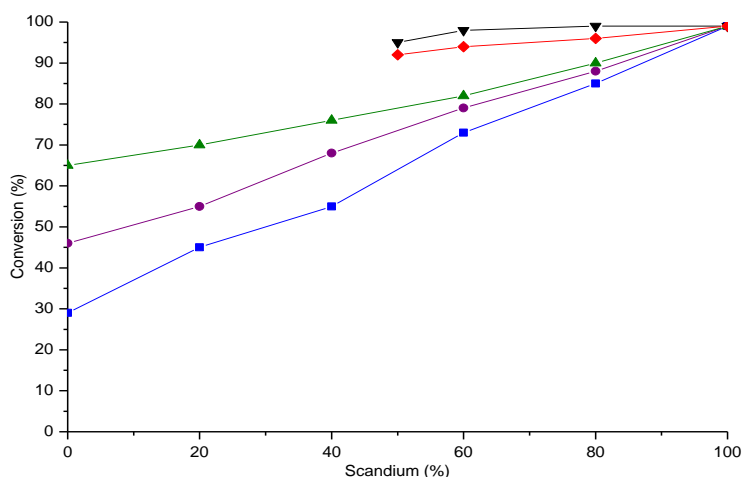
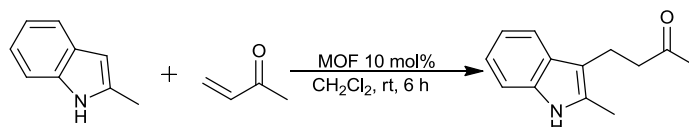


Figure 5.31: Conversion after 6 h in the reaction of α -methylstyrene with ethyl trifluoropyruvate catalysed by the following series of materials: MIL-100(Sc/Fe)Xs (black), MIL-100(Sc/Fe)X₅ (red) (mass adjusted on basis of metal content – see text), MIL-100(Sc/Cr) (green), MIL-100(Sc/Fe) (purple) and MIL-100(Sc/Al) (blue)

5.5.2. Conjugate addition of electron deficient olefins to indole

The effect of the introduction of Fe³⁺ was also investigated in the conjugate addition of 2-methylindole to methyl vinyl ketone (Table 5.8). The introduction of iron was of interest due to its reduced cost and low toxicity. The activity is seen to drop as the amount of scandium decreases in the MIL-100(Sc/Fe) series. The decrease however is not as steep as seen in the carbonyl ene reaction, and the MIL-100(Sc₆₀/Fe₄₀) material gives 80% conversion (Table 5.8, entry 4). The materials containing α -Fe₂O₃ nanoparticles were seen to show high levels of activity and conversions, greater than for MIL-100(Sc).

Table 5.8: Conjugate addition of indole to methyl vinyl ketone catalysed by MIL-100(Sc/Fe) series



Entry	MOF	Product (%) ^a
1	No catalyst	0
2	MIL-100(Sc)	92
3	MIL-100(Sc ₈₀ /Fe ₂₀)	88
4	MIL-100(Sc ₆₀ /Fe ₄₀)	80
5	MIL-100(Sc ₄₀ /Fe ₆₀)	74
6	MIL-100(Sc ₂₀ /Fe ₈₀)	62
7	MIL-100(Sc ₈₀ /Fe ₂₀)Xs	99(99)
8	MIL-100(Sc ₆₀ /Fe ₄₀)Xs	98(98)
9	MIL-100(Sc ₅₀ /Fe ₅₀)Xs	95(93)
10	MIL-100(Fe)	40

2-methylindole (0.1312 g, 1 mmol) and methyl vinyl ketone (0.083 ml, 1 mmol) were added to a solution of CH₂Cl₂ (5 ml) with pre-activated MOF (10 mol%) and stirred for 6 h at RT.
^a Determined by ¹H NMR. Results in brackets represent catalysis using MIL-100(Sc/Fe)Xs with mass normalised so that the metal content was the same.

The conversion to product was investigated further to compare the activity of the α -Fe₂O₃ nanoparticle-containing MIL-100 mixed material with other MIL-100 materials (Figure 5.32). The initial rate of reaction for the reaction catalysed by mass balanced MIL-100(Sc₆₀/Fe₄₀)Xs is higher than that of MIL-100(Sc) and the catalyst maintains this higher rate of activity throughout the reaction. The initial rate of reaction of MIL-100(Sc₆₀/Fe₄₀) is slower than MIL-100(Sc₆₀/Fe₄₀)Xs and cannot maintain a high rate of activity giving it lower overall conversion to product. However, the rate of reaction of MIL-100(Sc₆₀/Fe₄₀) is much higher than MIL-100(Fe).

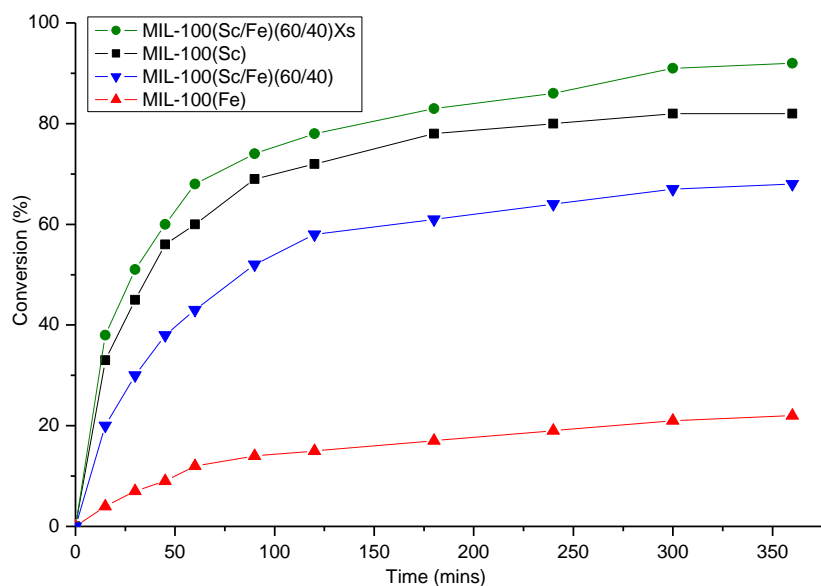


Figure 5.32: Formation of 4-(2-methyl-3-indolyl)butan-2-one catalysed by 5 mol% MIL-100(Sc)(black), MIL-100(Sc₆₀/Fe₄₀)Xs (green), MIL-100(Sc₆₀/Fe₄₀) (blue), and MIL-100(Fe)(red) over 6 h stirred at room temperature in dichloromethane

The introduction of divalent metals was also investigated in the reaction of 2-methylindole with methyl vinyl ketone (Table 5.9). This appeared to have a negative effect on the conversion to product. MIL-100(Sc₇₀/Mg₃₀) was the best example tested but is a poor catalyst relative to 100% Sc or even Sc/Fe 70/30 (Table 5.9, entry 3 versus entries 2 and 8). A similar conversion was observed for MIL-100(Sc₇₀/Ni₃₀) (Table 5.9, entry 5). This drop in activity was even more noticeable upon the introduction of cobalt, where MIL-100(Sc₇₀/Co₃₀) gives a conversion of only 25%.

Table 5.9: Conjugate addition of indole to methyl vinyl ketone catalysed by divalent and trivalent mixed metal MIL-100

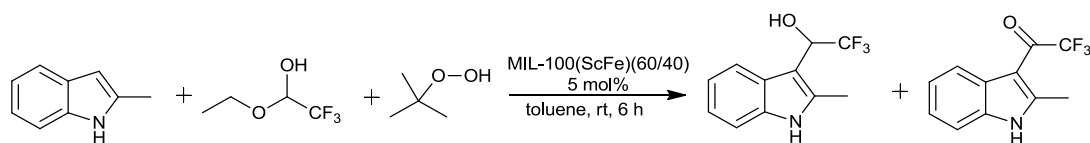
Entry	MOF	Product (%) ^a
1	No catalyst	0
2	MIL-100(Sc)	92
3	MIL-100(Sc ₇₀ /Mg ₃₀)	40
4	MIL-100(Sc ₇₀ /Ni ₃₀)	38
5	MIL-100(Sc ₇₀ /Co ₃₀)	25
6	MIL-100(Sc ₇₀ /Fe ₃₀)	83

2-methylindole (0.1312 g, 1 mmol) and methyl vinyl ketone (0.083 ml, 1 mmol) were added to a solution of CH₂Cl₂ (5 ml) with pre-activated MOF (10 mol%) and stirred for 6 h at RT.
^a Determined by ¹H NMR using 1-methylnaphthalene as internal standard.

The introduction of different trivalent or divalent metals into the MIL-100(Sc) structure reduces the activity of the MOF materials. This is particularly noticeable when divalent metals were introduced into the structure. The introduction of α -Fe₂O₃ nanoparticles enhances the Lewis acidity of the materials on a weight for weight basis and Fe³⁺ in the form of nanoparticles has a similar activity per mole to Sc³⁺ in framework positions.

5.6. Use of mixed metal MIL-100 in bifunctional catalysis

Due to the high performance of some of the mixed metal MIL-100 materials further investigation their use as multifunctional catalysts was carried out. The incorporation of transition metals such as Cr³⁺ and Fe³⁺ into the MIL-100 structure is known to promote activity in catalytic oxidation.^{33, 34} In particular the cheap and non-toxic Fe³⁺ is attractive in this regard. The mixed metal MIL-100(Sc/Fe) materials were therefore investigated for their activity in tandem reactions where a C-C bond forming reaction should be followed by an oxidation reaction. The overall target reaction is shown in Scheme 5.1.

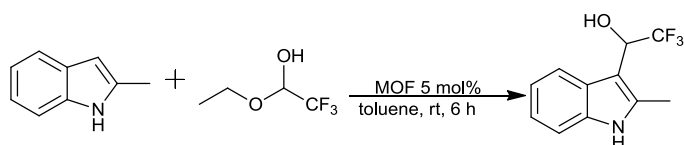


Scheme 5.1: Tandem reaction of 2-methylindole with trifluoroacetaldehyde ethyl hemiacetal and tert-butyl hydroperoxide catalysed by mixed metal MIL-100 materials

To assess the performance of the catalysts in this reaction their activity was first measured in the Lewis acid catalysed first step(s) and then (separately) in the oxidation step. Finally, the activity was measured in the one pot, tandem reaction where all reagents were added simultaneously.

5.6.1. Deacetalisation/Friedel-Crafts reaction of indole and related substrates with trifluoroacetaldehyde ethyl hemiacetal

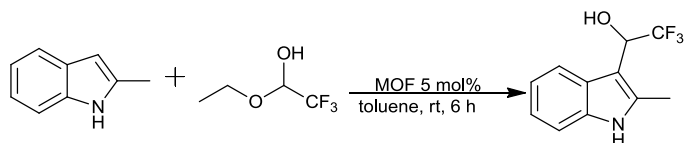
The deacetalisation/Friedel-Crafts reaction was chosen as a starting reaction for the use of mixed metal MOF materials in tandem C-C bond formation oxidation reactions. The initial reaction is itself a form of tandem reaction as it requires the removal of ethanol from the hemiacetal to give fluoral, the actual substrate in the Friedel-Crafts reaction (Scheme 5.2).



Scheme 5.2: Deacetalisation/Friedel-Crafts reaction of 2-methylindole with trifluoroacetaldehyde ethyl hemiacetal catalysed by MOF materials for 6 h at rt

The reaction was catalysed using mixed-metal MIL-100(Sc/Fe) materials as they had the most potential to be used as oxidation catalysts in subsequent reactions. As expected, MIL-100(Sc) material outperformed other materials used to catalyse the reaction (Table 5.10, entry 2). The widely used Lewis acid catalyst HKUST-1(Cu) gave low conversion compared to all the MIL-100 materials investigated including MIL-100(Fe).

Table 5.10: Friedel-Crafts conjugate addition of 2-methylindole to trifluoroacetaldehyde ethyl hemiacetal catalysed by various MOF materials to form 2,2,2-trifluoro-1-(2-methyl-1H-indol-3-yl)ethanol



Entry	MOF	Product (%) ^a
1	No catalyst	19
2	MIL-100(Sc)	98
3	MIL-100(Sc ₈₀ /Fe ₂₀)	89
4	MIL-100(Sc ₆₀ /Fe ₄₀)	78
5	MIL-100(Sc ₆₀ /Fe ₄₀) ^b	>99
6	MIL-100(Sc ₆₀ /Fe ₄₀) ^c	78
7	MIL-100(Sc ₄₀ /Fe ₆₀)	69
8	MIL-100(Sc ₂₀ /Fe ₈₀)	62
9	MIL-100(Sc ₈₀ /Fe ₂₀)Xs	99(98)
10	MIL-100(Sc ₆₀ /Fe ₄₀)Xs	98(96)
11	MIL-100(Sc ₂₀ /Fe ₈₀)Xs	95(89)
12	MIL-100(Fe)	55
13	HKUST-1(Cu)	28
14	HKUST-1(Cu ₉₀ /Ru ₁₀)	30

Reaction carried out using 1 mmol of 2-methylindole and 1.4 mmol trifluoroacetaldehyde ethyl hemiacetal in toluene at room temperature. ^a Determined by ¹H/¹⁹F NMR using 1-fluoronaphthalene as internal standard. ^b Reaction carried out over 16 h. ^c Recycled MIL-100. Results in brackets represent catalysis using MIL-100(Sc/Fe)Xs with mass normalised so that the metal content was the same.

The isomorphous substitution of iron into MIL-100(Sc) material reduced the conversion to product (Table 5.10). However, replacing 40% of the scandium with iron still allows

good conversion after 6 h (78%) and the reaction goes to completion if the reaction time is increased to 16 h (Table 5.10 entry 4 and 5).

The introduction of excess iron oxide nanoparticles into the MIL-100(Sc/Fe) improved the conversion to product of the MOF catalysts. These materials gave full conversion to product and this only dropped slightly when a ratio of 50/50 scandium/iron was used (Table 5.10). The rate of formation of product was investigated. The initial rate of conversion for both MIL-100(Sc) and MIL-100(Sc₆₀/Fe₄₀)Xs shows that both give conversions of over 80% within 2 h (Figure 5.33). Both MIL-100(Sc₆₀/Fe₄₀) and MIL-100(Fe) are slower, and conversion over MIL-100(Fe) levels off at ca 50%, while over MIL-100(Sc₆₀/Fe₄₀) the conversion steadily increases.

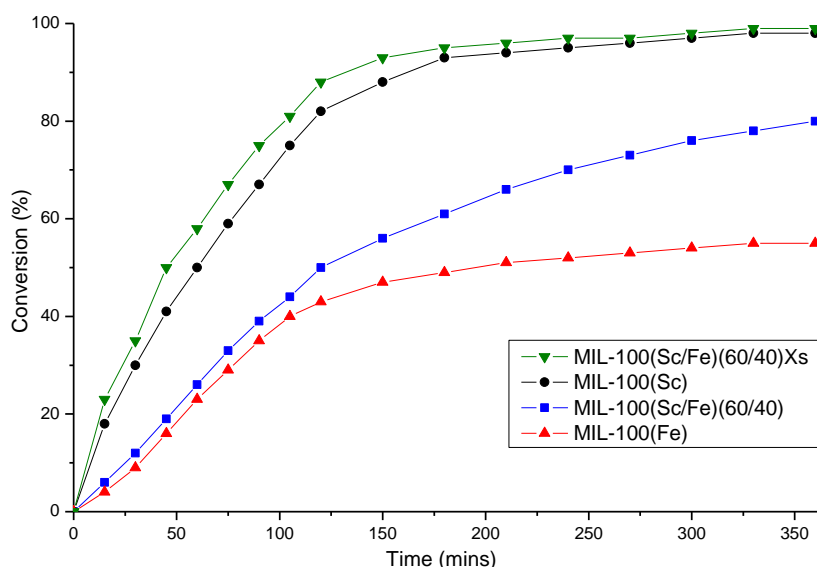
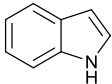
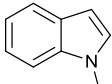
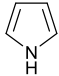
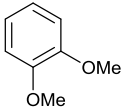


Figure 5.33: Formation of 2,2,2-trifluoro-1-(2-methyl-1H-indol-3-yl)ethanol catalysed by 5 mol% MIL-100(Sc₆₀/Fe₄₀)Xs (green), MIL-100(Sc) (black), MIL-100(Sc₆₀/Fe₄₀) (blue), and MIL-100(Fe) (red) over 6 h cycle stirred at room temperature in toluene

The scope of the reaction was investigated reacting different, and in some cases, less activated substrates with trifluoroacetaldehyde ethyl hemiacetal. Each substrate showed similar results to that obtained with 2-methylindole (Table 5.11) with regards to the best catalyst. MIL-100(Sc₆₀/Fe₄₀)Xs was the most active catalyst of those tested and in some cases outperformed MIL-100(Sc) (Table 5.11, entries 2 and 4). MIL-100(Sc₆₀/Fe₄₀) was not as active, but it is an improvement on MIL-100(Fe) (Table 5.11, entries 3 and 5). Using the less activated substrate veratrole the activity was strongly reduced for all catalysts tested.

Table 5.11: Friedel-Crafts conjugate addition of various substrates to trifluoroacetaldehyde ethyl hemiacetal catalysed by various MOF materials

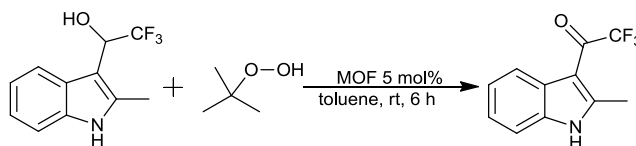
Entry	MOF	Substrate	Product (%) ^a
1	No catalyst		12
2	MIL-100(Sc)		90
3	MIL-100(Sc ₆₀ /Fe ₄₀)		80
4	MIL-100(Sc ₆₀ /Fe ₄₀)Xs		95
5	MIL-100(Fe)		45
6	HKUST-1(Cu)		22
7	No catalyst		
8	MIL-100(Sc)		89
9	MIL-100(Sc ₆₀ /Fe ₄₀)		78
10	MIL-100(Sc ₆₀ /Fe ₄₀)Xs		91
11	MIL-100Fe		50
12	No Catalyst		
13	MIL-100(Sc)		99 (7:1)
14	MIL-100(Sc ₆₀ /Fe ₄₀)		80(9:1)
15	MIL-100(Sc ₆₀ /Fe ₄₀)Xs		99(9:1)
16	MIL-100(Fe)		43(8:1)
17	No catalyst		
18	MIL-100(Sc)		50
19	MIL-100(Sc ₆₀ /Fe ₄₀)		40
20	MIL-100(Sc ₆₀ /Fe ₄₀)Xs		56
21	MIL-100(Fe)		19
22	HKUST-1(Cu)		0

Reaction carried out using 1 mmol of substrate and 1.4 mmol trifluoroacetaldehyde ethyl hemiacetal in toluene at room temperature. ^a Determined by ¹H/¹⁹F NMR using 1-fluoronaphthalene as internal standard. Number in brackets represents mono- to di-alkylated species ratio. Reaction entries 17-22 carried out at 90°C for 16 h.

5.6.2. Oxidation of alcohols catalysed by various MOF materials

The alcohols synthesised as discussed previously (section 5.5.1) could in principle undergo oxidation to ketones using *tert*-butyl hydroperoxide. Similar oxidations have previously been observed over MIL-100(Fe).^{33, 34} Therefore, the oxidation properties of MIL-100 materials containing iron were investigated. The reaction was initially carried out using 2,2,2-trifluoro-1-(2-methyl-1H-indol-3-yl)ethanol using a large range of MIL-100(Sc/Fe) materials. The oxidation did not proceed without a catalyst present. MIL-100(Sc), which has outstanding catalytic activity as a Lewis acid catalyst, was a very poor catalyst for the oxidation reaction (Table 5.12, entry 2). The conversion to product was shown to improve as more iron was introduced into the structure with MIL-100(Fe) achieving the highest conversion (85 %).

Table 5.12: Oxidation of 2,2,2-trifluoro-1-(2-methyl-1H-indol-3-yl)ethanol using *tert*-butyl hydroperoxide catalysed by various MOF materials



Entry	MOF	Product (%) ^a
1	No catalyst	0
2	MIL-100(Sc)	8
3	MIL-100(Sc ₈₀ /Fe ₂₀)	48
4	MIL-100(Sc ₆₀ /Fe ₄₀)	80
5	MIL-100(Sc ₆₀ /Fe ₄₀) ^b	79
6	MIL-100(Sc ₆₀ /Fe ₄₀) ^c	90
7	MIL-100(Sc ₆₀ /Fe ₄₀) ^d	>99
8	MIL-100(Sc ₄₀ /Fe ₆₀)	81
9	MIL-100(Sc ₂₀ /Fe ₈₀)	84
10	MIL-100(Sc ₈₀ /Fe ₂₀)Xs	57(56)
11	MIL-100(Sc ₆₀ /Fe ₄₀)Xs	70(70)
12	MIL-100(Sc ₅₀ /Fe ₅₀)Xs	74(72)
13	MIL-100(Fe)	85
14	HKUST-1(Cu)	9
15	HKUST-1(Cu ₉₀ /Ru ₁₀)	72

Reaction carried out using 1 mmol of 2,2,2-trifluoro-1-(2-methyl-1H-indol-3-yl)ethanol and 4 mmol *tert*-butyl hydroperoxide in toluene/decene and stirred at room temperature for 6 h. ^a Determined by ¹H/¹⁹F NMR using 1-fluoronaphthalene as internal standard. ^b Recycled MIL-100. ^c Alcohol substrate given 1 h incubation period before *tert*-butyl hydroperoxide is added ^d Stirred at room temperature for 16 h. Results in brackets represent catalysis using MIL-100(Sc/Fe)Xs with mass normalised so that the metal content was the same.

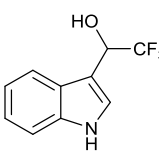
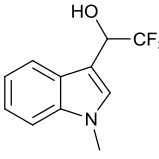
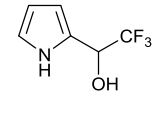
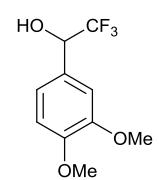
The materials that contained excess α -Fe₂O₃ nanoparticles did not perform as well as the materials that simply replaced scandium in the trimers of MIL-100 with iron (Table 5.12, entries 10-12). For MIL-100(Sc₆₀/Fe₄₀), which represents a good compromise composition for both Lewis acid and oxidation catalysis, there was 80% conversion after 6 h and complete conversion after 16 h (Table 5.12 entries 4 and 7).

It was found that by introducing ruthenium into HKUST-1 (Cu) that the oxidation properties of HKUST-1 are strongly enhanced as the conversion of alcohol to ketone increases from 9% to 72% (Table 5.12 entries 14 and 15). This is therefore another example of a potential bifunctional catalyst.

The reaction scope was investigated using the different alcohols shown in Table 5.13. Similar activity was observed to that of 2-methylindole. MIL-100(Sc) and HKUST-1(Cu) showed very low catalytic activity for each reactant and increase in catalytic activity was observed with increasing iron content in the MIL-100(Sc). The materials

that contained the iron in the trimer consistently outperformed the material containing α -Fe₂O₃ nanoparticles.

Table 5.13: Oxidation of various substrates using *tert*-butyl hydroperoxide catalysed by various MOF materials

Entry	MOF	Substrate	Product (%) ^a
1	No catalyst		0
2	MIL-100(Sc)		11
3	MIL-100(Sc ₆₀ /Fe ₄₀)		76
4	MIL-100(Sc ₆₀ /Fe ₄₀)Xs		72
5	MIL-100(Fe)		80
6	HKUST-1(Cu)		9
7	No catalyst		0
8	MIL-100(Sc)		6
9	MIL-100(Sc ₆₀ /Fe ₄₀)		70
10	MIL-100(Sc ₆₀ /Fe ₄₀)Xs		65
11	MIL-100(Fe)		78
12	No Catalyst		0
13	MIL-100(Sc)		11
14	MIL-100(Sc ₆₀ /Fe ₄₀)		95
15	MIL-100(Sc ₆₀ /Fe ₄₀)Xs		92
16	MIL-100(Fe)		96
17	No catalyst		0
18	MIL-100(Sc)		8
19	MIL-100(Sc ₆₀ /Fe ₄₀)		90
20	MIL-100(Sc ₆₀ /Fe ₄₀)Xs		80
21	MIL-100(Fe)		91
22	HKUST-1(Cu)		10

Reaction carried out using 1 mmol of 2,2,2-trifluoro-1-(2-methyl-1*H*-indol-3-yl)ethanol and 4 mmol *tert*-butyl hydroperoxide in toluene/decene and stirred at room temperature for 6 h. ^a Determined by ¹⁹F{¹H} NMR using 1-fluoronaphthalene as internal standard. ^b Recycled MIL-100. ^c Stirred at room temperature for 16 h. ^d Concentration of solvent doubled. ^e Concentration of solvent tripled. ^f Concentration of solvent halved. Reaction entries 17-22 carried out at 90°C for 16 h.

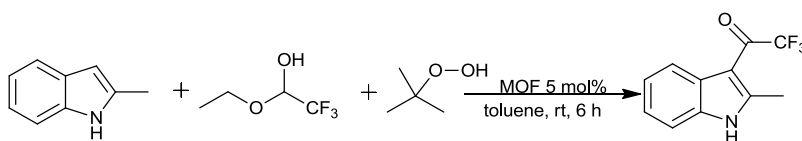
5.6.3. One-pot deacetalisation/Friedel-Crafts reaction and oxidation

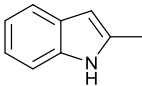
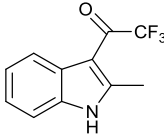
After the individual separate success of the deacetalisation/Friedel-Crafts and the oxidation reaction the introduction of all reactants at the same time in one-pot was investigated. The reaction was initially carried out using 2-methylindole as a substrate. The reaction was monitored using solution ¹⁹F and ¹H NMR. The deacetalisation reaction to form the aldehyde was of potential concern as the introduction of an oxidant might cause the formation of trifluoroacetic acid. However, no trace of this was found in the ¹⁹F NMR and very clean NMRs were obtained this reaction (see experimental

section 7.4.6). It is evident from the results given in Table 5.14 that a good balance between scandium (for C-C bond formation character) and iron (for oxidation) is required in the tandem reaction.

As might be expected, MIL-100(Sc) did not perform well in the tandem reaction. Although it outperforms many other MOF materials in Lewis acid reactions, it is a poor oxidation catalyst (Table 5.14, entry 2). MIL-100(Fe) shows an improvement in activity compared to MIL-100(Sc). This is because MIL-100(Fe) possesses Fe^{3+} sites active for both types of reaction. This activity is much improved by inclusion of both Fe^{3+} and Sc^{3+} into MIL-100. Introducing 20% iron into MIL-100(Sc) increases the activity 5-fold. The introduction of too much iron has a negative effect on the reaction; although this increases the rate of oxidation it decreases C-C bond formation.

Table 5.14: One-pot Friedel-Crafts addition and oxidation reaction of 2-methylindole with trifluoroacetaldehyde ethyl hemiacetal and tert-butyl hydroperoxide catalysed by various MOF materials



Entry	MOF	Substrate	Product	Conversion (%) ^a
1	No catalyst			0
2	MIL-100(Sc)			10
3	MIL-100(Sc ₈₀ /Fe ₂₀)			55
4	MIL-100(Sc ₆₀ /Fe ₄₀)			96
5	MIL-100(Sc ₆₀ /Fe ₄₀) ^b			96
6	MIL-100(Sc ₄₀ /Fe ₆₀)			78
7	MIL-100(Sc ₂₀ /Fe ₈₀)			67
8	MIL-100(Sc ₈₀ /Fe ₂₀)Xs			88
9	MIL-100(Sc ₆₀ /Fe ₄₀)Xs			90
10	MIL-100(Sc ₅₀ /Fe ₅₀)Xs			85
11	MIL-100(Fe)			60
12	HKUST-1(Cu)			12
13	HKUST-1(Cu ₉₀ /Ru ₁₀)			35

Reaction carried out using 1 mmol of 2-methylindole and 1.4 mmol trifluoroacetaldehyde ethyl hemiacetal 4 mmol *tert*-butyl hydroperoxide toluene/decene. ^a Determined by ¹⁹F{¹H} NMR using 1-fluoronaphthalene as internal standard. ^b Recycled MIL-100(Sc).

For the series of MIL-100(Sc/Fe) where both Sc and Fe are in the trimers, MIL-100(Sc₆₀/Fe₄₀) has the optimum ratio of metals. It shows very high activity in the tandem reaction (96 %) conversion using 5 mol% catalyst. This high activity can also be maintained when the catalyst is recycled (Table 5.14, entry 6). The reaction profile was

determined using NMR, taking samples of the reaction over a period of 6 h. This showed the increase in formation of alcohol which reaches a maximum at ~ 50 % minutes. This influences the rate of formation of ketone-hence the typical sigmoidal shape for a typical sequential reaction that is observed (Figure 5.34).

The activity of the materials in which scandium was directly replaced with iron was generally higher in the tandem reaction than the materials that for contain α -Fe₂O₃ nanoparticles. The C-C bond formation rate is increased by the presence of the α -Fe₂O₃; however, the rate of oxidation appears to decrease (Table 5.14 entries 8-10).

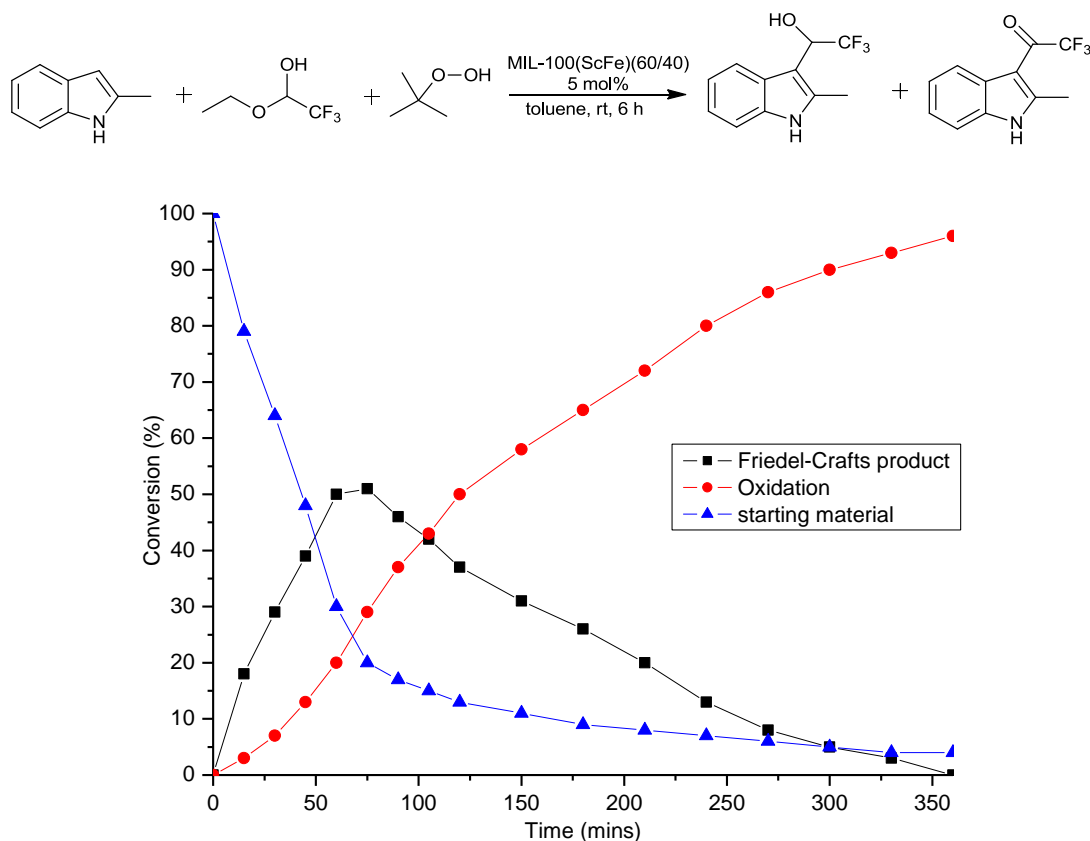


Figure 5.34: One-pot Friedel-Crafts addition and oxidation. Consumption of starting material (blue), formation of Friedel-Crafts product (black) and oxidation product (red)

Recycling of the MIL-100(Sc₆₀/Fe₄₀) was also successfully carried out. It was shown that after recovery and use of the previously used material the same high conversion as originally observed could be repeated (Table 5.14, entries 4 and 5). In order to determine that no metal leaching was occurring in the reaction the MIL-100(Sc₆₀/Fe₄₀) was removed from the reaction after 3 h (at a conversion of 58%). The reaction was

allowed to continue after catalyst removal and conversion was found to remain at 58% for a further 24 h.

The tandem reaction was also carried out using a chromium-containing MIL-100(Sc₆₀/Cr₄₀). MIL-100(Cr) was previously found to be a stronger Lewis acidic catalyst than MIL-100(Fe) and has also been found to catalyse oxidation. However, although the material did give a high conversion of trifluoroacetaldehyde ethyl hemiacetal only 52 % of this was selective to the desired product 2,2,2-trifluoro-1-(2-methyl-1H-indol-3-yl)ethanone. This shows the functional advantage of using the iron-containing material over the chromium-containing solid (additional to its lower toxicity).

Remarkably, the one-pot approach to the overall reaction gave product ketone more rapidly than carrying out the oxidation reaction separately. The oxidation reaction is slower. For MIL-100(Sc₆₀/Fe₄₀) material the oxidation step gives a conversion to product of 80% after 6 h for the oxidation to form 2,2,2-trifluoro-1-(2-methyl-1H-indol-3-yl)ethanone (Table 5.12, entry 4). This conversion to 2,2,2-trifluoro-1-(2-methyl-1H-indol-3-yl)ethanone is increased to 96% when the reaction is carried out in tandem (Table 5.14, entry 6) from the 2-methylindole starting material.

Diffusion of the substrates in and out of the MOF was investigated to determine if this had any influence on the activity. One explanation for why the conversion of alcohol to ketone was more complete for the one pot tandem reaction than in the separate 'oxidation-only' reaction might be that the first diffusion step is fast and the alcohol product is rapidly formed from 2-methylindole in the pores where it can be oxidised, but for the oxidation-only reaction the alcohol diffuses more slowly into the pores than the indole.

Uptake measurements for 2-methylindole and for the alcohol intermediate are shown in Figure 5.35. The 2-methylindole does enter the pores more quickly than the alcohol, particularly over the first hour. The oxidation-only reaction was then repeated, adding the peroxide only after the alcohol had been allowed to adsorb for 1 h. Conversion to ketone product increased from 79% to 90% over 6 h, similar to that observed in the tandem reaction over this timeframe (Table 5.12, entries 5 and 6). This suggests the tandem reaction is faster due to the generation of the alcohol in situ.

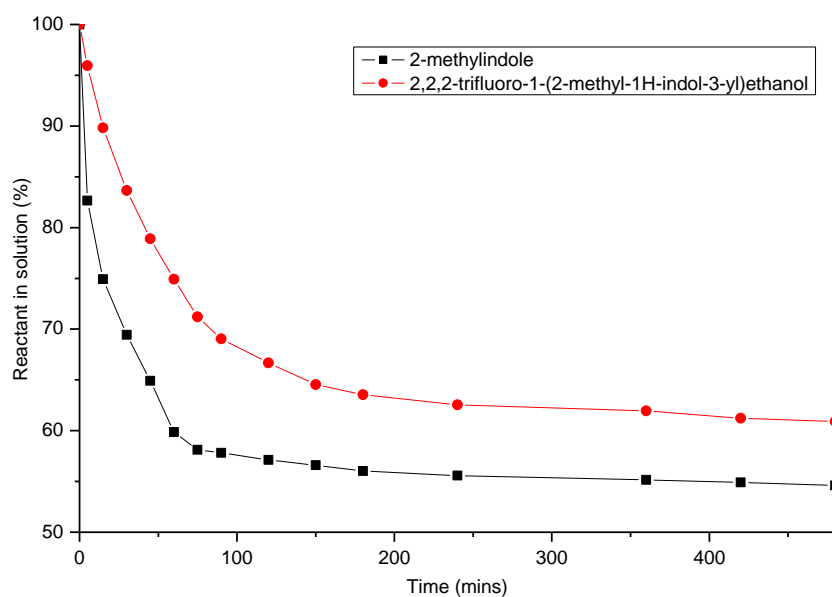
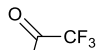
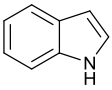
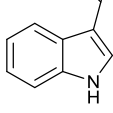
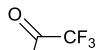
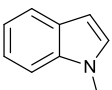
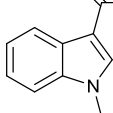
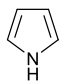
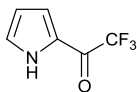
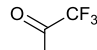
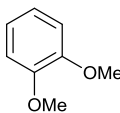
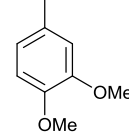


Figure 5.35: Diffusion of 2-methylindole (0.25 mmol) and 2,2,2-trifluoro-1-(2-methyl-1-indol-3-yl)ethanol (0.25 mmol) into mixed metal MIL-100(Sc_{60}/Fe_{40}) over an 8 h cycle stirred at room temperature in toluene. Using 1-methylnaphthalene as internal standard

The reaction was carried out using the same substrates as previously used in the Friedel-Crafts reaction (Table 5.15). The use of a one-pot approach again increased the rate of reaction compared to carrying out the oxidation reactions individually. Low conversions were observed with MIL-100(Sc) with each substrate. An increase is observed again when iron is introduced with the optimum material being MIL-100(Sc_{60}/Fe_{40}). High conversions were observed with activated heteroaromatics. However, with less activated veratrole lower conversions were observed. The Friedel-Crafts addition capability of the catalyst when using this substrate is reduced so in the tandem reaction the overall reaction conversion is lower (Table 5.15, entry 19).

Table 5.15: One-pot Friedel-Crafts addition and oxidation reaction of various substrates with trifluoroacetaldehyde ethyl hemiacetal and *tert*-butyl hydroperoxide catalysed by various MOF materials

Entry	MOF	Substrate	Product	Conversion (%)
1	No catalyst			0
2	MIL-100(Sc)			8
3	MIL-100(Sc ₆₀ /Fe ₄₀)			92
4	MIL-100(Sc ₆₀ /Fe ₄₀)Xs			87
5	MIL-100(Fe)			53
6	HKUST-1(Cu)			14
7	No catalyst			0
8	MIL-100(Sc)			7
9	MIL-100(Sc ₆₀ /Fe ₄₀)			93
10	MIL-100(Sc ₆₀ /Fe ₄₀)Xs			85
11	MIL-100(Fe)			51
12	No Catalyst			0
13	MIL-100(Sc)			9
14	MIL-100(Sc ₆₀ /Fe ₄₀)			97
15	MIL-100(Sc ₆₀ /Fe ₄₀)Xs			92
16	MIL-100(Fe)			48
17	No catalyst			0
18	MIL-100(Sc)			3
19	MIL-100(Sc ₆₀ /Fe ₄₀)			56
20	MIL-100(Sc ₆₀ /Fe ₄₀)Xs			51
21	MIL-100(Fe)			20
22	HKUST-1(Cu)			0

Reaction carried out using 1 mmol of 2-methylindole and 1.4 mmol trifluoroacetaldehyde ethyl hemiacetal 4 mmol *tert*-butyl toluene/decene. ^a Determined by ¹⁹F{¹H} NMR using 1-fluoronaphthalene as internal standard. Reaction entries 17-22 carried out at 90°C for 16 h.

In addition a physical mixture of MIL-100(Sc) and MIL-100(Fe) was used in the one pot reaction with 2-methylindole. Although this was found to be active the activity was not as high as what was observed for the mixed metal MIL-100(Sc₆₀/Fe₄₀) (78% cf. 95% after 31 h). This shows that some benefits are gained by having both metals present in the same MIL-100 material. The use of MIL-100(Sc/Fe) material has therefore been shown to be a successful catalyst in deacetalisation/Friedel-Crafts reaction and oxidation, both independently and in a one-pot system. By simply optimising the amount of each metal contained in MIL-100 a catalyst that can catalyse both reactions has been designed.

5.7. Conclusion

The synthesis of mixed metal MOFs have been carried out and discussed. Initial synthesis of mixed metal MOFs involved simple replacement of scandium with another trivalent metal. The introduction of iron was achieved over the complete compositional solid solution and PXRD confirmed MIL-100 was prepared in each case. The materials were shown to have a reduced unit cell volume as the amount of iron incorporated was increased. The N₂ adsorption of each material was similar; each showing mesoporous character. UV-visible spectroscopy showed an increase in absorption as iron content was increased, as expected. In other syntheses of mixed metal MIL-100(Sc/Fe) material an interesting series was formed when excess iron salt was added to the reaction. The material had a distinctively different colour (pink compared to orange when using the simple synthesis method). Unlike the previously discussed MIL-100(Sc/Fe), an introduction of 50% iron was the maximum that could be synthesised. The materials were initially analysed using PXRD showed saw a difference in peak intensity in the lower range of the pattern and distinctive differences were observed by UV-visible spectroscopy. N₂ uptake at 77 K was reduced as the amount of iron was increased in the material and the amount of mass remaining after calcination increased. The analysis gave evidence that the cause of the reduction in adsorption was caused by iron oxide nanoparticles in the pores of the material. XANES and EXAFS analysis concluded that the nanoparticle contained in the mixed metal material was α -Fe₂O₃ hematite. The amount of the nanoparticle could be calculated by TGA and the amount of iron in the framework structure predicted by calculating the *a* parameter of the material. In order to probe whether mixed metal materials consisted of mixed metal trimers, solid state NMR analysis was performed on Sc/Al mixed metal MOFs. The solid state NMR showed that the mixed metal materials consisted of scandium and aluminium within trimers but due to similarity in shifts no clear evidence for mixed metal or segregated trimers was obtained. The introduction of divalent metals into the MIL-100(Sc) was also achieved. Due to charge balance requirements the maximum amount of divalent metal introduced was ca. 30%. The inclusion of divalent metals was shown to have little effect on PXRD, BET surface area or TGA measurements. The UV-visible spectrum of the cobalt and nickel materials showed increases in absorption as the amount of metal was increased. The nature of the absorption gave evidence to suggest that the metals were incorporated into the trimer.

The mixed metal materials were tested in a range of reactions to gauge their catalytic activity and the effects of changing metal ratios. The initial tests in Lewis acid catalysed reactions showed that the replacement of scandium with other trivalent metal cations leads to a decline in conversion as the amount of scandium was decreased. Interestingly, the mixed metal MIL-100(Sc/Fe)_Xs material showed very high catalytic activity, with similar and sometimes higher conversions to product than over MIL-100(Sc) for the Lewis acid-catalysed Friedel-Crafts and carbonyl ene reactions. The introduction of divalent metals was detrimental to the catalytic activity, resulting in a dramatic reduction of activity.

The most important discovery was tandem Lewis acid/oxidation catalysis carried out using mixed metal MIL-100(Sc/Fe) which showed good activity when using heteroaromatic substrates. A good balance between scandium sites for C-C bond formation reactions and iron for oxidation reactions was required. MIL-100(Sc₆₀/Fe₄₀) was the best catalyst for this reaction with high conversions for the one-pot reactions and the Friedel-Crafts and oxidation reactions separately. Remarkably, the use of a one-pot approach to the reaction behaved better than carrying out both reactions separately. Diffusion of the substrate for oxidation in the MOF was slower for the alcohol substrate than 2-methylindole. So the oxidation reactions are limited by diffusion, but the tandem process enables oxidation of the alcohol intermediate before it leaves the MOF.

This work has shown that by replacing a metal with another, new properties can be introduced into the catalyst. The mixed metal materials can make use of the different metals in the framework to promote a useful process.

5.8. References

1. S. H. Cho, B. Q. Ma, S. T. Nguyen, J. T. Hupp and T. E. Albrecht-Schmitt, *Chem. Commun.*, 2006, 2563-2565.
2. F. Song, C. Wang, J. M. Falkowski, L. Ma and W. Lin, *J. Am. Chem. Soc.*, 2010, **132**, 15390-15398.
3. Y. Ren, X. Cheng, S. Yang, C. Qi, H. Jiang and Q. Mao, *Dalton Trans.*, 2013, **42**, 9930-9937.
4. A. M. Shultz, A. A. Sarjeant, O. K. Farha, J. T. Hupp and S. T. Nguyen, *J. Am. Chem. Soc.*, 2011, **133**, 13252-13255.
5. A. Arnanz, M. Pintado-Sierra, A. Corma, M. Iglesias and F. Sanchez, *Adv. Synth. Catal.*, 2012, **354**, 1347-1355.
6. M. Pintado-Sierra, A. M. Rasero-Almansa, A. Corma, M. Iglesias and F. Sanchez, *J. Catal.*, 2013, **299**, 137-145.

7. F. Ke, J. Zhu, L.-G. Qiu and X. Jiang, *Chem. Commun.*, 2013, **49**, 1267-1269.
8. A. Corma, M. Iglesias, F. Xamena and F. Sanchez, *Chem. -Eur. J.*, 2010, **16**, 9789-9795.
9. F. Xamena, A. Abad, A. Corma and H. Garcia, *J. Catal.*, 2007, **250**, 294-298.
10. F.-N. Shi, A. R. Silva, T.-H. Yang and J. Rocha, *Crystengcomm*, 2013, **15**, 3776-3779.
11. Y. Wan, C. Chen, W. Xiao, L. Jian and N. Zhang, *Microporous Mesoporous Mater.*, 2013, **171**, 9-13.
12. C. B. Liu, R. A. S. Ferreira, F. A. A. Paz, A. Cadiau, L. D. Carlos, L. S. Fu, J. Rocha and F. N. Shi, *Chem. Commun.*, 2012, **48**, 7964-7966.
13. M. I. Breeze, G. Clet, B. C. Campo, A. Vimont, M. Daturi, J.-M. Greneche, A. J. Dent, F. Millange and R. I. Walton, *Inorg. Chem.*, 2013, **52**, 8171-8182.
14. R. Canioni, C. Roch-Marchal, F. Secheresse, P. Horcajada, C. Serre, M. Hardidan, G. Ferey, J.-M. Greneche, F. Lefebvre, J.-S. Chang, Y.-K. Hwang, O. Lebedev, S. Turner and G. Van Tendeloo, *J. Mater. Chem.*, 2011, **21**, 1226-1233.
15. A. B. Blake and A. Yavari, *J. Chem. Soc., Chem. Commun.*, 1982, 1247-1249.
16. A. B. Blake, A. Yavari, W. E. Hatfield and C. N. Sethulekshmi, *J. Chem. Soc. Dalton Trans.*, 1985, 2509-2520.
17. V. Gia-Thanh, P. Minh-Hao and D. Trong-On, *Crystengcomm*, 2013, **15**, 9694-9703.
18. R. D. Shannon, *Acta Crystallogr. Sec. A*, 1976, **32**, 751-767.
19. P. Horcajada, S. Surble, C. Serre, D.-Y. Hong, Y.-K. Seo, J.-S. Chang, J.-M. Greneche, I. Margiolaki and G. Ferey, *Chem. Commun.*, 2007, 2820-2822.
20. T. Birsa Celic, M. Rangus, K. Lazar, V. Kaucic and N. Zabukovec Logar, *Angew. Chem. Int. Ed.*, 2012, **51**, 12490-12494.
21. A. Vimont, J. M. Goupil, J. C. Lavalley, M. Daturi, S. Surble, C. Serre, F. Millange, G. Ferey and N. Audebrand, *J. Am. Chem. Soc.*, 2006, **128**, 3218-3227.
22. C. Volkringer, D. Popov, T. Loiseau, G. Ferey, M. Burghammer, C. Riekel, M. Haouas and F. Taulclle, *Chem. Mater.*, 2009, **21**, 5695-5697.
23. L. J. Daumann, P. Comba, J. A. Larrabee, G. Schenk, R. Stranger, G. Cavigiasso and L. R. Gahan, *Inorg. Chem.*, 2013, **52**, 2029-2043.
24. J. M. Herrera, A. Bleuzen, Y. Dromzee, M. Julve, F. Lloret and M. Verdaguer, *Inorg. Chem.*, 2003, **42**, 7052-7059.
25. M. J. Borah, R. K. B. Singh, U. B. Sinha, T. Swu and P. J. Borah, *J. Chem. Crystallogr.*, 2012, **42**, 67-75.
26. O. Kozachuk, K. Yussenko, H. Noei, Y. Wang, S. Walleck, T. Glaser and R. A. Fischer, *Chem. Commun.*, 2011, **47**, 8509-8511.
27. C. R. Wade and M. Dinca, *Dalton Trans.*, 2012, **41**, 7931-7938.
28. R. Noyori and S. Hashiguchi, *Acc. Chem. Res.*, 1997, **30**, 97-102.
29. T. Naota, H. Takaya and S. I. Murahashi, *Chem. Rev.*, 1998, **98**, 2599-2660.
30. R. Noyori and T. Ohkuma, *Angew. Chem. Int. Ed.*, 2001, **40**, 40-73.
31. R. Noyori, *Angew. Chem. Int. Ed.*, 2002, **41**, 2008-2022.
32. A. Corma, H. Garcia and F. X. L. Xamena, *Chem. Rev.*, 2010, **110**, 4606-4655.
33. A. Dhakshinamoorthy, M. Alvaro, Y. K. Hwang, Y.-K. Seo, A. Corma and H. Garcia, *Dalton Trans.*, 2011, **40**, 10719-10724.
34. A. Dhakshinamoorthy, M. Alvaro, P. Horcajada, E. Gibson, M. Vishnuvarthan, A. Vimont, J.-M. Greneche, C. Serre, M. Daturi and H. Garcia, *ACS Catal.*, 2012, **2**, 2060-2065.

6. Post synthetic modification

6.1. Introduction

The use of post-synthetic modification in MOFs has proved a useful method for the introduction of different functionalities that cannot normally be achieved via direct MOF synthesis. Some examples of this are discussed in Chapter 1. This led to the idea of synthesising mixed metal materials by introducing a secondary metal post-synthesis. This idea was employed by taking two different approaches. The first approach was carried out by using the ligand 2,2'-bipyridine-5,5-dicarboxylic acid (bpydc) which contains two free nitrogen atoms that could be used to bind a second metal (Figure 6.1 route A). In this case the coordination reaction of the second metal occurs on the intact MOF. The second method is the post-synthetic introduction of a secondary ligand that could be used to attach a further metal. In this case the ligand is synthesised on an intact MOF and then the second metal is coordinated (Figure 6.1 route B).

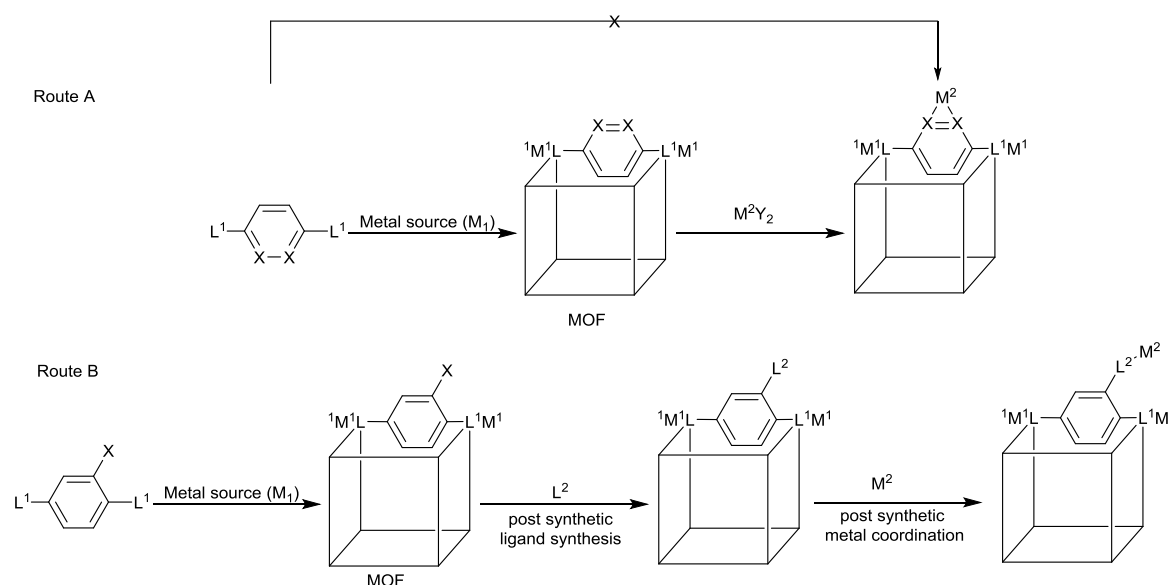
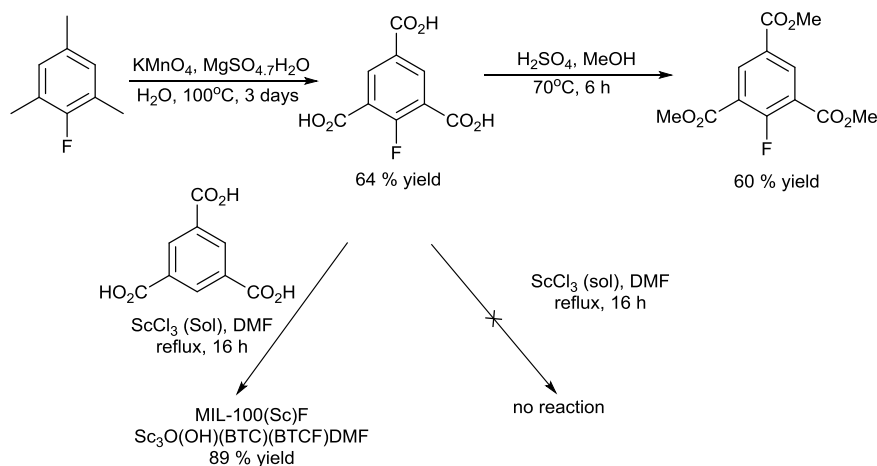


Figure 6.1: Schematic representation of potential ways in which post synthetic modification can be used to add a second metal to a MOF

Both routes of introduction of a secondary metal were attempted, however route A did not provide any materials additional to these already synthesised.¹ Therefore we focused on route B as a method of post-synthetic synthesis of mixed metal MOFs.

6.2. Synthesis of MIL-100(Sc) with diphenylphosphine ligand

The synthesis of MOF materials that do not just act as a support but also a catalyst in their own right is of great interest. Another approach we took with this in mind was the introduction of diphenylphosphino groups into the structure. Although there have been previous examples of MOFs that contain phosphorus entities that could be post synthetically modified to anchor another metal,²⁻⁷ there are no examples of doing this by post synthetic nucleophilic substitution of the ligand. In order to synthesise a MOF with a diphenylphosphine ligand, a MOF that contained a substituent that could be post-synthetically exchanged was synthesised. In this case we chose to synthesise a MIL-100(Sc) MOF that contained fluorine on the trimesic acid. This would allow for a nucleophilic aromatic substitution (S_NAr) to be carried out on the C-F bond with potassium diphenyl phosphide. In order to do this, the first step was to synthesise the fluorinated trimesic acid ligand. This was carried out using slow oxidation of 2,4,6-trimethylfluorobenzene using potassium permanganate, magnesium sulfate heptahydrate and water and refluxing for 3 days (Scheme 1) (see Experimental Section 7.2 for details).^{8,9}



Scheme 6.1: Oxidation of 2,4,6-trimethylfluorobenzene to form 1-fluoro-2,4,6-tricarboxylic acid which was then used to synthesis MIL-100(Sc)F

The synthesis of MIL-100(Sc) with 1-fluoro-2,4,6-tricarboxylic acid was attempted. Synthesis temperatures from 373 - 433 K were tried using different solvents (DMF, DMA, water, ethanol and acetone) and different solvent ratios. However, only starting material was returned. The synthesis was then attempted using the ester of 1-fluoro-

2,4,6-tricarboxylic acid as the ester is more soluble than the acid. This however did not give the desired MIL-100 material and again only starting materials were obtained.

In order to try and help the formation of MIL-100(Sc) using the fluorinated ligand a mixture of 1-fluoro-2,4,6-tricarboxylic acid and 1,3,5-tricarboxylic acid was attempted. This was successful and a MIL-100(Sc) material that contained different mixtures of both ligands was synthesised with maximum of 50% fluorinated ligand. A schematic representation of part of the structure is given below (Figure 6.2)

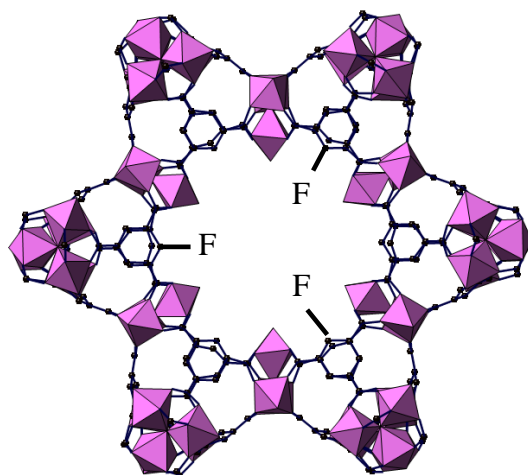


Figure 6.2: Schematic representation of a part of MIL-100(Sc)F

For the synthesis of a 50/50 ligand mixture MIL-100(Sc), scandium chloride (aq), 1-fluoro-2,4,6-tricarboxylic acid and 1,3,5-tricarboxylic acid in DMF (3:1:1:600) were heated under reflux for 16 h. A yellow powder was obtained with 89% yield and initially analysed by PXRD. This showed a crystalline material with peaks in the same places as MIL-100(Sc) synthesised with just 1,3,5-tricarboxylic acid (Figure 6.6). Further to this, N₂ adsorption was carried out and the material was found to have a BET surface area of 1089 m²g⁻¹. This was also carried out for BTC:BTCF ratios of 90:10 and 70:30. PXRD of each of these materials show a crystalline material comparable to that of MIL-100(Sc) was synthesised (Figure 6.3).

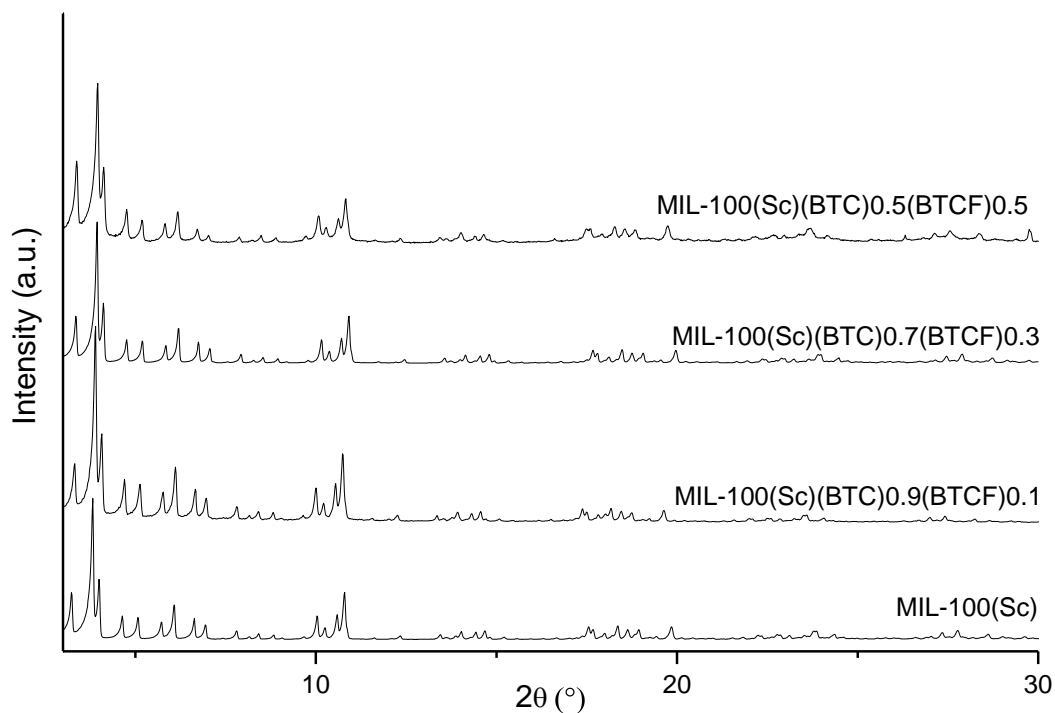


Figure 6.3: PXRD patterns of mixed ligand MIL-100(Sc) materials

TGA analysis showed a slight increase in residual mass as the amount of fluorine in the material was increased (Figure 6.4). A small decrease in N₂ adsorption was also seen as the amount of fluorine in the MOF was increased (Figure 6.5). This could be caused by the fluorine taking up more space in the pore of the material.

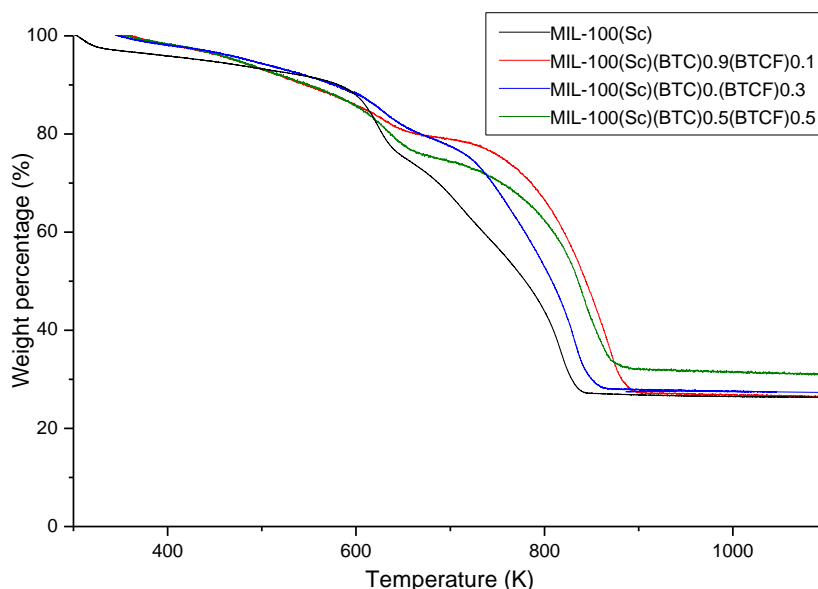


Figure 6.4: TGA carried out in air of (a) MIL-100(Sc) (black)
 (b) MIL-100(Sc)(BTC)_{0.9}(BTCF)_{0.1} (red) (c) MIL-100(Sc)(BTC)_{0.7}(BTCF)_{0.3} (blue)
 (d) MIL-100(Sc)(BTC)_{0.5}(BTCF)_{0.5} (green)

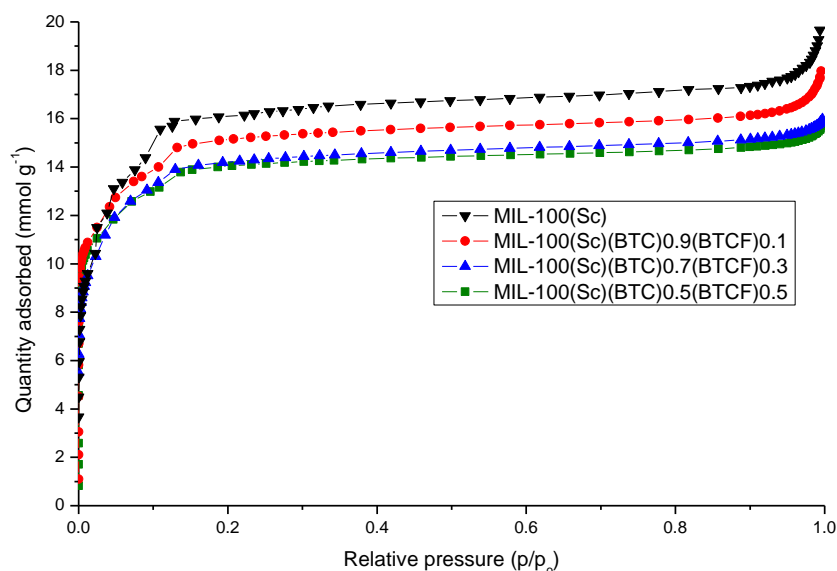


Figure 6.5: N_2 adsorption at 77 K comparison of mmol g^{-1} uptake of mixed ligand MIL-100 materials

In order to determine if the fluorinated ligand was present both EDX analysis (Table 6.1) and solution-phase NMR was carried out. The amount of fluorinated ligand in the material could be indirectly determined by solution phase $^1\text{H-NMR}$ as the shifts of the both starting materials differ. The MOF was therefore digested in acid before analysis and thereby broken down into starting ligand. In order to do this 10 mg of the synthesised material was placed in a vial with d_6 -DMSO (0.5 ml) and 0.1 M nitric acid (0.2 ml) and the mixture was dissolved, aided by sonication. The peaks due to both the 1-fluoro-2,4,6-tricarboxylic acid and 1,3,5-tricarboxylic acid were differentiated by their shift in $^1\text{H NMR}$. The 1,3,5-tricarboxylic acid shows a singlet 3 H peak (at 8.87 ppm) and 1-fluoro-2,4,6-tricarboxylic acid is slightly shifted downfield to give a 2 H doublet peak (at 8.62 ppm).

Table 6.1: Ratios of BTC and BTCF in the synthesis of mixed ligand MIL-100(Sc)

Entry	Ratio (Sc:BTC:BTCF:DMF)	MOF	Sc/F ratio by EDX
1	3:1:1:600	MIL-100(Sc)(BTC) _{0.5} (BTCF) _{0.5}	74:26
2	3:1.4:0.6:600	MIL-100(Sc)(BTC) _{0.7} (BTCF) _{0.3}	83:17
3	3:1.8:0.2:600	MIL-100(Sc)(BTC) _{0.9} (BTCF) _{0.1}	93:7

6.3. Functionalisation of MIL-100(Sc) with diphenylphosphine

The introduction of the fluoro- group onto the aromatic rings in MIL-100(Sc) gave the potential for further post synthetic reactions to be carried out on the material. In order to carry out post synthetic modification, the MOF was dehydrated to remove any solvent that could hinder reactivity. In initial reactions an excess of potassium diphenylphosphide in THF and toluene was stirred with the MOF at 343 K for 6 h. Once the reaction was complete and purified the MOF material was analysed. The PXRD pattern shows that the synthesised material has peaks in the same positions as MIL-100(Sc) although some crystallinity has been lost (Figure 6.6).

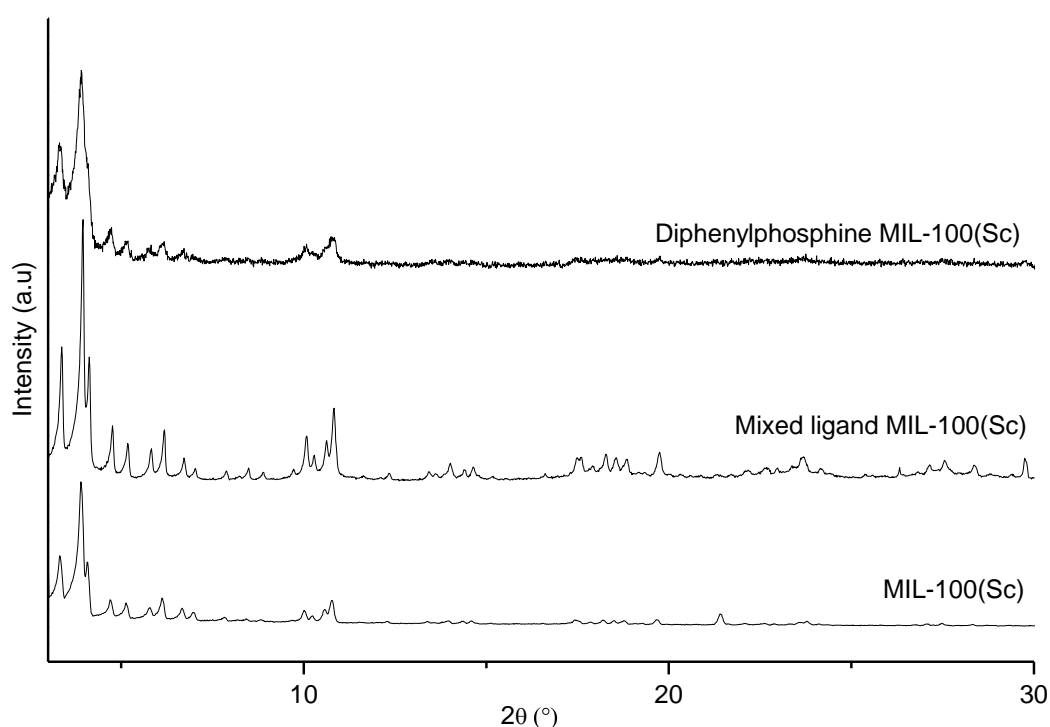


Figure 6.6: PXRD patterns of MIL-100(Sc) synthesised using trimesic acid compared to MIL-100(Sc) synthesised using a 50/50 mixture of 1-fluoro-2,4,6-tricarboxylic acid and 1,3,5-tricarboxylic acid and after post synthetic modification with diphenylphosphine

The MOF was dissolved in 0.1 M nitric acid and d_6 -DMSO and NMR analysis carried out. This showed that phosphorus was present in the solution with a peak at 23.59 ppm, being consistent with the oxide of a biarylphosphine. (It is expected that DMSO or aqueous nitric acid should oxidise the phosphine).

EDX analysis showed that phosphorus was now present in the material and comparison with the material before post-synthetic modification showed that although some (4 % F

compared to Sc wt %) fluorine is present in the product structure, the amount present is reduced. N₂ adsorption showed very low uptake with a very small BET surface area. This may be due to the bulky diphenylphosphine blocking the pores.

To overcome the large reduction in porosity it was thought the amount of diphenylphosphine replacing fluorine could be reduced. The amount of diphenylphosphine with respect to fluorine added was reduced in several reactions using between 1 and 30% potassium diphenylphosphide in the MIL-100 material. These reactions were all carried out using MIL-100(Sc) synthesised from a 50/50 mixture of fluorinated and non-fluorinated ligands. PXRD analysis showed that in these materials there was a slight reduction in crystallinity as the amount of diphenylphosphine introduced was increased (Figure 6.7).

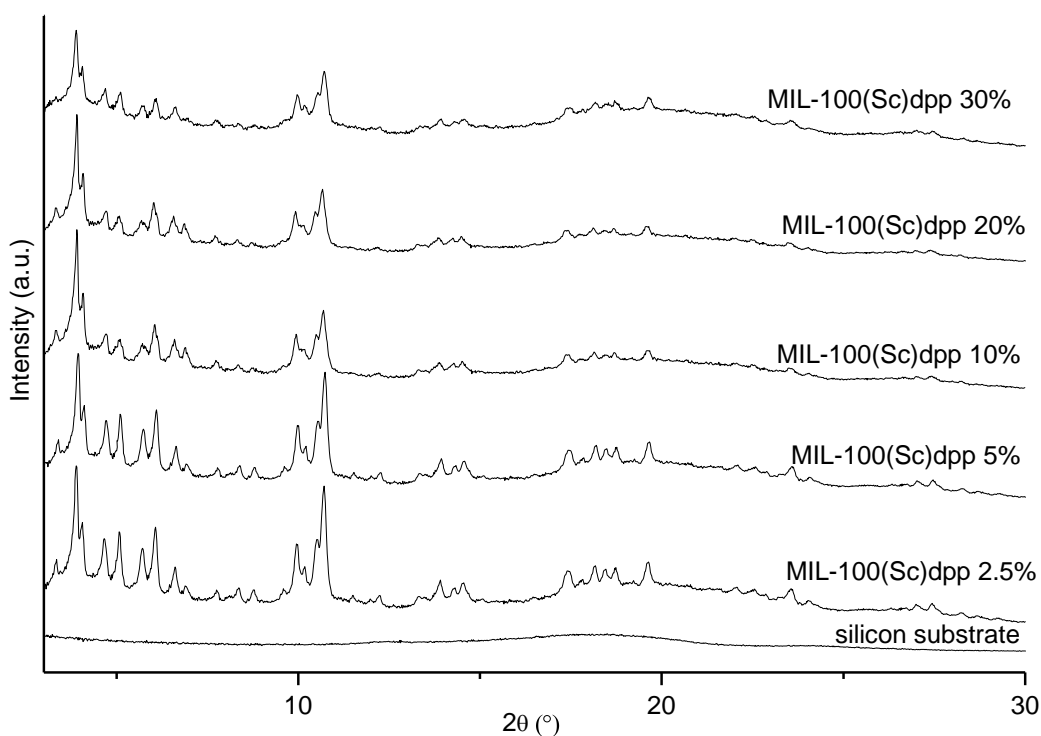


Figure 6.7: PXRD of MIL-100(Sc)dpp with varying amounts of diphenylphosphine compared to silicon substrate used to carry out PXRD due to small amount of material

It was confirmed that the phosphorus was present in these diphenylphosphine containing materials by both NMR on the digested ligands and EDX (Table 6.2). N₂ adsorption of the materials showed that a decrease in adsorption is observed as the amount of diphenylphosphine was increased. This was expected as the diphenylphosphine will take up some of the pore volume (Figure 6.8).

Table 6.2: Ratio of amount of phosphorus compared to fluorine in different MIL-100(Sc) materials containing diphenylphosphino-functionalised aromatic rings

MOF	Ratio of phosphorus to fluorine established by EDX analysis
MIL-100(Sc)dpp30%	31.0:69.0
MIL-100(Sc)dpp20%	23.2:76.8
MIL-100(Sc)dpp10%	9.9:90.1
MIL-100(Sc)dpp5%	5.7:94.3
MIL-100(Sc)dpp2.5%	2.5:97.5
MIL-100(Sc)dpp1%	1.2:98.8

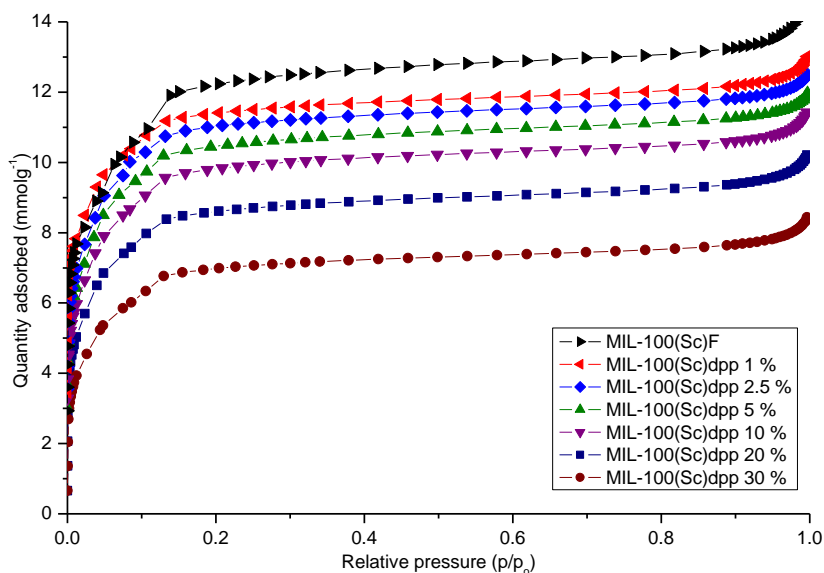


Figure 6.8: N_2 adsorption at 77 K of MIL-100(Sc) containing varying amounts of diphenylphosphino-functionalised aromatic rings (dpp)

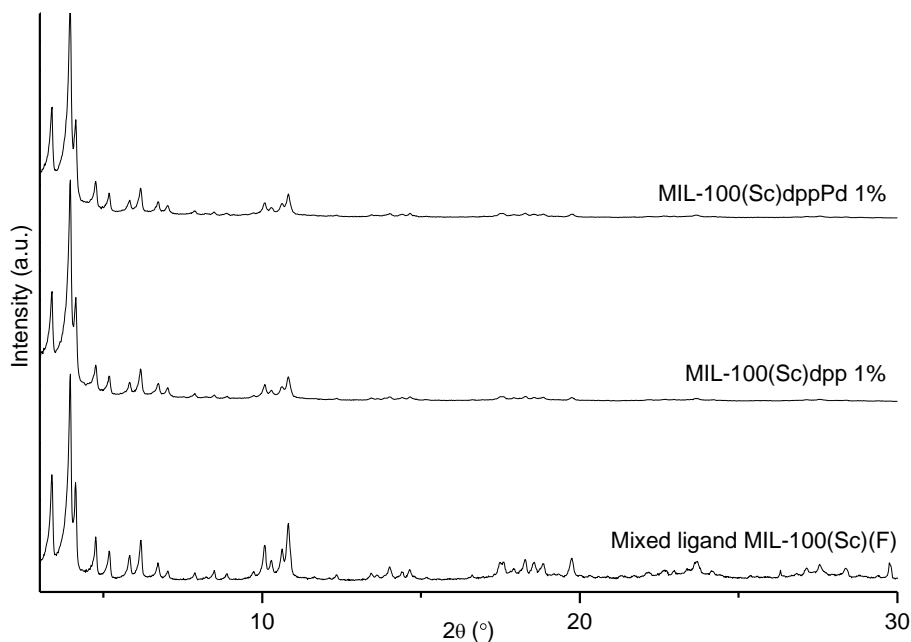


Figure 6.9: PXRD of MIL-100(Sc)(F) after introduction of diphenylphosphine and allylpalladium dichloride dimer

The synthesis of a porous material that contained a phosphine ligand could allow the addition of complexed palladium. This was achieved by stirring the MIL-100(Sc)-dpp-1% in dichloromethane and allylpalladium dichloride dimer. PXRD analysis shows that the crystallinity of the material is retained and no presence of metal oxide is observed.

A further reduction in N₂ adsorption was observed in the material after introduction of palladium (Figure 6.10).

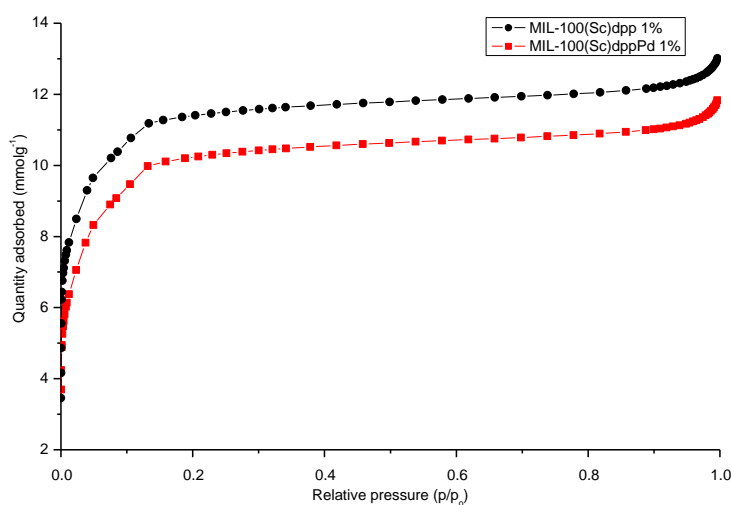


Figure 6.10: N₂ adsorption of MIL-100(Sc)-dpp-1% before and after addition of allylpalladium dichloride dimer (at 77 K)

The presence of palladium in the material was confirmed by EDX and was shown to be homogeneously distributed throughout the MOF. It was thought that the presence of palladium bound to phosphorus would be observed by solid state ^{31}P NMR since phosphines shift downfield from around 0 ppm to around 30 ppm when coordinated. This was not observed (Figure 6.11). It was found that the MIL-100(Sc)-dpp material was oxidised even before addition of palladium. These were only preliminary attempts at the potentially important approach of making C-P bond in intact MOFs. Modification of the reaction conditions should make it possible to introduce phosphine without oxidation.

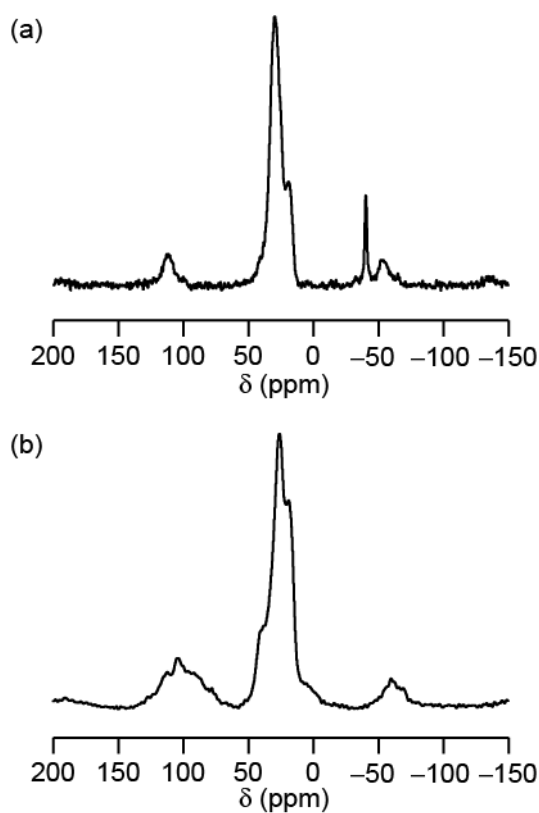
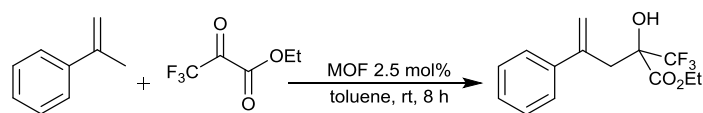


Figure 6.11: ^{31}P NMR spectrum of (a) MIL-100(Sc)dpp and (b) MIL-100(Sc)dppPd

Some initial catalytic testing was carried out to see if the scandium sites were still Lewis acidic. The activity of the scandium site on the MOF was tested by carrying out a simple carbonyl ene reaction as discussed in section 4.1.2. A small reduction in catalytic activity was observed with a conversion to product of 89% after 8 h using 2.5 mol% catalyst loading (Scheme 6.2). This may be due to the reduced surface area of the material making it harder to access the Lewis acid sites caused by all the extra bulk in the structure. The palladium was not tested in catalysis as palladium complexes of phosphine oxides do not have such a rich catalysis chemistry as that of phosphines.



Scheme 6.2: Intermolecular carbonyl ene reaction of α -methyl styrene with ethyl trifluoropyruvate catalysed by MIL-100(Sc)dpp-10%

6.4. Conclusion

The use of post-synthetic modification has been implemented in order to synthesis bimetallic MOF materials. The synthesis of mixed ligand MIL-100(Sc) was carried out using 50% BTC and 50% BTCF and the material was characterised by PXRD, EDX, N₂ adsorption and both solid and solution phase NMR. This material opens up the potential for some interesting chemistry as the fluoro-group present in the material could be made use of in nucleophilic aromatic substitution reactions in order to replace the C-F bond with different functionalities. In this case we chose to add the diphenylphosphino group. This was successfully added in different ratios and the materials were characterised. It was found by solid state NMR that the diphenylphosphine added had oxidised making it less desirable for catalysis however it could possibly be reduced post-preparatively or retained in oxygen-free environment before use. Although the use of both metals in the material was thus not possible, the concept of using the fluorine on the trimesic acid to add new substrates provides new possibilities for post-synthetic modification of MOF materials.

6.5. References

1. E. D. Bloch, D. Britt, C. Lee, C. J. Doonan, F. J. Uribe-Romo, H. Furukawa, J. R. Long and O. M. Yaghi, *J. Am. Chem. Soc.*, 2010, **132**, 14382-14384.
2. J. Vaclavik, M. Servalli, C. Lothschuetz, J. Szlachetko, M. Ranocchiari and J. A. van Bokhoven, *ChemCatChem*, 2013, **5**, 692-696.
3. A. J. Nunez, M. S. Chang, I. A. Ibarra and S. M. Humphrey, *Inorg. Chem.*, 2014, **53**, 282-288.
4. S. Zhang, Q. Liu, M. Shen, B. Hu, Q. Chen, H. Li and J.-P. Amoureux, *Dalton Trans.*, 2012, **41**, 4692-4698.
5. X. Tan, L. Li, J. Zhang, X. Han, L. Jiang, F. Li and C.-Y. Su, *Chem. Mater.*, 2012, **24**, 480-485.
6. N. Nasser and R. J. Puddephatt, *Cryst. Growth Des.*, 2012, **12**, 4275-4282.
7. F. L. Morel, M. Ranocchiari and J. A. van Bokhoven, *Ind. Eng. Chem. Res.*, 2014, **22**, 9120-9127.
8. F. Micheel and W. Busse, *Chemische Berichte-Recueil*, 1957, **90**, 2049-2053.
9. K. Peikert, F. Hoffmann and M. Froeba, *Chem. Commun.*, 2012, **48**, 11196-11198.

7. Experimental

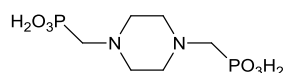
7.1. General procedures

Chemicals were purchased from commercial suppliers. Dry solvents were used in reactions that were carried out under N₂. Thin layer chromatography was carried out on pre-coated 0.2 Å Machery-Nagel Polygram SIL G/UV254 silicon plates. Absorption under UV light was visualised as well as thermal decomposition after dipping in aqueous solution of potassium permanganate if required. Column chromatography was performed using Davisil silica gel Fluorochem 60 Å, particle size 35-70 micron. ¹H NMR, ¹³C NMR, ¹⁹F NMR, and ³¹P NMR were carried out using a Bruker Avance III 500 spectrometer at 500 Hz, Bruker Avance II 400 spectrometer at 400 Hz or Bruker Avance 300 spectrometer at 300 Hz. Chemical shift information for each signal is given in part per million (ppm) relative to trimethylsilane (TMS). Chemical shifts for ¹⁹F are relative to CFCl₃ and ³¹P relative to phosphoric acid. The number of protons is denoted by nH reported from their resonance signal and the multiplicity represented by s,d,t,m and br where s is singlet, d is double, t is triplet, m is multiplet and b is broad. Coupling constants (J) are quoted to the nearest 0.1 Hz. The notation Ar is representative of an aryl group. All spectra were recorded at room temperature in varying solvents which are given in the parentheses.

7.2. Ligand synthesis

Phosphonate ligand synthesis (1)

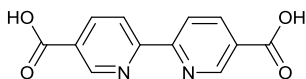
The phosphonic acids used in synthesis of STA-12 (H₄L ligand) and STA-16 (H₄LL) Ligand were prepared using a modified Mannich type reaction according to the literature procedure.¹



In a typical synthesis of STA-12 ligand N,N'-piperazinebis-(methylenephosphonic acid) (H₄L), piperazine (7.75 g 0.09 mol) was dissolved in phosphorous acid (19.19 g, 0.27 mol), hydrobromic acid (74 ml, 48 wt%) and distilled water (70 ml) in a three neck flask, fitted to a condenser and dropping funnel. Formaldehyde (38.5 ml, 35 wt%) was added drop wise over 30 minutes. The reaction was then heated to reflux at 393 K for 20 h. The reaction mixture was allowed to cool to room temperature causing a white

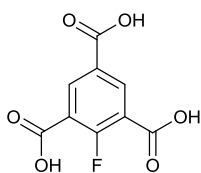
precipitate to form. The precipitate was filtered under vacuum filtration, washed using an ethanol:water mixture (90:10) 3 times and dried overnight in 313 K oven. Product was obtained in 82% yield, 20.22g, 74 mmol. ^1H NMR δ_{H} (400 MHz, D_2O) δ_{H} 2.38 (8 H, br s, CH_2), 2.25 (4 H, d, J 12, CH_2). ^{13}C NMR (75 MHz, D_2O) δ_{C} 57.1 (d, J 140), 53.7 (d, J 8.5). $^{31}\text{P}\{^1\text{H}\}$ NMR (121 MHz, D_2O) δ_{P} 14.45 (t, J 12.2 Hz).

Synthesis of 2,2'-bipyridine-5,5-dicarboxylic acid (2)



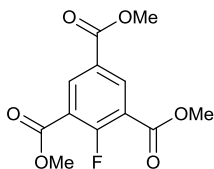
Synthesised using a modified literature prep.² 5,5'-dimethyl-2,2'-bipyridine (1 g, 5.42 mmol) was heated in water (60 ml) to 363 K. KMnO_4 (5.5 g, 34.82 mmol) was added in 4 portions over 8 h. The solution was stirred until the purple colour could no longer be observed. The mixture was cooled and brown precipitate filtered off. Extraction using diethylether was used to remove any unreacted 5,5'-dimethyl-2,2'-bipyridine. The solution was acidified using HCl (pH 2) and white precipitate that formed filtered off and dried under vacuum to give 2,2'-bipyridine-5,5-dicarboxylic acid (74%, 4.87 g, 19.8 mmol). This compound has been reported before using a similar procedure.² ^1H NMR (300 MHz, D_2O) δ_{H} 8.68 (1 H, dd, J 2.1, 0.7, Ar- H), 7.99 (1 H, dd, J 8.2, 2.1, Ar- H), 7.68 (1 H, dd, J 8.3, 0.6, Ar- H). ^{13}C NMR (75 MHz, D_2O) δ_{C} 172.8, 155.9, 149.8, 138.7, 132.4, 122.1. ESI [M- H] calculated 243.0411 found 243.0465. $\text{C}_{12}\text{H}_8\text{N}_2\text{O}_4$ (Found C, 59.02; H, 3.3; N, 11.47; Required C, 58.89; H, 3.28; N, 11.46)

1-fluorobenzene-2,4,6-tricarboxylic acid ligand synthesis (3+4)^{3, 4}



2,4,6-trimethylfluorobenzene (0.97 g, 7 mmol) was suspended in 50 ml of boiling water. The suspension was combined with a mixture of KMnO_4 (5.18 g, 32.8 mmol) and $\text{MgSO}_4 \cdot 7\text{H}_2\text{O}$ (4.14 g, 16.8 mmol) in 5 portions with 12 h gaps in between. The solution volume was halved under vacuum, separated from MnO through suction and the latter boiled in 20 ml of water, twice. The combined solutions were reduced to 60 ml, left in the fridge overnight and the precipitate separated by filtration. The obtained solution was reduced again to 30 ml and acidified with conc. H_2SO_4 (pH 3). The precipitate was

left in the fridge overnight. The crude acid was obtained through suction could not be recrystallized but was used as obtained (64%, 1.02 g, 4.47 mmol). This compound has been reported before using a similar procedure.³



In order to obtain analytical data on 1-fluorobenzene-2,4,6-tricarboxylic acid, its ester form was synthesised. 1-fluorobenzene-2,4,6-tricarboxylic acid (0.5 g, 2.19 mmol) was boiled with MeOH (10 ml) and conc. H₂SO₄ (0.12 ml) for 6h. The solution volume was halved under vacuum, poured over water (20 ml) and neutralized by adding an aqueous solution of sodium carbonate. The precipitated ester was filtered and recrystallized several times in MeOH (60%, 0.39 g, 1.44 mmol). This compound has been reported before using a similar procedure.⁴ ¹H NMR (400 MHz, CDCl₃) δ_H 8.72 (2 H, d, *J* 6.4, *Ar-H*), 3.94 (6 H, s, CH₃), 3.93 (3 H, s, CH₃). ¹³C NMR (75 MHz, CDCl₃) δ_C 164.7, 163.45 (d, *J*_{C-F} 4), 162.9 (d, *J*_{C-F} 252), 137.8 (d, *J*_{C-F} 3), 126.2 (d, *J*_{C-F} 4.8), 119.9 (d, *J*_{C-F} 11.8), 52.7, 52.4. ¹⁹F{¹H} NMR (471 MHz, CDCl₃) δ_F -118.8.

7.3. MOF synthesis

Synthesis of CPO-27(Ni),⁵ HKUST-1,⁶ MIL-88B(Sc),⁷ MIL-100(Cr)⁸ and MIL-101(Cr)⁸ were carried out using literature preps.

STA-12

N,N'-piperazinebis-(methylenephosphonic acid) (0.203 g, 0.74 mmol) was placed in a Teflon insert, dissolved in water (20 ml) and nickel acetate tetrahydrate (0.368 g, 1.48 mmol) added. This was left to stir for 30 minutes, Teflon liner placed in a steel autoclave and heated to 493 K for 3 days. The resulting precipitate is filtered under vacuum, washed with water and dried in 313 K oven overnight. The green powder product was characterised using PXRD, N₂ adsorption, TGA, EDX, and compared to literature.⁹

MIL-100(Sc)

Benzene-1,3,5-tricarboxylic acid (0.0905 g, 0.43 mmol,) and scandium chloride (aq) (1.45 M, 0.86 mmol, 0.6 ml) were dissolved in dimethylformamide, DMF (20 mL) and heated in a Teflon lined steel autoclave at 423 K for 48 h. The resulting solid was filtered under suction, washed with ethanol and water and dried at 313 K. Product was stirred in methanol for 24 h, filtered and dried at 313 K to activate. The white powder product was characterised using PXRD, N₂ adsorption, TGA, EDX, IR and UV spectroscopy, and compared to literature.⁷

MIL-100(Sc) and STA-12 synthesis have been optimised using various synthesis techniques and alternative solvents discussed in chapter 3.

MIL-100(Sc/Fe)(60/40)

Benzene-1,3,5-tricarboxylic acid (0.0908 g, 0.43 mmol), scandium chloride (aq) (1.45 M, 0.39 mmol, 0.27 ml) and iron (III) chloride hexahydrate (Aldrich, 0.26 mmol, 0.0701 g) were dissolved in DMF (10 mL) and heated in a Teflon lined steel autoclave at 383 K for 24 h. The resulting solid was filtered under suction, washed with ethanol and water and dried at 313 K. Product was stirred in methanol for 24 h, filtered and dried at 313 K to activate. The orange powder product was characterised using PXRD, N₂ adsorption, TGA, EDX, UV spectroscopy, XANES, and EXAFS, and compared to literature.⁷ The metal ratios of Sc/Fe of 100:0, 80:20, 60:40, 40:60 and 20:80 were used keeping the molar ratio of metal : BTC : DMF at 3:2:600.

MIL-100(Sc/Fe)(60/40)Xs

Benzene-1,3,5-tricarboxylic acid (0.0908 g, 0.43 mmol), scandium chloride (aq) (1.45 M, 0.43 mmol, 0.298 ml) and iron (III) chloride hexahydrate (Aldrich, 0.87 mmol, 0.234 g) were dissolved in DMF (10 mL) and heated in a Teflon lined steel autoclave at 383 K for 24 h. The resulting solid was filtered under suction, washed with ethanol and water and dried at 313 K. Product was stirred in methanol for 24 h, filtered and dried at 313 K to activate. The orange powder product was characterised using PXRD, N₂ adsorption, TGA, EDX, UV spectroscopy, XANES, and EXAFS, and compared to literature.⁷ The metal ratios of Sc/Fe of 2:2 to 5 were used keeping the molar ratio of BTC : DMF at 2:600.

MIL-100(Sc/Al)(60/40)

Benzene-1,3,5-tricarboxylic acid (0.0908 g, 0.43 mmol), scandium chloride (aq) (1.45 M, 0.39 mmol, 0.27 ml) and aluminium nitrate nonahydrate (Aldrich, 0.26 mmol, 0.0973 g) were dissolved in DMF (10 mL) and heated in a Teflon lined steel autoclave at 383 K for 24 h. The resulting solid was filtered under suction, washed with ethanol and water and dried at 313 K. Product was stirred in methanol for 24 h, filtered and dried at 313 K to activate. The white powder product was characterised using PXRD, N₂ adsorption, TGA, EDX, MASNMR and compared to literature.⁷ The metal ratios of Sc/Al of 100:0, 80:20, 70:30, 60:40, 50:50, 40:60, 30:70, 20:80 and 10:90 were used keeping the molar ratio of metal : BTC : DMF at 3:2:600.

MIL-100(Sc/Cr)(60/40)

Benzene-1,3,5-tricarboxylic acid (0.0908 g, 0.43 mmol), scandium chloride (aq) (1.45 M, 0.39 mmol, 0.27 ml) and chromium chloride hexahydrate (Aldrich, 0.26 mmol, 0.0619 g) were dissolved in DMF (10 mL) and heated in a Teflon lined steel autoclave at 383 K for 24 h. The resulting solid was filtered under suction, washed with ethanol and water and dried at 313 K. Product was stirred in methanol for 24 h, filtered and dried at 313 K to activate. The green powder product was characterised using PXRD, N₂ adsorption, TGA, EDX, UV spectroscopy, and compared to literature.⁷ The metal ratios of Sc/Cr of 100:0, 80:20, 60:40, 40:60 and 20:80 were used keeping the molar ratio of metal : BTC : DMF at 3:2:600.

A range of mixed metal MIL-100 materials have been synthesised and characterised which is discussed in chapter 5.

HKUST-1(Cu/Ru)

Benzene-1,3,5-tricarboxylic acid (0.174 g, 0.83 mmol), copper nitrate trihydrate (Aldrich, 1.36 mmol, 0.328 g) and ruthenium trichloride hydrate (Aldrich, 0.15 mmol, 0.031 g) were dissolved in water (5 mL) and ethanol (5 ml) and heated in a Teflon lined steel autoclave at 383 K for 16 h. The resulting solid was filtered under suction, washed with ethanol and water and dried at 313 K. Product was stirred heated in ethanol for 24 h at 363 K, filtered and dried at 313 K to activate. The green powder product was characterised using PXRD, N₂ adsorption, TGA, EDX, and compared to literature.⁶

Synthesis of scandium MOF using the ligand 2,2'-bipyridine-5,5-dicarboxylic acid

2,2'-bipyridine-5,5-dicarboxylic acid (0.151 g, 0.618 mmol), scandium chloride (aq) (1.45 M, 0.21 ml), aluminium chloride hexahydrate (0.075 g, 0.309 mmol) were dissolved in DMF (10 mL) and heated under reflux for 16 h. The resulting solid was filtered under suction, washed with ethanol and water and dried at 313 K. Product was heated in ethanol for 24 h at 383 K in Teflon lined steel autoclave, filtered and dried at 313 K to activate. The white powder product was characterised using PXRD, N₂ adsorption, TGA, EDX, and compared to literature.¹⁰ Further details and characterisation of material is reported in chapter 6.

Synthesis of MIL-100PPH₂(Sc)

Benzene-1,3,5-tricarboxylic acid (0.064 g, 0.3 mmol), 1-fluorobenzene-2,4,6-tricarboxylic acid (0.069 g, 0.3 mmol), scandium chloride (aq) (1.45 M, 0.84 ml, 1.2 mmol) were dissolved in DMF (20 mL) and heated under reflux for 16 h. The resulting solid was filtered under suction, washed with ethanol and water and dried at 313 K. Product was stirred in methanol for 24 h, filtered and dried at 313 K to activate. The yellow powder product obtained in 89% yield (0.311 g) was characterised using PXRD, N₂ adsorption, TGA, EDX and compared to literature.⁷

Mixed ligand MIL-100(Sc)(F) (0.13 g) was heated under vacuum for 5 h at 383 K. Potassium diphenylphosphide solution (0.5M in THF, 0.025 mmol, 0.05 ml) was added and stirred in toluene at 343 K for 6 h. The reaction mixture was cooled and methanol added to quench the reaction. Using a cannula the solution was separated. The resulting solid was filtered under suction, washed with ethanol and water and dried at 313 K. The yellow powder product obtained in 82 % yield (0.165 g) was characterised using PXRD, N₂ adsorption, TGA, EDX, and solid state NMR, and compared to literature.⁷ Solid state ³¹P NMR δ_p 23.5. In order to obtain further evidence of diphenylphosphine in the MOF the material was broken down. Solution phase NMR and mass spectrometry was carried out on the resultant mixture. MIL-100(Sc)(F)(dpp) (10 mg) was dissolved in a mixture of d₆-DMSO (0.5 ml) and 0.1M nitric acid (0.2 ml) and sonicated for 10 minutes. ³¹P{¹H} NMR (121 MHz, DMSO) δ_p 23.59. ESI [M+H] calculated 395.0679 found 395.0683.

Addition of allylpalladium dichloride to MIL-100(Sc) with diphenylphosphine ligand

Mixed ligand MIL-100(Sc)(F)(dpp) (0.15 g) was heated under vacuum for 5 h at 383 K. Allylpalladium dimer (0.00225 mmol, 0.0004 g) was added and stirred in CH₂Cl₂ for 6 h at room temperature. The product was filtered, washed with ethanol and water and dried at 313 K. The resultant MOF material obtained in 96 % yield (0.144 g) was characterised using PXRD, N₂ adsorption, TGA, EDX, and solid state NMR, and compared to the literature.

7.4. FTIR experiments

This was carried out by pressing ($\sim 10^6$ torr) the MOF material into small pellets (2 cm², 10-15 mg) and placing them in a quartz cell that contained a KBr window. The movable quartz cell allowed for the beam to be placed in the infra-red beam and also to be placed in a furnace in the cell to allow for thermal treatment. The cell was connected to a vacuum to allow for cell evacuation, dehydration of the MOF material and also to pass gases into the cell. Transmission IR spectra were recorded in the 400–4000 cm⁻¹ range (with a 4 cm⁻¹ resolution), on a Nicolet Nexus spectrometer equipped with an extended KBr beam splitting device and a mercury cadmium telluride (MCT) cryodetector. The thermal behaviour of the materials was recorded at a range of temperatures using a ramp rate of 5 K /min⁻¹ and measurements were also taken at room temperature. Before both probing with CD₃CN and CO, the materials were dehydrated for 5 h at 423 K under secondary vacuum. The probing of the strength of Lewis acid sites was carried out using CD₃CN and the stretching frequency on $\nu(\text{CN})$ was recorded. Spectra were recorded at room temperature. In the experiment to probe the number of Lewis acid sites CO adsorption was used. The stretching frequency of CO was recorded at 100 K by cooling the sample holder using liquid nitrogen. The CO was introduced in increments (1.04 μ mol) via a calibrated volume (1.75 cm³) connected to a pressure gauge for the control of the probe pressure (0–10⁴ Pa range). The CO pressure inside the IR cell was controlled by another pressure gauge (0–10³ Pa range).

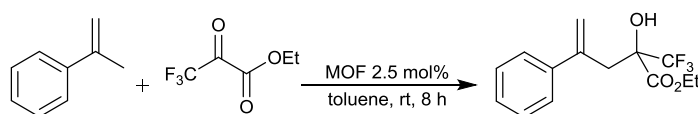
7.5. MOF catalysis

7.5.1. Carbonyl ene reaction

General comments

MOF catalyst was activated by heating under vacuum for 5 h between 423 – 523 K or in the case of MIL-100(Sc), by washing with methanol and MIL-101(Cr) was heated under solvothermal conditions for 12 h at 363 K in EtOH (20ml) and further washed with NH₄Cl.

Catalysed formation of ethyl-2-hydroxy-4-phenyl-2-trifluoromethyl)pent-4-enoate (5)



Ethyl trifluoropyruvate (0.298 ml, 2.25 mmol), α -methylstyrene (0.351 ml, 2.7 mmol, 1.2 eq.) and 1-fluoronaphthalene (0.29 ml, 2.25 mmol) (internal standard) were added to a solution of activated MIL-100(Sc) (17 mg, 2.5 mol%) in toluene (5 ml). The solution was stirred for 8 h at room temperature under N₂. The reaction mixture was filtered and the solute concentrated under vacuum and purified by column chromatography using a hexane:ethyl acetate (6:1) mixture yielding a colourless oil (0.59 g, 90%, 2 mmol). Reported previously using a different synthetic procedure.¹¹

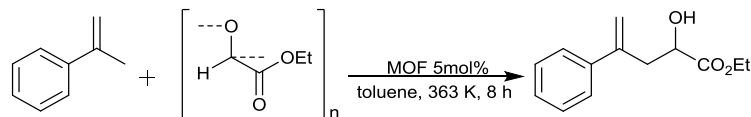
¹H NMR (300 MHz, CDCl₃) δ _H 7.28 – 7.13 (5 H, m, Ar-H), 5.30 (1H, s, C=CHH'), 5.19 (1 H, s, C=CHH'), 3.93 (1 H, dq, *J* 10.7, 7.2 Hz, CHH'), 3.74 (1 H, s, OH), 3.53 (1 H, dq, *J* 10.7, 7.2 Hz, CHH'), 3.20 (1 H, d, *J* 14.0 Hz, CHH'), 2.95 (1 H, d, *J* 14.0 Hz, CHH'), 1.01 (3 H, t, *J* 7.2 Hz, CH₃). ¹³C NMR (75 MHz, CDCl₃) δ _C 169.4, 141.5, 141.3, 128.6, 128.1, 127.2, 123.8 (q, *J*_{C-F} 286), 119.8, 77.3 (q, *J*_{C-F} 28.7), 63.9, 37.5, 13.9. ¹⁹F{¹H} NMR (282 MHz, CDCl₃) δ _F -78.9. ESI [M+H] calculated 289.1046 found 289.1049. C₁₄H₁₅F₃O₃ (Found C, 58.17; H, 5.08; Required C, 58.33; H, 5.24).

Catalysed formation of ethyl-2-hydroxy-4-phenyl-2-trifluoromethyl)pent-4-enoate by tandem dehydration followed by carbonyl ene reaction

Ethyl 3,3,3-trifluoro-2,2-dihydroxypropanoate (0.25 ml, 2.7 mmol), α -methylstyrene (0.351 ml, 2.7 mmol, 1.2 eq.) and 1-fluoronaphthalene (0.29 ml, 2.25 mmol, 1 eq.) (internal standard) were added to a solution of activated MIL-100(Sc) (40.9 mg, 5 mol%) in toluene (5 ml). The solution was stirred for 16 h at room temperature under

N₂. The reaction mixture was filtered and the solute concentrated under vacuum (95%, 0.739 g, 2.57 mmol).

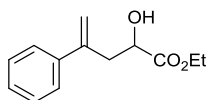
Catalysed formation of ethyl-2-hydroxy-4-phenyl-2-pent-4-enoate (6)



Formation of ethyl glyoxalate monomer

Ethyl glyoxalate polymer was heated to 383 K for 30 minutes. The temperature was increased to 403 K to distil off excess toluene. The temperature was further increased to 423 K to distil ethyl glyoxalate monomer as a 65:35 mixture with toluene.

Ene reaction to give ethyl-2-hydroxy-4-phenylpent-4-enoate



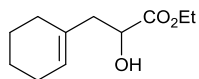
Ethyl glyoxalate (0.36 ml, 2.7 mmol, 1 eq.) and α -methylstyrene (0.35 ml, 2.7 mmol, 1 eq.) was added to a solution of activated MIL-100(Sc) (40.9 mg, 5 mol%) in toluene (5 ml). The solution was stirred for 8 h at 363 K under N₂. Reaction mixture was filtered under suction, concentrated under vacuum and purified by column chromatography using hexane:ethyl acetate (5:1) mixture yielding a colourless oil (0.536 g, 89%, 2.4 mmol). Reported previously using a different synthetic procedure.¹² ¹H NMR (300 MHz, CDCl₃) δ _H 7.37 – 7.30 (2 H, m, Ar-H), 7.30 – 7.17 (3 H, m, Ar-H), 5.32 (1 H, s, C=CHH'), 5.13 (1 H, s, C=CHH'), 4.25 – 4.12 (1 H, m, CH), 4.11 – 3.86 (2 H, m, CH₂), 2.99 (1 H, dd, *J* 14.4, 4.5, CHH'), 2.77 (1 H, dd, *J* 14.4, 7.6, CHH'), 2.66 (1 H, br s, OH), 1.15 (3 H, t, *J* 7.1 Hz, CH₃). ¹³C NMR (75 MHz, CDCl₃) δ _C 174.41, 143.6, 140.4, 128.4, 127.7, 126.4, 116.2, 69.2, 61.6, 40.5, 14.1. ESI [M+H] calculated 221.1172 found 221.1176. C₁₂H₁₆O₃ (Found C, 70.95; H, 7.35; Required C 70.89; H, 7.32).

Catalysed formation of ethyl-2-hydroxy-4-phenyl-2-pent-4-enoate using ethyl glyoxalate polymer

Ethyl glyoxalate in 50% toluene (0.54 ml, 2.7 mmol,) and α -methylstyrene (0.35ml, 2.7 mmol, 1 eq) was added to a solution of activated MIL-100(Sc) (40.9 mg 5 mol%) in toluene (5 ml). The solution was stirred for 8 h at 363 K under N₂. Reaction mixture

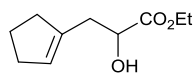
was filtered under suction and concentrated under vacuum yielding a colourless oil (0.573 g, 96%, 2.59 mmol).

Ene reaction to give ethyl 3-cyclohexenyl-2-hydroxypropanoate (7)



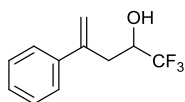
Ethyl glyoxalate (0.36 ml, 2.7 mmol) and methylene cyclohexane (0.32 ml, 2.7 mmol) was added to a solution of activated MIL-100(Sc) (40.9 mg, 5 mol%) in toluene (5 ml). The solution was stirred for 8 h at 363 K under N₂. Reaction mixture was filtered under suction, concentrated under vacuum yielding a colourless oil (98%, 0.524 g, 2.65 mmol). Reported previously using a different synthetic procedure.¹³ ¹H NMR (300 MHz, CDCl₃) δ_H 5.45 (1 H, s, CH), 4.15 (2 H, q, *J* 7.2, CH₂), 2.81 (1 H, br s, OH), 2.36 (1 H, dd, *J* 13.9, 4.6, CHH'), 2.21 (1 H, dd, *J* 13.9, 7.9, CHH'), 1.92 (4 H, m, CH₂), 1.52 (4 H, dtd, *J* 15.6, 5.8, 3, CH₂), 1.22 (3 H, t, *J* 7.2, CH₃). ¹³C NMR (101 MHz, CDCl₃) δ 174.9, 133.0, 125.1, 69.3, 61.3, 43.2, 28.4, 25.2, 22.8, 22.1, 14.2. ESI [M+H] calculated 199.1329 found 199.1334. C₁₂H₁₆O₃ (Found C, 66.42; H, 9.02; Required C 66.64; H, 9.15).

Ene reaction to give ethyl 3-cyclopentyl-2-hydroxypropanoate (8)



Ethyl glyoxalate (0.36 ml, 2.7 mmol) and methylene cyclopentane (0.28 ml, 2.7 mmol) was added to a solution of activated MIL-100(Sc) (40.9 mg, 5 mol%) in toluene (5 ml). The solution was stirred for 8 h at 363 K under N₂. Reaction mixture was filtered under suction, concentrated under vacuum yielding a colourless oil (99%, 0.492 g, 2.67 mmol). Reported previously using a different synthetic procedure.¹³ ¹H NMR (300 MHz, CDCl₃) δ_H 5.43 (1 H, s, CH), 4.24 (1 H, dd, *J* 7.3, 4.6, CH), 4.15 (2 H, qd, *J* 7.4, 1.3, CH₂), 2.86 (1 H, br s, OH), 2.53 (1 H, dd, *J* 14.0, 5.2, CHH'), 2.41 (1 H, dd, *J* 14.6, 7.3, CHH'), 2.29 – 2.15 (4 H, m, CH₂), 1.79 (2 H, q, *J* 7.2 Hz, CH₂), 1.22 (3 H, t, *J* 7.1, CH₃). ¹³C NMR (75 MHz, CDCl₃) δ_C 174.7, 133.7, 126.1, 69.43, 61.42, 42.3, 34.5, 32.3, 22.7, 14.71.

Ene reaction to give 1,1,1-trifluoro-4-phenylpent-4-en-2-ol (9)



Trifluoroacetaldehyde ethyl hemiacetal (0.32 ml, 2.7 mmol) and α -methylstyrene (0.35 ml, 2.7 mmol) was added to a solution of activated MIL-100(Sc) (40.9 mg, 5 mol%) in toluene (5 ml). The solution was stirred for 8 h at 363 K under N_2 . Reaction mixture was filtered under suction, concentrated under vacuum yielding a yellow oil (99%, 0.58 g, 2.7 mmol). *1,1,1-trifluoro-4-phenylpent-4-en-2-ol* 1H NMR (300 MHz, $CDCl_3$) δ_H 7.33 – 7.15 (5 H, m, Ar-H), 5.34 (1 H, s, C=CHH'), 5.13 (1 H, s, C=CHH'), 3.93 – 3.78 (1 H, m, CH), 2.95 (1 H, dd, J 14.8, 1.8, CHH'), 2.57 (1 H, dd, J 14.8, 10.2, CHH'), 2.40 (1 H, br s, OH). ^{13}C NMR (75 MHz, $CDCl_3$) δ_C 141.5, 138.3, 127.6, 127.0, 125.8, 125.1, 115.7, 67.7 (q J_{C-F} 31 Hz), 34.66. ^{19}F { 1H } NMR (282 MHz, $CDCl_3$) δ_F -80.00.

7.5.2. Conjugate addition of indole to electron-deficient olefins

General comments

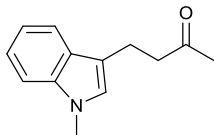
MOF catalyst was activated by heating under vacuum for 5 h between 423 – 523 K or in the case of MIL-100(Sc), by washing with methanol and MIL-101(Cr) was heated under solvothermal conditions for 12 h at 363 K in EtOH (20 ml) and further washed with NH_4Cl .

Formation of 4-(2-methyl-3-indolyl)butan-2-one (10)

MIL-100(Sc) (30 mg 10 mol%) was heated to 423 K under vacuum for 5 h, 2-methylindole (0.13 g, 1 mmol), methyl vinyl ketone (0.08 ml, 1 mmol), 1-methylnaphthalene (0.07 ml, 0.5 mmol) and CH_2Cl_2 (5 ml) was added and stirred for 6 h at room temperature. The reaction mixture was filtered and solution washed with water (5 ml), product extracted by CH_2Cl_2 (2 \times 5 ml) and dried ($MgSO_4$). The product was concentrated under vacuum and purified by column chromatography hexane: ethyl acetate (4:1), yielding a white solid (89%, 0.18 g, 0.09 mmol). Reported previously from a different synthetic procedure.¹⁴ 1H NMR (400MHz, $CDCl_3$): 1H NMR (300 MHz, $CDCl_3$) δ_H 7.79 (1 H, s, NH), 7.44 – 7.28 (1 H, m, Ar-H), 7.13 – 7.05 (1 H, m, Ar-H), 7.04 – 6.90 (2 H, m, Ar-H), 2.86 (2 H, t, J 7.8, CH_2), 2.64 (2H, t, J 7.6, CH_2), 2.21 (3 H, s, CH_3), 1.97 (3 H, s, CH_3). ^{13}C NMR (75 MHz, $CDCl_3$) δ_C 209.8, 135.8, 131.8, 128.7, 121.4, 119.5, 118.2, 110.9, 110.7, 44.7, 30.7, 18.9, 11.9. ESI [M+H]

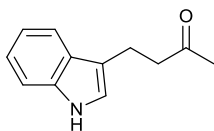
calculated 202.1226 found 202.1227. C₁₃H₁₅NO (Found C, 77.62; H, 7.42; N, 6.85; Required C, 77.58; H, 7.51; N, 6.96)

Formation of 4-(1-methyl-1H-indol-3-yl)butan-2-one (11)



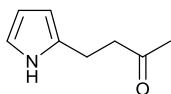
Experimental procedure similar to that for the synthesis of 4-(1-methyl-3-indolyl)butan-2-one. The product was concentrated under vacuum and purified by column chromatography hexane: ethyl acetate (4:1), yielding a yellow oil (85%, 0.17 g, 0.08 mmol). Reported previously using a different synthetic procedure.¹⁵ ¹H NMR (300 MHz, CDCl₃) δ_H 7.47 (1 H, dt, *J* 7.9, 1.0, Ar-*H*), 7.21 – 7.07 (2 H, m, Ar-*H*), 7.00 (1 H, ddd, *J* 8.0, 6.6, 1.4, Ar-*H*), 6.71 (1 H, s, Ar-*H*), 3.58 (3 H, s, CH₃), 2.92 (2 H, t, *J* 7.4, CH₂), 2.70 (2 H t, *J* 7.4, CH₂), 2.01 (3 H, s, CH₃). ¹³C NMR (75 MHz, CDCl₃) δ_C 209.2, 137.5, 128.1, 126.9, 122.1, 119.2, 119.2, 114.1, 109.7, 44.8, 33.0, 30.5, 19.7. ESI [M+H] calculated 202.1226 found 202.1221. C₁₃H₁₅NO (Found C, 77.69; H, 7.45; N, 6.88; Required C, 77.58; H, 7.51; N, 6.96)

Formation of 4-(1H-indol-3-yl)butan-2-one (12)

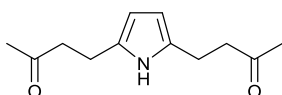


Experimental procedure similar to synthesis of 4-(1-methyl-3-indolyl)butan-2-one. The product was concentrated under vacuum and purified by column chromatography hexane: ethyl acetate (4:1), yielding a yellow oil (87%, 0.16 g, 0.09 mmol). Reported previously from a different synthetic procedure.¹⁴ ¹H NMR (300 MHz, CDCl₃) δ_H 7.94 (1 H, s, NH), 7.51 (1 H, d, *J* 7.8, Ar-*H*), 7.26 (1 H, d, *J* 6.9, Ar-*H*), 7.15 – 6.98 (2 H, m, Ar-*H*), 6.88 (1 H, s, Ar-*H*), 2.97 (2 H, t, *J* 7.4, CH₂), 2.76 (2 H, t, *J* 7.4, CH₂), 2.06 (3 H, s, CH₃). ¹³C NMR (75 MHz, CDCl₃) δ_C 209.3, 136.7, 127.6, 122.5, 121.9, 119.7, 119.1, 115.5, 111.6, 44.5, 30.5, 19.8. ESI [M+H] calculated 188.1070 found 188.1069. C₁₂H₁₃NO (Found C, 76.84; H, 6.99; N, 7.39; Required C, 76.98; H, 6.99; N, 7.48).

Formation of 4-(1H-pyrrole-2-yl)butan-2-one and 4'4'-(1H-pyrrole-2,5-diyl)bis(butan-2-one) (13 and 14)



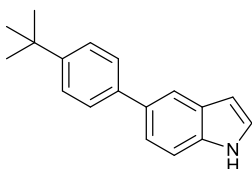
MIL-100(Sc) (30, mg 10 mol%) was heated to 423-523 K under vacuum for 5 h. Pyrrole (0.07 ml, 1 mmol), methyl vinyl ketone (0.08 ml, 1 mmol), 1-methylnaphthalene (0.07 ml, 0.5mmol) and CH₂Cl₂ (5 ml) was added and the reaction mixture stirred for 6 h at room temperature. The reaction mixture was filtered and solution washed with water (5 ml), product extracted by CH₂Cl₂ (2×5 ml) and dried (MgSO₄). The product was concentrated under vacuum and separated into mono and di substituted pyrroles by column chromatography hexane: ethyl acetate (4:1) to yield both mono- (70%, 0.09 g, 0.07 mmol) and di- (5 %, 0.01g, 0.005mol) substituted product. This compound has been reported previously from a different synthetic procedure.¹⁶ ¹H NMR (300 MHz, CDCl₃) δ_H 8.44 (1 H, s, NH), 6.58 (1 H, td, *J* 2.6, 1.6, Ar-*H*), 6.01 (1 H, q, *J* 2.8, Ar-*H*), 5.85 – 5.71 (1 H, m, Ar-*H*), 2.84 – 2.68 (m, 4H, CH₂), 2.09 (3 H, s, CH₃). ¹³C NMR (75 MHz, CDCl₃) δ_C 209.8, 126.1, 117.1, 108.3, 105.7, 44.6, 30.5, 21.7. C₈H₁₁NO (Found C, 70.13; H, 8.06; N, 10.11; Required C, 70.01; H, 8.06; N, 10.26).



4'4'-(1H-pyrrole-2,5-diyl)bis(butan-2-one) ¹H NMR (300 MHz, CDCl₃) δ 8.40 (1 H, s, NH), 5.64 (2 H, d, *J* 2.6, Ar-*H*), 2.75 – 2.61 (8 H, m, CH₂), 2.09 (6 H, s, CH₃). ¹³C NMR (75 MHz, CDCl₃) δ_C 209.6, 130.8, 105.2, 44.4, 30.4, 21.9. C₁₂H₁₇NO₂ (Found C, 69.91; H, 8.02; N, 10.11; Required C, 70.01; H, 8.06; N, 10.26)

7.5.3. Synthesis of larger substrates for the indole reaction

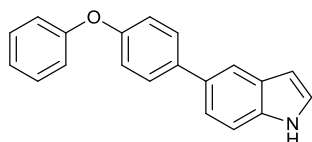
Synthesis of 5-(4-(*tert*-butyl)phenyl)-1H-indole via Suzuki coupling reaction(15)



Para-*tert*-phenylboronic acid (0.79 g, 4.46 mmol, 1.75 eq.), [PdCl₂(PCy₃)₂] (9.41 × 10⁻³ g, 1.27 × 10⁻³ mmol, 4 mol%) and potassium phosphate (1.62g, 7.65 mmol, 3 eq) were added to a flask that was flushed with argon. Dry degassed toluene (10 ml) and 5-

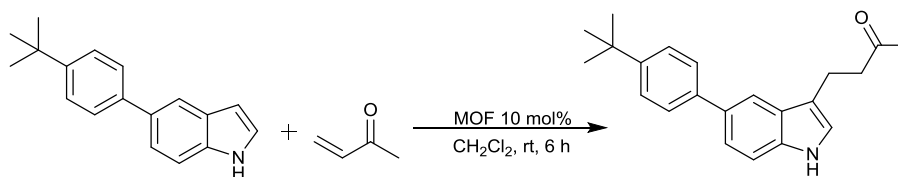
bromoindole (0.5 g, 2.55 mmol, 1 eq.) was added to the flask and the reaction mixture was heated to 363 K. This was left to stir at 363 K for 16 h under an argon atmosphere. The reaction was concentrated under vacuum and purified by column chromatography hexane: ethyl acetate (5:1). This yields a white crystalline powder (0.39 g, 62%, 1.56 mmol). ^1H NMR (400 MHz, CDCl_3) δ_{H} 8.05 (1 H, s, NH), 7.78 (1 H, dt, J 1.6, 0.8, Ar-H), 7.56 – 7.48 (2 H, m, Ar-H), 7.46 – 7.27 (4 H, m, Ar-H), 7.14 (1 H, dd, J 3.2, 2.4, Ar-H), 6.52 (1 H, ddd, J 3.0, 2.1, 0.8, Ar-H), 1.30 (9 H, s, $\text{C}(\text{CH}_3)_3$). ^{13}C NMR (300 MHz, CDCl_3) 149.2, 139.6, 135.2 133.3, 128.4, 127.0, 125.6, 124.70 4, 121.9, 119.1, 111.2, 103.0, 34.5, 31.5. $\text{C}_{18}\text{H}_{19}\text{N}$ (Found C, 86.63; H, 7.59; N, 5.62; Required C, 86.7; H 7.68; N 5.62). ESI $[\text{M}+\text{H}]$ calculated 250.1590 found 250.1593. Mp: 435-436 K. $\nu_{\text{max}}(\text{KBr})/\text{cm}^{-1}$ 3434(NH), 2953(CH), 1463 (C=C), 1407 (C=C), 1384 (CH₃), 1264 (CN), 1096, 885, 810, 723.

Synthesis of 5-(4-phenoxyphenyl)-1H-indole via Suzuki coupling reaction(16)

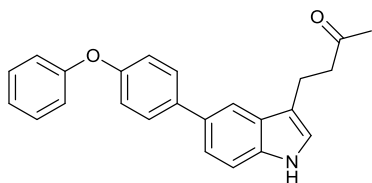


Para-4-phenoxyphenylboronic acid (0.955 g, 4.46 mmol, 1.75 eq.), $[\text{PdCl}_2(\text{PCy}_3)_2]$ (9.41×10^{-3} g, 1.27×10^{-3} mmol, 4 mol%) and potassium phosphate (1.62g, 7.65 mmol, 3 eq) were added to a flask that was then flushed with argon. Dry degassed toluene (10 ml) and bromoindole (0.5 g, 2.55 mmol, 1eq) was added to the flask and the reaction mixture was heated to 363 K. This was left to stir at 363 K for 16 h under argon. The reaction was concentrated under vacuum and purified by column chromatography hexane: ethyl acetate (5:1). This yielded a brown solid (0.37 g, 52%, 1.3 mmol). ^1H NMR (300 MHz, CDCl_3) δ 8.04 (1 H, s, NH), 7.74 (1 H, s, Ar-H), 7.56 – 7.46 (2 H, m, Ar-H), 7.34 (2 H, d, J 1.2, Ar-H), 7.29 – 7.20 (2 H, m, Ar-H), 7.13 (1 H, dd, J 5.8, 3.0, Ar-H), 7.06 – 6.94 (5 H, m, Ar-H), 6.51 (1 H, dd, J 3.1, 2.0, Ar-H). ^{13}C NMR (101 MHz, CDCl_3) δ_{C} 157.4, 156.0, 137.9, 135.1, 132.8, 129.8, 128.7, 128.4, 124.9, 123.2, 121.8, 119.2, 119.0, 118.9, 111.3, 103.0. ESI $[\text{M}+\text{H}]$ calculated 286.1226 found 286.1230. $\text{C}_{19}\text{H}_{15}\text{NO}$ (Found C, 84.19; H,5.31; N,4.91; Required C, 84.36; H, 5.42; N, 4.98). Mp: 393-395 K. $\nu_{\text{max}}(\text{KBr})/\text{cm}^{-1}$ 3340(NH), 2927 CH), 1586, 1488(C=C), 1465 (C=C), 1235 (C-N), 1165 (C-O), 1020, 805, 755.

7.5.4. Conjugate addition of large substrate indole to electron-deficient olefins



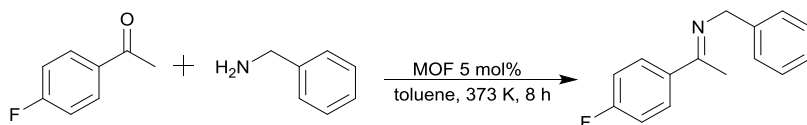
Sc(OTf)₃ (1 mol%) was added to a flask that was flushed with nitrogen. 5-(4-(tert-butyl)phenyl)-1H-indole (0.25 g, 1 mmol), methyl vinyl ketone (0.08 ml, 1 mmol), and CH₂Cl₂ (5 ml) was added and stirred for 6 h at room temperature. The reaction mixture was filtered and solution washed with water (5 ml), product extracted by CH₂Cl₂ (2×5 ml) and dried (MgSO₄). The product was concentrated under vacuum and purified by column chromatography hexane: ethyl acetate (4:1), yielding a yellow oil (82%, 0.26 g, 0.82 mmol). 4-(5-(4-tert-butyl)phenyl-1H-indol-3-yl)butan-2-one (17). ¹H NMR (300 MHz, CDCl₃) ¹H NMR (300 MHz, CDCl₃) δ 7.96 (1 H, s, Ar-H), 7.71 – 7.65 (1 H, m, Ar-H), 7.51 (2 H, d, *J* 8.2, Ar-H), 7.42 – 7.33 (3 H, m, Ar-H), 7.28 (1 H, d, *J* 8.4, Ar-H), 6.88 (1 H, d, *J* 2.2, Ar-H), 2.99 (2 H, t, *J* 7.4, CH₂), 2.77 (2 H, t, *J* 7.4, CH₂), 2.05 (3 H, s, CH₃), 1.29 (9 H, s, C(CH₃)₃). ¹³C NMR (75 MHz, CDCl₃) δ_C 207.8, 148.2, 138.6, 134.7, 131.8, 126.6, 125.9, 124.6, 121.1, 120.8, 115.98, 114.4, 110.3, 43.0, 30.4, 29.0, 18.3. ESI [M+H] calculated 320.2009 found 320.2014. C₂₂H₂₅NO (Found C, 82.95; H, 7.95; N, 4.55; Required C, 82.72; H 7.89; N 4.38)



Experimental procedure as for the synthesis of 4-(5-(4-tert-butyl)phenyl)-1H-indol-3-yl)butan-2-one (65%, 0.23 g, 0.65 mmol). 4-(5-(4-phenoxyphenyl)-1H-indol-3-yl)butan-2-one (18) ¹H NMR (400 MHz, CDCl₃) δ 8.00 (1 H, s, Ar-H), 7.65 (1 H, s, Ar-H), 7.51 (2 H, dt, *J* 8.5, 2.1, Ar-H), 7.31 (1 H, dd, *J* 8.5, 1.7, Ar-H), 7.28 – 7.23 (2 H, m, Ar-H), 7.04 – 6.93 (5 H, m, Ar-H), 6.88 (1 H, s, Ar-H), 2.98 (2 H, t, *J* 7.4, CH₂), 2.76 (2 H, t, *J* 7.4, CH₂), 2.04 (3 H, s, CH₃). ESI [M+H] calculated 356.1645 found 356.1649. C₂₄H₂₁NO₂ (Found C, 81.22; H, 5.82; N, 3.72; Required C, 81.10; H 5.96; N 3.94)

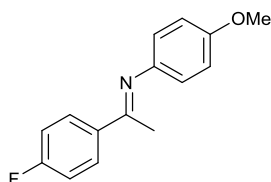
7.5.5. Imine synthesis over MOFs

Imine synthesis of (E)-N-(1-(4-fluorophenyl)ethylidene)(phenyl)methanamine (19)



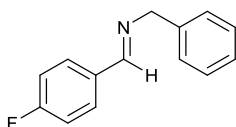
MIL-100(Sc) (10 mg, 5 mol%) was heated to 423K under vacuum for 5 h, 4-fluoroacetophenone (0.08ml, 0.65 mmol), benzylamine (0.14 ml, 1.3 mmol), 1-methylnaphthalene (0.4 mmol) and toluene (5 ml) were added and the reaction was stirred at 373 K for 8 h. The reaction mixture was diluted using toluene, filtered through Na₂SO₄, washed using 0.1M HCl solution and concentrated under vacuum to yield a brown oil (90%, 0.133 g, 0.58 mmol). Reported previously using a different synthetic procedure.¹⁷ ¹H NMR (300 MHz, C₆D₆) δ_H 7.97 (2 H, ddd, *J* 8.5, 5.3, 2.6, Ar-*H*), 7.53 (2 H, d, *J* 7.5), 7.46 (2 H, td, *J* 6.7, 6.2, 1.7, Ar-*H*), 7.40 – 7.28 (2 H, m, Ar-*H*), 7.19 – 7.11 (2 H, m, Ar-*H*), 4.81 (2 H, s, CH₂), 2.39 (3 H, s, CH₃). ¹³C NMR (75 MHz, C₆D₆) δ_C 166.3 (d, *J*_{C-F} 250), 141.2, 137.9, 131.6, 129.5, 129.4, 129.2 (d, *J*_{C-F} 7.8), 128.4, 127.4 (d, *J*_{C-F} 1.8), 56.4, 16.2. ¹⁹F{¹H} NMR (282 MHz, CDCl₃) δ_F -112.4. C₁₅H₁₄FN Found C, 79.14; H, 6.19; N, 6.11; Required C, 79.27; H 6.21; N 6.16.

Imine synthesis of (E)-N-(1-(4-fluorophenyl)ethylidene)4-methoxyaniline (20)



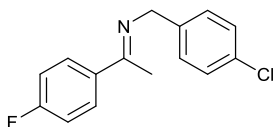
MIL-100(Sc) (10 mg, 5 mol%) was heated to 523 K under vacuum for 5 h, 4-fluoroacetophenone (0.08 ml, 0.65 mmol), 4-methoxyaniline (0.16 g, 1.3 mmol), 1-methylnaphthalene (0.4 mmol) and toluene (5 ml) were added and stirred at 373 K for 8 h. The reaction mixture was diluted using toluene, filtered through Na₂SO₄, washed using 0.1M HCl solution and concentrated under vacuum yielding a yellow oil (75%, 0.12 g, 0.49 mmol). ¹H NMR (300 MHz, CD₃OD) δ_H 7.93 – 7.79 (2 H, m, Ar-*H*), 7.15 – 7.00 (2 H, m, Ar-*H*), 6.91 – 6.78 (2 H, m, Ar-*H*), 6.70 – 6.58 (2 H, m, Ar-*H*), 3.70 (3 H, s, CH₃), 2.15 (3 H, s, CH₃). ¹³C NMR (75 MHz, CD₃OD) δ_C 165.3 (d, *J*_{C-F} 250), 158.1, 141.8, 132.2, 129.4, 128.5, 128.3, 126.5, 113.6 (d, *J*_{C-F} 1.8), 55.2, 15.3. ¹⁹F{¹H} NMR (282 MHz, C₆D₆) δ_F -111.3.

Imine synthesis of Benzylidenebenzylamine (21)



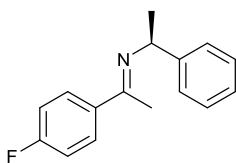
MIL-100(Sc) (10 mg, 5 mol%) was heated to 523 K under vacuum for 5 h, 4-fluorobenzaldehyde (0.08 ml, 0.65 mmol), benzylamine (0.07 ml, 0.65 mmol), 1-methylnaphthalene (0.4 mmol) and toluene (5 ml) were added and stirred at room temperature for 8 h. The reaction mixture was diluted using toluene, filtered through Na_2SO_4 and concentrated under vacuum yielding a yellow oil (98%, 0.14 g, 6.4 mmol). Reported previously using a different synthetic procedure.¹⁸ ^1H NMR (300 MHz, CD_3OD) δ_{H} 8.53 (1 H, s, CH), 7.79 – 7.76 (2 H, m, Ar-H), 7.49 – 7.45 (3 H, m, Ar-H), 7.36 – 7.32 (4 H, m, Ar-H), 7.26 – 7.27 (1 H, m, Ar-H), 4.85 (s, 2H, CH_2), ^{13}C NMR (75 MHz, CD_3OD) δ_{C} 161.9 (d, $J_{\text{C-F}}$ 244), 137.2, 136.5, 130.9, 130.1 (d, $J_{\text{C-F}}$ 8.8), 128.7, 128.6, 127.8, 126.1 (d, $J_{\text{C-F}}$ 21), 64.8. $^{19}\text{F}\{^1\text{H}\}$ NMR (282 MHz, C_6D_6) δ_{F} -106.8.

Imine synthesis of 1-(4-chlorophenyl)-N-(1-(4-fluorophenyl)ethylidene)methanamine (21)



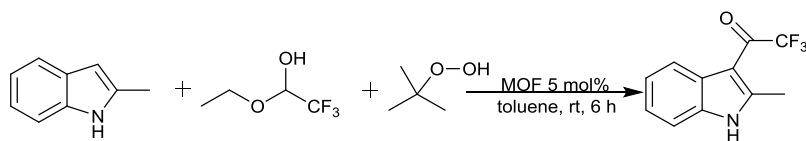
MIL-100(Sc) (10 mg, 5 mol%) was heated to 423 K under vacuum for 5 h, 4-fluoroacetophenone (0.08ml, 0.65 mmol), 4-chlorobenzylamine (0.16 ml, 1.3 mmol), 1-methylnaphthalene (0.4 mmol) and hexane (5 ml) were added and stirred at 343 K for 8 h. The reaction mixture was diluted using toluene, filtered through Na_2SO_4 , washed using methanol and concentrated under vacuum yielding a yellow oil (0.155 g, 91%, 0.59 mmol). ^1H NMR (300 MHz, C_6D_6) δ_{H} 7.80-7.73 (2 H, m, Ar-H), 7.34-7.10 (3 H, m, Ar-H), 6.97-6.89 (2 H, m, Ar-H), 4.31 (2 H, s, CH_2), 1.74 (3 H, s, CH_3). ^{13}C NMR (75 MHz, C_6D_6) δ_{C} 164.2 (d, J 250), 140.4, 133.0, 129.4 (d, J_{CF} 8.4), 129.1, 128.8, 128.4, 128.1, 115.5 (d, J_{CF} 1.5), 55.2, 15.2. $\{^1\text{H}\}^{19}\text{F}$ NMR (282 MHz, C_6D_6) -112.2.

Imine synthesis of 1-(4-fluorophenyl)ethylidene-1-phenylethanamine (22)

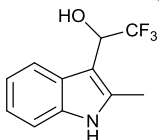


MIL-100(Sc) (10 mg, 5 mol%) was heated to 423 K under vacuum for 5 h, 4-fluoroacetophenone (0.08 ml, 0.65 mmol), (s)-1-phenylethan-1-amine (0.17 ml, 1.3 mmol), 1-methylnaphthalene (0.4 mmol) and toluene (5 ml) were added and stirred at 373 K for 8 h using dean stark apparatus to remove excess water. The reaction mixture was diluted using toluene, filtered through Na₂SO₄, washed using methanol and concentrated under vacuum yielding a colourless oil (0.15 g, 94%, 0.61 mmol). Reported previously using a different synthetic procedure.¹⁹ ¹H NMR (300 MHz, C₆D₆) δ_H 7.83-7.76 (2 H, m, Ar-H), 7.59-7.55 (2 H, m, Ar-H), 7.37-7.17 (3 H, m, Ar-H), 6.96-6.90 (2 H, m, Ar-H), 4.70 (1 H, q, *J* 6.6, CH), 1.79 (3H, s, CH₃), 1.59 (3 H, d, *J* 6.6, CH₃). ¹⁹F{¹H} NMR (282 MHz, C₆D₆) δ_H -112.6.

7.5.6. Tandem C-C bond forming-oxidation catalysis



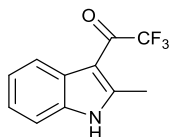
Formation of 2,2,2-trifluoro-1-(2-methyl-1H-indol-3-yl)ethanol (23)



MIL-100(Sc/Fe)(60/40) (15.4 mg, 5 mol%) was heated to 423 K under vacuum for 5 h, 2-methylindole (0.13 g, 1 mmol), trifluoroacetaldehyde ethyl hemiacetal (0.12 ml, 1.4 mmol), 1-fluoronaphthalene (0.07 ml, 0.5 mmol) and toluene (5 ml) was added and stirred for 6 h at room temperature. The reaction mixture was filtered and MIL-100(Sc/Fe)(60/40) washed with methanol. The product was filtered through silica using dichloromethane (to remove any unreacted 2-methylindole), followed by ether:dichloromethane (1:4) eluent and concentrated under vacuum yielding a colourless oil obtained in 74 % yield, 0.17 g, 0.73 mmol. This product has been reported previously using a different synthetic procedure.²⁰ ¹H NMR (500 MHz, (CD₃)₂CO) δ_H 10.18 (1 H, s, NH), 7.78 (1 H, d, *J* 7.8, Ar-H), 7.34 (1 H, dd, *J* 7.8, 1.2, Ar-H), 7.07 (2 H, dtd, *J* 23.2, 7.1, 1.2, Ar-H), 5.49 – 5.41 (1 H, m, CH), 3.32 (1 H, s, OH), 2.51 (3 H, s,

CH_3). ^{13}C NMR (126 MHz, $(CD_3)_2CO$) δ_C 126.3 (q, J_{CF} 282.1), 127.5, 135.7, 134.8, 120.8, 119.6, 119.1, 110.2, 105.4, 66.9 (q, J_{CF} 32.8), 11.18. $^{19}F\{^1H\}$ NMR (471 MHz, $(CD_3)_2CO$) δ_F -78.01. ESI [M-H] calculated 228.0642 found 228.0641. $C_{11}H_{10}F_3NO$ (Found C, 57.49; H, 4.45; N, 6.14; Required C, 57.64 ; H, 4.40; N, 6.11)

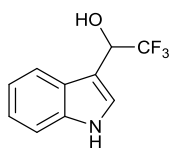
Formation of 2,2,2-trifluoro-1-(2-methyl-1H-indol-3-yl)ethanone (24)



Oxidation of Friedel Crafts product example procedure: 2,2,2-trifluoro-1-(2-methyl-1H-indol-3-yl)ethanol (0.23 g, 1 mmol), *tert*-butyl hydroperoxide (4 mmol, 0.36 g), 1-fluoronaphthalene (0.07 ml, 0.5 mmol) and toluene (5 ml) was added to activated MIL-100(Sc/Fe)(60/40) (15.4 mg, 5 mol%) and stirred for 6 h at room temperature. The reaction mixture was filtered, concentrated under vacuum. The crude residue was dissolved in acetone and reduced under vacuum to remove volatiles from the mixture to obtain a white powder in 79% yield, 0.18 g, 0.79 mmol.

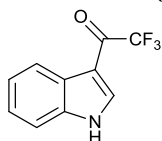
Tandem method: MIL-100(Sc/Fe)(60/40) (15.4 mg, 5 mol%) was heated to 150°C under vacuum for 5 h, 2-methylindole (0.13 g, 1 mmol), ethyl trifluoroacetaldehyde ethyl hemiacetal (0.12 ml, 1.4 mmol), *tert*-butyl hydroperoxide (4 mmol, 0.36 g), 1-fluoronaphthalene (0.07 ml, 0.5mmol) and toluene (5 ml) was added and stirred for 6 h at room temperature. The reaction mixture was filtered and MIL-100(Sc/Fe)(60/40) washed with methanol and concentrated under vacuum. The material was filtered through silica using a ether:dichloromethane (1:4) eluent and concentrated under vacuum. The crude residue was dissolved in acetone and reduced under vacuum to remove volatiles from the mixture to obtain a white powder in 90 % yield, 0.2 g, 0.9 mmol. This product has been reported previously using a different synthetic procedure.²¹ 1H NMR (300 MHz, $(CD_3)_2CO$) δ_H 11.53 (1 H, s, NH), 8.08 – 7.97 (1 H, m, Ar-H), 7.55 – 7.42 (1 H, m, Ar-H), 7.26 (2 H, ddd, J 5.6, 3.1, 1.3, Ar-H), 2.78 (3 H, s, CH_3). ^{13}C NMR (101 MHz, $(CD_3)_2CO$) δ_C 205.5, 205.1, 174.3 (q, J_{CF} 35.6), 149.8, 135.4, 126.2, 123.2, 122.7, 120.4, 117.3 (q, J_{CF} 289.4), 111.7, 107.3, 14.6. $^{19}F\{^1H\}$ NMR (471 MHz, $(CD_3)_2CO$) δ_F -75.82. ESI [M+H] calculated 228.0631 found 228.0625. $C_{11}H_8F_3NO$ (Found C, 58.02; H, 3.44; N, 6.13; Required C, 58.16; H, 3.55; N, 6.17).

Formation of 2,2,2-trifluoro-1-(1H-indol-3-yl)ethanol (25)



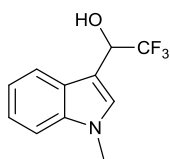
Experimental procedure similar to that for the synthesis of 2,2,2-trifluoro-1-(1H-indol-3-yl)ethanol. To purify, the product was filtered through silica using dichloromethane (to remove any unreacted indole), followed by ether:dichloromethane (1:4) eluent and concentrated under vacuum to obtain product 25 in 68 % yield, 0.15 g, 0.68 mmol. This product has been reported previously using a different synthetic procedure.²⁰ ¹H NMR (300 MHz, (CD₃)₂CO) δ_{H} 10.26 (1 H, s, NH), 7.62 (1 H, d, *J* 8.5, Ar-*H*), 7.39 – 7.25 (1 H, m, Ar-*H*), 7.06 – 6.87 (1 H, m, Ar-*H*), 5.36 – 5.33 (2 H, m, CH). ¹³C NMR (126 MHz, (CD₃)₂CO) δ_{C} 136.7, 126.3, 125.9 (q, *J*_{CF} 281.7), 124.6, 121.8, 119.6, 119.4, 111.5, 110.1, 66.9 (q, *J*_{CF} 32.6). ¹⁹F{¹H} NMR (282 MHz, (CD₃)₂CO) δ_{F} -79.08. ESI [M-H] calculated 214.0485 found 214.0483.

Formation of 2,2,2-trifluoro-1-(1H-indol-3-yl)ethanone (26)



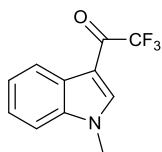
Experimental procedure similar to that for the oxidation and tandem synthesis of 2,2,2-trifluoro-1-(2-methyl-1H-indol-3-yl)ethanone. Oxidation product was purified by dissolving crude product in acetone and reducing under vacuum to remove volatiles from the mixture to obtain a white powder 57% yield, 0.14 g, 0.66 mmol. Tandem product purified by filtering through silica using a ether:dichloromethane eluent (1:4) and concentrated under vacuum. The crude residue was dissolved in acetone and reduced under vacuum to remove volatiles from the mixture to obtain a white powder in 81% yield, 0.17 g, 0.8 mmol. This product has been reported previously using a different synthetic procedure.²¹ ¹H NMR (300 MHz, d6-DMSO) δ_{H} 12.71 (1 H, s, NH), 8.48 (1 H, dq, *J* 3.8, 1.9, Ar-*H*), 8.26 – 8.11 (1 H, m, Ar-*H*), 7.66 – 7.51 (1 H, m, Ar-*H*), 7.41 – 7.23 (2 H, m, Ar-*H*). ¹³C NMR (75 MHz, d6-DMSO) δ_{C} 174.2 (q, *J* 33.8), 137.9 (q, *J* 4.8), 137.0, 126.1, 124.6, 123.7, 121.4, 117.2 (q, *J* 291.6), 113.3, 109.2. ¹⁹F{¹H} NMR (282 MHz, d6-DMSO) δ_{F} -71.83. ESI [M-H] calculated 212.0329 found 212.0323.

Formation of 2,2,2-trifluoro-1-(1-methyl-1H-indol-3-yl)ethanol (27)



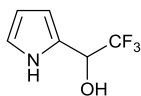
Experimental procedure similar to that for the synthesis of 2,2,2-trifluoro-1-(1H-indol-3-yl)ethanol. To purify, the product was filtered through silica using dichloromethane (to remove any unreacted indole), followed by ether:dichloromethane (1:4) eluent and concentrated under vacuum to obtain a yellow oil in 65 % yield, 0.15 g, 0.65 mmol. This product has been reported previously using a different synthetic procedure.²⁰ ¹H NMR (500 MHz, (CD₃)₂CO) δ _H 7.76 (1 H, d, *J* 8.0, Ar-*H*), 7.47 – 7.39 (2 H, m, Ar-*H*), 7.22 (1 H, ddd, *J* 8.2, 7.0, 1.2, Ar-*H*), 7.10 (1 H, td, *J* 7.4, 1.0, Ar-*H*), 5.47 (1 H, q, *J* 7.3, CH), 3.86 (3 H, s, CH₃). ¹³C NMR (126 MHz, (CD₃)₂CO) δ _C 137.09, 126.88, 128.71, 125.69 (q, *J*_{CF} 264.4), 121.65, 119.70, 119.31, 109.57, 109.06, 66.64 (q, *J*_{CF} 32.7), 32.05. ¹⁹F{¹H} NMR (471 MHz, (CD₃)₂CO) δ _F -78.52. ESI [M+H] calculated 216.0642 found 216.0641.

Formation of 2,2,2-trifluoro-1-(1-methyl-1H-indol-3-yl)ethanone (28)

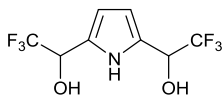


Experimental procedure similar to that for the oxidation and tandem synthesis of 2,2,2-trifluoro-1-(2-methyl-1H-indol-3-yl)ethanone. Oxidation product was purified by dissolving crude product in acetone and reducing under vacuum to remove volatiles from the mixture to obtain a yellow powder in 62% yield, 0.14 g, 0.62 mmol. Tandem product purified by filtering through silica using a ether:dichloromethane (1:4) eluent and concentrated under vacuum. The crude residue was dissolved in acetone and reduced under vacuum to remove volatiles from the mixture to obtain a yellow powder in 72% yield, 0.16 g, 0.72 mmol. This product has been reported previously using a different synthetic procedure.²¹ ¹H NMR (500 MHz, (CD₃)₂CO) δ _H 8.38 (1 H, dt, *J* 3.0, 1.4, Ar-*H*), 8.32 (1 H, dd, *J* 7.4, 1.5, Ar-*H*), 7.63 (1 H, d, *J* 8.1, Ar-*H*), 7.42 (1 H, m, Ar-*H*), 7.41 (1 H, m, Ar-*H*), 4.06 (3 H, s, CH₃). ¹³C NMR (126 MHz, (CD₃)₂CO) δ _C 173.84 (q, *J*_{CF} 34.2), 139.8, 137.8, 126.8, 124.4, 123.7, 121.7, 117.2 (q, *J*_{CF} 291.0), 111.0, 108.5, 33.3. ¹⁹F{¹H} NMR (282 MHz, (CD₃)₂CO) δ _F -73.34. ESI [M+H] calculated 228.0361 found 228.0636.

Formation of 2,2,2-trifluoro-1-(1H-pyrrol-2-yl)ethanol and Formation of 1,1'-(1H-pyrrole-2,5-diyl)bis(2,2,2-trifluoroethanol) (29+30)

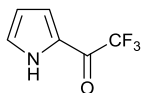


Experimental procedure similar to that for the synthesis of 2,2,2-trifluoro-1-(1H-indol-3-yl)ethanol. The product was isolated by column chromatography using hexane:ethyl acetate (5:1) as eluent to yield a yellow oil (65%, 0.11g, 0.65 mmol). This product has been reported previously using a different synthetic procedure.²² ¹H NMR (500 MHz, (CD₃)₂CO) δ_H 10.06 (1 H, s, NH), 6.83 (1 H, td, *J* 2.7, 1.6, Ar-*H*), 6.22 (1 H, s, Ar-*H*), 6.09 (1 H, q, *J* 2.6 Ar-*H*), 5.33-5.09 (1 H, m, CH). ¹³C NMR (126 MHz, (CD₃)₂CO) δ_C 125.3, 124.9 (q, *J*_{CF} 281.4 Hz), 118.6, 107.8, 107.7, 66.7 (q, *J*_{CF} 32.6 Hz). ¹⁹F{¹H} NMR (282 MHz, (CD₃)₂CO) δ_F -79.9.



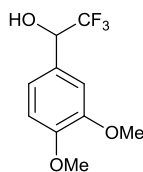
Product obtained in 4% yield, 0.01g, 0.04mmol. ¹H NMR (300 MHz, (CD₃)₂CO) δ_H 10.04 (1 H, s, NH), 5.66 (2 H, d, *J* 5.6, Ar-*H*), 5.06 (2 H, q, *J* 6.9, CH). ¹⁹F{¹H} NMR (282 MHz, (CD₃)₂CO) δ_F -79.42.

Formation of 2,2,2-trifluoro-1-(1H-pyrrol-2-yl)ethanone



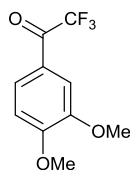
Experimental procedure similar to that for the synthesis of 2,2,2-trifluoro-1-(2-methyl-1H-indol-3-yl)ethanone. Oxidation product was purified by dissolving crude product in acetone and reducing under vacuum to remove volatiles from the mixture to obtain a brown oil in 81% yield, 0.13 g, 0.81 mmol. Tandem product purified by filtering through silica using a ether:dichloromethane (1:4) eluent and concentrated under vacuum. The crude residue was dissolved in acetone and reduced under vacuum to remove volatiles from the mixture to obtain a brown powder in 72% yield, 0.12 g, 0.72 mmol. This product has been reported previously using a different synthetic procedure.²³ ¹H NMR (500 MHz, CDCl₃) δ_H 11.89 (1 H, s, NH), 7.50 (1 H, s, Ar-*H*), 7.25 – 7.21 (1 H, m, Ar-*H*), 6.45 (1 H, d, *J* 3.1, Ar-*H*). ¹³C NMR (126 MHz, CDCl₃) δ_C 170.3 (q, *J*_{CF} 36.8), 129.1, 125.9, 121.8, 116.9 (q, *J*_{CF} 289.0), 112.7. ¹⁹F{¹H} NMR (471 MHz, CDCl₃) δ_F -73.08. ESI [M-H] calculated 162.0172 found 162.0167.

Formation of 1-(3,4-dimethoxyphenyl)-2,2,2-trifluoroethanol (31)



MIL-100(Sc/Fe)(60/40) (15.4 mg, 5 mol%) was heated to 423 K under vacuum for 5 h, 1,2-dimethoxybenzene (0.13 ml, 1 mmol), ethyl trifluoroacetaldehyde ethyl hemiacetal (0.12 ml, 1.4 mmol), 1-fluoronaphthalene (0.07 ml, 0.5 mmol) and toluene (5 ml) was added and stirred for 16 h at 90°C. The reaction mixture was filtered and solution washed with water (5 ml), and methanol. The product was isolated by column chromatography using hexane:ethyl acetate (5:1) as eluent (22%, 0.05 g, 0.22 mmol). ^1H NMR (300 MHz, CDCl_3) δ_{H} 7.19 – 6.99 (1 H, m, Ar-H), 6.96 (1 H, d, J 8.1, Ar-H), 6.85 (1 H, dd, J 17.5, 10.9, Ar-H), 5.17 (1 H, q, J 7.15, CH), 3.83 (6 H, d, J 6.9, CH_3). ^{13}C NMR (75 MHz, CDCl_3) δ_{C} 151.1, 149.1, 132.5, 125.1 (q, J_{CF} 290), 120.1, 112.9, 110.6, 68.8 (q, J_{CF} 32.7 Hz), 54.89. $^{19}\text{F}\{^1\text{H}\}$ NMR (282 MHz, CDCl_3) δ_{F} -78.34.

Formation of 1-(3,4-dimethoxyphenyl)-2,2,2-trifluoroethanone (32)



Oxidation of Friedel Crafts product example procedure: 1-(3,4-dimethoxyphenyl)-2,2,2-trifluoroethanone (0.05 g, 0.2 mmol), *tert*-butyl hydroperoxide (0.09 ml, 1 mmol), 1-fluoronaphthalene (0.07 ml, 0.5 mmol) and toluene (5 ml) was added to MIL-100(Sc/Fe)(60/40) (15.4 mg, 5 mol%) and stirred for 16 h at 90°C. Product was isolated by column chromatography using hexane:ethyl acetate (5:1) as eluent (21%, 0.04 g, 0.19 mmol). Tandem method: MIL-100(Sc/Fe)(60/40) (15.4 mg, 5 mol%) was heated to 150°C under vacuum for 5 h, 2-methylindole (0.13 g, 1 mmol), ethyl trifluoroacetaldehyde ethyl hemiacetal (0.12 ml, 1.4 mmol), *tert*-butyl hydroperoxide (0.36 ml, 4 mmol), 1-fluoronaphthalene (0.07 ml, 0.5 mmol) and toluene (5 ml) was added and stirred for 16 h. The reaction mixture was filtered and solution washed with methanol and concentrated under vacuum. The product was isolated by column chromatography using hexane:ethyl acetate (5:1) as eluent (23%, 0.05 g, 0.23 mmol). ^1H NMR (500 MHz, CDCl_3) δ_{H} 7.71 (1 H, t, J 7.6, 1, Ar-H), 7.53 (1 H, d, J 7.9, Ar-H), 6.93 – 9.77 (1 H, m, Ar-H), 3.83 (6 H, d, J 6.7, CH_3). ^{13}C NMR (75 MHz, CDCl_3) δ_{C}

176.1 (q, J_{CF} 35.2), 156.3, 150.4, 121.5, 117.2 (q, J_{CF} 290.05 Hz), 115.7, 113.1, 112.4, 55.4. $^{19}\text{F}\{^1\text{H}\}$ NMR (471 MHz, CDCl_3) δ_{F} -72.17. ESI [M-H] calculated 233.0431 found 233.0434.

7.6. References

1. J. A. Groves, S. R. Miller, S. J. Warrender, C. Mellot-Draznieks, P. Lightfoot and P. A. Wright, *Chem. Commun.*, 2006, 3305-3307.
2. N. A. Uhlich, P. Sommer, C. Buehr, S. Schuerch, J.-L. Reymond and T. Darbre, *Chem. Commun.*, 2009, 6237-6239.
3. F. Micheel and W. Busse, *Chem. Ber.*, 1957, **90**, 2049-2053.
4. K. Peikert, F. Hoffmann and M. Froeba, *Chem. Commun.*, 2012, **48**, 11196-11198.
5. P. D. C. Dietzel, Y. Morita, R. Blom and H. Fjellvag, *Angew. Chem, Int. Ed.*, 2005, **44**, 6354-6358.
6. L. Alaerts, E. Seguin, H. Poelman, F. Thibault-Starzyk, P. A. Jacobs and D. E. De Vos, *Chem. Eur. J.*, 2006, **12**, 7353-7363.
7. J. P. S. Mowat, S. R. Miller, A. M. Z. Slawin, V. R. Seymour, S. E. Ashbrook and P. A. Wright, *Microporous Mesoporous Mater.*, 2011, **142**, 322-333.
8. G. Férey, C. Mellot-Draznieks, C. Serre, F. Millange, J. Dutour, S. Surble and I. Margiolaki, *Science*, 2005, **309**, 2040-2042.
9. S. R. Miller, G. M. Pearce, P. A. Wright, F. Bonino, S. Chavan, S. Bordiga, I. Margiolaki, N. Guillou, G. Feerey, S. Bourrelly and P. L. Llewellyn, *J. Am. Chem. Soc.*, 2008, **130**, 15967-15981.
10. E. D. Bloch, D. Britt, C. Lee, C. J. Doonan, F. J. Uribe-Romo, H. Furukawa, J. R. Long and O. M. Yaghi, *J. Am. Chem. Soc.*, 2010, **132**, 14382-14384.
11. M. L. Clarke, C. E. S. Jones and M. B. France, *Beilstein J. Org. Chem.*, 2007, **3**.
12. D. A. Evans, S. W. Tregay, C. S. Burgey, N. A. Paras and T. Vojtkovsky, *J. Am. Chem. Soc.*, 2000, **122**, 7936-7943.
13. J.-F. Zhao, H.-Y. Tsui, P.-J. Wu, J. Lu and T.-P. Loh, *J. Am. Chem. Soc.*, 2008, **130**, 16492.
14. J. S. Yadav, S. Abraham, B. V. S. Reddy and G. Sabitha, *Synthesis-Stuttgart*, 2001, 2165-2169.
15. J. S. Yadav, B. V. S. Reddy, G. Baishya, K. V. Reddy and A. V. Narsaiah, *Tetrahedron*, 2005, **61**, 9541-9544.
16. J. S. Yadav, S. Abraham, B. V. S. Reddy and G. Sabitha, *Tetrahedron Let.*, 2001, **42**, 8063-8065.
17. C. Wang, X. Wu, L. Zhou and J. Sun, *Chem. Eur. J.*, 2008, **14**, 8789-8792.
18. G. D. Joly and E. N. Jacobsen, *J. Am. Chem. Soc.*, 2004, **126**, 4102-4103.
19. M. Kanai, M. Yasumoto, Y. Kuriyama, K. Inomiya, Y. Katsuhara, K. Higashiyama and A. Ishii, *Chem. Let.*, 2004, **33**, 1424-1425.
20. Y. Maki, H. Kimoto, S. Fujii, M. Senga and L. A. Cohen, *J. Fluor. Chem.*, 1988, **39**, 47-59.
21. A. Cipiciani, S. Clementi, G. Giulietti, G. Marino, G. Savelli and P. Linda, *J. Chem. Soc. Perkin Trans. 2*, 1982, 523-530.
22. S. M. Landge, D. A. Borkin and B. Toeroek, *Tetrahedron Let.*, 2007, **48**, 6372-6376.
23. I. A. Ushakov, A. V. Afonin, V. K. Voronov, Z. V. Stepanova, L. N. Sobenina and A. I. Mikhaleva, *Russ. J. Org. Chem.*, 2003, **39**, 1318-1324.

8. Conclusions and future work

8.1. Conclusions

The first aim of this project was to synthesise MOF materials and investigate their use in Lewis acid catalysis. Initially a range of known MOFs was synthesised and the syntheses methods for both STA-12(Ni) and MIL-100(Sc) were optimised. After various attempts using various solvents and conditions the synthesis of STA-12(Ni) at room temperature was largely unsuccessful. It was found that for the hydrothermal synthesis of STA-12(Ni) the material was dependent on synthesis time and temperature and larger surface areas were obtained for materials synthesised over 72 h compared to 24 h. STA-12(Ni) could be synthesised efficiently using reflux and microwave techniques rather than the previously used hydrothermal synthesis techniques. This significantly reduced the time required to synthesise the material and also had an influence on the resultant particle size. Similarly, MIL-100(Sc) was also found to synthesise materials of high crystallinity and surface area when using both reflux and microwave techniques rather than the previously conventional solvothermal method. An alternative solvent for the synthesis of MIL-100(Sc) was sought due to the toxicity of the solvent DMF. Unfortunately, after various attempts it was found that the synthesis of MIL-100 required the presence of DMF in order to synthesise the desired material. The amount of DMF used in the synthesis of MIL-100(Sc) could be significantly reduced (to a 90:10 mixture of water:DMF) however, this did cause a slight decrease in crystallinity and surface area.

Previously MIL-100 and STA-12 materials had been probed by IR spectroscopy to determine Lewis acid strength and concentration of Lewis acid sites. MIL-100(Sc), however, had never been fully studied using this approach. This was carried out on both as-prepared MIL-100(Sc) and materials which had been activated using methanol; this had been previously found to increase the available surface area of the material. Initially the effect of heating the material was probed. It was shown that both the as-prepared material and methanol washed material contained DMF even after heating to 523 K, although a reduction in the amount of DMF present was apparent in the latter. The Lewis acid strength of MIL-100(Sc) was probed using CD₃CN and was shown to be similar to that of MIL-100(Sc, Cr) but weaker than that of MIL-100(Al). The amount of Lewis acid sites present in the material showed that the most sites were present when pre-heated to 523 K, however the amount of sites present were half of

what was observed previously for MIL-100(Fe,Cr) and equated to about 1.5 active sites per trimer.

In order to correlate the relationship between Lewis acid strength, concentration of sites and ability to catalyse a Lewis acid reaction, many different MOFs were synthesised and tested in the carbonyl ene reaction of α -methylstyrene with ethyl trifluoropyruvate. This also helped to determine the most important factors of a MOF for its use in catalysis. It was found that MIL-100(Sc) was the most successful MOF material tested in the carbonyl ene reaction. Other MIL-100 materials in the series were tested in order to determine if this was due to the nature of the large cage structure or if the metal had an influence on this high activity. MIL-100(Cr, Fe, Al), although previously found to be a stronger Lewis acid with more accessible Lewis acid sites, could not emulate the high activity shown by MIL-100(Sc). Further to this, other scandium containing MOFs were tested to determine if it was the metal that led to the high catalytic activity. No other scandium containing MOF could achieve this high activity. The large pore MIL-88D(Sc) was initially expected to show similar activity to that of MIL-100(Sc) however evidence has shown that this material is interpenetrated, making it difficult to access the Lewis acid site. MIL-101(Sc) was shown to break down to MIL-88B(Sc) when heated therefore could not be activated before use in catalysis. MIL-88B(Sc) was shown to remain in a closed pore structure when submerged in toluene (the solvent used for the carbonyl ene reaction) meaning substrates could not enter the pores to access Lewis acid sites. This showed that MIL-100(Sc) provided a good balance of Lewis acid strength and site accessibility to give high catalytic activity in the carbonyl ene reaction.

MIL-100(Sc) was shown to be an efficient catalyst in tandem carbonyl ene reactions carrying out dehydration, depolymerisation, and deactivation of substrates to form an activated material which could then go on to be used in a carbonyl ene reaction. Although MIL-100(Cr) was shown to be active for this type of reaction it did not provide the high activity observed in MIL-100(Sc). MIL-100(Sc) was shown to have its limitations however and when tested with less activated alkenes the performance of the material was much lower than previously observed. This shows that although MIL-100(Sc) is an efficient Lewis acid catalyst it is not strong and is much more efficient with more activated substrates. The material was shown to be easily recycled maintaining high activity even after five cycles with the structural integrity of the material the same after each cycle.

The high activity of MIL-100(Sc) compared to other MOF catalysts was not confined to the carbonyl ene reaction but was also the case for conjugate addition of electron deficient olefins to indoles and for imine formation reactions. The conjugate addition of electron deficient olefins to indole gave an interesting opportunity to try and determine if the catalysis was occurring in the pore of the material or on the surface. In order to do this, larger substrates that would be too large to fit in the material were synthesised. MIL-100(Sc) was shown to have much reduced activity compared to that previously observed with smaller substrates providing evidence that although there may be some surface catalysis most of the catalysis occurs in the pore.

Mixed metal MOFs have been previously synthesised using various techniques, however the introduction of two different structural metals and their use in catalysis has not been widely probed. The introduction of various trivalent and divalent metals to the synthesis of mixed metal MIL-100 materials led to MOF materials with interesting properties. It was shown that a series of mixed metal MIL-100(Sc/Fe) materials could be easily synthesised in a range of metal ratios. The materials were analysed using PXRD, N₂ adsorption, TGA, UV-vis spectroscopy and EDX which suggested no significant structural differences in the materials. Similar synthesis was carried out using an excess of iron metal source which formed a new series of mixed metal MIL-100(Sc/Fe)Xs materials. The materials were initially shown to differ by PXRD analysis, colour and UV-vis spectroscopy compared to the original MIL-100(Sc/Fe) series. The N₂ adsorption of the material was found to decrease as the amount of iron was increased and residual mass after calcination of the materials increased as iron content increased. In order to further probe the materials, XANES and EXAFS analysis was carried out and it was shown that these differences in properties were caused by the formation of α -Fe₂O₃ nanoparticulates in the pores of the MIL-100 materials.

A MIL-100(Sc/Al) series was synthesised as this allowed for the materials to be probed by solid state NMR. The materials were again shown to be similar by PXRD. Solid state NMR found that the hydroxide ion on the trimer was more likely on a scandium site compared to an aluminium site. It also showed that the materials contained aluminium and scandium in the trimers. However no clear evidence of whether there were mixed metal trimers or separate Al₃ and Sc₃ trimers was obtained. A MIL-100(Sc/Cr) series of materials was also prepared and characterised.

Divalent metals were also introduced into the MIL-100 structure. The introduction of trivalent metals into the materials was only obtained up to 30%. This was due to the charge balance of the trimer. The materials did show similar crystallinity and N₂ adsorption and the introduction of the metal could be visualised by UV-vis spectroscopy.

After the synthesis of the mixed metal MIL-100 materials the natural progression was to test these materials for suitability as Lewis acid catalysts. Initially, the previously tested carbonyl ene reaction was used to gauge the activity of the materials. In the MIL-100(Sc/Al), MIL-100(Sc/Cr) and MIL-100(Sc/Fe) series it was shown that a reduction in scandium content reduced the overall activity of the materials. Interestingly, for the MIL-100(Sc/Fe)Xs material this was not the case. This series of materials maintained high activities compared to MIL-100(Sc) throughout the available composites. Further to this, the materials were tested in the conjugate addition of electron deficient indoles and the same pattern was observed. The introduction of divalent metals into MIL-100 appeared to have a detrimental effect on the overall conversion of the materials.

In order to determine the effectiveness of the mixed metal materials as tandem catalysts they were tested for their use in a deacetalisation/Friedel-Crafts-oxidation reaction. The MIL-100(Sc/Fe) and MIL-100(Sc/Fe)Xs materials were chosen as the main focus for these reactions. It was shown that although the MIL-100(Sc/Fe)Xs materials were more effective at deacetalisation/Friedel-Crafts reactions the MIL-100(Sc/Fe) were better at oxidation reactions. The conversion of the deacetalisation/Friedel-Crafts reaction was shown to decrease as scandium content was decreased and oxidation activity increased as iron content was increased. An optimum activity for the tandem reaction was achieved at MIL-100(Sc₆₀/Fe₄₀). Interestingly the materials performed more effectively in the tandem process than in each reaction individually. It was found that this was largely due to diffusion of substrates and products in and out of the pore of the catalysts.

To continue with MIL-100(Sc), post synthetic modification was carried out on the material to potentially synthesise a mixed metal bifunctional catalyst. A mixed ligand MIL-100(Sc) material was synthesised consisting of fluorinated trimesic acid. This allowed for post synthetic nucleophilic substitution to be carried out on the ligand. In this case the substitution with diphenylphosphine was selected as these types of ligands are widely used in catalysis. This was successfully carried out using various amounts of diphenylphosphine. The materials were shown to maintain crystallinity and N₂ adsorption was shown to reduce as the amount of

diphenylphosphine added into the MOF was increased. The addition of palladium to the material was also carried out which again maintained crystallinity. Unfortunately, it was found by solid state NMR that the diphenylphosphine had oxidised therefore any palladium added to the ligand would be rendered catalytically inactive.

8.2. Future Work

This work has shown that MOFs can be successfully synthesised using a range of different synthetic techniques. The use of MOFs in different catalytic reactions has been implemented with outstanding performances from MIL-100(Sc) compared to other MOF materials in Lewis acid catalysed C-C and C=N bond formation. Further work into the use of this material along with metal nanoparticles in the pore is already being investigated for use as a mixed metal bifunctional catalyst.

It would be beneficial to gain more of an understanding as to what controls the catalytic activity of these materials. This could allow for a MOF to be tailor-made for a particular catalytic reaction. This could allow for MOFs to be used in flow chemistry, by tailoring different MOF materials with different catalytic properties

Further investigation into the use of nucleophilic substitution in post synthetic modification could open up potential for the addition of new ligands. This approach could be used to include a structural (Lewis acidic) metal and a late transition metal such as Rh, Ir, or Ru in the MOF and so to investigate tandem catalysis including asymmetric catalysis.

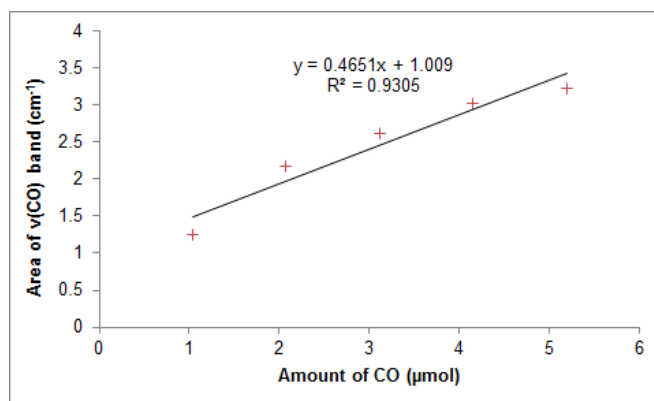
9. Appendix

9.1. Calculation of molar absorption coefficient used to determine number of Lewis acid sites

9.1.1. As-prepared MIL-100(Sc) heated at 423 K and CO dosed at 100 K

Table 9.1: Area of CO band after each dose and the amount of μmol introduced

area CO (cm^{-1})	Pressure (torr)	μmol
1.24	10	10.0
2.18	10	20.0
2.61	10	30.0
3.03	10	40.0
3.23	10	50.0

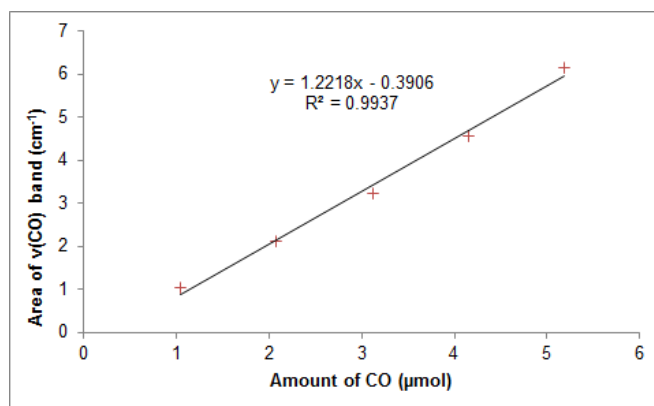


Graph 9.1: Area of $\nu(\text{CO})$ of coordinated CO species versus amount of CO introduced into the IR cell to give the adsorption molar coefficient. Calculation of Lewis acid sites using molar adsorption coefficient

9.1.2. As-prepared MIL-100(Sc) heated at 523 K and CO dosed at 100 K

Table 9.2: Area of CO band after each dose and the amount of μmol introduced

area CO (cm^{-1})	Pressure (torr)	μmol
1.02	10	10.0
2.12	10	20.0
3.24	10	30.0
4.56	10	40.0
6.14	10	50.0

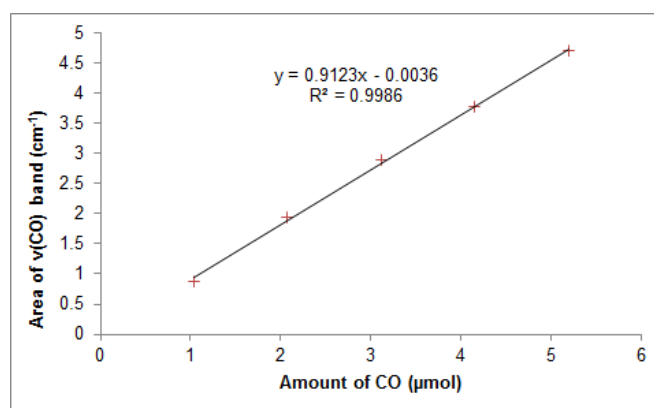


Graph 9.2: Area of $\nu(\text{CO})$ of coordinated CO species versus amount of CO introduced into the IR cell to give the adsorption molar coefficient. Calculation of Lewis acid sites using molar adsorption coefficient

9.1.3. Methanol-activated MIL-100(Sc) heated at 423 K and CO dosed at 100 K

Table 9.3: Area of CO band after each dose and the amount of μmol introduced

area CO (cm ⁻¹)	pressure (torr)	μmol
0.88	10	10.0
1.95	10	20.0
2.89	10	30.0
3.78	10	40.0
4.69	10	50.0



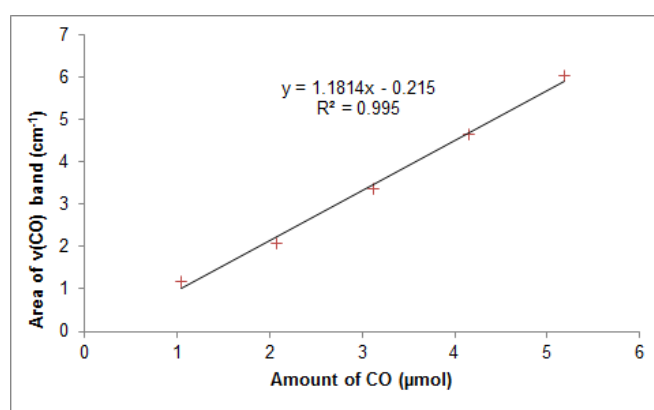
Graph 9.3: Area of $\nu(\text{CO})$ of coordinated CO species versus amount of CO introduced into the IR cell to give the adsorption molar coefficient. Calculation of Lewis acid sites using molar adsorption coefficient

9.1.4. Methanol-activated MIL-100(Sc) heated at 523 K and CO dosed at 100 K

Table 9.4: Area of CO band after each dose and the amount of μmol introduced

area CO (cm^{-1})	pressure (torr)	pressure (torr)	μmol
1.18	10	10.0	1.04
2.09	10	20.0	2.08
3.38	10	30.0	3.12
4.64	10	40.0	4.15
6.04	10	50.0	5.19

Table 9.5: Area of CO band after each dose and the amount of μmol introduced



Graph 9.4: Area of $\nu(\text{CO})$ of coordinated CO species versus amount of CO introduced into the IR cell to give the adsorption molar coefficient. Calculation of Lewis acid sites using molar adsorption coefficient.

9.2. Crystallographic details of samples

9.2.1. STA-12(Ni) (chapter 3)

	STA-12(Ni) 24 hrs hydrothermal	STA-12(Ni) 72 hrs hydrothermal
Unit cell	$\text{Ni}_{18}\text{P}_{18}\text{O}_{126}\text{N}_{18}\text{C}_{54}\text{H}_{216}$	$\text{Ni}_{18}\text{P}_{18}\text{O}_{126}\text{N}_{18}\text{C}_{54}\text{H}_{216}$
Temperature/K	298	298
Space group	R -3	R -3
X-ray source	Cu	Cu
Diffractometer	PANalytical	PANalytical
Wavelength (\AA)	1.54056	1.54056
$a/\text{\AA}$	27.9142(15)	27.9368(3)
$b/\text{\AA}$	27.9142(15)	27.9368(3)
$c/\text{\AA}$	6.23142(28)	6.23212(9)
Volume/ \AA^3	4205.1(4)	4215.2(5)
R_p	0.456	0.0352
R_{wp}	0.0651	0.0499

	STA-12(Ni) microwave	STA-12(Ni) reflux
Unit cell	Ni ₁₈ P ₁₈ O ₁₂₆ N ₁₈ C ₅₄ H ₂₁₆	Ni ₁₈ P ₁₈ O ₁₂₆ N ₁₈ C ₅₄ H ₂₁₆
Temperature/K	298	298
Space group	R -3	R -3
X-ray source	Cu	Cu
Diffractometer	PANalytical	PANalytical
Wavelength (Å)	1.54056	1.54056
a/ Å	27.904(7)	27.9459(7)
b/ Å	27.904(7)	27.9459(7)
c/ Å	6.2167(10)	6.23385(14)
Volume/Å ³	4192.1(16)	4216.22(18)
R _p	0.0434	0.0338
R _{wp}	0.0689	0.0489

9.2.2. MIL-100 materials (Chapter 5)

	MIL-100(Sc)	MIL-100(Fe)	MIL-100(Al)	MIL-100(Cr)
Unit cell	Sc ₈₁₆ O ₉₇₁₂ C ₄₈₉₆	Fe ₈₁₆ O ₉₇₁₂ C ₄₈₉₆	Al ₈₁₆ O ₉₇₁₂ C ₄₈₉₆	Cr ₈₁₆ O ₉₇₁₂ C ₄₈₉₆
Temperature/K	298	298	298	298
Space group	F d -3 m	F d -3 m	F d -3 m	F d -3 m
X-ray source	Cu	Cu	Cu	Cu
Diffractometer	PANalytical	PANalytical	PANalytical	PANalytical
Wavelength (Å)	1.54056	1.54056	1.54056	1.54056
a/ Å	75.436(8)	73.5821(4)	73.2356(20)	73.6525(19)
Volume/Å ³	429275.35(15)	398397.44(3)	392795.71(8)	399542.04(8)
R _p	0.0281	0.0381	0.038	0.0324
R _{wp}	0.0372	0.0499	0.050	0.0391

9.2.3. Mixed metal MIL-100(Sc/Fe) (Chapter 5)

	MIL-100(Sc₈₀/Fe₂₀)	MIL-100(Sc₆₀/Fe₄₀)
Unit cell	Sc ₆₅₃ Fe ₁₆₃ O ₉₇₁₂ C ₄₈₉₆	Sc ₄₉₀ Fe ₃₂₆ O ₉₇₁₂ C ₄₈₉₆
Temperature/K	298	298
Space group	F d -3 m	F d -3 m
X-ray source	Cu	Cu
Diffractometer	PANalytical	PANalytical
Wavelength (Å)	1.54056	1.54056
a/ Å	75.0561(14)	74.755(3)
Volume/Å ³	422822.4(6)	417759.15(9)
R _p	0.0284	0.0293
R _{wp}	0.0375	0.0388

	MIL-100(Sc₄₀/Fe₆₀)	MIL-100(Sc₂₀/Fe₈₀)
Unit cell	Sc ₃₂₆ Fe ₄₉₀ O ₉₇₁₂ C ₄₈₉₆	Sc ₁₆₃ Fe ₆₅₃ O ₉₇₁₂ C ₄₈₉₆
Temperature/K	298	298
Space group	F d -3 m	F d -3 m
X-ray source	Cu	Cu
Diffractometer	PANalytical	PANalytical
Wavelength (Å)	1.54056	1.54056
a/ Å	74.5501(14)	74.22093(16)
Volume/Å ³	414329.39(6)	408864.28(2)
R _p	0.0348	0.0365
R _{wp}	0.0449	0.0462

9.2.4. Mixed metal MIL-100(Sc/Fe)Xs (Chapter 5)

	MIL-100(Sc₈₀/Fe₂₀)Xs	MIL-100(Sc₆₀/Fe₄₀)Xs	MIL-100(Sc₅₀/Fe₅₀)Xs
Unit cell	Sc ₆₅₃ Fe ₁₆₃ O ₉₇₁₂ C ₄₈₉₆	Sc ₄₉₀ Fe ₃₂₆ O ₉₇₁₂ C ₄₈₉₆	Sc ₄₀₈ Fe ₄₀₈ O ₉₇₁₂ C ₄₈₉₆
Temperature/K	298	298	298
Space group	F d -3 m	F d -3 m	F d -3 m
X-ray source	Cu	Cu	Cu
Diffractometer	PANalytical	PANalytical	PANalytical
Wavelength (Å)	1.54056	1.54056	1.54056
a/ Å	75.2241(6)	75.0666(14)	74.9223(18)
Volume/Å ³	425667.99(4)	422999.87(6)	420565.17(7)
R _p	0.0386	0.0362	0.0381
R _{wp}	0.0505	0.0487	0.0499

9.2.5. Mixed metal MIL-100(Sc/Al) (Chapter 5)

	MIL-100(Sc₈₀/Al₂₀)	MIL-100(Sc₆₀/Al₄₀)
Unit cell	Sc ₆₅₃ Al ₁₆₃ O ₉₇₁₂ C ₄₈₉₆	Sc ₄₉₀ Al ₃₂₆ O ₉₇₁₂ C ₄₈₉₆
Temperature/K	298	298
Space group	F d -3 m	F d -3 m
X-ray source	Cu	Cu
Diffractometer	PANalytical	PANalytical
Wavelength (Å)	1.54056	1.54056
a/ Å	74.9231(21)	74.6841(12)
Volume/Å ³	420578.64(8)	416566.61(6)
R _p	0.0279	0.0267
R _{wp}	0.0376	0.0362

	MIL-100(Sc₄₀/Al₆₀)	MIL-100(Sc₂₀/Fe₈₀)
Unit cell	Sc ₃₂₆ Al ₄₉₀ O ₉₇₁₂ C ₄₈₉₆	Sc ₁₆₃ Al ₆₅₃ O ₉₇₁₂ C ₄₈₉₆
Temperature/K	298	298
Space group	F d -3 m	F d -3 m
X-ray source	Cu	Cu
Diffractionmeter	PANalytical	PANalytical
Wavelength (Å)	1.54056	1.54056
a/ Å	74.3204(7)	73.9127(16)
Volume/Å ³	410510.35(5)	403791.53(7)
R _p	0.0374	0.0351
R _{wp}	0.0492	0.0456

9.2.6. Mixed metal MIL-100(Sc/Cr) (Chapter 5)

	MIL-100(Sc₈₀/Cr₂₀)	MIL-100(Sc₆₀/Cr₄₀)
Unit cell	Sc ₆₅₃ Cr ₁₆₃ O ₉₇₁₂ C ₄₈₉₆	Sc ₄₉₀ Cr ₃₂₆ O ₉₇₁₂ C ₄₈₉₆
Temperature/K	298	298
Space group	F d -3 m	F d -3 m
X-ray source	Cu	Cu
Diffractionmeter	PANalytical	PANalytical
Wavelength (Å)	1.54056	1.54056
a/ Å	75.1452(2)	74.8045(12)
Volume/Å ³	424329.99(2)	418584.53(6)
R _p	0.0339	0.0257
R _{wp}	0.0412	0.0354

	MIL-100(Sc₄₀/Cr₆₀)	MIL-100(Sc₂₀/Cr₈₀)
Unit cell	Sc ₃₂₆ Cr ₄₉₀ O ₉₇₁₂ C ₄₈₉₆	Sc ₁₆₃ Cr ₆₅₃ O ₉₇₁₂ C ₄₈₉₆
Temperature/K	298	298
Space group	F d -3 m	F d -3 m
X-ray source	Cu	Cu
Diffractionmeter	PANalytical	PANalytical
Wavelength (Å)	1.54056	1.54056
a/ Å	74.6121(15)	74.3145(5)
Volume/Å ³	415362.98(7)	410412.59(4)
R _p	0.035	0.0295
R _{wp}	0.0451	0.0404